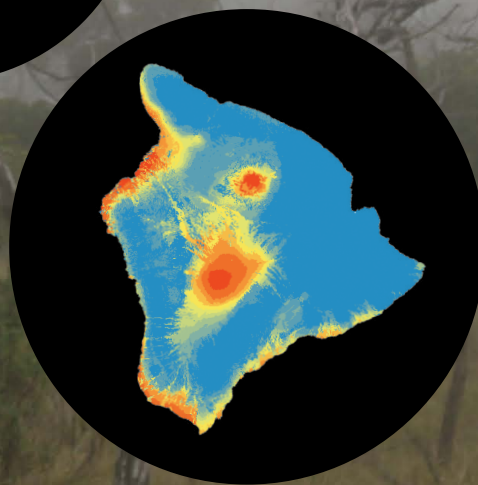
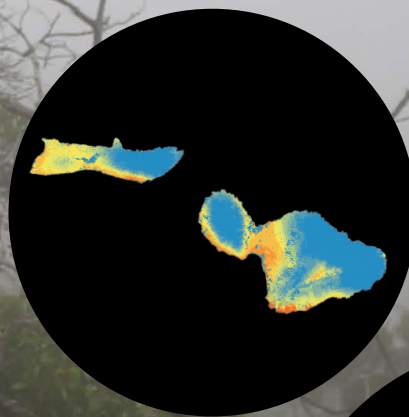
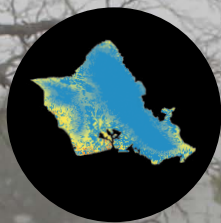
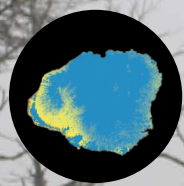


Prepared in cooperation with the Pacific Islands Climate Adaptation Science Center

Effects of Drought and Cloud-Water Interception on Groundwater Recharge and Wildfire Hazard for Recent and Future Climate Conditions, Kauaʻi, Oʻahu, Molokaʻi, Maui, and the Island of Hawaiʻi



Scientific Investigations Report 2023–5141

Cover. Map showing the relative frequency of monthly mean soil moisture less than or equal to a threshold value of 0.074, expressed as a fraction of available water capacity, during the Non-Drought scenario for Kaua'i, O'ahu, Moloka'i, Maui, and the Island of Hawai'i. Non-Drought scenario is rainfall during 1990–97 and 2003–06, and 2020 land cover. Relative frequency is shown using a spectral color scale with blue representing low frequency and red representing high frequency. This map is a modified version of [figure 18](#) in the report. Background image, Photograph of shrubland immersed in clouds at an altitude of approximately 5,400 feet in Nakula, Maui. Photograph by Joseph Kennedy, U.S. Geological Survey, January 2018.

Effects of Drought and Cloud-Water Interception on Groundwater Recharge and Wildfire Hazard for Recent and Future Climate Conditions, Kauaʻi, Oʻahu, Molokaʻi, Maui, and the Island of Hawaiʻi

By Alan Mair, Delwyn S. Oki, Heidi L. Kāne, Adam G. Johnson, and Kolja Rotzoll

Prepared in cooperation with the Pacific Islands Climate Adaptation Science Center

Scientific Investigations Report 2023–5141

**U.S. Department of the Interior
U.S. Geological Survey**

U.S. Geological Survey, Reston, Virginia: 2024

For more information on the USGS—the Federal source for science about the Earth, its natural and living resources, natural hazards, and the environment—visit <https://www.usgs.gov> or call 1–888–ASK–USGS.

For an overview of USGS information products, including maps, imagery, and publications, visit <https://store.usgs.gov>.

Any use of trade, firm, or product names is for descriptive purposes only and does not imply endorsement by the U.S. Government.

Although this information product, for the most part, is in the public domain, it also may contain copyrighted materials as noted in the text. Permission to reproduce copyrighted items must be secured from the copyright owner.

Suggested citation:

Mair, A., Oki, D.S., Kāne, H.L., Johnson, A.G., and Rotzoll, K., 2024, Effects of drought and cloud-water interception on groundwater recharge and wildfire hazard for recent and future climate conditions, Kauaʻi, Oʻahu, Molokaʻi, Maui, and the Island of Hawaiʻi: U.S. Geological Survey Scientific Investigations Report 2023–5141, 98 p., <https://doi.org/10.3133/sir20235141>.

Associated data for this publication:

Mair, A., 2024, Frequency characteristics of soil moisture, evapotranspiration, and climatic water deficit for Kauaʻi, Oʻahu, Molokaʻi, Maui, and the Island of Hawaiʻi, for a set of rainfall and land-cover conditions: U.S. Geological Survey data release, <https://doi.org/10.5066/P9HGHWS4>.

Mair, A., 2024, Mean annual groundwater recharge rates for Kauaʻi, Oʻahu, Molokaʻi, Maui, and the Island of Hawaiʻi, for a set of drought and land-cover conditions: U.S. Geological Survey data release, <https://doi.org/10.5066/P9DDP1C6>.

Acknowledgments

This study was conducted in cooperation with the Pacific Islands Climate Adaptation Science Center. The authors are grateful to Abby Frazier (Clark University) and Clay Trauernicht (University of Hawai'i at Mānoa) for contributing expertise and data to this study.

The authors also wish to thank John Engott (U.S. Geological Survey California Water Science Center), Christian Giardina (U.S. Forest Service, Pacific Southwest Research Station, Institute of Pacific Islands Forestry), and Clay Trauernicht (University of Hawai'i at Mānoa) for providing comments on the draft version of the report.

Contents

Acknowledgments	iii
Abstract	1
Introduction.....	1
Purpose and Scope	6
Previous Studies	6
Effects of Drought on Groundwater Recharge	6
Effects of Soil and Plant Moisture on Wildfire Hazard and Behavior	8
Effects of Cloud-Water Interception on Total Precipitation, Groundwater Recharge, and Wildfire Hazard	8
Study Area	10
Physical Setting	10
Climate	11
Land Cover	12
Groundwater Recharge	14
Wildfires	16
Selection of Climate and Land-Cover Conditions	18
Historical Drought Conditions	18
Future Climate Conditions	18
Hypothetical Land-Cover Conditions	18
Water-Budget Model.....	20
Water-Budget Scenarios.....	20
Effects of Drought and Reduced Cloud-Water Interception on Groundwater Recharge	20
Effects of Drought and Reduced Cloud-Water Interception on Soil Moisture, Evapotranspiration, and Climatic Water Deficit.....	23
Groundwater-Recharge Estimates	24
Effects of Drought	24
Kauaʻi	24
Oʻahu	24
Molokaʻi	30
Maui	32
Island of Hawaiʻi	35
Effects of Drought and Reduced Cloud-Water Interception	35
Oʻahu	38
Maui	38
Island of Hawaiʻi	38
Soil Moisture, Evapotranspiration, and Climatic Water Deficit Frequency Characterization	39
Frequency Characteristics for Reference Condition	39
Effects of Drought	39
Kauaʻi	43
Oʻahu	46
Molokaʻi	50
Maui	54
Island of Hawaiʻi	58
Effects of Drought and Reduced Cloud-Water Interception	62

O‘ahu	62
Maui	62
Island of Hawai‘i	62
Implications of Drought and Reduced Cloud-Water Interception for Groundwater Recharge, Soil Moisture, Evapotranspiration, and Climatic Water Deficit	63
Groundwater Recharge	63
Soil Moisture, Evapotranspiration, and Climatic Water Deficit	63
Study Limitations	64
Summary	67
References Cited	68
Appendix 1. Model Input	78
Appendix 2. Evaluation of Moisture-Stress Thresholds for Soil Moisture, Evapotranspiration, and Climatic Water Deficit	90

Figures

1. Maps showing the main Hawaiian Islands showing the general topography of individual islands	2
2. Maps showing the aquifer systems for Kaua‘i, O‘ahu Moloka‘i, Maui, and the Island of Hawai‘i	4
3. Maps showing the mean annual rainfall in the main Hawaiian Islands, excluding Ni‘ihau	11
4. Maps showing the land cover in 2020 for Kaua‘i, O‘ahu, Moloka‘i, Maui, and the Island of Hawai‘i	13
5. Maps showing the mean annual groundwater recharge for 1978–2007 climate and 2020 land cover for Kaua‘i, O‘ahu, Moloka‘i, Maui, and the Island of Hawai‘i	15
6. Maps showing the land cover within wildfire perimeters during 1999–2012 for Kaua‘i, O‘ahu, Moloka‘i, Maui, and the Island of Hawai‘i	17
7. Maps showing the land-cover conversions on O‘ahu, Maui, and the Island of Hawai‘i for two hypothetical land-cover conditions	21
8. Maps showing the distribution of estimated change in mean annual groundwater recharge for two water-budget scenarios for Kaua‘i	26
9. Maps showing the estimated change in mean annual groundwater recharge by aquifer system for two water-budget scenarios for Kaua‘i	27
10. Maps showing the distribution of estimated change in mean annual groundwater recharge for six water-budget scenarios for O‘ahu	28
11. Maps showing the estimated change in mean annual groundwater recharge by aquifer system for six water-budget scenarios for O‘ahu	29
12. Maps showing the distribution of estimated change in mean annual groundwater recharge for two water-budget scenarios for Moloka‘i	30
13. Maps showing the estimated change in mean annual groundwater recharge by aquifer system for two water-budget scenarios for Moloka‘i	31
14. Maps showing the distribution of estimated change in mean annual groundwater recharge for six water-budget scenarios for Maui	33
15. Maps showing the estimated change in mean annual groundwater recharge by aquifer system for six water-budget scenarios for Maui	34
16. Maps showing the distribution of estimated change in mean annual groundwater recharge for six water-budget scenarios for the Island of Hawai‘i	36

17.	Maps showing the estimated change in mean annual groundwater recharge by aquifer system for six water-budget scenarios for the Island of Hawai'i	37
18.	Maps showing the relative frequency of monthly mean soil moisture less than or equal to a threshold value of 0.074 during the Non-Drought scenario for Kaua'i, O'ahu, Moloka'i, Maui, and the Island of Hawai'i	40
19.	Maps showing the relative frequency of monthly evapotranspiration less than or equal to a threshold value of 0.96 inches during the Non-Drought scenario for Kaua'i, O'ahu, Moloka'i, Maui, and the Island of Hawai'i	41
20.	Maps showing the relative frequency of monthly climatic water deficit greater than or equal to a threshold value of 0.77 during the Non-Drought scenario for Kaua'i, O'ahu, Moloka'i, Maui, and the Island of Hawai'i	42
21.	Maps showing estimated increases in relative frequency of monthly mean soil moisture less than or equal to a value of 0.074 for three water-budget scenarios for Kaua'i	43
22.	Maps showing estimated increases in relative frequency of monthly evapotranspiration less than or equal to a value of 0.96 inches for three water-budget scenarios for Kaua'i	44
23.	Maps showing estimated increases in relative frequency of monthly climatic water deficit greater than or equal to a value of 0.77 for three water-budget scenarios for Kaua'i	45
24.	Maps showing estimated increases in relative frequency of monthly mean soil moisture less than or equal to a value of 0.074 for nine water-budget scenarios for O'ahu	47
25.	Maps showing estimated increases in relative frequency of monthly evapotranspiration less than or equal to a value of 0.96 inches for nine water-budget scenarios for O'ahu	48
26.	Maps showing estimated increases in relative frequency of monthly climatic water deficit greater than or equal to a value of 0.77 for nine water-budget scenarios for O'ahu	49
27.	Maps showing estimated increases in relative frequency of monthly mean soil moisture less than or equal to a value of 0.074 for three water-budget scenarios for Moloka'i	51
28.	Maps showing estimated increases in relative frequency of monthly evapotranspiration less than or equal to a value of 0.96 inches for three water-budget scenarios for Moloka'i	52
29.	Maps showing estimated increases in relative frequency of monthly climatic water deficit greater than or equal to a value of 0.77 for three water-budget scenarios for Moloka'i	53
30.	Maps showing estimated increases in relative frequency of monthly mean soil moisture less than or equal to a value of 0.074 for nine water-budget scenarios for Maui	55
31.	Maps showing estimated increases in relative frequency of monthly evapotranspiration less than or equal to a value of 0.96 inches for nine water-budget scenarios for Maui	56
32.	Maps showing estimated increases in relative frequency of monthly climatic water deficit greater than or equal to a value of 0.77 for nine water-budget scenarios for Maui	57
33.	Maps showing estimated increases in relative frequency of monthly mean soil moisture less than or equal to a value of 0.074 for nine water-budget scenarios for the Island of Hawai'i	59
34.	Maps showing estimated increases in relative frequency of monthly evapotranspiration less than or equal to a value of 0.96 inches for nine water-budget scenarios for the Island of Hawai'i	60
35.	Maps showing estimated increases in relative frequency of monthly climatic water deficit greater than or equal to a value of 0.77 for nine water-budget scenarios for the Island of Hawai'i	61

Tables

1. Selected water-budget studies comparing drought and reference conditions for Kaua‘i, O‘ahu, Moloka‘i, Lāna‘i, Maui, and the Island of Hawai‘i.....	7
2. Summary of wildfire activity during 1999–2012	16
3. Fraction of area affected by wildfire activity during 1999–2012 by land cover	16
4. Summary of mean annual island-wide rainfall for selected periods during 1920–2012 and projected climate conditions for Kaua‘i, O‘ahu, Moloka‘i, Maui, and the Island of Hawai‘i.....	19
5. Summary of water-budget scenarios for Kaua‘i, O‘ahu, Moloka‘i, Maui, and the Island of Hawai‘i.....	22
6. Mean annual groundwater recharge and change in recharge relative to 1978–2007 scenario for Kaua‘i, O‘ahu, Moloka‘i, Maui, and the Island of Hawai‘i.....	25

Conversion Factors

U.S. customary units to International System of Units

Multiply	By	To obtain
Length		
inch (in.)	2.54	centimeter (cm)
inch (in.)	25.4	millimeter (mm)
foot (ft)	0.3048	meter (m)
mile (mi)	1.609	kilometer (km)
Area		
acre	4,047	square meter (m ²)
acre	0.4047	hectare (ha)
square mile (mi ²)	259.0	hectare (ha)
square mile (mi ²)	2.590	square kilometer (km ²)
Volume		
gallon (gal)	3.785	liter (L)
gallon (gal)	0.003785	cubic meter (m ³)
million gallons (Mgal)	3,785	cubic meter (m ³)
Flow rate		
million gallons per day (Mgal/d)	0.04381	cubic meter per second (m ³ /s)

Temperature in degrees Celsius (°C) may be converted to degrees Fahrenheit (°F) as follows:

$$^{\circ}\text{F} = (1.8 \times ^{\circ}\text{C}) + 32.$$

Temperature in degrees Fahrenheit (°F) may be converted to degrees Celsius (°C) as follows:

$$^{\circ}\text{C} = (^{\circ}\text{F} - 32) / 1.8.$$

Datum

Vertical coordinate information is referenced to local mean sea level.

Horizontal coordinate information is referenced to the North American Datum of 1983 (NAD 83).

Altitude, as used in this report, refers to distance above the vertical datum.

Abbreviations

CWD	climatic water deficit
CWI	cloud-water interception
CWRM	State of Hawai'i Commission on Water Resource Management
ET	evapotranspiration
OSDS	onsite sewage disposal systems
RCP	Representative Concentration Pathway
RCM	regional climate model
TMK	tax map key
TWI	trade-wind inversion
USGS	U.S. Geological Survey
WATRMod	Water-budget Accounting for Tropical Regions Model

Effects of Drought and Cloud-Water Interception on Groundwater Recharge and Wildfire Hazard for Recent and Future Climate Conditions, Kauaʻi, Oʻahu, Molokaʻi, Maui, and the Island of Hawaiʻi

By Alan Mair, Delwyn S. Oki, Heidi L. Kāne, Adam G. Johnson, and Kolja Rotzoll

Abstract

The Water-budget Accounting for Tropical Regions Model (WATRMd) code was used for Kauaʻi, Oʻahu, Molokaʻi, Maui, and the Island of Hawaiʻi to estimate the spatial distribution of groundwater recharge, soil moisture, evapotranspiration, and climatic water deficit for a set of water-budget scenarios. The scenarios included historical and future drought conditions, and a land-cover condition where shrubland and forest within the cloud zone were converted to grassland. For the historical drought condition, island-wide mean annual recharge estimates range from a decrease of 30 percent (239 million gallons per day [Mgal/d]) for Kauaʻi to a decrease of 39 percent (2,706 Mgal/d) for the Island of Hawaiʻi, relative to the reference condition consisting of 1978–2007 rainfall and 2020 land cover. For the future drought condition, estimates of island-wide mean annual recharge range from a decrease of 40 percent (477 Mgal/d) on Maui to a decrease of 51 percent (116 Mgal/day) on Molokaʻi. Complete conversion of all shrubland and forest within the cloud zone to grassland for each drought condition produces estimated land-cover-related decreases in island-wide mean annual recharge (in addition to the drought-related decreases) of 11–12 Mgal/d on Oʻahu, 119–135 Mgal/day on Maui, and 689–849 Mgal/d on the Island of Hawaiʻi. The spatial distributions of increases in conditions indicative of moisture stress and potential wildfire hazard were quantified using the relative frequency of soil moisture less than a selected threshold value (monthly mean soil moisture less than 0.074, expressed as a fraction of available water capacity), evapotranspiration less than a selected threshold value (monthly evapotranspiration less than 0.96 inches), and climatic water deficit greater than a selected threshold value (monthly climatic water deficit greater than 0.77, expressed as fraction of potential evapotranspiration). For the historical drought condition, the greatest increases in the relative frequency for the moisture-stress indicators occur across parts of east and southwest Kauaʻi; central, east, and west Oʻahu; central Molokaʻi; central Maui and low- to mid-altitude parts of West Maui volcano; and the northwestern and southern parts of the Island of Hawaiʻi. For the future drought condition, the greatest increases in the relative frequency of the

moisture-stress indicators occur across parts of west Kauaʻi; central and west Oʻahu and Molokaʻi; a band of mid-altitude area on the southern slope of West Maui volcano and across the southwestern slope of Haleakalā; and mid-altitude areas of the northwestern and southern parts of the Island of Hawaiʻi. Complete conversion of all shrubland and forest within the cloud zone to grassland for each drought condition results in land-cover-related increases in the relative frequency of moisture-stress indicators around Kaʻala in the Waiʻanae Range and the southeastern part of the Koʻolau Range on Oʻahu, the southern part of West Maui volcano and the southwestern slope of Haleakalā on Maui, and the upland regions of the western and southern parts of the Island of Hawaiʻi.

Introduction

Changes and extremes in climate, as reflected in drought, can have profound effects on freshwater availability, and wildfire frequency, severity, duration, and extent through change in the biomass and moisture content of living and dead vegetation. In areas affected by drought or in areas where the climate becomes drier, reduced groundwater recharge could result in higher salinity groundwater and reduced base flow in streams, which could affect potable resources for humans and habitat for aquatic ecosystems that rely on fresh groundwater discharge. Reduced rainfall, streamflow, and soil moisture also could enhance wildfire hazard, diminish freshwater availability, and threaten native species. Wildfire hazard can be described qualitatively as a fire environment—fuel (living and dead vegetation), weather, topography, and ignitions—with potential for causing harm or damage (Scott and others, 2013). In this study, freshwater availability refers to the amount of water that is available for human and ecological uses, whereas wildfire hazard refers to the prevalence of moisture stress in living vegetation that is favorable for wildfire occurrence and propagation. Cloud-water interception (CWI) is the process by which fog or cloud-water droplets are captured, accumulate on, and potentially drip from the leaves and branches of plants (Tseng and others, 2021). Rates of CWI are mainly controlled by the amount of cloud water supplied to vegetation and the vegetation's ability to capture the cloud water (Tseng, 2021).

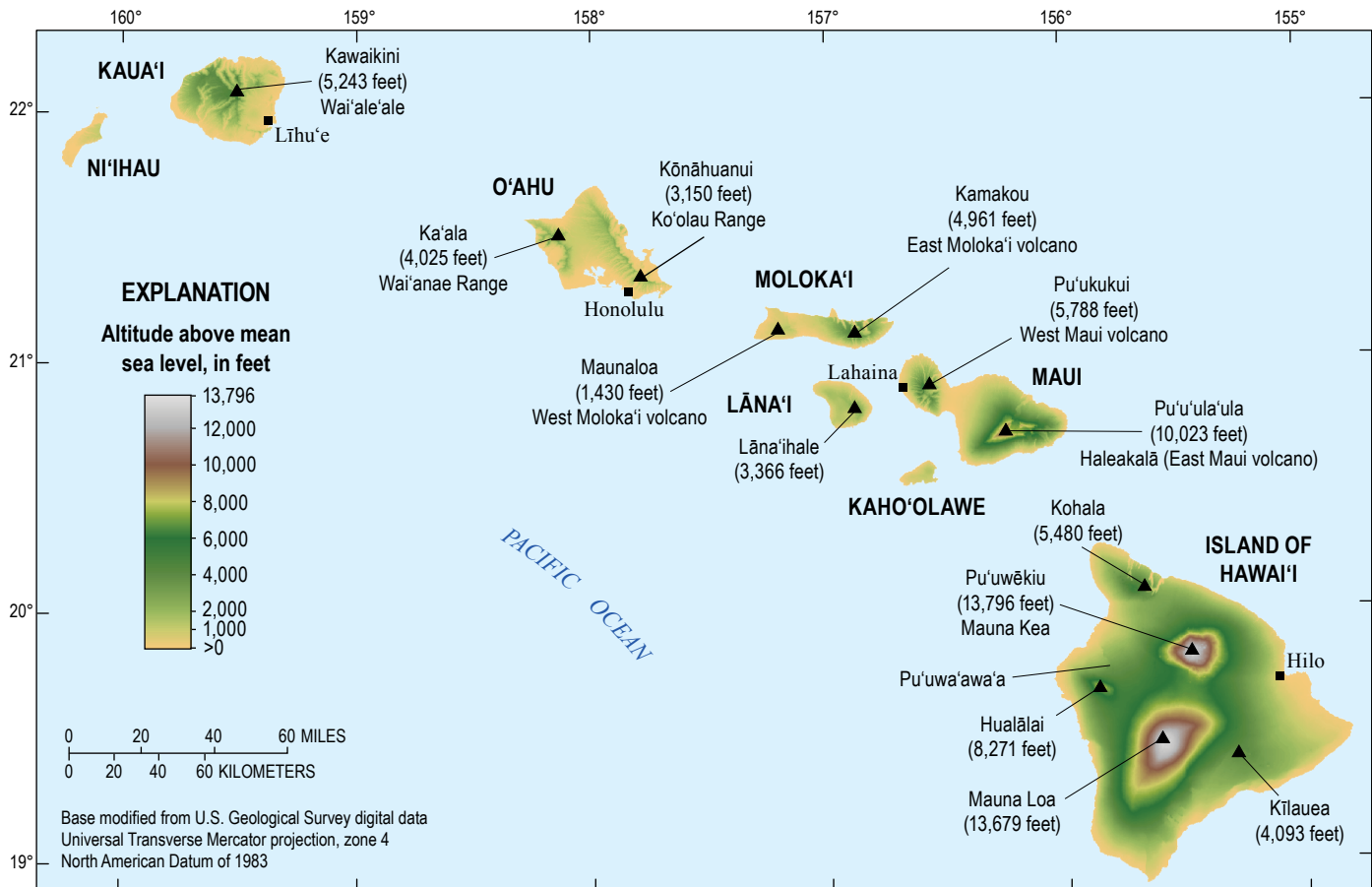


Figure 1. Maps showing the main Hawaiian Islands showing the general topography of individual islands.

Hence, CWI may be reduced during drought, in areas where the future climate becomes drier, or where changes in vegetation type and structure diminish the capture of cloud water. Reduced CWI has the potential to exacerbate the effects of drought on freshwater availability and wildfire hazard. However, during periods of drought, CWI might be a critical source of water that provides moisture for plants, reduces wildfire hazard within the zone where the fog occurs, and contributes to groundwater recharge that sustains base flow in streams. Thus, understanding the effects of drought and CWI on groundwater recharge and wildfire hazard is critical to Hawai'i's water-resource managers, farmers, ranchers, and forest, watershed, and wildfire managers for developing adaptive management strategies (Kunz, 2021; Longman and others, 2022). Estimation of these effects is important for understanding how climate and land-cover changes affect native plant and animal species preservation, and Native Hawaiian traditional and customary practices, such as kalo (taro) cultivation, that depend on consistent supplies of freshwater.

Climate and land cover in the Hawaiian Islands (fig. 1) have changed over the last century with wide-ranging implications for freshwater availability, agriculture, ecosystem integrity, and wildfire hazard (Bassiouni and Oki, 2013; Longman and others, 2015; Frazier and Giambelluca, 2017; McKenzie and others, 2019; Clilverd and others, 2019;

Frazier and others, 2022). Recent studies have shown that observed long-term trends and changes in climate have already affected water resources in the Hawaiian Islands with decreased rainfall across more than 90 percent of the State (Frazier and Giambelluca, 2017), increased drought duration and magnitude across the State (Frazier and others, 2022), and increased surface temperature, particularly at higher altitudes (Giambelluca and others, 2008; Diaz and others, 2011; McKenzie and others, 2019), which coincides with decreased stream base flow (Oki, 2004; Bassiouni and Oki, 2013; Clilverd and others, 2019). Observed increases in the strength and frequency of occurrence of the trade-wind inversion (TWI) in the main Hawaiian Islands coincide with observed decreases in rainfall and increases in solar radiation at higher altitudes (Longman and others, 2014; 2015), and the observed decline in population and range of an alpine silversword plant species (*Argyroxiphium sandwicense* subspecies *macrocephalum*) (Krushelnycky and others, 2013, 2016). Mortality among three native plant species in Hawai'i (*Coprosma ernodeoides*, *Leptecophylla tameiameiae*, and *Vaccinium reticulatum*) has been observed during extreme drought, which can contribute to shifts from dominance by woody species to more fire-prone herbaceous species (Lohse and others, 1995). A widespread native forest species in the main Hawaiian Islands (*Metrosideros polymorpha*) has shown

greater recruitment sensitivity to drying in wet areas than in dry areas, which indicates that long-term drying trends in wet areas could contribute to substantial declines in populations (Barton and others, 2020). The historical hydrologic changes imply a decreasing trend in groundwater recharge and storage, and an overall decline in groundwater availability. Furthermore, observed changes in climate may be affecting the population and range of native plant species.

For the main Hawaiian Islands, several published climate projections for the middle and end of the 21st century (Elison Timm and others, 2015; Zhang and others, 2016; Zhang and Wang, 2017) estimate decreases in rainfall across large areas on each island. In response to these projected changes in rainfall, groundwater recharge is anticipated to decrease across extensive areas of each island (Kāne and others, 2024a). Groundwater provides 99 percent of Hawai‘i’s drinking water and about 50 percent of all freshwater used in the State (Gingerich and Oki, 2000; Izuka and others, 2018). Demand for freshwater in Hawai‘i during 2020–35 is projected to increase by 13 percent, from about 239 to 269 million gallons per day (Mgal/d) (Townscape, Inc., 2019). The estimated decrease in groundwater recharge coupled with the anticipated increase in freshwater demand have important implications for future groundwater availability.

Wildfires are affected by several factors including temperature, humidity, and the moisture content of living and dead vegetation (<https://www.noaa.gov/noaa-wildfire/wildfire-climate-connection>). In the Western United States, the observed doubling of the number of large wildfires during 1984–2015 has been linked to enhanced drying of living and dead vegetation driven by observed warming (Abatzoglou and Williams, 2016). Wildfires in the Hawaiian Islands, as measured by the total area burned, have increased over the last century and were most frequent in dry non-native grasslands and shrublands that cover 24 percent of the State of Hawai‘i’s total land area (Trauernicht and others, 2015). During 2005–11, the mean annual area burned state-wide as a fraction of total land area was greater than in the 12 fire-prone states in the Western United States (Trauernicht and others, 2015). Wildfire danger assessments in the continental United States have used variables, such as soil moisture, evapotranspiration (ET), and climatic water deficit (CWD), to identify areas at risk for wildfires (Westerling and Bryant, 2008; Kane and others, 2015; Krueger and others, 2015; Abatzoglou and Williams, 2016; Krueger and others, 2017; Jensen and others, 2018; Sharma and others, 2021; Sharma and Dhakal, 2021). Climatic water deficit is the evaporative demand that exceeds available water and is calculated as the difference between potential ET and actual ET (Flint and others, 2015). Estimates of soil moisture are a useful surrogate for estimates of live fuel moisture, that is, the moisture content within living vegetation and a key influence on fire behavior, because soil moisture is linked to the physical interactions between soils and plants (Hillel, 1998). In the Hawaiian Islands, estimates of soil moisture and plant moisture also have been used to assess wildfire hazard and behavior (Burgan, 1976; Dolling and others, 2005, 2009; Ellsworth and others, 2013; 2014). Projected decreases in rainfall during the

middle and end of the 21st century combined with projected increases in surface temperature across many parts of the main Hawaiian Islands (Elison Timm and others, 2015; Elison Timm, 2017; Fandrich and others, 2022) can increase moisture stress on vegetation, which will further increase wildfire hazard (Trauernicht, 2019).

Estimates of the spatial distribution of groundwater recharge, soil moisture, ET, and CWD are needed for the main Hawaiian Islands to provide information for evaluating the effects of severe drought, future climate conditions, and reduced CWI on freshwater availability and wildfire hazard. Water-budget models have been developed for the main Hawaiian Islands’ diverse topography and climate to produce spatially distributed estimates of recharge rates for average climate and recent land-cover conditions in Hawai‘i (Engott and others, 2017; Izuka and others, 2018; Johnson and others, 2018; Oki and others, 2020). These models were used to assess the effects of projected climate and hypothetical land-cover conditions on recharge rates for several of the main Hawaiian Islands (Mair and others, 2019; Brewington and others, 2019; Rotzoll and Johnson, 2023; Kāne and others, 2024a). Estimates of recharge are used by the State of Hawai‘i Commission on Water Resource Management (CWRM) in the calculation of sustainable-yield values for groundwater withdrawal (Townscape, Inc., 2019) from aquifer systems on each of the main Hawaiian Islands (fig. 2). Spatially distributed estimates of recharge are also a critical input to numerical groundwater models that can be used to assess groundwater availability under different recharge and demand conditions. Numerical groundwater models have been used to help inform decisions by water-resource managers in the State of Hawai‘i (Oki, 2005; Gingerich, 2008; Oki and others, 2020; Izuka and Rotzoll, 2021; Rotzoll and others, 2022). Estimates of soil moisture, ET, and CWD are important for resource managers to understand increased wildfire hazard and can be used in wildfire danger assessments. Identifying areas of increased wildfire hazard is also important for developing strategic monitoring programs to help assess and predict the effects of wildfire on freshwater supplies and aquatic ecosystems (Stebblein and others, 2021; Murphy and others, 2023).

For this study, the water-budget models developed for Kaua‘i, O‘ahu, Moloka‘i, Maui, and the Island of Hawai‘i (fig. 1) were used to develop estimates of groundwater recharge, soil moisture, ET, and CWD to analyze changes between recent, drought, and future climate conditions; illustrate the effects of reduced CWI for recent, drought, and future climate conditions; and highlight areas of increased potential wildfire hazard during drought and future climate conditions. The recharge estimates can be used in numerical groundwater models to evaluate the additional effects of groundwater withdrawals on groundwater levels, freshwater volume in the aquifer, streamflow, coastal discharge, and salinity of water withdrawn from production wells. The estimates of soil moisture, ET, and CWD can be used by natural resource managers to help evaluate the effects of drought and future long-term drying on moisture stress in vegetation and wildfire hazard.

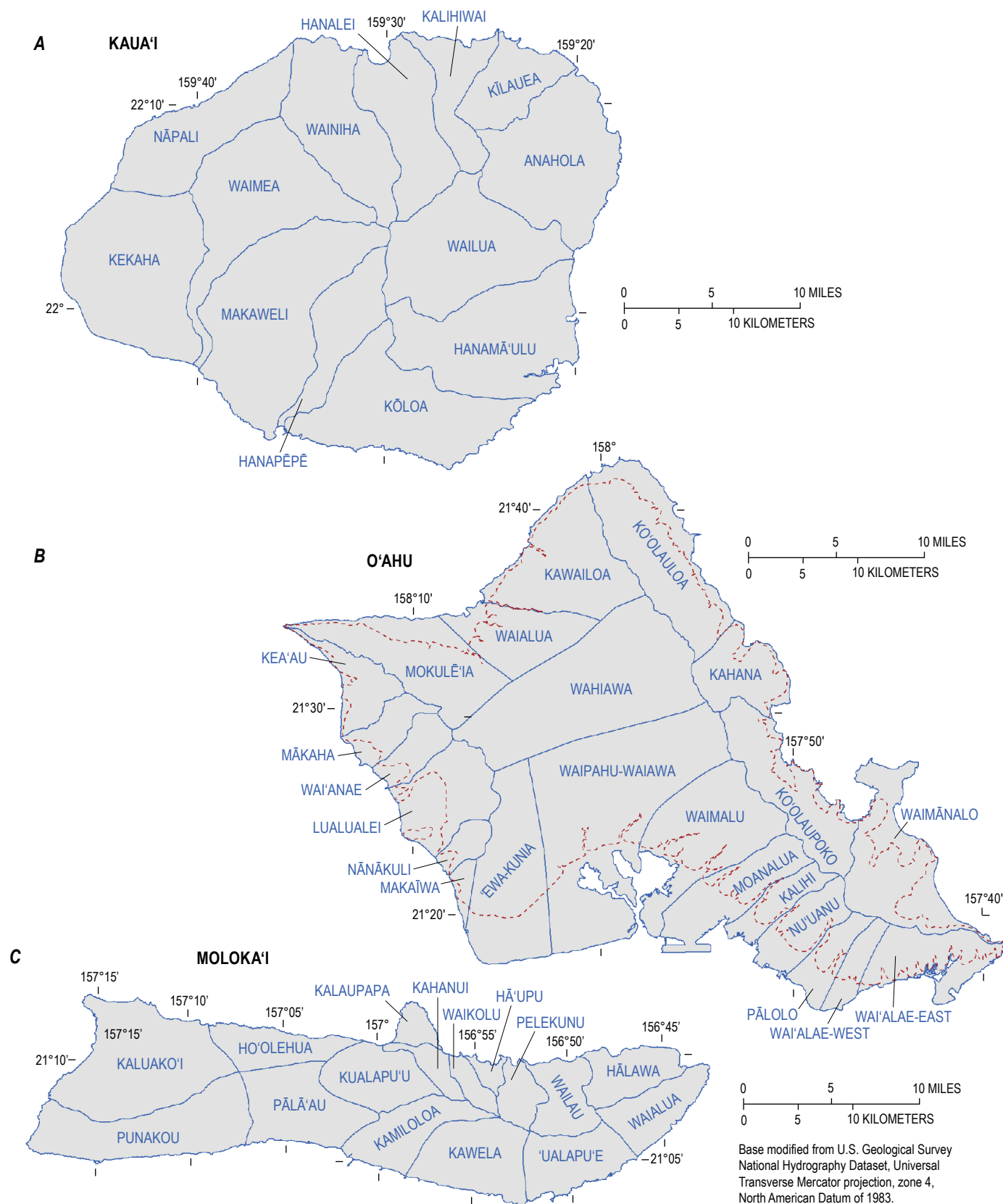


Figure 2. Maps showing the aquifer systems for Kaua'i (A), O'ahu (B), Moloka'i (C), Maui (D), and the Island of Hawai'i (E).

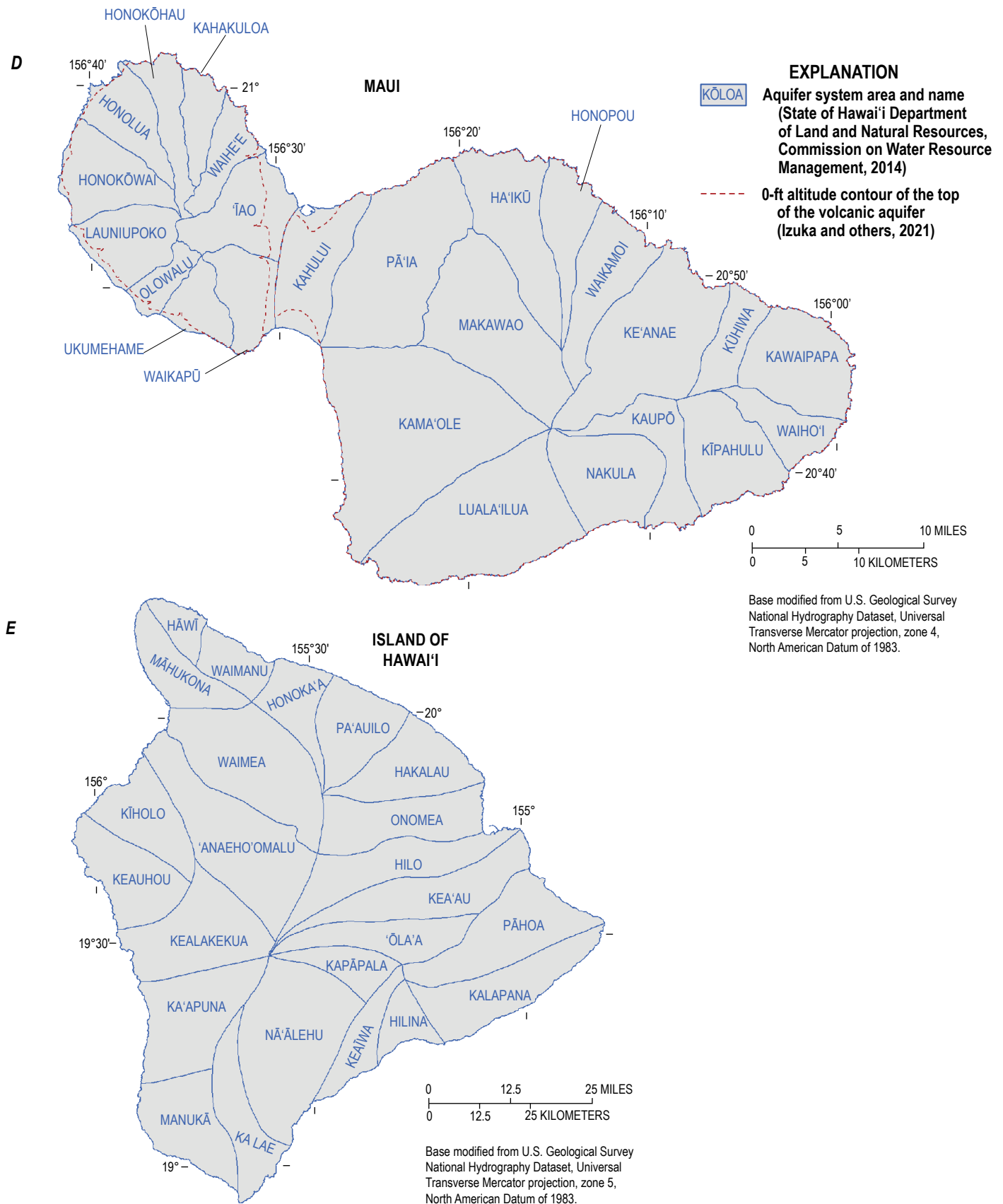


Figure 2. —Continued

Purpose and Scope

The purpose of this study was to provide information for (1) assessing the effects of climate variability, drought, and long-term drying on vegetation (moisture stress), wildfire hazard, groundwater recharge, and freshwater availability for recent and future climate conditions, and (2) evaluating the capacity of CWI to mitigate the hydrologic effects of drought. Specific objectives of the study were to estimate changes in groundwater recharge, soil moisture, ET, and CWD during periods of episodic drought and long-term drying for recent and future climate conditions; and quantify the effects of reduced CWI on groundwater recharge, soil moisture, ET, and CWD. The study area consists of Kauaʻi, Oʻahu, Molokaʻi, Maui, and the Island of Hawaiʻi.

In the first part of this study, the water-budget models were used to quantify the effects of drought and reduced CWI on groundwater recharge for historical and future dry-climate conditions. Two drought conditions were defined for each island in the study area as follows: (1) a historical drought condition representative of the driest period during 1920–2012, and (2) a future drought condition representative of the driest period during a future dry-climate condition. A map of land-cover conditions in 2020 (Kāne and others, 2024a, b), hereinafter 2020 land-cover condition, was used in the model simulations for both drought conditions. For this study, a future dry-climate condition was developed using projected rainfall conditions during 2071–99 from Elison Timm and others (2015) for a Representative Concentration Pathway (RCP) warming scenario with a total radiative forcing of 8.5 watts per square meter (W/m^2) by the year 2100 (RCP8.5 2071–99 projection) (Intergovernmental Panel on Climate Change, 2014). In the model calculations, CWI is applied only to non-native forest, native forest, tree plantation, kiawe, shrubland, coffee, and macadamia land cover within the cloud zone. The effects of reduced CWI were evaluated in the model simulations by converting forest and shrubland land cover within the cloud zone to grassland, for which CWI was considered negligible. To simulate the effects of reduced CWI, two hypothetical land-cover conditions were defined for Oʻahu, Maui, and the Island of Hawaiʻi as follows: (1) a land-cover condition in which roughly 50 percent of shrubland and forest areas within the cloud zone were converted to grassland, and (2) a land-cover condition in which 100 percent of shrubland and forest areas within the cloud zone were converted to grassland. The water-budget models were used to estimate groundwater recharge for the two drought conditions for each island and the two hypothetical land-cover conditions for Oʻahu, Maui, and the Island of Hawaiʻi. Island-wide summaries of groundwater recharge were computed to illustrate the effects of historical and future drought conditions, and reduced CWI on groundwater recharge.

In the second part of this study, the water-budget models were used to quantify the effects of drought and reduced CWI on soil moisture, ET, and CWD for historical and

future climate conditions. For the purpose of quantifying the effects of drought and climate change, four climate conditions were defined for each island in the study area as follows: (1) a reference condition representative of non-drought climate conditions during 1990–2012, (2) a historical drought condition representative of the driest period during 1920–2012, (3) a future non-drought condition representative of non-drought climate conditions for a RCP8.5 2071–99 projection, and (4) a future drought condition representative of the driest period for a RCP8.5 2071–99 projection. A map of 2020 land-cover conditions (Kāne and others, 2024a, b) was used in the model simulations for each climate condition. The added effects of reduced CWI on soil moisture, ET, and CWD were evaluated using the two hypothetical land-cover conditions for Oʻahu, Maui, and the Island of Hawaiʻi. Monthly time-series outputs from the model simulations were analyzed to determine the relative frequency of soil moisture, ET, and CWD estimates that were greater or less than selected moisture-stress thresholds for each island in the study area. Island-wide summaries of changes in the relative frequency between the reference condition, and the different drought and hypothetical land-cover conditions were used to identify areas of increased moisture stress and potential wildfire hazard.

Previous Studies

Effects of Drought on Groundwater Recharge

The most recent estimates of regional and island-wide groundwater recharge for historical drought conditions for Kauaʻi, Oʻahu, Molokaʻi, Lānaʻi, Maui, and the Island of Hawaiʻi were developed from water-budget studies that used a range of drought and land-cover conditions ([table 1](#)). Although Lānaʻi is excluded from this study, it is included in this summary because the effect of historical drought conditions on island-wide groundwater recharge for Lānaʻi was recently evaluated by Kāne and others (2024a). To the authors' knowledge, no published study documents the effects of projected future drought conditions on island-wide groundwater recharge for Kauaʻi, Oʻahu, Molokaʻi, Lānaʻi, Maui, and the Island of Hawaiʻi.

Izuka and others (2005) used a water-budget model to estimate regional groundwater recharge in southeast Kauaʻi for two land-cover conditions and four climate conditions, including a 1916–83 reference-climate condition and three drought conditions. The three drought conditions were developed using observed rainfall measurements collected during 1952–2003 from a rain gage in southeast Kauaʻi. For a 1981 land-cover condition, regional recharge estimates for the three drought conditions in southeast Kauaʻi decreased between 50 and 68 percent relative to the 1916–83 reference-climate condition ([table 1](#)). For a 1998 land-cover condition, regional recharge estimates for the three drought conditions decreased between 54 and 72 percent relative to the 1916–83 reference-climate condition.

Table 1. Selected water-budget studies comparing drought and reference conditions for Kauaʻi, Oʻahu, Molokaʻi, Lānaʻi, Maui, and the Island of Hawaiʻi.

[Mgal/d, million gallons per day.]

Island	Reference	Region	Land-cover condition (year)	Rainfall condition		Recharge (Mgal/d)
				Type	Time period	
Kauaʻi	Izuka and others (2005)	Southeast Kauaʻi	1981	Reference	1916–83	264
				Drought	3 conditions ^a	84–131
			1998	Reference	1916–83	246
				Drought	3 conditions ^a	69–114
Oʻahu	Engott and others (2017)	Island-wide	2010	Reference	1978–2007	660
				Drought	1998–2002	417
Molokaʻi	Oki and others (2020)	Island-wide	2000s	Reference	1978–2007	227
				Drought	1998–2002	140
Lānaʻi	Kāne and others (2024a)	Island-wide	2020	Reference	1978–2007	27
				Drought	2008–12	12
Maui	Johnson and others (2018)	Island-wide	2010	Reference	1978–2007	1,308
				Drought	1998–2002	1,010
Hawaiʻi	Engott (2011)	Island-wide	2008	Reference	1916–83	6,595
				Drought	Lowest 5-year average ^b	4,271

^aDrought conditions of “moderately dry,” “very dry,” and “extremely dry” determined from observed rainfall during 1952–2003 at the Līhuʻe Airport rain gage, Kauaʻi.

^bSelected as period with lowest 5-year average rainfall during 1916–83 in each of six rainfall-variability zones.

Engott (2011) used a water-budget model to estimate groundwater recharge on the Island of Hawaiʻi for a 2008 land-cover condition and two climate conditions—a 1916–83 reference-climate condition and one drought condition. He selected the drought condition as the period with the lowest 5-year average rainfall during 1916–83 in each of six zones. Island-wide recharge estimates for the drought condition decreased by 35 percent relative to the 1916–83 reference-climate condition and 2008 land-cover condition (table 1).

A water-budget model was used to estimate groundwater recharge on Oʻahu and Maui for a 2010 land-cover condition and two climate conditions—a 1978–2007 reference-climate condition and one drought condition (Engott and others, 2017; Johnson and others, 2018). Rainfall during 1998–2002 was selected to represent drought conditions on Oʻahu and Maui because this period had the lowest 5-year average rainfall during 1978–2007. Island-wide recharge estimates for the 1998–2002 drought decreased by 37 percent for Oʻahu and by 23 percent for Maui, relative to the 1978–2007 reference-climate condition (table 1).

Oki and others (2020) used a water-budget model to estimate groundwater recharge on Molokaʻi for a land-cover condition during the 2000s and two climate conditions—a 1978–2007 reference-climate condition and one drought condition. They selected rainfall during 1998–2002 to represent drought conditions on Molokaʻi because this period had the lowest 5-year average rainfall during 1920–2012. Island-wide recharge estimates for the 1998–2002 drought decreased by 38 percent relative to the 1978–2007 reference-climate condition (table 1).

Kāne and others (2024a) used a water-budget model to estimate groundwater recharge on Lānaʻi for a 2020 land-cover condition and two climate conditions, including a 1978–2007 reference-climate condition and one drought condition. They selected rainfall during 2008–2012 to represent drought conditions on Lānaʻi because this period had the lowest 5-year average rainfall during 1920–2012. Island-wide recharge estimates for the 2008–12 drought decreased by 54 percent relative to the 1978–2007 reference-climate condition (table 1).

Effects of Soil and Plant Moisture on Wildfire Hazard and Behavior

The moisture content of living and dead vegetation, collectively referred to as fuel-moisture content in wildfire science, is an important characteristic for assessing wildfire hazard because it can influence wildfire propagation (Schroeder and Buck, 1970). Vegetation (or fuels) can be divided into two groups as follows: (1) fine fuels consisting of leaf litter, grasses, and small shrubs, and (2) coarse fuels consisting of larger shrubs, trees, and dead woody debris (Trauernicht and Kunz, 2019). When fuel-moisture content is high, wildfires are more difficult to ignite and tend to burn poorly because more energy is needed to evaporate water before burning organic tissues. When fuel-moisture content is low, wildfires can start easily, and can rapidly spread and intensify given appropriate conditions of fuel continuity and weather. Grass-dominated fuel types quickly cure during dry weather, ignite easily, and provide conditions for fast-spreading wildfires (Cheney and Sullivan, 2008). In contrast, coarse fuels typical of forest areas cure more slowly and require more energy to ignite. However, coarse fuels can burn longer and at higher intensity (that is, at higher temperatures and with longer flame lengths) once they are ignited, especially during severe drought conditions. More than 98 percent of wildfires in Hawai'i are caused by human activity (Pickett, 2016; <https://www.hawaiiwildfire.org/home>) and environmental conditions such as land-cover type, antecedent moisture, and high winds can exacerbate wildfire hazard in Hawai'i (Nugent and others, 2020; Partyka and Erdman, 2023). The most wildfire-prone areas in Hawai'i are grasslands dominated by fine fuels, such as native and non-native grasses, small shrubs, and ferns (Trauernicht and Kunz, 2019).

On O'ahu, Ellsworth and others (2013) measured the temporal variability in soil and fuel moisture during 2008–10 at four sites dominated by a non-native grass (*Megathyrsus maximus*). Their analysis indicated a high correlation between fuel moisture and soil moisture, relative humidity, air temperature, and antecedent rainfall. Their results indicate that measurements of soil moisture and commonly quantified meteorological variables can be used in Hawai'i to quantify fuel moisture across large areas and improve assessments of wildfire hazard. Ellsworth and others (2014) measured fuel biomass and moisture at two sites on O'ahu dominated by non-native forest and a non-native grass (*M. maximus*) and used these data to model potential wildfire behavior. Their model simulations indicated that wildfire spreads 3 to 5 times more rapidly in grassland than in forest and that flame lengths were 2 to 3 times longer in grassland than in forest. They also analyzed aerial imagery taken during 1950–2011 in two areas on O'ahu and found that non-native grassland expanded at rates ranging from 4.5 to 6.5 acres per year, with more rapid rates of conversion before the early 1990s when active fire management practices were implemented. Trauernicht

(2019) used a probability-based wildfire occurrence model and historical wildfire records to estimate annual wildfire probability for a set of land-cover and climate conditions for the northwest quadrant of the Island of Hawai'i. He found that annual wildfire probability was highest for grassland, dominated by non-native grasses including *Cenchrus setaceus* and *Cenchrus clandestinus*, relative to shrubland or forest in the same region. He also noted that antecedent wet years increased wildfire hazard in grassland more than drought conditions during the year that a wildfire occurred. The combined effects of projected future drying and warming across the region increased wildfire probability by as much as 375 percent and shifted areas of peak landscape flammability to higher altitudes.

Several studies in the Hawaiian Islands have used the Keetch-Byram Drought Index (KBDI), an index that describes the soil-moisture deficit to assess the relation of soil- and fuel-moisture content to wildfire hazard (Burgan, 1976; Dolling and others, 2005; 2009). The KBDI is computed using inputs of daily rainfall, daily maximum temperature, and mean annual rainfall, and assumes a maximum soil-moisture storage capacity (for example, 8 inches) for all soil types (Heim, 2002). Burgan (1976) assessed the relation between the KBDI and measurements of fuel moisture on O'ahu and the Island of Hawai'i for three types of non-native grass species (*C. setaceus*, *Andropogon virginicus*, *Bothriochloa pertusa*) and one native shrub species (*Dodonaea viscosa*). He noted the KBDI adequately described the general wetting and drying cycles but did not adequately correlate with measurements of fuel-moisture content. Dolling and others (2005) assessed the relation between the KBDI computed for 16 rain-gage stations and wildfires during 1976–96 on Kaua'i, O'ahu, Maui, and the Island of Hawai'i. Their study indicated a strong relation between the KBDI and the total area burned on O'ahu, Maui, and the Island of Hawai'i. Dolling and others (2009) analyzed the natural variability of the KBDI and assessed the relation of the KBDI computed at 27 locations on six islands (Kaua'i, O'ahu, Moloka'i, Lāna'i, Maui, and Hawai'i) to atmospheric circulations and sea-surface temperatures. They concluded that the highest KBDI values, which imply the greatest wildfire hazard, tend to occur as equatorial sea-surface temperatures cool after an El Niño event, and persist into the autumn months whenever an El Niño event is followed by a La Niña event.

Effects of Cloud-Water Interception on Total Precipitation, Groundwater Recharge, and Wildfire Hazard

Contributions of CWI to precipitation in the cloud forests of the main Hawaiian Islands are substantial and vary widely with location and vegetation type (Ekern, 1964; Juvik and Ekern, 1978; Juvik and Nullet, 1995; Juvik and others, 2011; Giambelluca and others, 2011; Takahashi and others, 2011; Tseng, 2021). On Lāna'i, CWI from one non-native forest

species, *Araucaria columnaris*, accounted for 38 to 82 percent of total annual precipitation (Ekern, 1964; Juvik and others, 2011). On Maui, CWI accounted for 15 and 32 percent of total annual precipitation in two cloud forest sites with windward areas receiving proportionally greater inputs of cloud water than leeward areas (Giambelluca and others, 2011). On the Island of Hawai‘i, Takahashi and others (2011) monitored CWI at two windward sites, one dominated by a native forest species (*Metrosideros polymorpha*) and one dominated by a non-native forest species (*Psidium cattleianum*), and found that CWI accounted for 27 and 16 percent, respectively, of total annual precipitation. Tseng (2021) monitored CWI at five cloud-forest sites on O‘ahu, Maui, and the Island of Hawai‘i and found that CWI accounted for 3 to 34 percent of total annual precipitation.

Changes in land-cover and climate conditions can also affect CWI and groundwater recharge rates. Wada and others (2017) conducted an ecosystem-services assessment to estimate groundwater recharge near Pu‘uwa‘awa‘a, Island of Hawai‘i (fig. 1), for a current land-cover condition and two hypothetical land-cover conditions, and a 1978–2007 reference-climate condition and one projected climate condition. In their analysis, CWI was assumed to occur only in areas with shrubland or forest within the cloud zone, which they defined as extending from an altitude equal to or greater than 750 m. They defined two hypothetical land-cover conditions as follows: (1) a partial restoration condition with conversion of grassland, non-native forest, and non-native shrubland to native forest in selected areas, and (2) a full restoration condition with conversion of grassland, non-native forest, and non-native shrubland to native forest in the entire watershed. They reported that full restoration effectively increased CWI, which helped increase total recharge across their study area by 5 and 6 percent relative to a 1978–2007 reference-climate condition and a projected climate condition, respectively. Brewington and others, (2019) utilized a water-budget model to estimate the spatial distribution of CWI and groundwater recharge on Maui for four hypothetical land-cover conditions and two future climate conditions. In their analysis, CWI was assumed to occur only in areas with non-native forest, native forest, tree plantation, kiawe, shrubland, coffee, and macadamia land cover within the cloud zone, which they defined as extending from an altitude equal to or greater than 2,000 feet. They assumed CWI from all other land covers within the cloud zone was negligible. They reported that the conversion of grassland to forest within the cloud zone on Maui effectively increased island-wide rates of CWI and groundwater recharge. Bremer and others (2021) combined land-cover and water-balance modeling to quantify the potential effects of native forest restoration on groundwater recharge in three areas of the Island of Hawai‘i. They reported that hypothetical conversions of grassland to native forest increased CWI within the cloud zone, which increased estimates of groundwater recharge in selected areas by as much 88,900 cubic meters per hectare (or 9.5 million gallons

per acre) over a 50-year simulation period. Kāne and others (2024a) estimated the spatial distribution of CWI within the cloud zone on Kaua‘i, O‘ahu, Moloka‘i, Lāna‘i, Maui, and the Island of Hawai‘i using water-budget models for a 2020 land-cover condition, and a 1978–2007 reference-climate condition and three projected climate conditions. For the 1978–2007 climate, island-wide rates of CWI ranged from about 1 Mgal/d (about 1 percent of total precipitation) on Lāna‘i to about 1,018 Mgal/d (about 7 percent of total precipitation) on the Island of Hawai‘i.

Although CWI may be supplying a considerable amount of freshwater in Hawai‘i, few studies have quantified the contributions of CWI to groundwater recharge and streamflow. Hardy (1996) used a water-budget analysis to estimate that about 62 percent of the recharge within the cloud zone on Lāna‘i is derived from CWI. Scholl and Giambelluca (2010) used isotopic analyses of CWI and stream water to estimate that cloud water supplied about 37 percent of high-altitude streamflow year-round.

Contributions of moisture derived from CWI also have the potential to increase fuel moisture, thereby decreasing wildfire hazard, but to the authors’ knowledge, no published study documents the effect of CWI on wildfire hazard in Hawai‘i. However, the effects of forest restoration on landscape flammability have been assessed in the western parts of the Island of Hawai‘i (Wada and others, 2017; Bremer and others, 2018). Wada and others (2017) evaluated changes in landscape flammability near Pu‘uwa‘awa‘a, Island of Hawai‘i, including extensive areas within the cloud zone, for a current land-cover condition and two hypothetical land-cover conditions (described earlier in this section), and a 1978–2007 reference-climate condition and one projected climate condition. They reported that full restoration increased CWI and helped to decrease landscape flammability across much of their study area for both climate conditions. Bremer and others (2018) also conducted an ecosystem services assessment to evaluate changes in landscape flammability for the western part of the Island of Hawai‘i, including extensive areas within the cloud zone, for three land-use conditions (native forest and agroforestry, coffee, and one future climate condition). They reported that landscape flammability was lowest for the native forest and agroforestry land-cover condition for both recent and future climate conditions, which implies that conversions of grassland to forest might decrease fuel moisture loss and decrease wildfire hazard. Along the coast of southern California, Emery and others (2018) investigated the effect of dry-season fog on live fuel moisture in six dominant shrub species. They found that fog deposition slowed rates of fuel moisture loss for species that were exposed to consistent fog during the dry season. Emery (2016) measured foliar uptake of fog water in dominant California shrub species following exposure to isotopically labeled fog water. They reported a minimal effect of foliar water uptake on live fuel moisture, which indicates that live fuel moisture in drought-tolerant species may be more directly affected by changes in soil moisture.

Study Area

The descriptions in this section were modified from Kāne and others (2024a). The Hawaiian archipelago is located in the North Pacific Ocean where it is geographically isolated from continental landmasses. The eight main islands—Ni‘ihau, Kaua‘i, O‘ahu, Moloka‘i, Lāna‘i, Kaho‘olawe, Maui, and the Island of Hawai‘i (fig. 1)—are the emergent tops of basaltic shield volcanoes that rise from the floor of the Pacific Ocean, hereinafter the Hawaiian Islands. The older islands are in the northwest part of the chain and the younger islands are in the southeast. Ni‘ihau and Kaua‘i are the oldest islands at over 5.1 million years old, whereas the Island of Hawai‘i is the youngest island with active volcanism still occurring (Macdonald and others, 1983). Each island is made up of one or more shield volcanos formed by thousands of lava flows emanating from vents in rift zones and, in most cases, a central caldera. Lava flows on the dike-free flanks of the volcanoes form productive aquifers containing freshwater-lens systems, which consist of a lens-shaped freshwater body, a brackish intermediate transition zone, and underlying saltwater. These aquifer systems are the primary sources of freshwater for the 1.5 million residents of the Hawaiian Islands (U.S. Census Bureau, 2021), and also are important for agricultural pursuits, industries, and the U.S. military. Fresh groundwater in coastal aquifer systems is vulnerable to the effects of short and long-term climatic changes and human activity (Izuka and others, 2018). The five islands considered in this study are Kaua‘i, O‘ahu, Moloka‘i, Maui, and Hawai‘i and have a combined land area of about 6,166 square miles (mi²). The CWRM divides each island into aquifer systems for management purposes, with boundaries delineated on the basis of geologic, topographic, and geographic considerations (fig. 2). The CWRM estimates groundwater sustainable-yield values for each aquifer system using an analytical model that requires an estimate of recharge as input. The groundwater-recharge estimates for this study are summarized by the CWRM aquifer system.

Physical Setting

The five islands considered for this study constitute 96 percent of the total land area in the Hawaiian archipelago. The islands range in size from 260 (Moloka‘i) to 4,029 mi² (Island of Hawai‘i) and the peak altitudes range from 4,025 (O‘ahu) to 13,796 feet (ft) (Island of Hawai‘i). O‘ahu is the most densely populated of the islands—about 1 million or 70 percent of the State of Hawai‘i’s population lives on O‘ahu (U.S. Census Bureau, 2021).

Kaua‘i covers an area of 554 mi². The prevailing view in current geologic literature is that the bulk of Kaua‘i was built by a single shield volcano (Izuka and others, 2018). Stream erosion carved a generally radial pattern of valleys in the original shield surface of Kaua‘i, but large-scale faulting and collapse during and after the shield stage also modified the topography, altered erosion patterns, and influenced the deposition of younger rock units. Sediments also contributed

to filling the depressions, and to the formation of a coastal plain. The highest point on Kaua‘i is Kawaikini on Wai‘ale‘ale at 5,243 ft (fig. 1).

O‘ahu has an area of about 595 mi². O‘ahu is formed by two elongated shield volcanoes, the eroded remnants of which are the Wai‘anae Range in western O‘ahu and the Ko‘olau Range in eastern O‘ahu (fig. 1). Weathering and erosion have greatly modified the volcanoes carving out large amphitheater valleys leaving steep inter-fluvial ridges in the interior of the island. O‘ahu has extensive coastal-plain deposits that partly overlie the lava flows of the shield volcanoes and almost completely encircle the island. The coastal-plain sediments and rejuvenated-stage volcanic rocks on O‘ahu have been referred to as “caprock” because they act as a semi-confining unit over parts of the high-permeability lava-flow aquifers (Sherrod and others, 2007; Izuka and others, 2018). The highest points on O‘ahu are Ka‘ala at 4,025 ft in the Wai‘anae Range and Kōnāhuanui at 3,150 ft in the Koolau Range. O‘ahu is the center of commerce, industry, and government in Hawai‘i and the site of the State capital, Honolulu.

Moloka‘i occupies an area of 260 mi² and primarily consists of two shield volcanoes. The older West Moloka‘i volcano rises to an altitude of 1,430 ft at Maunaloa and the younger East Moloka‘i volcano which rises to an altitude of 4,961 ft at Kamakou (fig. 1) (Stearns and Macdonald, 1947). Between the summit areas of the volcanoes is a relatively flat area of land in the central saddle of the island.

Maui has an area of about 728 mi². The island is formed by two shield volcanoes, the West Maui volcano and the East Maui volcano known as Haleakalā. An intervening saddle of broad, gently sloping land sits between the two volcanoes (fig. 1). Erosion of West Maui volcano has carved deep valleys resulting in sharp-crested ridges. On Haleakalā, the valleys on the rainy northeastern (windward) slope are separated by broad areas and ridges, whereas the drier southwestern (leeward) slope is less incised and retains the broad shield shape of the volcano. Wedges of low-permeability sedimentary material, referred to as caprock, impede the seaward flow of fresh groundwater in freshwater-lens systems along parts of the northeast and southwest flanks of West Maui volcano (Sherrod and others, 2007; Izuka and others, 2018). Wedges of caprock between West Maui volcano and Haleakalā also impede the flow of fresh groundwater between West Maui volcano and the saddle of land between the two volcanos. The highest points on Maui are Pu‘ukukui at 5,788 ft on West Maui volcano and Pu‘u‘ula‘ula at 10,023 ft on Haleakalā.

The Island of Hawai‘i lies at the southeastern end of the Hawaiian Islands (fig. 1). Comprising an area of about 4,029 mi², it is nearly twice as large as the combined areas of the other Hawaiian Islands (Macdonald and others, 1983). The island consists of five volcanoes: Kohala, Mauna Kea, Hualālai, Mauna Loa, and Kīlauea. Mauna Kea is the highest of these volcanoes, rising to an altitude of 13,796 ft, and Mauna Loa is the largest by volume. With the exception of the northeastern slopes of Kohala and Mauna Kea, the geologically youthful land surface generally retains a broad,

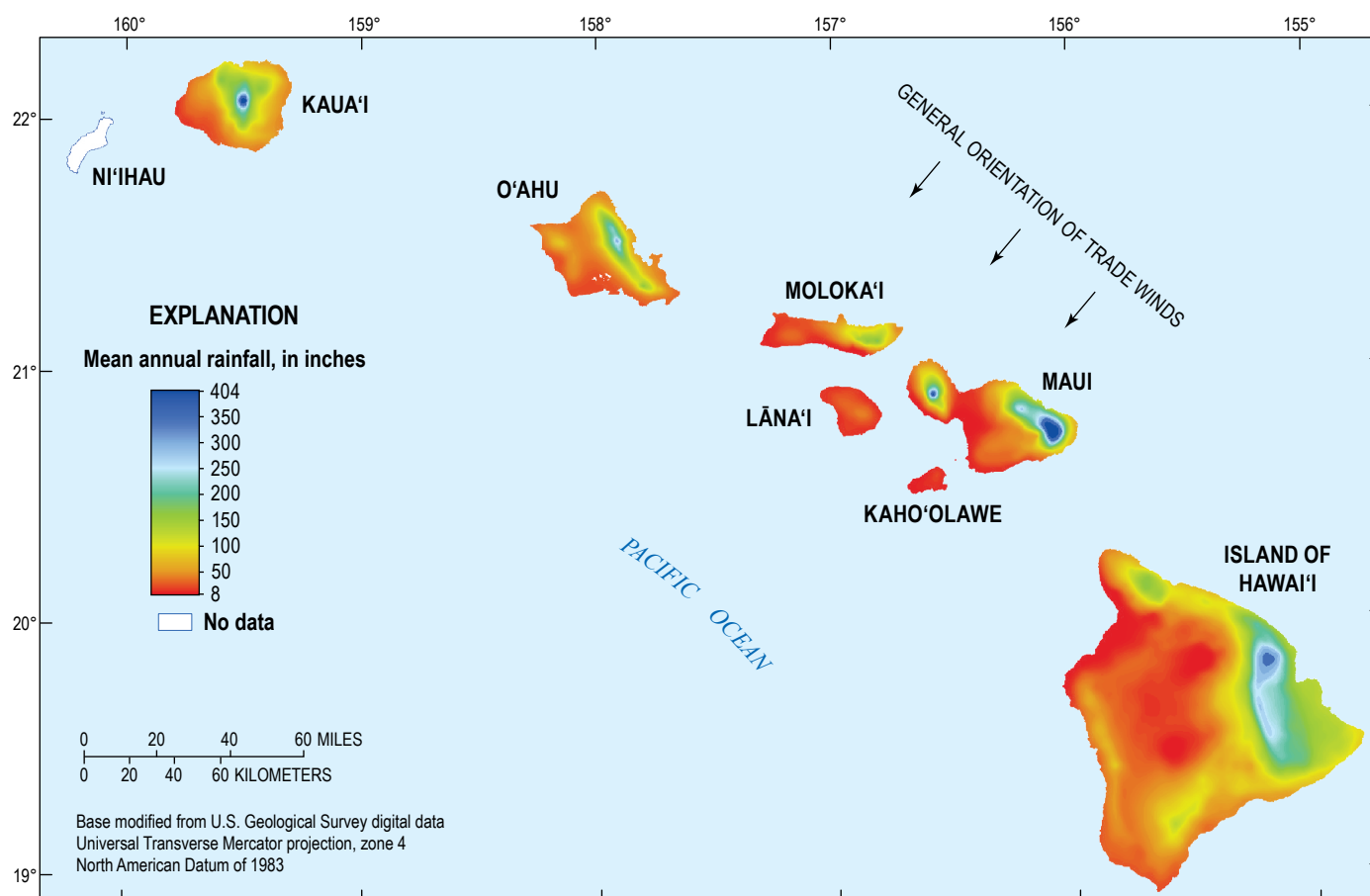


Figure 3. Maps showing the mean annual rainfall in the main Hawaiian Islands, excluding Ni'ihau. Modified from Giambelluca and others (2013).

shield-shaped morphology from the volcanic summits to the ocean, except where modified by faulting, volcanic vents, or erosion. On the northeastern sides of Kohala and Mauna Kea, large streams, resulting from high rainfall, have carved deep valleys in these relatively older volcanoes.

Climate

The Hawaiian Islands lie in the trade-wind belt of the North Pacific anticyclone. The climate for most of the islands is characterized by mild temperatures, moderate humidity, and prevailing northeasterly trade winds (Giambelluca and Schroeder, 1998). The climate of the Hawaiian Islands is diverse, however, and includes deserts, tropical rain forests, and snow-capped mountains. Climate distribution is influenced by the prevailing northeasterly trade winds and their interaction with the islands' volcanic mountains. Since the 1970s, the direction, frequency, and strength of trade winds in the main Hawaiian Islands have shifted to less frequent but stronger northeasterly trade winds and more frequent easterly trade winds (Garza and others, 2012).

Rain is generated by the orographic effect—trade winds blow against the mountain slopes and air carrying moisture from the ocean is forced to rise and cool adiabatically, causing condensation of water vapor. As a result, rainfall amounts are high over mountain crests and on northeast-facing (windward)

slopes and low in leeward areas (fig. 3). The mean annual rainfall gradient between dry leeward areas and wet windward slopes is substantial—mean annual rainfall ranges from less than 10 inches on some leeward coasts to as much as 404 inches on the windward slopes and can vary by more than an order of magnitude within 5 horizontal miles (Giambelluca and Schroeder, 1998; Giambelluca and others, 2013). The interaction of trade winds and mountains thus provides a voluminous and persistent influx of freshwater to Hawai'i; without the orographic effect, rainfall would be less than 30 inches per year (in/yr), similar to that of the open ocean in this region of the Pacific (Giambelluca and Schroeder, 1998). The orographic effect and the rainfall it generates are typically limited to about 8,200 ft altitude by the TWI (DeLay and Giambelluca, 2010). Thus, the climate at the peaks of the highest mountains—Haleakalā on Maui, and Mauna Kea and Mauna Loa on the Island of Hawai'i—is dry, with the lowest mean annual rainfall values in the main Hawaiian Islands (figs. 1, 3). The southwest-facing slopes of the Island of Hawai'i, although sheltered from the trade winds, receive air flow as the trade winds wrap around Mauna Loa and from sea breezes generated by the diurnal heating and cooling of the large land mass of the Island of Hawai'i; these winds produce a band of higher precipitation on the middle-altitude slopes (Giambelluca and Schroeder, 1998; Giambelluca

and others, 2013). The Hawaiian Islands also receive rain from occasional migratory storm systems unrelated to the orographic effect. These storms can bring heavy rain to any part of an island and are the main source of rainfall for the dry leeward areas and on mountain tops above the base of the TWI (Giambelluca and others, 2013). Rainfall at high altitudes in the Hawaiian Islands is inversely correlated with the TWI frequency (Longman and others, 2015). For example, an increase in the mean frequency of the TWI since the 1990s has corresponded with decreases in mean dry- and wet-season rainfall at high altitudes.

In the Hawaiian Islands, clouds can form when a moist air mass cools and condenses as it is forced upslope by trade winds or by thermal circulation systems such as sea breezes. As clouds flow near the land surface, some of the cloud moisture may accumulate on vegetation through CWI. At places where CWI is frequent, intercepted cloud moisture that reaches the ground can be a substantial part of the water budget (Ekern, 1964; Juvik and Ekern, 1978; Juvik and Nullet, 1995; Heath and Huebert, 1999; Giambelluca and others, 2011; Takahashi and others, 2011; Tseng, 2021). The cloud zone includes areas that frequently have clouds and is typically between altitudes of about 2,000 and 8,200 ft in the main Hawaiian Islands (DeLay and Giambelluca, 2010). However, the altitudinal boundaries of the cloud zone can vary temporally and spatially across the main Hawaiian Islands (Diaz and others, 2011; Zhang and others, 2012; Longman and others, 2015; Kagawa-Viviani and Giambelluca, 2020). Furthermore, clouds can also form in areas above the generalized cloud zone (Juvik and Ekern, 1978) and some of the cloud moisture in these areas can accumulate on vegetation through CWI. In this study, the cloud zone on each island was defined as follows, consistent with earlier studies (Kāne and others, 2024a; Johnson and others, 2023). For Kauaʻi, Oʻahu, and Molokaʻi, all areas at or above 2,000 ft were assumed to be within the cloud zone and all areas below 2,000 ft were assumed to be below the cloud zone (figs. 4A–C). In windward areas of Maui and the Island of Hawaiʻi, all areas at or above 2,000 ft were assumed to be within the cloud zone and all areas below 2,000 ft were assumed to be below the cloud zone (fig. 4D, E). In leeward areas of Maui and the Island of Hawaiʻi, all areas at or above 2,600 ft were assumed to be within the cloud zone and all areas below 2,600 ft were assumed to be below the cloud zone.

The seasonal rainfall cycle across much of the Hawaiian Islands is characterized by a dry season and a wet season. The dry season (May to September) is characterized by warm temperatures and steady trade winds, whereas the wet season (October to April) has cooler temperatures and less persistent trade winds (Sanderson, 1993; Blumenstock and Price, 1994). In drier leeward areas, where most rainfall comes from storms, mean monthly rainfall is highest in December and January and lowest in June and July (Giambelluca and others, 2013; Frazier and others, 2016). In wet windward areas that receive abundant orographic rainfall, mean monthly rainfall tends to be more evenly distributed throughout the year. On the

southwest-facing slopes of the Island of Hawaiʻi, rainfall tends to be highest from May to September when the sea breezes generated by the diurnal heating and cooling of the large land mass are strongest.

Rainfall in Hawaiʻi also varies with multi-year cycles linked to ocean and atmosphere cycles, such as El Niño and La Niña, which repeat at a frequency of about 2 to 7 years and have events that typically last about 9 to 12 months; the Pacific Decadal Oscillation (PDO); and the Pacific North American pattern (PNA). The El Niño, La Niña, PDO, and PNA cycles cause some years to be wetter or drier than the long-term average (Chu and Chen, 2005; Frazier and others, 2018). For example, the Hawaiian Islands tend to be dry during most El Niño events and wet during most La Niña events. El Niño (La Niña) years also tend to have less (more) extreme rainfall events (Chu and others, 2010). Over the last century, El Niño events have been associated with most droughts in the Hawaiian Islands (Frazier and others, 2022). El Niño events can be broadly separated into two types: central Pacific or Modoki events with peak sea-surface temperature anomalies located in the central equatorial Pacific, and eastern Pacific or canonical El Niño events with peak sea-surface temperature anomalies in the eastern equatorial Pacific (Kug and others, 2009). In the Hawaiian Islands, eastern Pacific El Niño events are more unfavorable for wet-season rainfall than central Pacific El Niño events (Lu and others, 2020). Since the 1980s, wet-season rainfall during La Niña years has declined due to variations in tropical sea-surface temperatures and the atmospheric circulation in the North Pacific Ocean (O'Connor and others, 2015). Future El Niño events are projected to increase in strength, grow at a faster rate, persist for longer durations, and have greater effects on climate variability (Geng and others, 2022; Lopez and others, 2022).

Land Cover

Changes in land cover can have a substantial effect on water resources. The diversity of land cover in the Hawaiian Islands reflects the influence of island age, steep climate gradients, agricultural practices, and land development (fig. 4). The islands are dominated by native and non-native forests, shrubland, grassland, and varying amounts of agriculture. Developed regions are distributed in and around the main metropolitan areas. Large tracts of forest, commonly dominated by native canopy species, exist in the wetter areas of the island, with shrubland and grassland in the drier areas (fig. 4). Sparsely vegetated land generally exists on lava flows that have not been sufficiently weathered to allow for plant colonization, along dry ridges, and coastlines. Small wetlands exist in some of the flat summits of old volcanic craters, such as Kawaikini on Kauaʻi, Kaʻala on Oʻahu, Puʻukukui on West Maui volcano, and upland areas of eastern Haleakalā (figs. 1, 4).

On Kauaʻi, non-native forest and shrubland dominate the eastern wet upland areas within the cloud zone with wetland areas occurring near Kawaikini on Waiʻaleʻale (figs. 1, 4A). The western wet upland slope of Waiʻaleʻale is dominated by

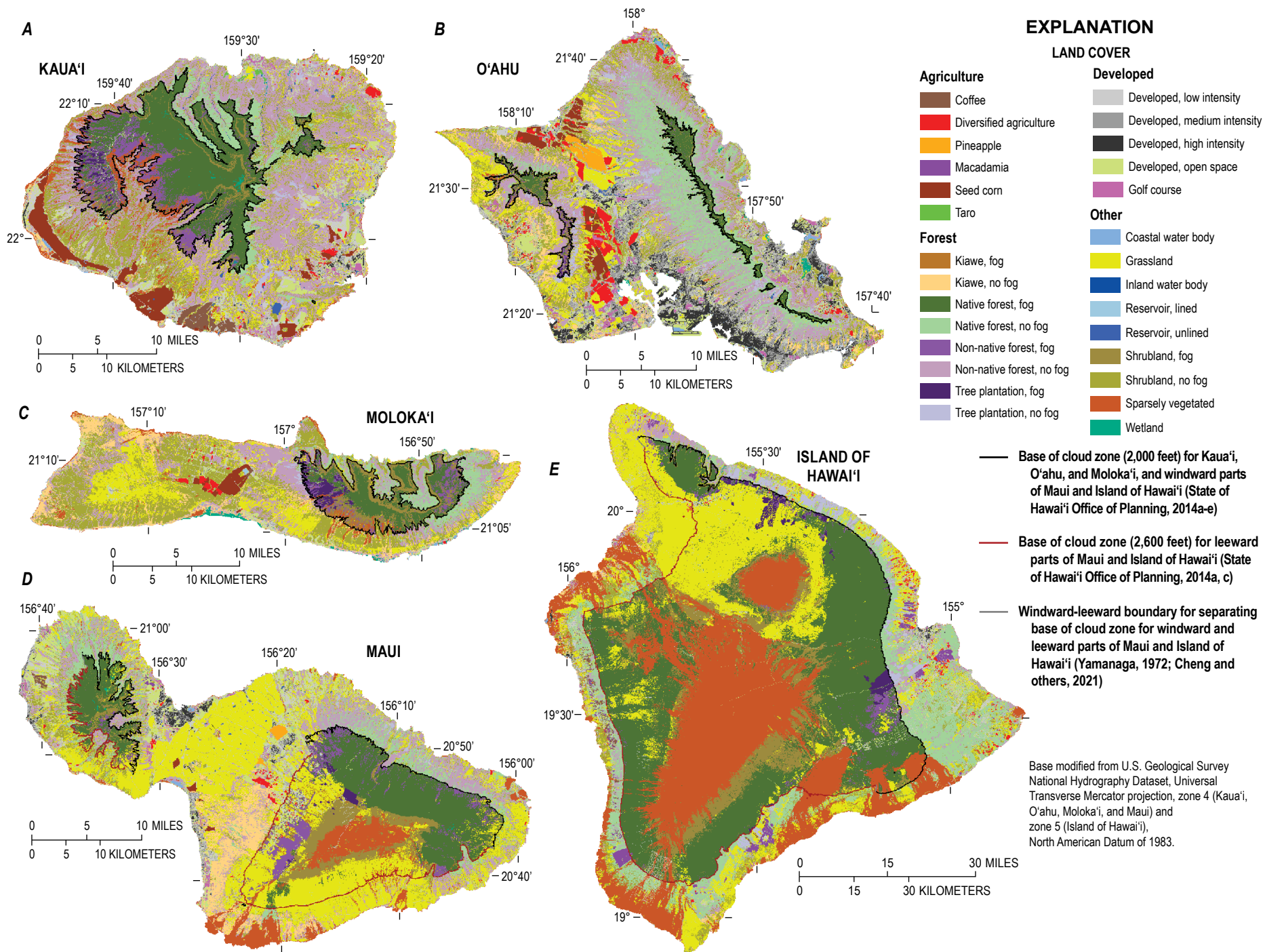


Figure 4. Maps showing the land cover in 2020 for Kaua'i (A), O'ahu (B), Moloka'i (C), Maui (D), and the Island of Hawai'i (E). Modified from Kāne and others (2024a).

native forest and non-native forest within and below the cloud zone. The mid-altitude areas on the windward side are partially developed but are mainly covered by grassland, shrubland, and non-native forest areas. The southern and southwestern coastal lands have large areas of seed corn and coffee with patches of kiawe near the coast. The main developed regions are near the northern, eastern, and southern coastlines with the highest intensity of development occurring near Līhu‘e.

O‘ahu is the most developed island with the southern coastal lands and the Honolulu region having the largest extent of high-intensity developed areas (fig. 4B). The region between the Ko‘olau and Wai‘anae Ranges is covered in grassland and agriculture fields (seed corn, coffee, pineapple, and other diversified agriculture). The wet upland areas of the Wai‘anae Range have areas of native forest surrounded by non-native forest and shrubland. Lower in altitude near the southwestern coastline are shrubland and grassland areas. The wet upland regions of the Ko‘olau Range are dominated by native forest with non-native forest becoming more dominant on the mid-altitude slopes. The leeward coastal areas have mixed non-native forest, shrubland, and grassland with developed areas closest to the coast.

The wet upland areas of the East Moloka‘i volcano are dominated by native and non-native forests, and tree plantations (fig. 4C). The mid-to-low altitude areas along the slopes of the East Moloka‘i volcano are dominated by shrubland and grassland with patches of sparsely vegetated areas occurring in the southern region. Low-altitude areas in east and west Moloka‘i are covered in large areas of shrubland and grassland, with large patches of kiawe growing near the coast, the largest of which occurs along the northwestern coastline. The central saddle area of Moloka‘i has patches of diversified agriculture and seed corn.

On West Maui volcano, native forest and shrubland dominate the wet upland areas near Pu‘ukukui, whereas non-native forest, grassland, urban development, and agricultural fields (macadamia and coffee) cover the drier lowland areas (figs. 1, 4D). Mid-altitude areas on northwest Haleakalā are developed but also have patches of pineapple and diversified agriculture. In the high-altitude area of Haleakalā, the peak Pu‘u‘ula‘ula has sparsely vegetated barren rock, which is surrounded by a region of shrubland. Mostly native forest covers the mid-altitude wet northeastern slopes below the shrubland region and transitions to coastal regions dominated by non-native forest and grassland. Much of the arid southwestern slopes of Haleakalā are covered with non-native forest and grassland mixed with patches of development, native forest, and diversified agriculture. Coastal areas between West Maui volcano and Haleakalā are developed with grassland in between (fig. 4D).

On the Island of Hawai‘i, the mountains of Mauna Loa and Mauna Kea are active shield volcanoes that rise above the base of the TWI. Areas above the base of the TWI consist of sparsely vegetated barren rock that transitions into shrubland and native forest at lower altitudes (fig. 4E). The shrubland and native forest areas on Mauna Kea transition into grassland that extends northwest across the leeward slope of Mauna Kea down to the coast. The mid-altitude region of Mauna

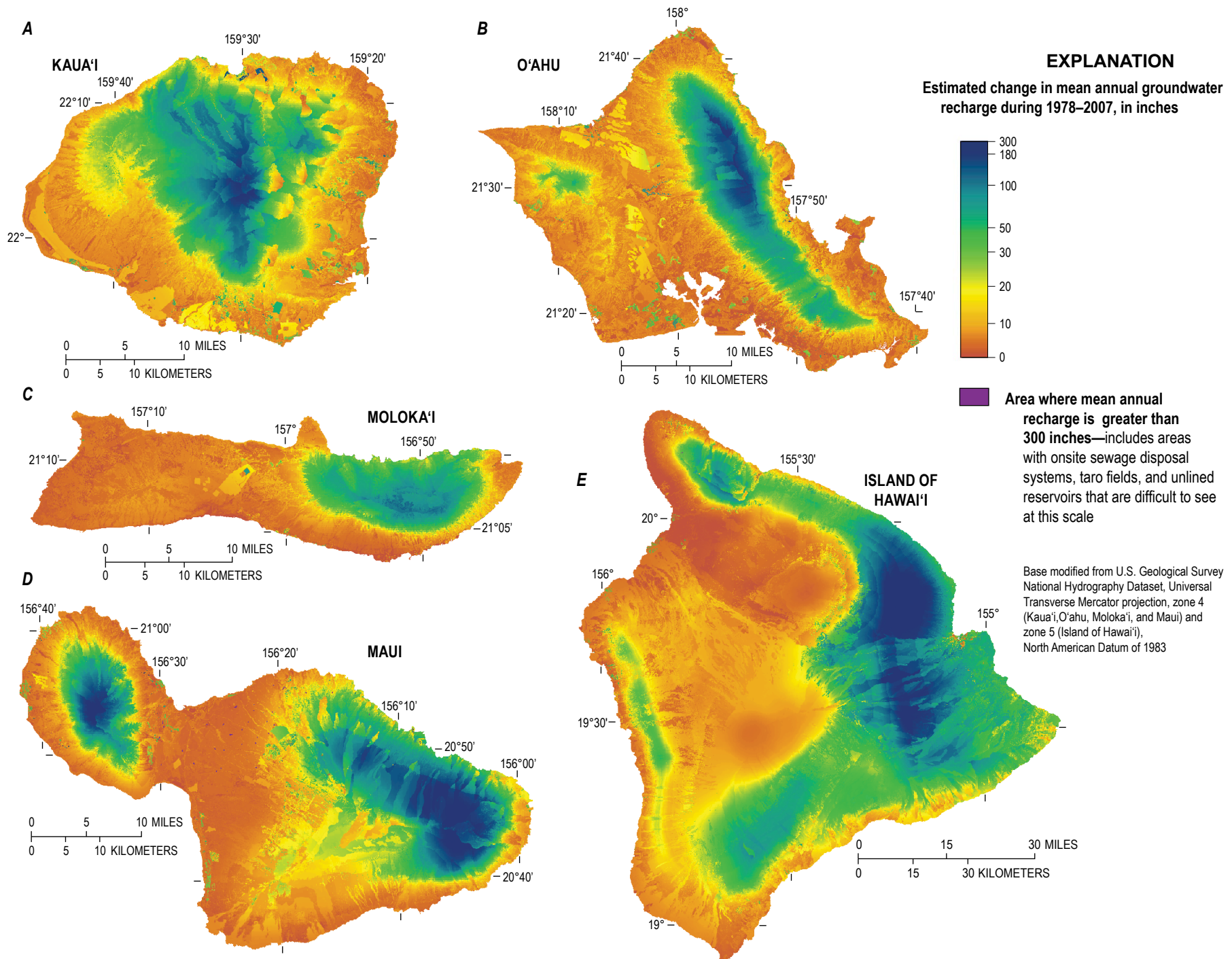
Loa and the eastern flank of Mauna Kea are mainly native and non-native forest with areas of tree plantations. Areas near the west, south, and southeast coast are mostly grassland and sparsely vegetated with small areas of developed land. The eastern, coastal areas of the island are covered by native and non-native forest with developed areas occurring around Hilo. The northern region of Kohala has native and non-native forest on the windward side but is mostly grassland and shrubland on the leeward side.

Groundwater Recharge

Groundwater recharge is water that flows into an aquifer from the ground surface or near it (ignoring recharge from injection wells that discharge water below the water table). Most of this water comes from rainfall and CWI but, in some places, irrigation or seepage from unlined reservoirs can contribute substantially to recharge. Other sources of water entering from near the surface include septic-system leachate and leaks from water systems, sewers, and cesspools. Kāne and others (2024a) estimated mean annual groundwater recharge rates on Kaua‘i, O‘ahu, Moloka‘i, Maui, and the Island of Hawai‘i for a reference condition consisting of 1978–2007 climate and 2020 land cover (fig. 5).

The spatial pattern of mean annual recharge on each island generally resembles the pattern of mean annual rainfall during the same reference period, which might be modified by land-cover conditions (fig. 3). Recharge is substantial on windward slopes and mountain tops below the base of the TWI. The mountains of Kaua‘i, the Ko‘olau Range (O‘ahu), East Moloka‘i volcano, West Maui, and Kohala (Island of Hawai‘i) are all below the base of the TWI. Thus, the areas of substantial recharge—as much as several hundred inches per year—on these mountains are at or near the summits. Ka‘ala on O‘ahu also is an area of locally substantial recharge, although the recharge is not as great or extensive as that on the Ko‘olau Range. The peaks of Haleakalā on Maui, and Mauna Kea and Mauna Loa on the Island of Hawai‘i, rise into the arid subalpine climates above the base of the TWI. Therefore, the areas with substantial recharge (hundreds of inches of recharge per year) are on the windward slopes at lower altitudes. The windward slopes of Mauna Kea, Mauna Loa, and Kīlauea on the Island of Hawai‘i form a zone in which rainfall and recharge are particularly substantial. The lower middle altitudes of leeward Mauna Loa and southwest Hualālai have somewhat elevated recharge because of the orographic rainfall generated by diurnal sea breezes (Giambelluca and others, 2013).

Recharge is generally less on the leeward sides of the islands, particularly on the low-lying coastal areas, which is consistent with the rainfall in these areas (fig. 3). The distribution pattern of recharge departs from that of rainfall where other sources of water contribute to and enhance recharge. Areas of enhanced recharge commonly occur in irrigated areas such as agricultural fields, golf courses, and residential developments. Enhanced recharge also commonly occurs in areas with standing water such as unlined reservoirs and taro fields.



-- **Figure 5.** Maps showing the mean annual groundwater recharge for 1978–2007 climate and 2020 land cover for Kaua'i (A), O'ahu (B), Moloka'i (C), Maui (D), and the Island of Hawai'i (E). Modified from Kāne and others (2024a).

Wildfires

Wildfires have not played a substantial role in the evolution of native ecosystems in the Hawaiian Islands (LaRosa and others, 2008) and many native forest species do not possess adaptations to survive or recover from a wildfire (Vitousek, 1992; D’Antonio and others, 2011). After a wildfire, the post-wildfire plant community is often characterized by rapid non-native grass regeneration, which increases the potential for more frequent and higher intensity wildfires (LaRosa and others, 2008; Ainsworth and Kauffman, 2010). This cycle of non-native grass invasion, wildfire, then non-native grass reinvasion, also known as the invasive-grass wildfire cycle, has led to large-scale land-cover change in the main Hawaiian Islands and many other parts of the world (D’Antonio and Vitousek, 1992; Hawbaker and others, 2017). The grassland and shrubland landscapes in the main Hawaiian Islands enable wildfires to propagate rapidly into the forested perimeters of the state’s watersheds, thereby posing a threat to ecosystem health, freshwater supplies, and human health and safety (Trauernicht and others, 2015). Over the last century, the occurrences of wildfire in the main Hawaiian Islands show a strong relation to El Niño events characterized by a cyclic

pattern where stocks of fuel (that is, living and dead vegetation) increase during the summer months preceding an El Niño event and then later cure during dry winter months, which results in increased wildfire risk (Frazier and others, 2022).

A total of 187 wildfires were documented on Kaua’i, O’ahu, Moloka’i, Maui, and the Island of Hawai’i during 1999–2012 (table 2). The 187 wildfires during 1999–2012 were selected from a larger dataset of documented wildfires during 1999–2019 across the Hawaiian Islands (University of Hawai’i at Mānoa, 2021) to overlap with the 1990–2012 time period used in the model simulations for this study (see “Water-Budget Model” section). Documented wildfires range in size from as small as 0.2 acres on O’ahu to as large as 25,590 acres on the Island of Hawai’i. About 80 percent of the total area within the wildfire perimeters on Kaua’i, O’ahu, Moloka’i, Maui, and the Island of Hawai’i is mapped as grassland or shrubland (fig. 6, table 3). About 13 percent of the total area is mapped as forest land cover including native and non-native forest and kiawe. Another 5 percent of the total area is mapped as developed or agricultural land cover. The remaining areas within the wildfire perimeters are mapped as sparsely vegetated. Most of the wildfires occurred in the drier, leeward parts of each island.

Table 2. Summary of wildfire activity during 1999–2012.

[Number, size, and location of wildfire perimeters determined from University of Hawai’i at Mānoa (2021). Product of number of wildfires and mean (in acres) might not equal total land area (in acres) because of rounding.]

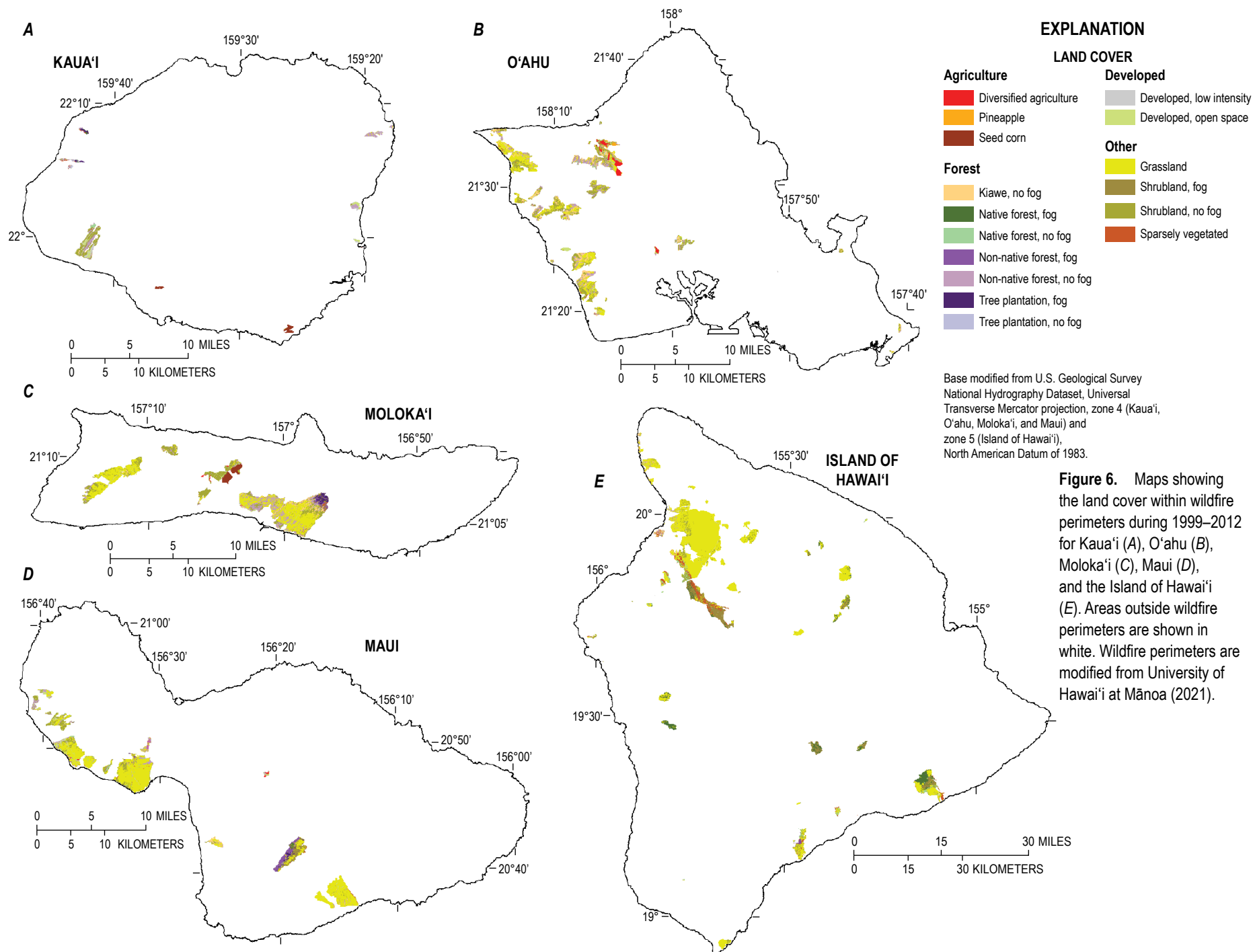
Island	Number of wildfires	Area burned					
		Mean (acres)	Minimum (acres)	Median (acres)	Maximum (acres)	Total land area (acres)	Total fraction of land area
Kaua’i	15	245	49	128	1,909	3,674	0.01
O’ahu	45	427	0.2	141	3,601	19,202	0.05
Moloka’i	9	1,560	22	467	8,357	14,037	0.08
Maui	22	1,093	73	279	4,810	24,055	0.05
Hawai’i	96	1,279	1.0	195	25,590	122,744	0.05
All islands	187	982	0.2	196	25,590	183,711	0.05

Table 3. Fraction of area affected by wildfire activity during 1999–2012 by land cover.

[Land-cover type from map of 2020 land-cover by Kāne and others (2024a). Sum of fractions for each island might not sum to 1.]

Land-cover type	Kaua’i	O’ahu	Moloka’i	Maui	Island of Hawai’i	All islands
Diversified agriculture	0.00	0.04	0.00	0.00	0.00	0.01
Pineapple	0.00	0.01	0.00	0.00	0.00	0.00
Seed corn	0.09	0.00	0.04	0.00	0.00	0.01
Developed, open space	0.13	0.03	0.03	0.04	0.01	0.02
Developed, low-intensity	0.11	0.01	0.01	0.01	0.01	0.01
Grassland	0.02	0.34	0.47	0.71	0.70	0.63
Shrubland, fog	0.00	0.00	0.01	0.05	0.09	0.07
Shrubland, no fog	0.27	0.28	0.22	0.07	0.05	0.10
Sparsely vegetated	0.02	0.01	0.00	0.01	0.04	0.03

Land-cover type	Kaua’i	O’ahu	Moloka’i	Maui	Island of Hawai’i	All islands
Native forest, fog	0.01	0.00	0.00	0.00	0.06	0.04
Native forest, no fog	0.02	0.01	0.00	0.01	0.02	0.02
Non-native forest, fog	0.01	0.00	0.01	0.03	0.00	0.01
Non-native forest, no fog	0.26	0.14	0.14	0.04	0.01	0.04
Tree plantation, fog	0.03	0.00	0.02	0.01	0.00	0.00
Tree plantation, no fog	0.02	0.00	0.00	0.00	0.00	0.00
Kiawe, no fog	0.01	0.13	0.05	0.01	0.01	0.02



Selection of Climate and Land-Cover Conditions

The effect of drought conditions and reduced CWI on recharge, soil moisture, ET, and CWD was evaluated using historical and projected future drought conditions. Gridded maps of rainfall for the 1,116 months during 1920–2012 (Frazier and others, 2016) were used to identify historical drought conditions. Climate projections developed for a set of global emission and warming scenarios adopted by Nakićenović and others (2000) and the Intergovernmental Panel on Climate Change (2014) were used to develop a drought condition for projected future climate conditions. A map of 2020 land cover and two modified versions of the map were used to develop a set of land-cover conditions for simulating the hydrologic effects of reduced CWI.

Historical Drought Conditions

The Standard Precipitation Index (SPI) is a common drought index for assessing meteorological drought and is based solely on rainfall (McKee and others, 1993). In a recent study, Frazier and others (2022) used gridded maps of monthly rainfall from Frazier and others (2016) during 1920–89 and from Lucas and others (2022) during 1990–2019 to compute gridded SPI maps at multiple timescales during 1920–2019 (for example, from one month up to 60 months). Frazier and others (2022) used the 12-month SPI, or SPI-12, to identify the most severe droughts in the Hawaiian Islands during 1920–2019. To determine the most severe droughts, they considered a set of five characteristics derived from the SPI-12 that included average intensity, peak intensity, duration, magnitude, and maximum percentage of land area with an SPI-12 value of less than -1 during the event. The 2007–14 drought followed by the 1998–2002 drought were ranked as the two most severe statewide droughts on record. However, they ranked the 1998–2002 drought as the most severe island-wide drought for Kauaʻi, Oʻahu, Maui, Lānaʻi, Kahoʻolawe, and Molokaʻi (fig. 1). For the Island of Hawaiʻi, they ranked the 2007–14 drought as the most severe island-wide drought.

We conducted a separate analysis to identify the driest time periods, in terms of mean annual island-wide rainfall, for each island. The 93-year gridded dataset of monthly rainfall maps during 1920–2012 (Frazier and others, 2016) was used to identify a 5-year and a 6-year period with the lowest mean annual island-wide rainfall. A 5-year period has been used in earlier water-budget studies to identify the driest time period (Engott, 2011; Engott and others, 2017; Johnson and others, 2018; Oki and others, 2020; Kāne and others, 2024a). A 6-year period was added to this analysis to enable identification of longer duration droughts as identified by Frazier and others (2022). The 1920–2012 dataset from Frazier and others (2016) was used for this analysis to be consistent with the dataset of monthly rainfall used in the water-budget modeling (see

“[Water-Budget Model](#)” section). For the 5-year period, mean annual island-wide rainfall was lowest on Kauaʻi, Oʻahu, and Molokaʻi during 1998–2002, and on Maui and the Island of Hawaiʻi during 2008–12. For the 6-year period, mean annual island-wide rainfall was lowest on Kauaʻi, Oʻahu, and Molokaʻi during 1998–2003, and on Maui and the Island of Hawaiʻi during 2007–12.

We used the results of the drought analyses by Frazier and others (2022) and the analyses of mean annual island-wide rainfall to identify a historical drought condition during 1920–2012 for each island. We selected the 1998–2002 and 2007–12 time periods as the two drought periods for Kauaʻi, Oʻahu, Molokaʻi, Maui, and the Island of Hawaiʻi. For assessing the effect of drought on groundwater recharge, the 1998–2002 time period was selected as the historical drought condition for Kauaʻi, Oʻahu, and Molokaʻi, whereas the 2007–12 time period was selected for Maui and the Island of Hawaiʻi (table 4). For assessing the effect of drought on soil moisture, ET, and CWD, we grouped the 1998–2002 and 2007–12 time periods into one discontinuous 11-year drought period for each island to enable the calculation of relative frequency of soil moisture, ET, and CWD for a single drought period (see “[Water-Budget Scenarios](#)” section).

Future Climate Conditions

Kāne and others (2024a) examined a range of future climate projections to determine a range of projected changes in rainfall and temperature for Kauaʻi, Oʻahu, Molokaʻi, Maui, and the Island of Hawaiʻi. On the basis of projected changes in mean annual rainfall, they selected two climate projections to capture a range of future climate conditions: (1) a dry-climate condition, and (2) a wet-climate condition. For the dry-climate condition, they selected the projected rainfall conditions during 2071–99 from Elison Timm and others (2015) for a Representative Concentration Pathway (RCP) warming scenario with a total radiative forcing of 8.5 watts per square meter (W/m^2) by the year 2100 (Intergovernmental Panel on Climate Change, 2014), hereinafter RCP8.5 2071–99 projection, for each island because it represents the driest condition among the available set of rainfall projections (Elison Timm and others, 2015; Zhang and others, 2016; Zhang and Wang, 2017). For this study, the RCP8.5 2071–99 projection from Elison Timm and others (2015) also was chosen as the future climate condition for assessing the effects of future drought and long-term drying on groundwater recharge, soil moisture, ET, and CWD.

Hypothetical Land-Cover Conditions

In this study, the effects of reduced CWI on groundwater recharge during drought were evaluated for three islands. Maui and the Island of Hawaiʻi were selected to assess the effect of reduced CWI because both have large areas within the cloud zone. Oʻahu was also selected to assess the effect of reduced

Table 4. Summary of mean annual island-wide rainfall for selected periods during 1920–2012 and projected climate conditions for Kauaʻi, Oʻahu, Molokaʻi, Maui, and the Island of Hawaiʻi.

[Mgal/d, million gallons per day; --, not applicable; RCP8.5, Representative Concentration Pathway warming scenario with total radiative forcing of 8.5 watts per square meter by the year 2100 from Intergovernmental Panel on Climate Change (2014); 1978–2007 reference is 1978–2007 rainfall from Frazier and others (2016); Drought 1 rainfall is 1998–2002 rainfall from Frazier and others (2016); Drought 2 rainfall is 2007–12 rainfall from Frazier and others (2016); Drought 3 rainfall is 1998–2002 and 2007–12 rainfall; RCP8.5 2071–99 Drought 1 rainfall is 1998–2002 rainfall from Frazier and others (2016) adjusted for a RCP8.5 2071–99 projection from Elison Timm and others (2015); RCP8.5 2071–99 Drought 2 rainfall is 2007–12 rainfall from Frazier and others (2016) adjusted for a RCP8.5 2071–99 projection from Elison Timm and others (2015); RCP8.5 2071–99 Drought 3 rainfall is 1998–2002 and 2007–12 rainfall from Frazier and others (2016) adjusted for a RCP8.5 2071–99 projection from Elison Timm and others (2015); Non-Drought rainfall is 1990–97 and 2003–06 rainfall from Frazier and others (2016); RCP8.5 2071–99 Non-Drought rainfall is 1990–97 and 2003–06 rainfall from Frazier and others (2016) adjusted for a RCP8.5 2071–99 projection from Elison Timm and others (2015).]

Period description	Island	Time period	Rainfall condition	Mean annual island-wide rainfall		
				inches	Mgal/d	Change, in percent, from 1978–2007 reference (change in Mgal/d)
30-year reference rainfall	Kauaʻi	1978–2007	1978–2007 reference	84.2	2,221	--
	Oʻahu	1978–2007	1978–2007 reference	64.0	1,813	--
	Molokaʻi	1978–2007	1978–2007 reference	49.1	607	--
	Maui	1978–2007	1978–2007 reference	81.0	2,805	--
	Hawaiʻi	1978–2007	1978–2007 reference	72.7	13,937	--
Non-drought rainfall	Kauaʻi	1990–97, 2003–06	Non-Drought	87.2	2,300	4 (79)
	Oʻahu	1990–97, 2003–06	Non-Drought	67.4	1,910	5 (96)
	Molokaʻi	1990–97, 2003–06	Non-Drought	53.2	658	8 (51)
	Maui	1990–97, 2003–06	Non-Drought	80.5	2,788	–0.6 (–17)
	Hawaiʻi	1990–97, 2003–06	Non-Drought	73.1	14,013	0.5 (76)
Projected non-drought rainfall	Kauaʻi	--	RCP8.5 2071–99 Non-Drought	65.9	1,738	–22 (–483)
	Oʻahu	--	RCP8.5 2071–99 Non-Drought	52.5	1,487	–18 (–326)
	Molokaʻi	--	RCP8.5 2071–99 Non-Drought	42.3	523	–14 (–84)
	Maui	--	RCP8.5 2071–99 Non-Drought	69.8	2,417	–14 (–388)
	Hawaiʻi	--	RCP8.5 2071–99 Non-Drought	60.8	11,655	–16 (–2,282)
Lowest 5-year rainfall	Kauaʻi	1998–2002	Drought 1	66.0	1,741	–22 (–480)
	Oʻahu	1998–2002	Drought 1	47.3	1,340	–26 (–473)
	Molokaʻi	1998–2002	Drought 1	36.3	449	–26 (–158)
Projected lowest 5-year rainfall	Kauaʻi	--	RCP8.5 2071–99 Drought 1	52.0	1,372	–38 (–849)
	Oʻahu	--	RCP8.5 2071–99 Drought 1	37.4	1,060	–42 (–754)
	Molokaʻi	--	RCP8.5 2071–99 Drought 1	28.5	353	–42 (–255)
Lowest 6-year rainfall	Maui	2007–12	Drought 2	56.2	1,946	–31 (–859)
	Hawaiʻi	2007–12	Drought 2	50.9	9,755	–30 (–4,182)
Projected lowest 6-year rainfall	Maui	--	RCP8.5 2071–99 Drought 2	49.1	1,700	–39 (–1,105)
	Hawaiʻi	--	RCP8.5 2071–99 Drought 2	44.7	8,565	–39 (–5,372)
11-year drought rainfall	Kauaʻi	1998–2002, 2007–12	Drought 3	70.2	1,851	–17 (–369)
	Oʻahu	1998–2002, 2007–12	Drought 3	50.3	1,425	–21 (–388)
	Molokaʻi	1998–2002, 2007–12	Drought 3	38.1	471	–22 (–136)
	Maui	1998–2002, 2007–12	Drought 3	60.6	2,098	–25 (–707)
	Hawaiʻi	1998–2002, 2007–12	Drought 3	57.2	10,964	–21 (–2,973)
Projected 11-year drought rainfall	Kauaʻi	--	RCP8.5 2071–99 Drought 3	53.1	1,400	–37 (–820)
	Oʻahu	--	RCP8.5 2071–99 Drought 3	39.6	1,122	–38 (–691)
	Molokaʻi	--	RCP8.5 2071–99 Drought 3	30.2	374	–38 (–234)
	Maui	--	RCP8.5 2071–99 Drought 3	53.2	1,842	–34 (–963)
	Hawaiʻi	--	RCP8.5 2071–99 Drought 3	49.6	9,507	–32 (–4,429)

CWI because of the high utilization of groundwater resources on the island. In the model calculations, CWI is assumed to be negligible for all land-cover classes except for non-native forest, native forest, tree plantation, kiawe, shrubland, coffee, and macadamia land cover within the cloud zone. The effect of reduced CWI was evaluated in the water-budget model simulations by converting forest and shrubland land cover within the cloud zone to grassland, for which CWI was considered negligible. Two hypothetical land-cover conditions were defined for O‘ahu, Maui, and the Island of Hawai‘i to simulate the effects of reduced CWI on groundwater recharge, soil moisture, ET, and CWD: (1) a land-cover condition in which roughly 50 percent of shrubland and forest areas within the cloud zone were converted to grassland, hereinafter Conversion 1 land cover, and (2) a land-cover condition in which 100 percent of shrubland and forest areas within the cloud zone were converted to grassland, hereinafter Conversion 2 land cover (fig. 7).

Water-Budget Model

The water-budget code known as WATRM_{od}, a Water-budget Accounting for Tropical Regions Model (Oki, 2022), was used to estimate spatially variable daily water-budget components, including groundwater recharge, soil moisture, and ET, on Kaua‘i, O‘ahu, Moloka‘i, Maui, and the Island of Hawai‘i. The WATRM_{od} code, hereinafter WATRM_{od}, is a modified version of the code used in earlier studies to estimate groundwater recharge for Pacific islands. Detailed descriptions of WATRM_{od} are provided by Oki (2022).

Groundwater recharge replenishes aquifers and is mainly fed by precipitation and irrigation that infiltrates the ground surface and percolates beyond the plant-root zone. Regional estimates of recharge were made using a threshold-type water-budget model approach in which recharge was assumed to occur when water in the plant-root zone exceeded the soil’s moisture-storage capacity. A water budget of the plant-soil system accounts for water inputs (rainfall, CWI, irrigation, septic-system discharge, and other inputs), water outputs (runoff, ET, and recharge), and changes in stored water (soil moisture) during a specified time interval.

WATRM_{od} computes a daily water budget for each hydrologically independent subarea within the overall study area. Each subarea is defined by its climatic, soil, land-cover, and human-related (for example, adding irrigation or other water) characteristics (see Appendix 1 for a description of model input datasets). WATRM_{od} can represent processes including rainfall, CWI, irrigation, septic-system discharge, direct recharge that bypasses the plant-soil system, runoff, canopy evaporation in forest areas, ET, changes in soil moisture, and groundwater recharge. WATRM_{od} is designed to simulate the hydrologic processes and physical conditions that affect recharge on the islands on a daily basis. Hydrologic processes simulated by the model include rainfall, CWI, irrigation, runoff, and ET. WATRM_{od} represents physical conditions by using parameters that include the moisture-storage capacity

of soils and properties of the vegetation and land cover that affect ET. For each model subarea, WATRM_{od} calculates daily recharge, soil moisture, ET, and other water-budget components during the simulation period.

Water-Budget Scenarios

A set of water-budget scenarios was developed for this study to estimate the effects of drought and reduced CWI on groundwater recharge, soil moisture, ET, and CWD (table 5). Each water-budget scenario consisted of a combination of a rainfall condition and a land-cover condition selected from a range of rainfall and land-cover conditions considered for this study. Each rainfall condition corresponds to a historical or projected future climate condition, whereas each land-cover condition corresponds to one of three conditions, consisting of 2020 land cover, Conversion 1 land cover, and Conversion 2 land cover. WATRM_{od} was used to estimate recharge, soil moisture, ET, and CWD for each water-budget scenario. The water-budget scenarios used a 23-year simulation period during 1990–2012 to reflect the overlapping period of available gridded monthly maps of rainfall during 1920–2012 from Frazier and others (2016) and gridded daily maps of rainfall during 1990–2014 from Longman and others (2019). The 1990–2012 simulation period captures the two droughts identified for each island during the 93-year period during 1920–2012, including the 5-year drought during 1998–2002 and the 6-year drought during 2007–12. The results for each water-budget scenario were processed to compare estimates of groundwater recharge, soil moisture, ET, and CWD to a reference condition.

Effects of Drought and Reduced Cloud-Water Interception on Groundwater Recharge

A reference condition consisting of 1978–2007 rainfall and 2020 land cover, hereinafter the 1978–2007 scenario, from Kāne and others (2024a) was used for comparison with recharge estimates from each water-budget scenario (table 5). Two water-budget scenarios were developed to quantify the effects of severe drought and future climate conditions on groundwater recharge for each island as follows: (1) rainfall conditions representative of the driest conditions during 1920–2012 and 2020 land cover, and (2) rainfall conditions representative of the driest conditions during a future dry-climate condition and 2020 land cover.

For Kaua‘i, O‘ahu, and Moloka‘i, rainfall amounts during 1998–2002 (hereinafter Drought 1 rainfall) were selected to represent the driest period during 1920–2012 and used with 2020 land cover (hereinafter Drought 1 scenario) (table 5). Rainfall amounts during 1998–2002 adjusted for the RCP8.5 2071–99 projection (hereinafter RCP8.5 2071–99 Drought 1 rainfall) were selected to represent the driest period for the future dry-climate condition and used with 2020 land cover (hereinafter Future Drought 1 scenario). For Maui and the Island of Hawai‘i, rainfall amounts during 2007–12

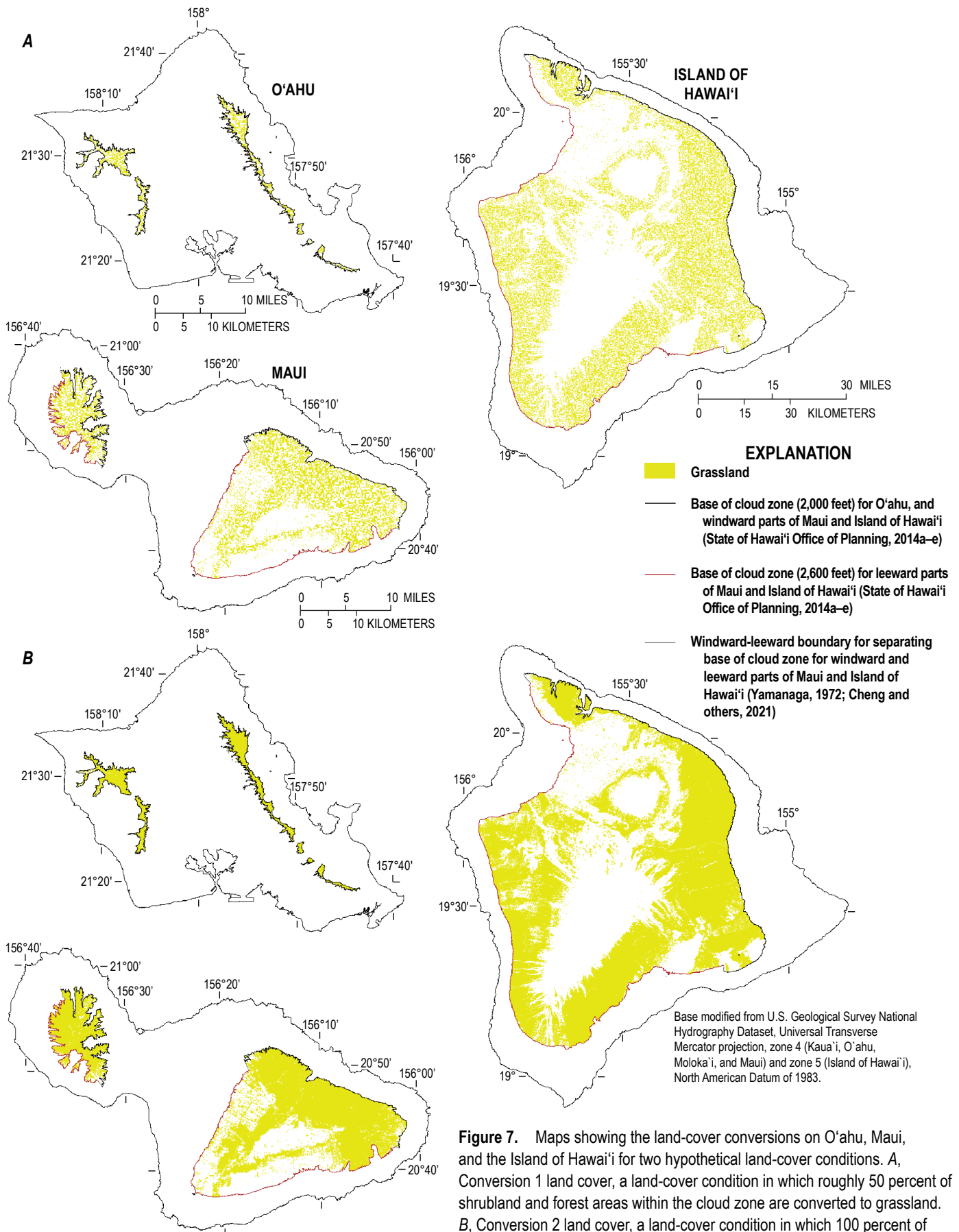


Figure 7. Maps showing the land-cover conversions on O'ahu, Maui, and the Island of Hawai'i for two hypothetical land-cover conditions. *A*, Conversion 1 land cover, a land-cover condition in which roughly 50 percent of shrubland and forest areas within the cloud zone are converted to grassland. *B*, Conversion 2 land cover, a land-cover condition in which 100 percent of shrubland and forest areas within the cloud zone are converted to grassland. Only areas subject to conversion to grassland are shown.

(hereinafter Drought 2 rainfall) were selected to represent the driest period during 1920–2012 and used with 2020 land cover (hereinafter Drought 2 scenario) (table 5). Rainfall amounts during 2007–12 adjusted for the RCP8.5 2071–99 projection (hereinafter RCP8.5 2071–99 Drought 2 rainfall) were selected to represent the driest period for the future dry-climate condition and used with 2020 land cover (hereinafter Future Drought 2 scenario).

Each drought condition was combined with two hypothetical land-cover conditions to produce four additional water-budget scenarios each for O‘ahu, Maui, and the Island

of Hawai‘i (table 5), which enabled evaluation of the added effects of reduced CWI on groundwater recharge. For O‘ahu, the four additional scenarios were:

1. Drought 1 rainfall and Conversion 1 land cover (hereinafter Drought 1 Conversion 1 scenario),
2. Drought 1 rainfall and Conversion 2 land cover (hereinafter Drought 1 Conversion 2 scenario),
3. RCP8.5 2071–99 Drought 1 rainfall and Conversion 1 land cover (hereinafter Future Drought 1 Conversion 1 scenario), and

Table 5. Summary of water-budget scenarios for Kaua‘i, O‘ahu, Moloka‘i, Maui, and the Island of Hawai‘i.

[S, selected water-budget scenario; --, not applicable; RCP8.5, Representative Concentration Pathway warming scenario with total radiative forcing of 8.5 watts per square meter by the year 2100 from Intergovernmental Panel on Climate Change (2014); 1978–2007 rainfall is 1978–2007 rainfall from Frazier and others (2016); Drought 1 rainfall is 1998–2002 rainfall from Frazier and others (2016); Drought 2 rainfall is 2007–12 rainfall from Frazier and others (2016); Drought 3 rainfall is 1998–2002 and 2007–12 rainfall from Frazier and others (2016); RCP8.5 2071–99 Drought 1 rainfall is 1998–2002 rainfall from Frazier and others (2016) adjusted for a RCP8.5 2071–99 projection from Elison Timm and others (2015); RCP8.5 2071–99 Drought 2 rainfall is 2007–12 rainfall from Frazier and others (2016) adjusted for a RCP8.5 2071–99 projection from Elison Timm and others (2015); RCP8.5 2071–99 Drought 3 rainfall is 1998–2002 and 2007–12 rainfall from Frazier and others (2016) adjusted for a RCP8.5 2071–99 projection from Elison Timm and others (2015); Non-Drought rainfall is 1990–97 and 2003–06 rainfall from Frazier and others (2016); RCP8.5 2071–99 Non-Drought rainfall is 1990–97 and 2003–06 rainfall from Frazier and others (2016) adjusted for a RCP8.5 2071–99 projection from Elison Timm and others (2015); 2020 land cover is land-cover condition in 2020 from Kāne and others (2024a); Conversion 1 land cover is land-cover condition in which roughly 50 percent of shrubland and forest areas within the cloud zone are converted to grassland; Conversion 2 land cover is land-cover condition in which 100 percent of shrubland and forest areas within the cloud zone are converted to grassland.]

Water-budget scenario name	Rainfall condition	Land-cover condition	Kaua‘i	O‘ahu	Moloka‘i	Maui	Island of Hawai‘i
Groundwater recharge							
1978–2007	1978–2007	2020	S	S	S	S	S
Drought 1	Drought 1	2020	S	S	S	--	--
Drought 1 Conversion 1	Drought 1	Conversion 1	--	S	--	--	--
Drought 1 Conversion 2	Drought 1	Conversion 2	--	S	--	--	--
Drought 2	Drought 2	2020	--	--	--	S	S
Drought 2 Conversion 1	Drought 2	Conversion 1	--	--	--	S	S
Drought 2 Conversion 2	Drought 2	Conversion 2	--	--	--	S	S
Future Drought 1	RCP8.5 2071–99 Drought 1	2020	S	S	S	--	--
Future Drought 1 Conversion 1	RCP8.5 2071–99 Drought 1	Conversion 1	--	S	--	--	--
Future Drought 1 Conversion 2	RCP8.5 2071–99 Drought 1	Conversion 2	--	S	--	--	--
Future Drought 2	RCP8.5 2071–99 Drought 2	2020	--	--	--	S	S
Future Drought 2 Conversion 1	RCP8.5 2071–99 Drought 2	Conversion 1	--	--	--	S	S
Future Drought 2 Conversion 2	RCP8.5 2071–99 Drought 2	Conversion 2	--	--	--	S	S
Soil moisture, total evapotranspiration, and climatic water deficit							
Non-Drought	Non-Drought	2020	S	S	S	S	S
Drought 3	Drought 3	2020	S	S	S	S	S
Drought 3 Conversion 1	Drought 3	Conversion 1	--	S	--	S	S
Drought 3 Conversion 2	Drought 3	Conversion 2	--	S	--	S	S
Future Non-Drought	RCP8.5 2071–99 Non-Drought	2020	S	S	S	S	S
Future Non-Drought Conversion 1	RCP8.5 2071–99 Non-Drought	Conversion 1	--	S	--	S	S
Future Non-Drought Conversion 2	RCP8.5 2071–99 Non-Drought	Conversion 2	--	S	--	S	S
Future Drought 3	RCP8.5 2071–99 Drought 3	2020	S	S	S	S	S
Future Drought 3 Conversion 1	RCP8.5 2071–99 Drought 3	Conversion 1	--	S	--	S	S
Future Drought 3 Conversion 2	RCP8.5 2071–99 Drought 3	Conversion 2	--	S	--	S	S

4. RCP8.5 2071–99 Drought 1 rainfall and Conversion 2 land cover (hereinafter Future Drought 1 Conversion 2 scenario).

For Maui and the Island of Hawai‘i, the four additional scenarios were:

1. Drought 2 rainfall and Conversion 1 land cover (hereinafter Drought 2 Conversion 1 scenario),
2. Drought 2 rainfall and Conversion 2 land cover (hereinafter Drought 2 Conversion 2 scenario),
3. RCP8.5 2071–99 Drought 2 rainfall and Conversion 1 land cover (hereinafter Future Drought 2 Conversion 1 scenario), and
4. RCP8.5 2071–99 Drought 2 rainfall and Conversion 2 land cover (hereinafter Future Drought 2 Conversion 2 scenario).

For the water-budget scenarios using Drought 1 or 2 rainfall, estimates of mean annual recharge for each scenario were calculated from a time series of annual recharge estimates produced by the sequential 23-year 1990–2012 simulation. For example, mean annual recharge for each model subarea for a scenario using Drought 1 rainfall was calculated using annual values for 1998, 1999, 2000, 2001, and 2002 in the time series of annual recharge estimates from the 1990–2012 simulation. For the scenarios using RCP8.5 2071–99 Drought 1 or 2 rainfall, a 23-year simulation also was used, and mean annual recharge for each model subarea was computed using the same sequence of years as the 1990–2012 simulation. For example, annual time series of recharge estimates for scenarios using Drought 1 rainfall correspond to years 9–13 in the 1990–2012 simulation. Hence, mean annual recharge for scenarios using RCP8.5 2071–99 Drought 1 rainfall were calculated using estimates from years 9–13 in the time series of annual recharge estimates. Mean annual recharge for each of the island’s aquifer systems and the recharge for the total island were calculated by summing the values of the model subareas located within their respective boundaries.

Effects of Drought and Reduced Cloud-Water Interception on Soil Moisture, Evapotranspiration, and Climatic Water Deficit

A separate reference condition was developed for assessing the effects of soil moisture, ET, and CWD because the time period for the available dataset of gridded maps of daily rainfall needed for the WATMod simulations only covers 18 years (1990–2007) of the 30-year period used for the 1978–2007 scenario from Kāne and others (2024a). For soil moisture, ET, and CWD, a reference condition consisting of the non-drought periods during the 1990–2012 simulation period, including rainfall during 1990–97 and 2003–06, and 2020 land cover, hereinafter Non-Drought scenario, was developed (table 5). Island-wide mean annual rainfall for the Non-Drought scenario is between 0.5 and 8 percent greater on Kaua‘i, O‘ahu, Moloka‘i, and the Island of Hawai‘i, and 0.6 percent less on Maui, relative to the 1978–2007 scenario (table 4).

Four water-budget scenarios were developed to quantify the effects of drought on soil moisture, ET, and CWD for each island as follows:

1. A reference condition, the Non-Drought scenario, consisting of rainfall conditions during 1990–97 and 2003–06 and 2020 land cover;
2. Rainfall conditions representative of the driest periods during 1920–2012 and 2020 land cover;
3. Rainfall conditions representative of non-drought conditions during a future dry-climate condition and 2020 land cover; and
4. Rainfall conditions representative of the driest periods during a future dry-climate condition and 2020 land cover.

Rainfall conditions during 1998–2002 and 2007–12 (hereinafter Drought 3 rainfall) were selected to represent the driest periods during 1920–2012 and used with 2020 land cover (hereinafter Drought 3 scenario) (table 5). Rainfall conditions during 1990–97 and 2003–06 adjusted for a RCP8.5 2071–99 projection (hereinafter RCP8.5 2071–99 Non-Drought rainfall) were selected to represent non-drought conditions during the future dry-climate condition and used with 2020 land cover (hereinafter Future Non-Drought scenario). Island-wide mean annual rainfall for the Future Non-Drought scenario is between 14 and 22 percent less on Kaua‘i, O‘ahu, Moloka‘i, Maui, and the Island of Hawai‘i, relative to the 1978–2007 scenario (table 4). Finally, rainfall conditions during 1998–2002 and 2007–12 adjusted for a RCP8.5 2071–99 projection (hereinafter RCP8.5 2071–99 Drought 3 rainfall) were selected to represent the driest periods during the future dry-climate condition and used with 2020 land cover (hereinafter Future Drought 3 scenario) (table 5).

For O‘ahu, Maui, and the Island of Hawai‘i, a total of six additional water-budget scenarios (table 5) were developed to quantify the added effects of drought and reduced CWI on soil moisture, ET, and CWD as follows:

1. Drought 3 rainfall and Conversion 1 land cover (hereinafter Drought 3 Conversion 1 scenario),
2. Drought 3 rainfall and Conversion 2 land cover (hereinafter Drought 3 Conversion 2 scenario),
3. RCP8.5 2071–99 Non-Drought rainfall and Conversion 1 land cover (hereinafter Future Non-Drought Conversion 1 scenario),
4. RCP8.5 2071–99 Non-Drought rainfall and Conversion 2 land cover (hereinafter Future Non-Drought Conversion 2 scenario),
5. RCP8.5 2071–99 Drought 3 rainfall and Conversion 1 land cover (hereinafter Future Drought 3 Conversion 1 scenario), and
6. RCP8.5 2071–99 Drought 3 rainfall and Conversion 2 land cover (hereinafter Future Drought 3 Conversion 2 scenario).

A 23-year sequential simulation period was used for each water-budget scenario to produce a time series of monthly soil moisture, ET, and CWD estimates for each model subarea. For each scenario using Non-Drought rainfall, the time series of monthly values during 1990–97 and 2003–06 were grouped together for the frequency analysis. For each scenario using Drought 3 rainfall, the time series of monthly values during 1998–2002 and 2007–12 were grouped together for the frequency analysis. For each scenario using RCP8.5 2071–99 Non-Drought rainfall, the time series of monthly values from years 1–8 and 14–17 in the WATRMd simulations were grouped together for the frequency analysis. Finally, for each scenario using RCP8.5 2071–99 Drought 3 rainfall, the time series of monthly values from years 9–13 and 18–23 in the WATRMd simulations were grouped together for the frequency analysis. Monthly estimates within each group of water-budget model results were used to characterize the frequency characteristics of soil moisture, ET, and CWD for selected moisture-stress levels (see “Soil Moisture, Evapotranspiration, and Climatic Water Deficit Frequency Characterization” section).

Groundwater-Recharge Estimates

WATRMd was used to compute groundwater recharge for a set of drought conditions for Kauaʻi, Oʻahu, Molokaʻi, Maui, and the Island of Hawaiʻi. A set of hypothetical land-cover conditions was added for Oʻahu, Maui, and the Island of Hawaiʻi to assess the effect of reduced CWI on groundwater recharge during drought conditions. WATRMd recharge estimates for each water-budget scenario were compared with estimates for a reference condition consisting of 1978–2007 rainfall and 2020 land cover (1978–2007 scenario) (table 5).

Effects of Drought

Two water-budget scenarios were selected for each island as follows: (1) Drought 1 scenario for Kauaʻi, Oʻahu, and Molokaʻi, and Drought 2 scenario for Maui and the Island of Hawaiʻi, and (2) Future Drought 1 scenario for Kauaʻi, Oʻahu, and Molokaʻi, and Future Drought 2 scenario for Maui and the Island of Hawaiʻi (table 5). Estimates of island-wide groundwater recharge for the 1978–2007 scenario and two water-budget scenarios are shown in table 6 and summarized by subarea in Mair (2024b).

Kauaʻi

Island-wide mean annual rainfall for the Drought 1 scenario is less than rainfall for the 1978–2007 scenario by 480 Mgal/d (22 percent) (table 4). These changes in rainfall correspond to a decrease in island-wide mean annual recharge of 239 Mgal/d (30 percent) (table 6). Mean annual recharge is estimated to decrease across most of Kauaʻi for the Drought 1 scenario (fig. 8.4). The greatest decrease in recharge occurs across many parts of the upland regions of central Kauaʻi where recharge decreases by more than 15 inches. Small regions in the upland area of Kīlauea aquifer system show

slight increases in recharge (0.1 to 5 inches). This region of Kauaʻi has relatively low mean recharge (fig. 5.4), where episodic recharge events caused by more intense daily rainfall during dry periods or drought can result in slight increases in mean recharge. Decreases in aquifer-system recharge are estimated for all of Kauaʻi’s aquifer systems for the Drought 1 scenario (fig. 9.4). In terms of absolute difference in mean annual recharge, the greatest decreases in aquifer-system recharge are estimated for the Waimea, Wailua, and Makaweli aquifer systems, where decreases range from 28 to 29 Mgal/d relative to recharge for the 1978–2007 scenario. In terms of percentage change from the 1978–2007 scenario, the greatest decreases in aquifer-system recharge are estimated for the Kīlauea, Anahola, Hanamāʻulu, and Kekaha aquifer systems, where decreases range from 44 to 54 percent.

Island-wide mean annual rainfall for the Future Drought 1 scenario is less than rainfall for the 1978–2007 scenario by 849 Mgal/d (38 percent) (table 4). These changes in rainfall correspond to a decrease in island-wide mean annual recharge of 373 Mgal/d (46 percent) (table 6). Mean annual recharge is estimated to decrease across most of Kauaʻi for the Future Drought 1 scenario relative to the 1978–2007 scenario (fig. 8.8). The greatest decrease in recharge occurs across a small upland region of Waimea and Makaweli aquifer systems where recharge decreases by more than 50 inches. Small, isolated regions near the southeast coast of the island show slight increases in recharge (0.1 to 5 inches) due to increases in irrigation for golf courses. Decreases in aquifer-system recharge are estimated for all of Kauaʻi’s aquifer systems (fig. 9.8). In terms of absolute difference in mean annual recharge, the greatest decreases in aquifer-system recharge are estimated for the Waimea and Makaweli aquifer systems, where decreases range from 50 to 57 Mgal/d relative to recharge for the 1978–2007 scenario. In terms of percentage change from the 1978–2007 scenario, the greatest decreases in aquifer-system recharge are estimated for the Kīlauea, Kekaha, and Nāpali aquifer systems, where decreases range from 62 to 88 percent.

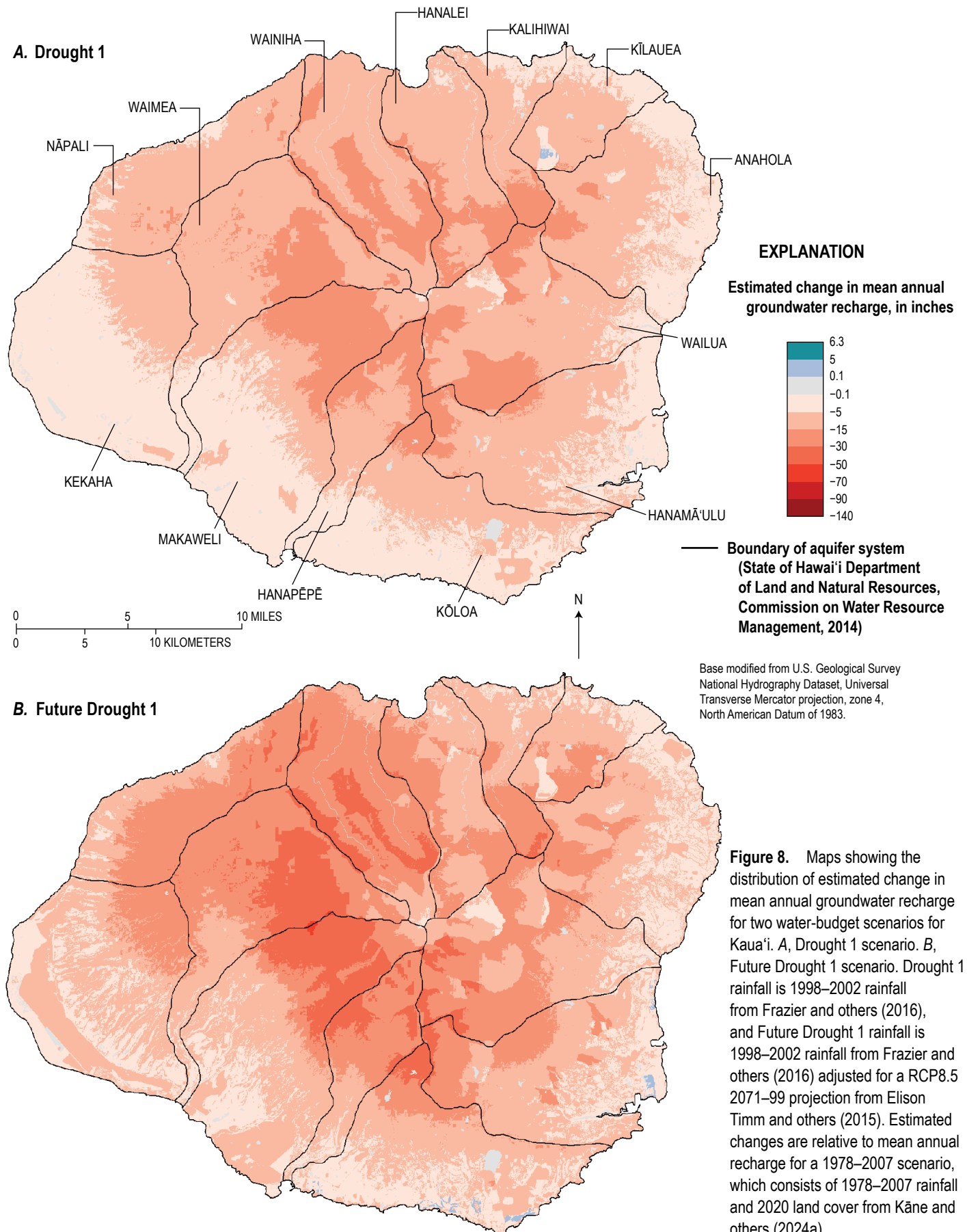
Oʻahu

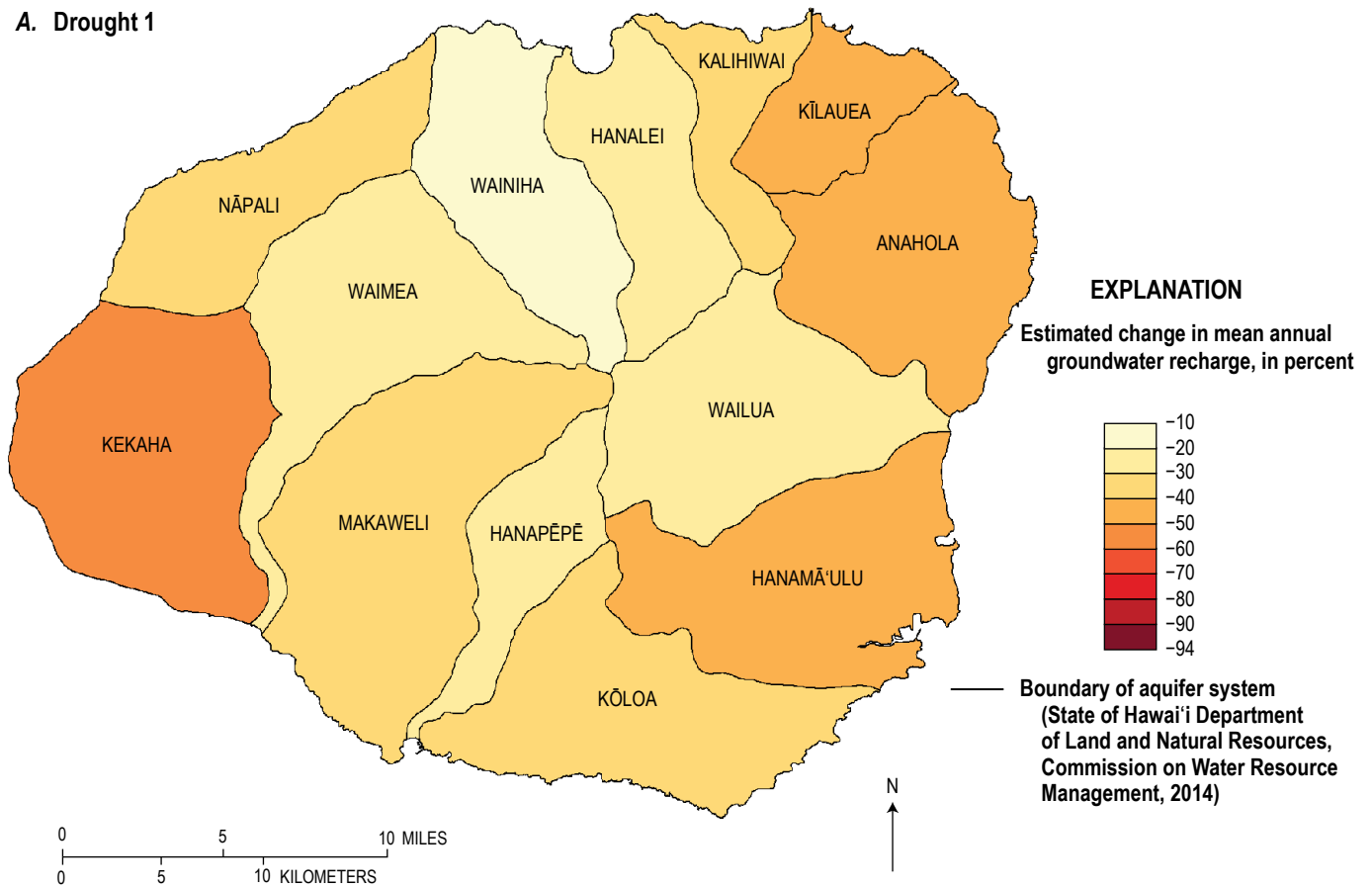
Island-wide mean annual rainfall for the Drought 1 scenario is less than rainfall for the 1978–2007 scenario by 473 Mgal/d (26 percent) (table 4). These changes in rainfall correspond to a decrease in island-wide mean annual recharge of 201 Mgal/d (34 percent) (table 6). Mean annual recharge is estimated to decrease across most of Oʻahu (fig. 10.4). The greatest decrease in recharge occurs across an upland region of Koʻolauloa aquifer system where recharge decreases by more than 30 inches. Small, isolated regions around the island show slight increases in recharge (0.1 to 5 inches) due to increased irrigation for golf courses. Decreases in aquifer-system recharge are estimated for all of Oʻahu’s aquifer systems (fig. 11.4). In terms of absolute difference in mean annual recharge, the greatest decreases in aquifer-system recharge are estimated for the Koʻolauloa, Wahiawa, and Waipahu-Waiawa

Table 6. Mean annual groundwater recharge and change in recharge relative to 1978–2007 scenario for Kauaʻi, Oʻahu, Molokaʻi, Maui, and the Island of Hawaiʻi.

[Mgal/d, million gallons per day; --, not applicable; RCP8.5, Representative Concentration Pathway warming scenario with total radiative forcing of 8.5 watts per square meter by the year 2100 from Intergovernmental Panel on Climate Change (2014); Conversion 1 land cover is land-cover condition in which roughly 50 percent of shrubland and forest areas within the cloud zone are converted to grassland; Conversion 2 land cover is land-cover condition in which 100 percent of shrubland and forest areas within the cloud zone are converted to grassland; 1978–2007 scenario is reference condition from Kāne and others (2024a) and consists of 1978–2007 rainfall from Frazier and others (2016), and 2020 land cover; Drought 1 scenario is 1998–2002 rainfall from Frazier and others (2016), and 2020 land cover; Drought 1 Conversion 1 scenario is 1998–2002 rainfall from Frazier and others (2016), and Conversion 1 land cover; Drought 1 Conversion 2 scenario is 1998–2002 rainfall from Frazier and others (2016), and Conversion 2 land cover; Drought 2 scenario is 2007–12 rainfall from Frazier and others (2016), and 2020 land cover; Drought 2 Conversion 1 scenario is 2007–12 rainfall from Frazier and others (2016), and Conversion 1 land cover; Drought 2 Conversion 2 scenario is 2007–12 rainfall from Frazier and others (2016), and Conversion 2 land cover; Future Drought 1 scenario is 1998–2002 rainfall from Frazier and others (2016) adjusted for a RCP8.5 2071–99 projection from Elison Timm and others (2015), and 2020 land cover; Future Drought 1 Conversion 1 scenario is 1998–2002 rainfall from Frazier and others (2016) adjusted for a RCP8.5 2071–99 projection from Elison Timm and others (2015), and Conversion 1 land cover; Future Drought 1 Conversion 2 scenario is 1998–2002 rainfall from Frazier and others (2016) adjusted for a RCP8.5 2071–99 projection from Elison Timm and others (2015), and Conversion 2 land cover; Future Drought 2 scenario is 2007–12 rainfall from Frazier and others (2016) adjusted for a RCP8.5 2071–99 projection from Elison Timm and others (2015), and 2020 land cover; Future Drought 2 Conversion 1 scenario is 2007–12 rainfall from Frazier and others (2016) adjusted for a RCP8.5 2071–99 projection from Elison Timm and others (2015), and Conversion 1 land cover; Future Drought 2 Conversion 2 scenario is 2007–12 rainfall from Frazier and others (2016) adjusted for a RCP8.5 2071–99 projection from Elison Timm and others (2015), and Conversion 2 land cover. Some recharge may discharge to streams as base flow.]

Water-budget scenario	Kauaʻi		Oʻahu		Molokaʻi		Maui		Island of Hawaiʻi	
	Recharge, in Mgal/d	Change in recharge, in percent (change in Mgal/d)	Recharge, in Mgal/d	Change in recharge, in percent (change in Mgal/d)	Recharge, in Mgal/d	Change in recharge, in percent (change in Mgal/d)	Recharge, in Mgal/d	Change in recharge, in percent (change in Mgal/d)	Recharge, in Mgal/d	Change in recharge, in percent (change in Mgal/d)
1978–2007	806.77	--	597.06	--	228.22	--	1,192.34	--	6,885.38	--
Drought 1	568.26	–30 (–238.51)	395.86	–34 (–201.20)	145.31	–36 (–82.91)	--	--	--	--
Drought 1 Conversion 1	--	--	389.82	–35 (–207.24)	--	--	--	--	--	--
Drought 1 Conversion 2	--	--	383.73	–36 (–213.33)	--	--	--	--	--	--
Drought 2	--	--	--	--	--	--	798.50	–33 (–393.84)	4,179.03	–39 (–2,706.35)
Drought 2 Conversion 1	--	--	--	--	--	--	730.89	–39 (–461.45)	3,755.97	–45 (–3,129.41)
Drought 2 Conversion 2	--	--	--	--	--	--	663.28	–44 (–529.06)	3,329.81	–52 (–3,555.57)
Future Drought 1	433.32	–46 (–373.45)	316.47	–47 (–280.59)	112.57	–51 (–115.65)	--	--	--	--
Future Drought 1 Conversion 1	--	--	311.09	–48 (–285.97)	--	--	--	--	--	--
Future Drought 1 Conversion 2	--	--	305.67	–49 (–291.39)	--	--	--	--	--	--
Future Drought 2	--	--	--	--	--	--	715.24	–40 (–477.10)	3,670.06	–47 (–3,215.32)
Future Drought 2 Conversion 1	--	--	--	--	--	--	655.77	–45 (–536.57)	3,327.09	–52 (–3,558.29)
Future Drought 2 Conversion 2	--	--	--	--	--	--	595.95	–50 (–596.39)	2,980.67	–57 (–3,904.71)



A. Drought 1

Base modified from U.S. Geological Survey
National Hydrography Dataset, Universal
Transverse Mercator projection, zone 4,
North American Datum of 1983.

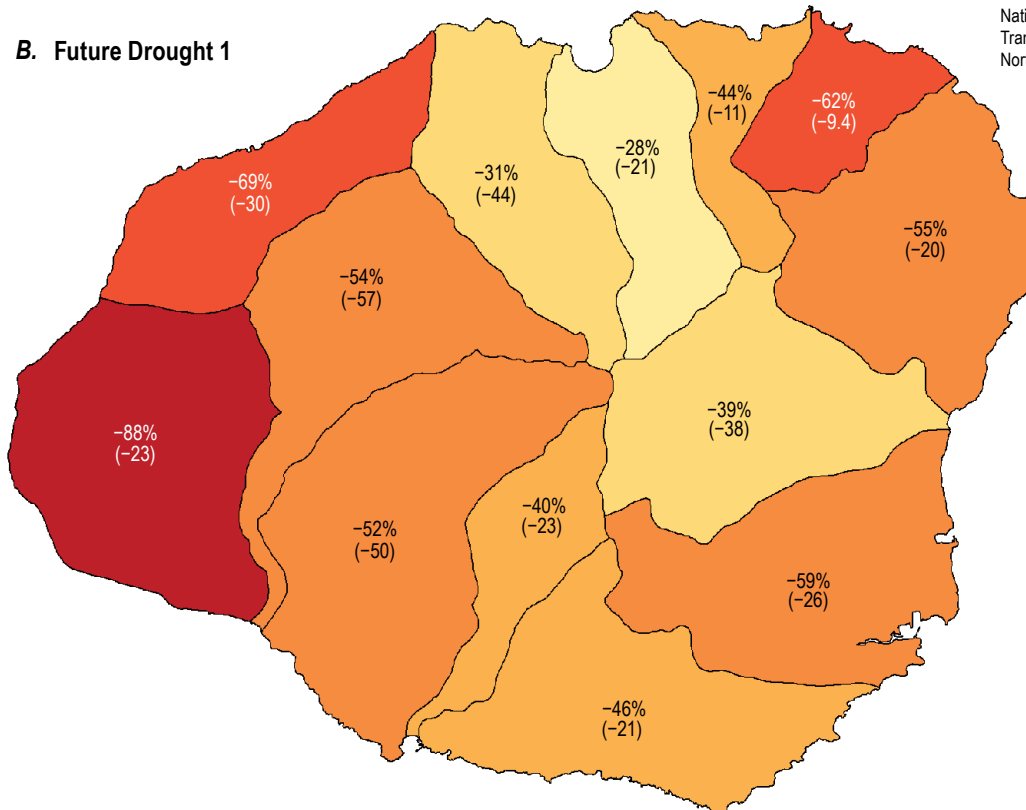
B. Future Drought 1

Figure 9. Maps showing the estimated change in mean annual groundwater recharge by aquifer system for two water-budget scenarios for Kaua'i. *A.* Drought 1 scenario. *B.* Future Drought 1 scenario. Drought 1 rainfall is 1998–2002 rainfall from Frazier and others (2016) and Future Drought 1 rainfall is 1998–2002 rainfall from Frazier and others (2016) adjusted for a RCP8.5 2071–99 projection from Elison Timm and others (2015). Estimated changes are relative to mean annual recharge for a 1978–2007 scenario, which consists of 1978–2007 rainfall and 2020 land cover from Kāne and others (2024a). Values in parentheses represent change in million gallons per day. %, percent.

aquifer systems, where decreases range from 21 to 29 Mgal/d relative to recharge for the 1978–2007 scenario. In terms of percentage change from the 1978–2007 scenario, the greatest decreases in aquifer-system recharge are estimated for the Mokulē‘ia, Kea‘au, Wai‘anae, Lualualei, Nānākuli, Makaīwa,

‘Ewa-Kunia, and Wai‘alae-East aquifer systems, where decreases range from 61 to 68 percent.

Island-wide mean annual rainfall for the Future Drought 1 scenario is less than rainfall for the 1978–2007 scenario by 754 Mgal/d (42 percent) (table 4). These changes in rainfall

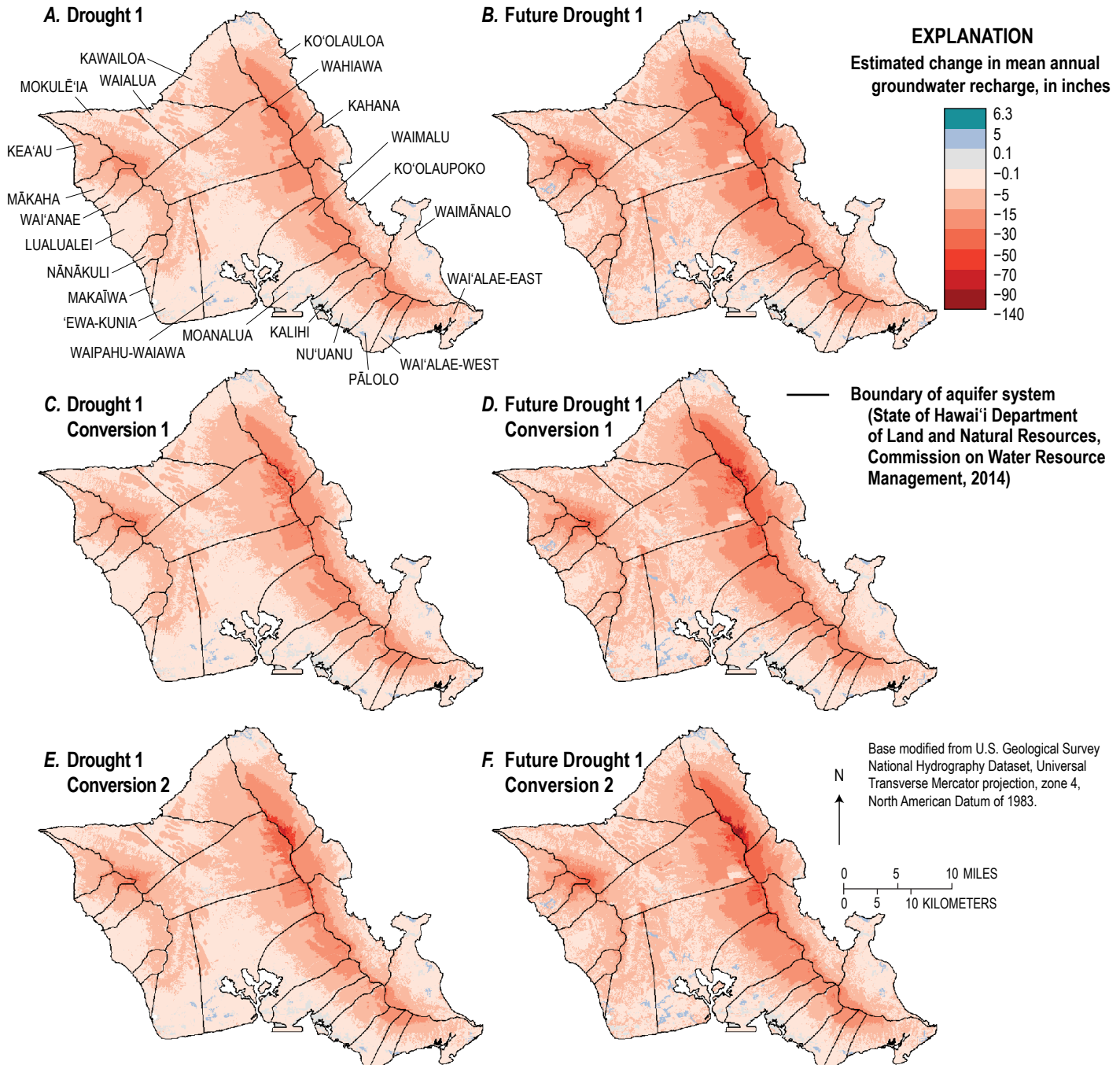


Figure 10. Maps showing the distribution of estimated change in mean annual groundwater recharge for six water-budget scenarios for O‘ahu. A, Drought 1 scenario. B, Future Drought 1 scenario. C, Drought 1 Conversion 1 scenario. D, Future Drought 1 Conversion 1 scenario. E, Drought 1 Conversion 2 scenario. F, Future Drought 1 Conversion 2 scenario. Drought 1 rainfall is 1998–2002 rainfall from Frazier and others (2016) and Future Drought 1 rainfall is 1998–2002 rainfall from Frazier and others (2016) adjusted for a RCP8.5 2071–99 projection from Elison Timm and others (2015). Conversion 1 land cover is land-cover condition in which roughly 50 percent of shrubland and forest areas within the cloud zone are converted to grassland; Conversion 2 land cover is land-cover condition in which 100 percent of shrubland and forest areas within the cloud zone are converted to grassland. Estimated changes are relative to mean annual recharge for a 1978–2007 scenario, which consists of 1978–2007 rainfall and 2020 land cover from Kāne and others (2024a).

correspond to a decrease in island-wide mean annual recharge of 281 Mgal/d (47 percent) (table 6). Mean annual recharge is estimated to decrease across most of O'ahu (fig. 10B). The greatest decrease in recharge occurs across an upland region of Ko'olauloa aquifer system where recharge decreases by more

than 50 inches. Small, isolated regions around the island show slight increases in recharge (0.1 to 5 inches) due to increased irrigation for golf courses. Decreases in aquifer-system recharge are estimated for all of O'ahu's aquifer systems (fig. 11B). In terms of absolute difference in mean annual

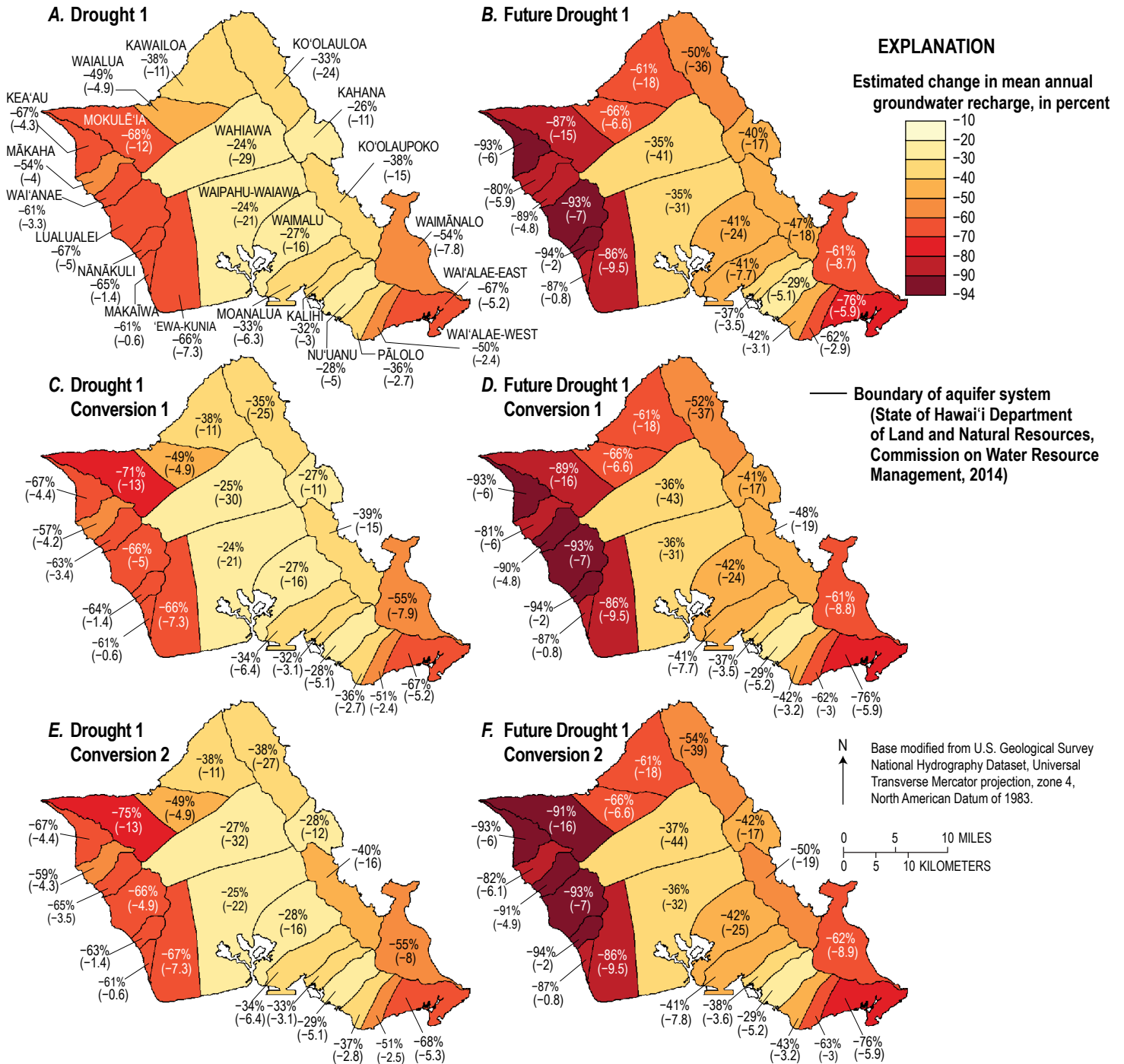


Figure 11. Maps showing the estimated change in mean annual groundwater recharge by aquifer system for six water-budget scenarios for O'ahu. A, Drought 1 scenario. B, Future Drought 1 scenario. C, Drought 1 Conversion 1 scenario. D, Future Drought 1 Conversion 1 scenario. E, Drought 1 Conversion 2 scenario. F, Future Drought 1 Conversion 2 scenario. Drought 1 is 1998–2002 rainfall from Frazier and others (2016) and Future Drought 1 rainfall is 1998–2002 rainfall from Frazier and others (2016) adjusted for a RCP8.5 2071–99 projection from Elison Timm and others (2015). Conversion 1 land cover is land-cover condition in which roughly 50 percent of shrubland and forest areas within the cloud zone are converted to grassland; Conversion 2 land cover is land-cover condition in which 100 percent of shrubland and forest areas within the cloud zone are converted to grassland. Estimated changes are relative to mean annual recharge for a 1978–2007 scenario, which consists of 1978–2007 rainfall and 2020 land cover from Kāne and others (2024a). Values in parentheses represent change in million gallons per day. %, percent.

recharge, the greatest decreases in aquifer-system recharge are estimated for the Koʻolauloa, Wahiawa, and Waipahu-Waiawa aquifer systems, where decreases range from 31 to 41 Mgal/d relative to recharge for the 1978–2007 scenario. In terms of percentage change from the 1978–2007 scenario, the greatest decreases in aquifer-system recharge are estimated for the Keaʻau, Lualualei, and Nānākuli aquifer systems, where decreases range from 93 to 94 percent.

Molokaʻi

Island-wide mean annual rainfall for the Drought 1 scenario is less than rainfall for the 1978–2007 scenario by 158 Mgal/d (26 percent) (table 4). These changes in rainfall correspond to a decrease in island-wide mean annual recharge of 83 Mgal/d (36 percent) (table 6). Mean annual recharge is estimated to decrease across most of Molokaʻi for the Drought

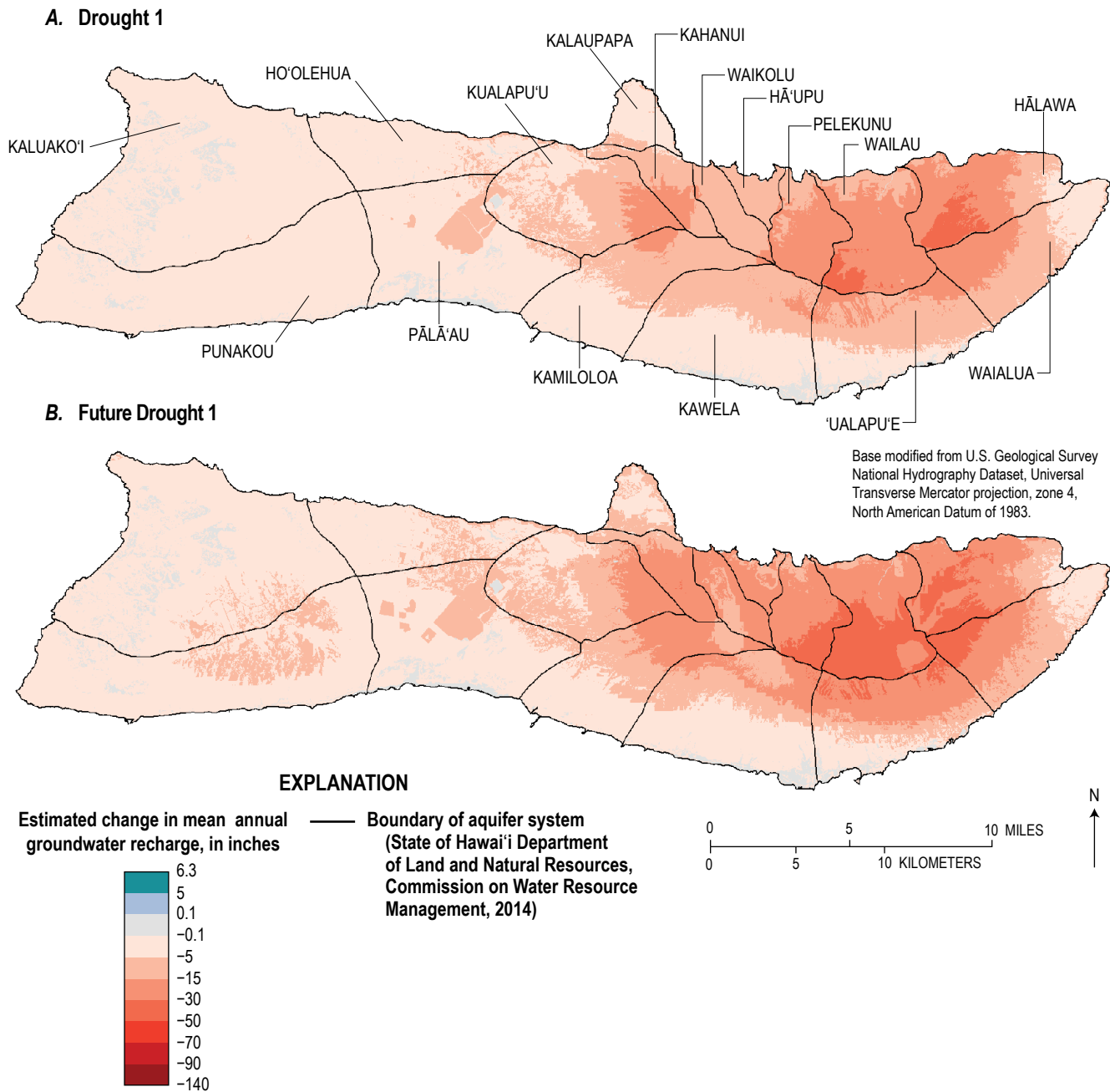


Figure 12. Maps showing the distribution of estimated change in mean annual groundwater recharge for two water-budget scenarios for Molokaʻi. *A*, Drought 1 scenario. *B*, Future Drought 1 scenario. Drought 1 rainfall is 1998–2002 rainfall from Frazier and others (2016) and Future Drought 1 rainfall is 1998–2002 rainfall from Frazier and others (2016) adjusted for a RCP8.5 2071–99 projection from Elison Timm and others (2015). Estimated changes are relative to mean annual recharge for a 1978–2007 scenario, which consists of 1978–2007 rainfall and 2020 land cover from Kāne and others (2024a).

1 scenario (fig. 12A). The greatest decrease in recharge occurs across the upland regions of Wailau and Hālawā aquifer systems where recharge decreases by more than 30 inches. Decreases in aquifer-system recharge are estimated for all of Molokaʻi's aquifer systems for the Drought 1 scenario (fig. 13A). In terms of absolute difference in mean annual recharge, the greatest decreases in aquifer-system recharge are estimated for the Wailau and Hālawā aquifer systems, where

decreases range from 12 to 13 Mgal/d relative to recharge for the 1978–2007 scenario. In terms of percentage change from the 1978–2007 scenario, the greatest decreases in aquifer-system recharge are estimated for the Hoʻolehūa and Pālāʻau aquifer systems, where decreases range from 64 to 66 percent.

Island-wide mean annual rainfall for the Future Drought 1 scenario is less than rainfall for the 1978–2007 scenario by 255 Mgal/d (42 percent) (table 4). These changes in rainfall

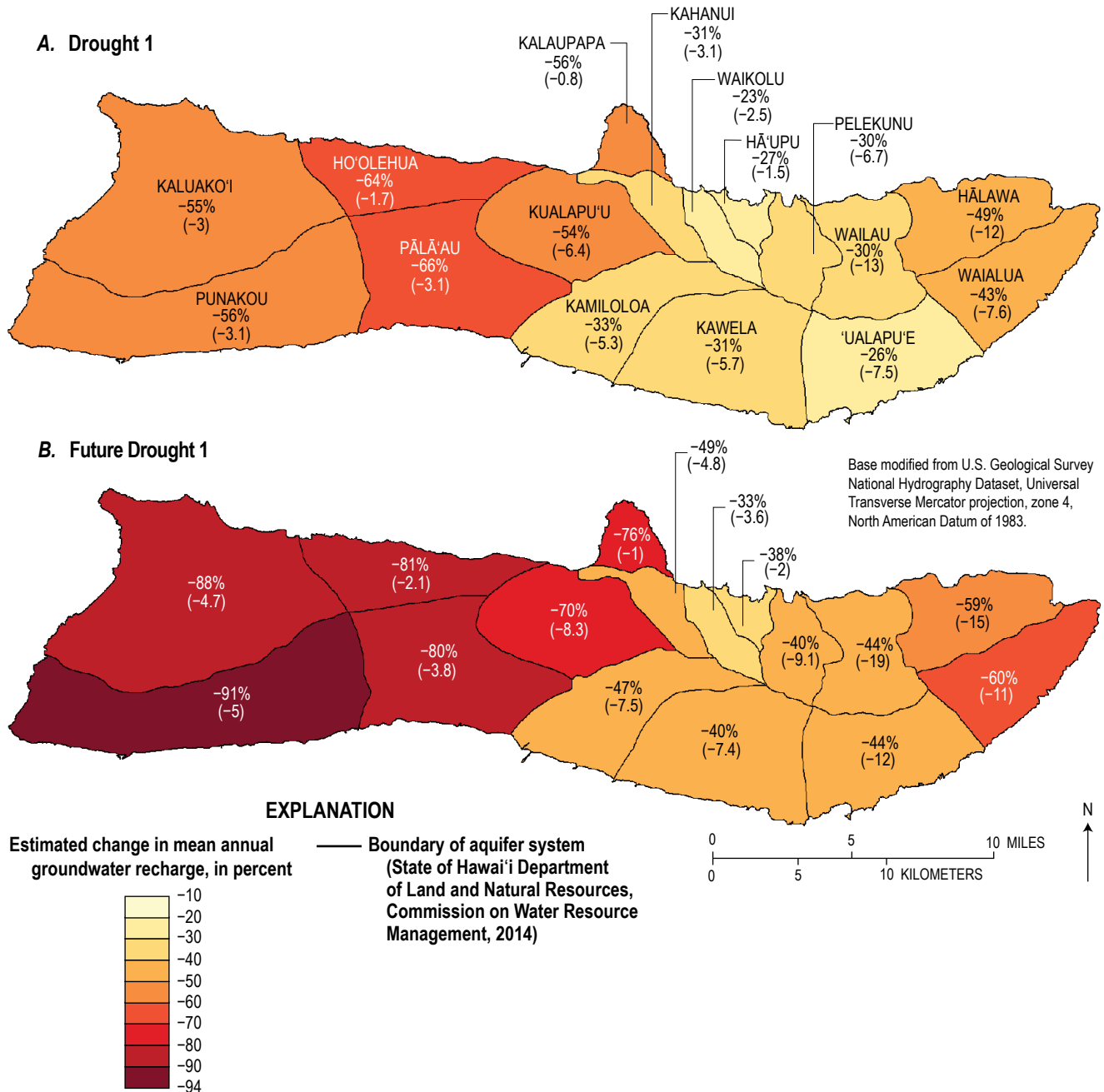


Figure 13. Maps showing the estimated change in mean annual groundwater recharge by aquifer system for two water-budget scenarios for Molokaʻi. A, Drought 1 scenario. B, Future Drought 1 scenario. Drought 1 rainfall is 1998–2002 rainfall from Frazier and others (2016) and Future Drought 1 rainfall is 1998–2002 rainfall from Frazier and others (2016) adjusted for a RCP8.5 2071–99 projection from Elison Timm and others (2015). Estimated changes are relative to mean annual recharge for a 1978–2007 scenario, which consists of 1978–2007 rainfall and 2020 land cover from Kāne and others (2024a). Values in parentheses represent change in million gallons per day. %, percent.

correspond to a decrease in island-wide mean annual recharge of 116 Mgal/d (51 percent) (table 6). Mean annual recharge is estimated to decrease across most of Molokaʻi (fig. 12B). The greatest decrease in recharge occurs across upland areas of Pelekunu, Wailau, Hālawā, Waialua, and ʻUalapuʻe aquifer systems where recharge decreases by more than 30 inches. Decreases in aquifer-system recharge are estimated for all of Molokaʻi's aquifer systems (fig. 13B). In terms of absolute difference in mean annual recharge, the greatest decreases in aquifer-system recharge are estimated for the Wailau and Hālawā aquifer systems, where decreases range from 15 to 19 Mgal/d relative to recharge for the 1978–2007 scenario. In terms of percentage change from the 1978–2007 scenario, the greatest decreases in aquifer-system recharge are estimated for the Kaluakoʻi, Hoʻolehua, Pālāʻau, and Punakou aquifer systems, where decreases range from 80 to 91 percent.

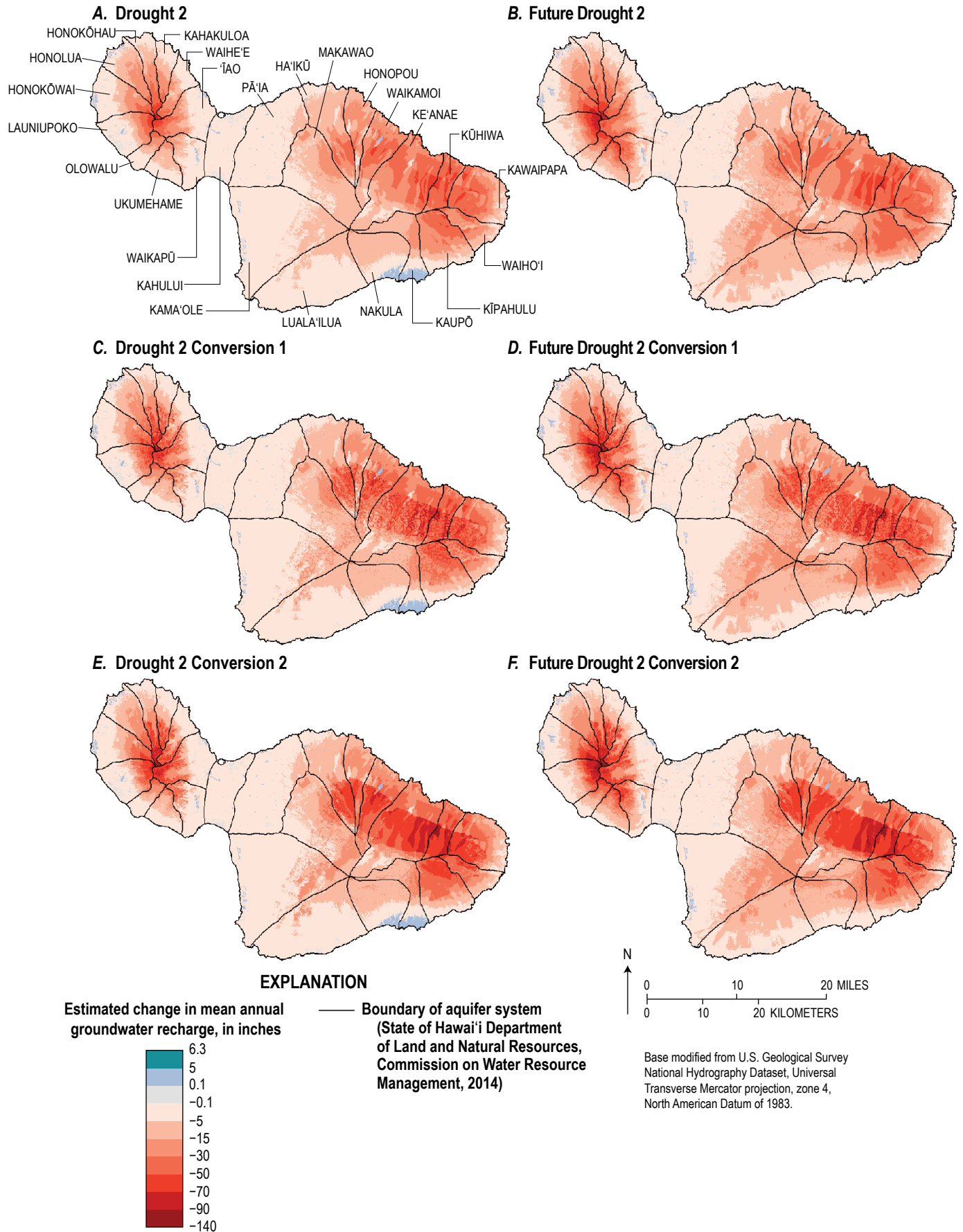
Maui

Island-wide mean annual rainfall for the Drought 2 scenario is less than rainfall for the 1978–2007 scenario by 859 Mgal/d (31 percent) (table 4). These changes in rainfall correspond to a decrease in island-wide mean annual recharge of 394 Mgal/d (33 percent) (table 6). Mean annual recharge is estimated to decrease across most of Maui (fig. 14A). The greatest decrease in recharge occurs across upland regions of Honokōhau and Kūhiwa aquifer systems where recharge decreases by more than 70 inches. Small, isolated regions around the island show slight increases in recharge (0.1 to 6.3 inches) due to increased irrigation for golf courses and more intense daily rainfall in low-recharge

areas. Decreases in aquifer-system recharge are estimated for all of Maui's aquifer systems (fig. 15A). In terms of absolute difference in mean annual recharge, the greatest decreases in aquifer-system recharge are estimated for the Keʻanae and Kawaipapa aquifer systems, where decreases range from 39 to 67 Mgal/d relative to recharge for the 1978–2007 scenario. In terms of percentage change from the 1978–2007 scenario, the greatest decreases in aquifer-system recharge are estimated for the Lualaʻilua and Makawao aquifer systems, where decreases range from 49 to 50 percent.

Island-wide mean annual rainfall for the Future Drought 2 scenario is less than rainfall for the 1978–2007 scenario by 1,105 Mgal/d (39 percent) (table 4). These changes in rainfall correspond to a decrease in island-wide mean annual recharge of 477 Mgal/d (40 percent) (table 6). Mean annual recharge is estimated to decrease across most of Maui (fig. 14B). The greatest decrease in recharge occurs across an upland region of Launiupoko aquifer system where recharge decreases by more than 90 inches. Small, isolated regions around the island show slight increases in recharge (0.1–5 inches) owing mainly to increased irrigation for golf courses. Decreases in aquifer-system recharge are estimated for all of Maui's aquifer systems (fig. 15B). In terms of absolute difference in mean annual recharge, the greatest decreases in aquifer-system recharge are estimated for the Keʻanae and Kawaipapa aquifer systems, where decreases range from 37 to 73 Mgal/d relative to recharge for the 1978–2007 scenario. In terms of percentage change from the 1978–2007 scenario, the greatest decreases in aquifer-system recharge are estimated for the Ukumehame, Kamaʻole, and Lualaʻilua aquifer systems, where decreases range from 81 to 85 percent.

Figure 14. Maps showing the distribution of estimated change in mean annual groundwater recharge for six water-budget scenarios for Maui. A, Drought 2 scenario. B, Future Drought 2 scenario. C, Drought 2 Conversion 1 scenario. D, Future Drought 2 Conversion 1 scenario. E, Drought 2 Conversion 2 scenario. F, Future Drought 2 Conversion 2 scenario. Drought 2 rainfall is 2007–12 rainfall from Frazier and others (2016) and Future Drought 2 rainfall is 2007–12 rainfall from Frazier and others (2016) adjusted for a RCP8.5 2071–99 projection from Elison Timm and others (2015). Conversion 1 land cover is land-cover condition in which roughly 50 percent of shrubland and forest areas within the cloud zone are converted to grassland; Conversion 2 land cover is land-cover condition in which 100 percent of shrubland and forest areas within the cloud zone are converted to grassland. Estimated changes are relative to mean annual recharge for a 1978–2007 scenario, which consists of 1978–2007 rainfall and 2020 land cover from Kāne and others (2024a).



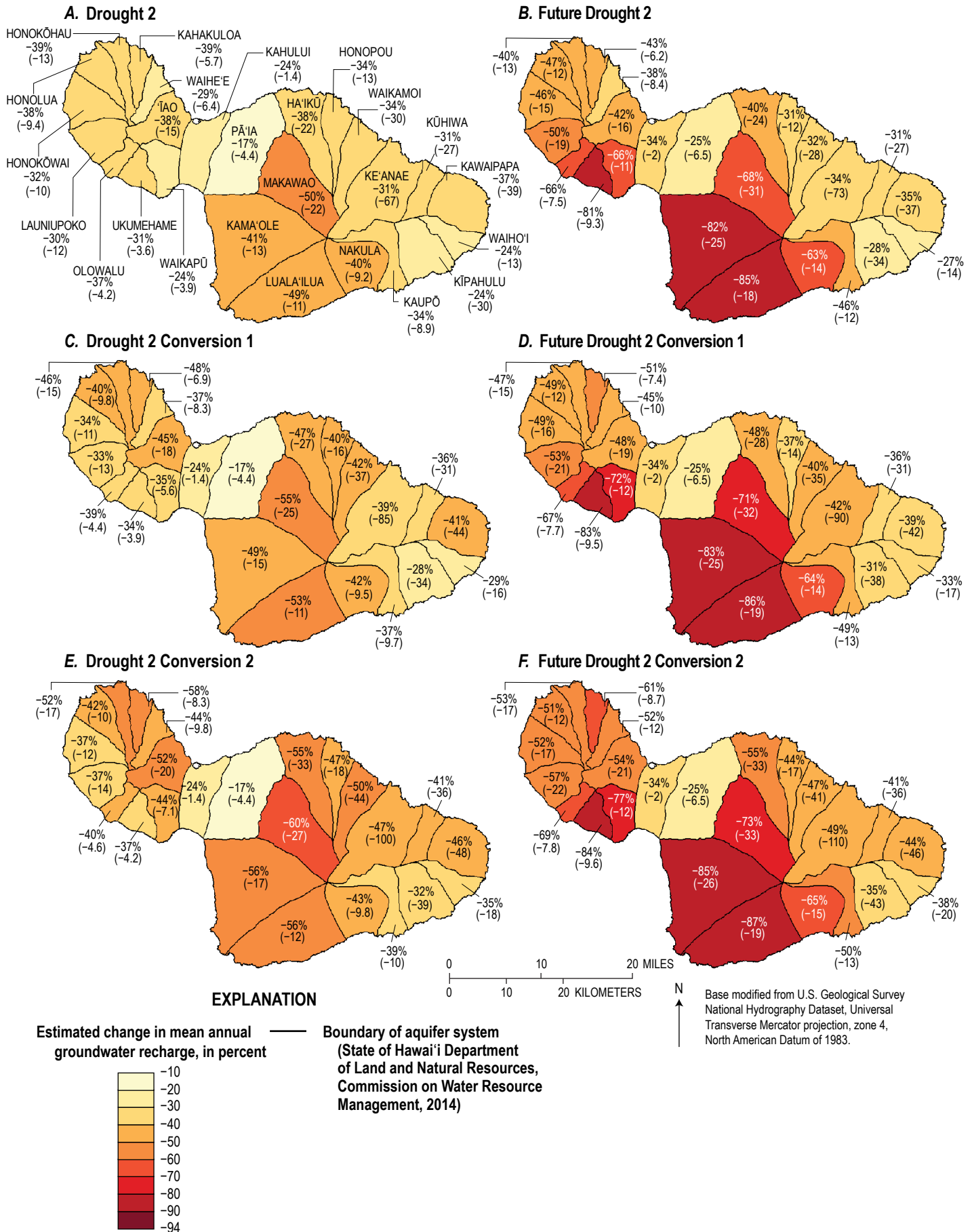


Figure 15. Maps showing the estimated change in mean annual groundwater recharge by aquifer system for six water-budget scenarios for Maui. A, Drought 2 scenario. B, Future Drought 2 scenario. C, Drought 2 Conversion 1 scenario. D, Future Drought 2 Conversion 1 scenario. E, Drought 2 Conversion 2 scenario. F, Future Drought 2 Conversion 2 scenario. Drought 2 rainfall is 2007–12 rainfall from Frazier and others (2016) and Future Drought 2 rainfall is 2007–12 rainfall from Frazier and others (2016) adjusted for a RCP8.5 2071–99 projection from Elison Timm and others (2015). Conversion 1 land cover is land-cover condition in which roughly 50 percent of shrubland and forest areas within the cloud zone are converted to grassland; Conversion 2 land cover is land-cover condition in which 100 percent of shrubland and forest areas within the cloud zone are converted to grassland. Estimated changes are relative to mean annual recharge for a 1978–2007 scenario, which consists of 1978–2007 rainfall and 2020 land cover from Kāne and others (2024a). Values in parentheses represent change in million gallons per day. %, percent.

Island of Hawai‘i

Island-wide mean annual rainfall for the Drought 2 scenario is less than rainfall for the 1978–2007 scenario by 4,182 Mgal/d (30 percent) (table 4). These changes in rainfall correspond to a decrease in island-wide mean annual recharge of 2,706 Mgal/d (39 percent) (table 6). Mean annual recharge is estimated to decrease across most of the Island of Hawai‘i (fig. 16A). The greatest decrease in recharge occurs across upland regions of Hakalau and Onomea aquifer systems where recharge decreases by more than 90 inches. Decreases in aquifer-system recharge are estimated for all of the aquifer systems on the Island of Hawai‘i (fig. 17A). In terms of absolute difference in mean annual recharge, the greatest decreases in aquifer-system recharge are estimated for the Hakalau, Onomea, Kea‘au, and Nā‘ālehu aquifer systems, where decreases range from 248 to 357 Mgal/d relative to recharge for the 1978–2007 scenario. In terms of percentage change from the 1978–2007 scenario, the greatest decrease in aquifer-system recharge is estimated for the Waimea aquifer systems, where a decrease of 74 percent is estimated.

Island-wide mean annual rainfall for the Future Drought 2 scenario is less than rainfall for the 1978–2007 scenario by 5,372 Mgal/d (39 percent) (table 4). These changes in rainfall correspond to a decrease in island-wide mean annual recharge of 3,215 Mgal/d (47 percent) (table 6). Mean annual recharge is estimated to decrease across most of the Island of Hawai‘i (fig. 16B). The greatest decrease in recharge occurs across upland regions of Hakalau, Onomea, Kea‘au, and Ōla‘a aquifer systems where recharge decreases by more than 70 inches. Decreases in aquifer-system recharge are estimated for all of the aquifer systems on the Island of Hawai‘i (fig. 17B). In terms of absolute difference in mean annual recharge, the greatest

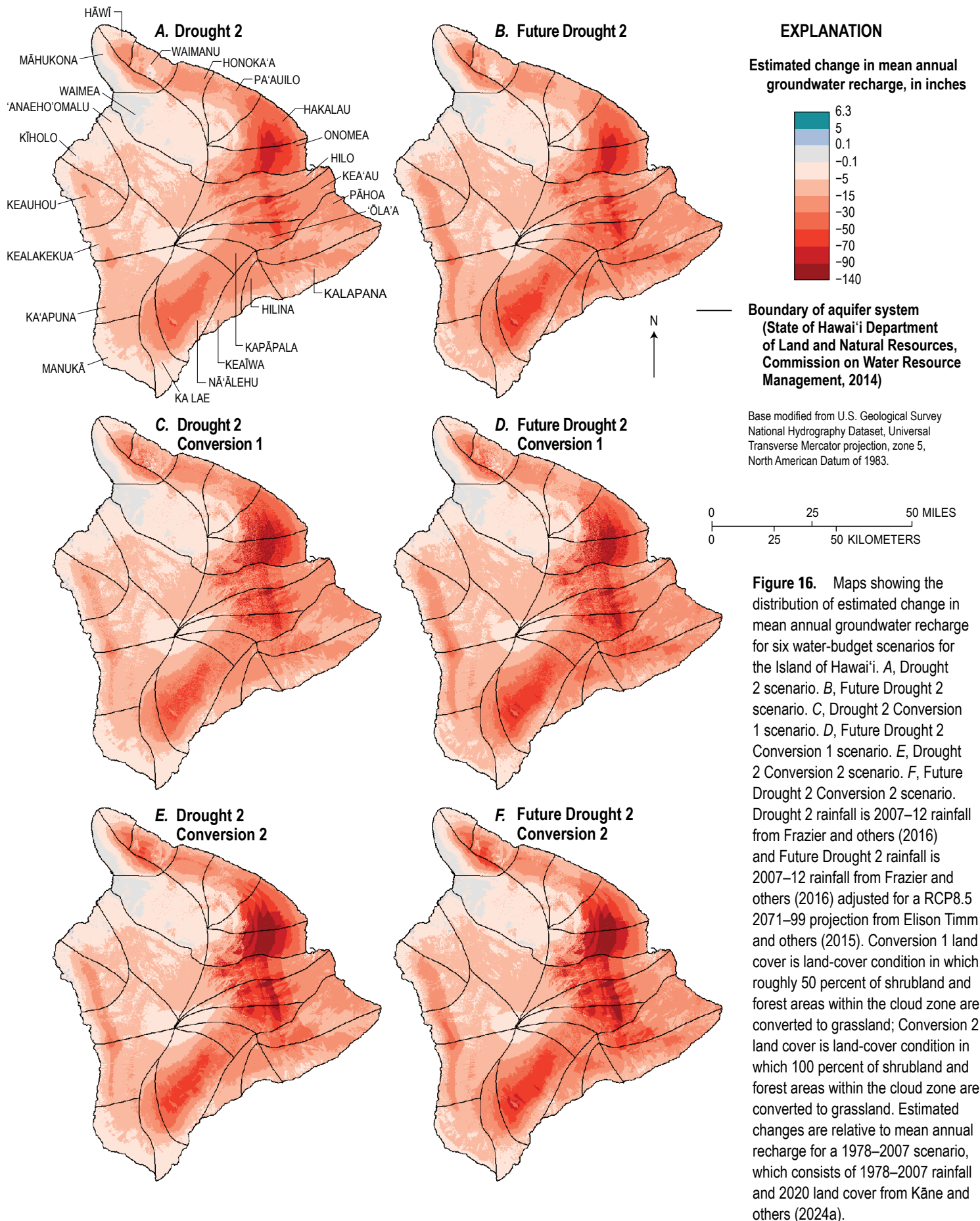
decreases in aquifer-system recharge are estimated for the Onomea and Nā‘ālehu aquifer systems, where decreases range from 312 to 513 Mgal/d relative to recharge for the 1978–2007 scenario. In terms of percentage change from the 1978–2007 scenario, the greatest decreases in aquifer-system recharge are estimated for the Waimea, Kīholo, Kealakekua, Ka‘apuna, Manukā, Ka Lae, and Nā‘ālehu aquifer systems, where decreases range from 80 to 88 percent.

Effects of Drought and Reduced Cloud-Water Interception

A total of four additional water-budget scenarios were included for O‘ahu, Maui, and the Island of Hawai‘i (table 5) to quantify the added effect of reduced CWI during drought conditions as follows:

1. Drought 1 Conversion 1 scenario (O‘ahu), or Drought 2 Conversion 1 scenario (Maui and Island of Hawai‘i),
2. Drought 1 Conversion 2 scenario (O‘ahu), or Drought 2 Conversion 2 scenario (Maui and Island of Hawai‘i),
3. Future Drought 1 Conversion 1 scenario (O‘ahu), or Future Drought 2 Conversion 1 scenario (Maui and Island of Hawai‘i), and
4. Future Drought 1 Conversion 2 scenario (O‘ahu) or Future Drought 2 Conversion 2 scenario (Maui and Island of Hawai‘i).

Estimates of island-wide groundwater recharge for the four added scenarios are shown in table 6 and summarized by subarea in Mair (2024b).



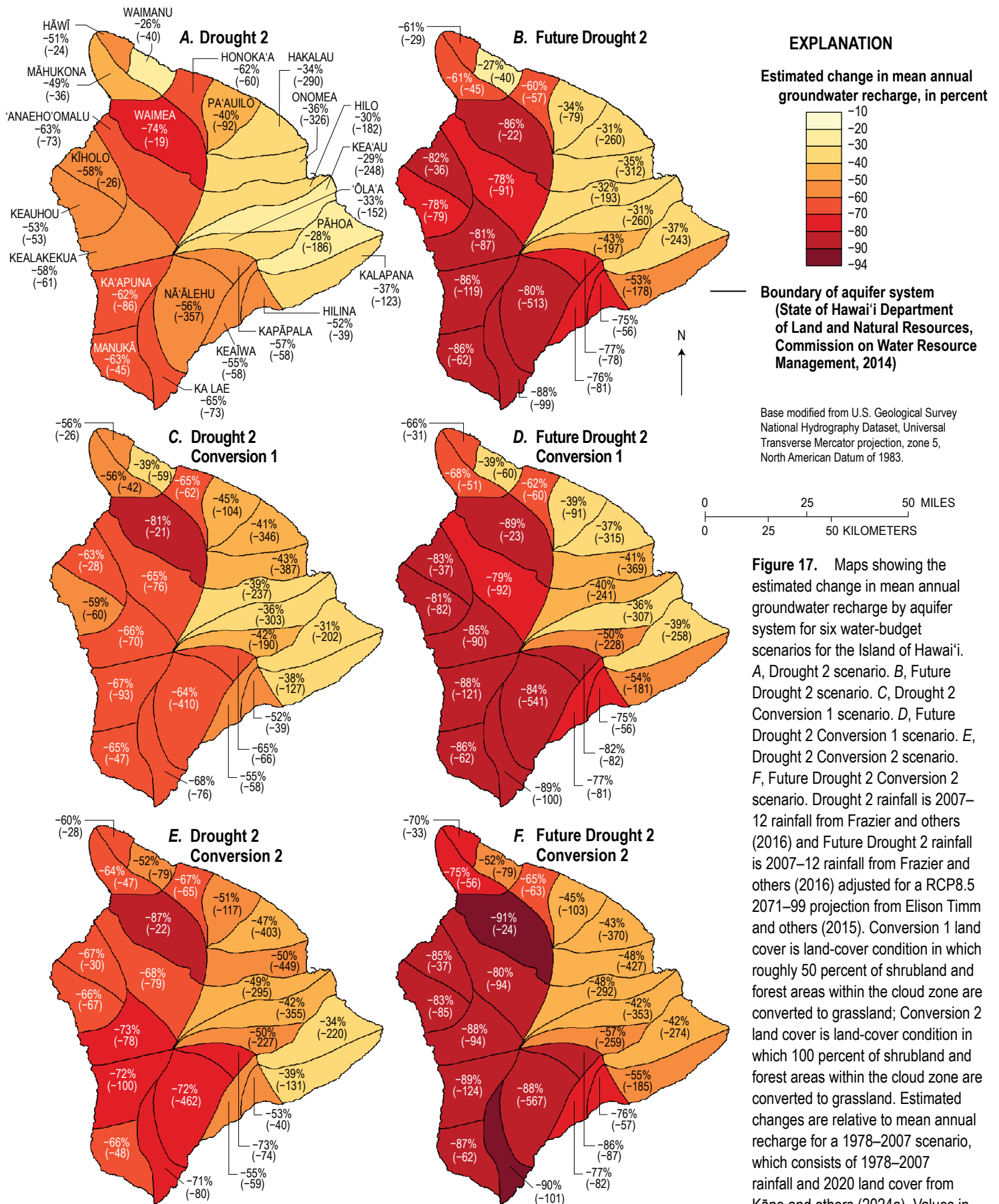


Figure 17. Maps showing the estimated change in mean annual groundwater recharge by aquifer system for six water-budget scenarios for the Island of Hawai'i. A, Drought 2 scenario. B, Future Drought 2 scenario. C, Drought 2 Conversion 1 scenario. D, Future Drought 2 Conversion 1 scenario. E, Drought 2 Conversion 2 scenario. F, Future Drought 2 Conversion 2 scenario. Drought 2 rainfall is 2007–12 rainfall from Frazier and others (2016) and Future Drought 2 rainfall is 2007–12 rainfall from Frazier and others (2016) adjusted for a RCP8.5 2071–99 projection from Elison Timm and others (2015). Conversion 1 land cover is land-cover condition in which roughly 50 percent of shrubland and forest areas within the cloud zone are converted to grassland; Conversion 2 land cover is land-cover condition in which 100 percent of shrubland and forest areas within the cloud zone are converted to grassland. Estimated changes are relative to mean annual recharge for a 1978–2007 scenario, which consists of 1978–2007 rainfall and 2020 land cover from Kāne and others (2024a). Values in parentheses represent change in million gallons per day. %, percent.

O'ahu

Island-wide mean annual recharge decreased by 207 Mgal/d (35 percent) for the Drought 1 Conversion 1 scenario and by 213 Mgal/d (36 percent) for the Drought 1 Conversion 2 scenario, relative to the 1978–2007 scenario (table 6). These hypothetical changes in land cover correspond to land-cover-related decreases in island-wide mean annual recharge ranging from 6 to 12 Mgal/d. Island-wide mean annual recharge decreased by 286 Mgal/d (48 percent) for the Future Drought 1 Conversion 1 scenario and by 291 Mgal/d (49 percent) for the Future Drought 1 Conversion 2 scenario, relative to the 1978–2007 scenario (table 6). These hypothetical changes in land cover correspond to land-cover-related decreases in island-wide mean annual recharge ranging from 5 to 11 Mgal/d. The effect of hypothetical land-cover conversion on recharge is most notable in the upland regions of the Ko'olauloa aquifer system where decreases in recharge intensify (fig. 10). Aquifer-system recharge decreases in those aquifer systems that are affected by the hypothetical changes in forest and shrubland land cover within the cloud zone. In terms of absolute difference in mean annual recharge, the greatest land-cover-related decreases in aquifer-system recharge are estimated for the Ko'olauloa and Wahiawa aquifer systems, where a land-cover-related decrease of up to 3 Mgal/d is estimated for each aquifer system across all four water-budget scenarios (fig. 11). In terms of percentage change from the 1978–2007 scenario, the greatest land-cover-related decreases in aquifer-system recharge are estimated for the Mākaha, Mokulē'ia, and Ko'olauloa aquifer systems, where complete conversion of forest and shrubland to grassland within the cloud zone decreases recharge by an additional 5 to 7 percent.

Maui

Island-wide mean annual recharge decreased by 461 Mgal/d (39 percent) for the Drought 2 Conversion 1 scenario and by 529 Mgal/d (44 percent) for the Drought 2 Conversion 2 scenario, relative to the 1978–2007 scenario (table 6). These hypothetical changes in land cover correspond to land-cover-related decreases in island-wide mean annual recharge ranging from 68 to 135 Mgal/d. Island-wide mean annual recharge decreased by 537 Mgal/d (45 percent) for the Future Drought 2 Conversion 1 scenario and by 596 Mgal/d (50 percent) for the Future Drought 2 Conversion 2 scenario, relative to the 1978–2007 scenario (table 6). These hypothetical changes in land cover correspond to land-cover-related decreases in island-wide mean annual recharge ranging from 59 to 119 Mgal/d. The effect of hypothetical land-cover conversions on recharge is most notable in the upland regions of West Maui and windward Haleakalā where decreases in

recharge intensify due to the conversion of forest and shrubland to grassland land cover (fig. 14). Aquifer-system recharge decreases in those aquifer systems that are affected by the hypothetical changes in forest and shrubland land cover within the cloud zone. In terms of absolute difference in mean annual recharge, the greatest land-cover-related decreases in aquifer-system recharge are estimated for the Waikamoi and Ke'anāe aquifer systems, where complete conversion of forest and shrubland to grassland for the Drought 2 Conversion 2 scenario decreases recharge by between 14 and 33 Mgal/d (fig. 15). In terms of percentage change from the 1978–2007 scenario, the greatest land-cover-related decreases in aquifer-system recharge are estimated for the Kahakuloa and Waikapū aquifer systems, where complete conversion of forest and shrubland to grassland within the cloud zone for the Drought 2 Conversion 2 scenario decreases recharge by an additional 19 to 20 percent.

Island of Hawai'i

Island-wide mean annual recharge decreased by 3,129 Mgal/d (45 percent) for the Drought 2 Conversion 1 scenario and by 3,556 Mgal/d (52 percent) for the Drought 2 Conversion 2 scenario, relative to the 1978–2007 scenario (table 6). These hypothetical changes in land cover correspond to land-cover-related decreases in island-wide mean annual recharge ranging from 423 to 849 Mgal/d. Island-wide mean annual recharge decreased by 3,558 Mgal/d (52 percent) for the Future Drought 2 Conversion 1 scenario and by 3,905 Mgal/d (57 percent) for the Future Drought 2 Conversion 2 scenario, relative to the 1978–2007 scenario (table 6). These hypothetical changes in land cover correspond to land-cover-related decreases in island-wide mean annual recharge ranging from 343 to 689 Mgal/d. The effect of land-cover conversion on recharge is most notable in the upland regions of the windward part of the Island of Hawai'i, where decreases in recharge intensify due to the conversion of forest and shrubland to grassland land cover (fig. 16). Aquifer-system recharge decreases in those aquifer systems that are affected by the hypothetical changes in forest and shrubland land cover within the cloud zone. In terms of absolute difference in mean annual recharge, the greatest land-cover-related decreases in aquifer-system recharge are estimated for the Hakalau, Onomea, Hilo, Kea'au, and Nā'ālehu aquifer systems, where complete conversion of forest and shrubland to grassland for the Drought 2 Conversion 2 scenario decreases recharge by between 105 and 123 Mgal/d (fig. 17). In terms of percentage change from the 1978–2007 scenario, the greatest land-cover-related decreases in aquifer-system recharge are estimated for the Hilo and 'Ōla'a aquifer systems, where complete conversion of forest and shrubland to grassland for the Drought 2 Conversion 2 scenario decreases recharge by an additional 17 to 19 percent.

Soil Moisture, Evapotranspiration, and Climatic Water Deficit Frequency Characterization

WATRMd was used to compute soil moisture, ET, and CWD for a set of drought conditions for Kaua'i, O'ahu, Moloka'i, Maui, and the Island of Hawai'i (table 5). A set of hypothetical land-cover conditions was added for O'ahu, Maui, and the Island of Hawai'i to assess the added effect of reduced CWI on soil moisture, ET, and CWD during drought conditions. WATRMd estimates within documented wildfires were evaluated at selected moisture-stress levels for soil moisture, ET, and CWD (see Appendix 2 for a description of the selection of moisture-stress levels for soil moisture, ET, and CWD). A threshold value of 0.074 was selected as the moisture-stress level for monthly mean soil moisture, expressed as a fraction of available water capacity. A threshold value of 0.96 inches was selected as the moisture-stress level for monthly ET and a threshold value of 0.77 was selected for monthly CWD, expressed as a fraction of potential ET. The selected moisture-stress levels were applied to a set of time series data of monthly estimates from WATRMd to calculate the frequency characteristics (or relative frequency) of soil moisture, ET, and CWD for each water-budget scenario (table 5). In this study, relative frequency describes the fraction of months that soil moisture or ET is less than or equal to the selected moisture-stress level (or greater than or equal to the selected level for CWD) without regard for the sequence or intensity of occurrence. The relative frequency was computed for each subarea on each of the five islands. The relative frequency of soil moisture, ET, and CWD for the selected moisture-stress levels are summarized by subarea in Mair (2024a).

Frequency Characteristics for Reference Condition

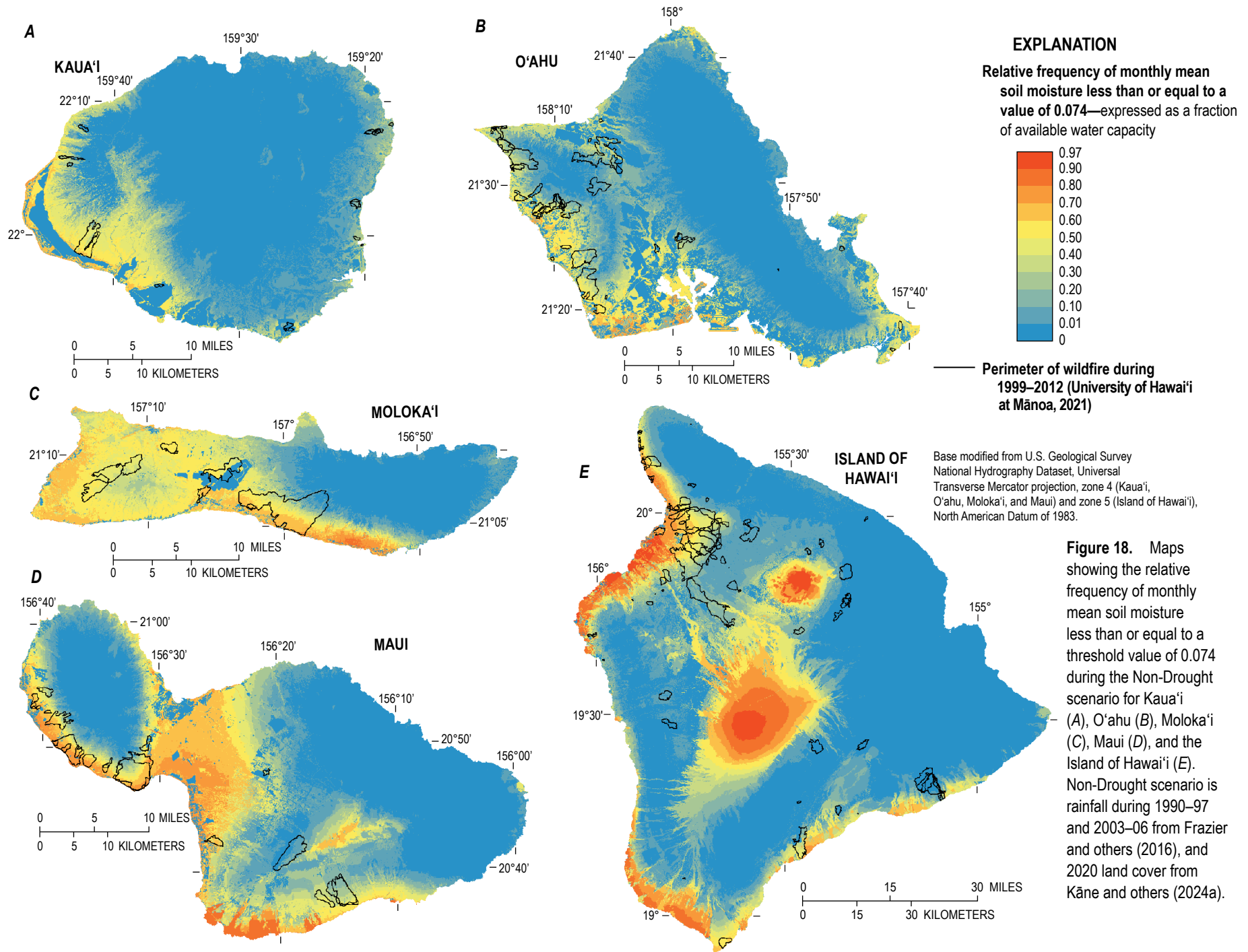
A Non-Drought scenario consisting of rainfall during 1990–97 and 2003–06, and 2020 land cover was used as the reference condition (table 5). For the Non-Drought scenario, the relative frequencies for soil moisture, ET, and CWD vary from zero to maximum values of 0.97, 0.87, and 0.99, respectively, across the five islands (figs. 18–20). Low relative frequency implies low moisture stress, whereas high relative frequency implies high moisture stress, increased flammability due to low fuel moisture, and increased potential wildfire hazard. Hence, the variability in relative frequency across the islands during the Non-Drought scenario indicates a wide range of moisture-stress on vegetation and potential wildfire hazard. For example, areas with the lowest relative frequency (less than 0.01) generally extend across the wet upland or windward regions of each island. Areas with agricultural, developed, and golf course land cover (fig. 4) also have

low relative frequency due to irrigation and include parts of southwestern Kaua'i; central, south, and west O'ahu; central Moloka'i; central Maui and western coastal areas of Maui; and isolated northwestern areas on the Island of Hawai'i. Areas with mid to high relative frequency (greater than 0.50), generally extend across the drier leeward parts of each island and across the drier summit areas of Haleakalā, Mauna Kea, and Mauna Loa (fig. 1).

Many of the 187 wildfires during 1999–2012 occurred in areas with mid to high relative frequency of moisture-stress indicators (figs. 18–20), which implies increased frequency of low fuel-moisture conditions and increased potential wildfire hazard. Numerous wildfires have occurred in or extended into areas with low relative frequency of moisture-stress indicators during the Non-Drought scenario simulation period (1990–97 and 2003–06). For example, several wildfires on the upland slopes of the Island of Hawai'i occurred in areas with low relative frequency of moisture-stress indicators. However, most of the wildfires in this area occurred during the Drought 3 scenario simulation period (1998–2002 and 2007–12), which was drier than the Non-Drought scenario simulation period. Also, low relative frequency of moisture-stress indicators implies decreased wildfire hazard but does not preclude the possibility of intermittent low-moisture conditions during the Non-Drought scenario. Relative frequency does not characterize the sequence or intensity of low-moisture conditions. Thus, a short, intense dry period during the Non-Drought scenario could produce low-moisture conditions for short durations without substantially increasing the relative frequency of any of the moisture-stress indicators.

Effects of Drought

Three water-budget scenarios were selected to evaluate the effect of drought on soil moisture, ET, and CWD for each island: (1) Drought 3 scenario, (2) Future Non-Drought scenario, and (3) Future Drought 3 scenario (table 5). The effect of drought and climate on moisture stress was evaluated by examining the change in relative frequency of the moisture-stress indicators between the Non-Drought scenario and the Drought 3, Future Non-Drought, and Future Drought 3 scenarios. The change in relative frequency was computed for each subarea as the difference in relative frequency from the Non-Drought scenario. Increases in the relative frequency indicate an increase in the fraction of months that soil moisture or ET (or CWD) is less than or equal to (or greater than or equal to) the selected threshold value. Hence, an increase in the relative frequency of low-moisture conditions implies higher moisture stress, increased flammability due to low fuel moisture, and greater wildfire hazard, relative to the Non-Drought scenario. The effect of drought for recent and projected climate conditions on the relative frequency of each moisture-stress indicator for Kaua'i, O'ahu, Moloka'i, Maui, and the Island of Hawai'i is described in the following sections.



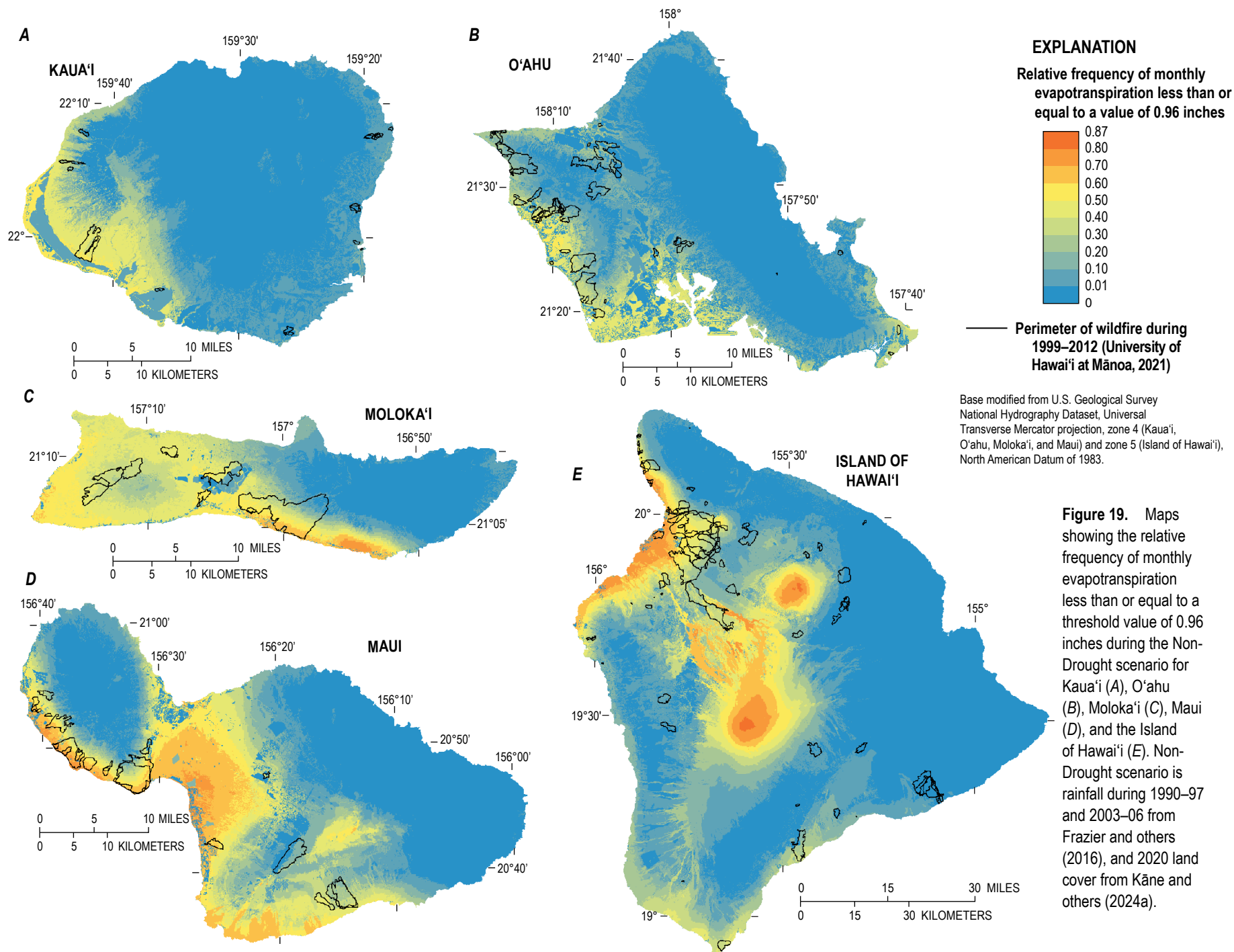
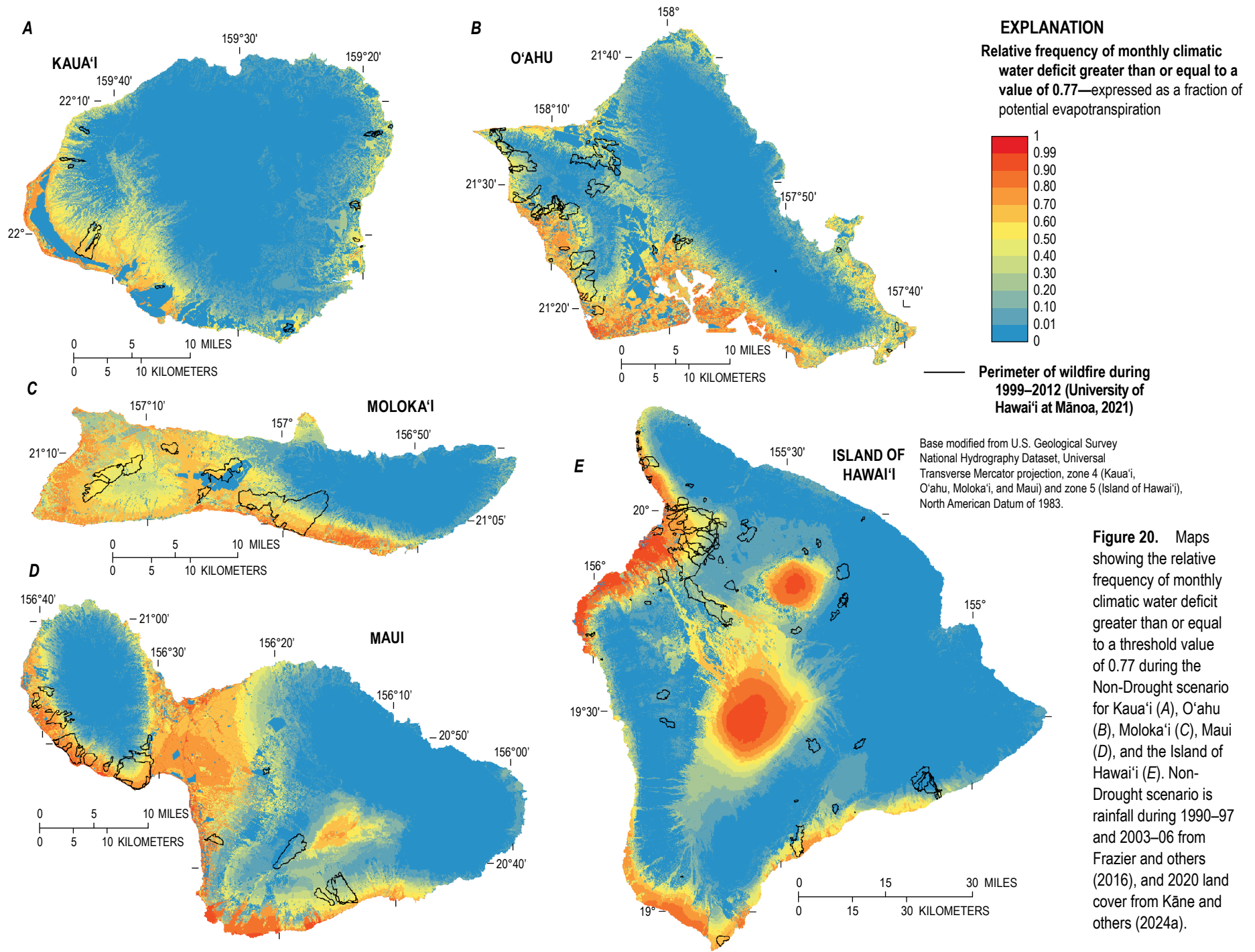


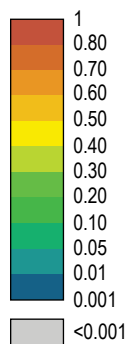
Figure 19. Maps showing the relative frequency of monthly evapotranspiration less than or equal to a threshold value of 0.96 inches during the Non-Drought scenario for Kaua'i (A), O'ahu (B), Moloka'i (C), Maui (D), and the Island of Hawai'i (E). Non-Drought scenario is rainfall during 1990–97 and 2003–06 from Frazier and others (2016), and 2020 land cover from Kāne and others (2024a).



Kauaʻi

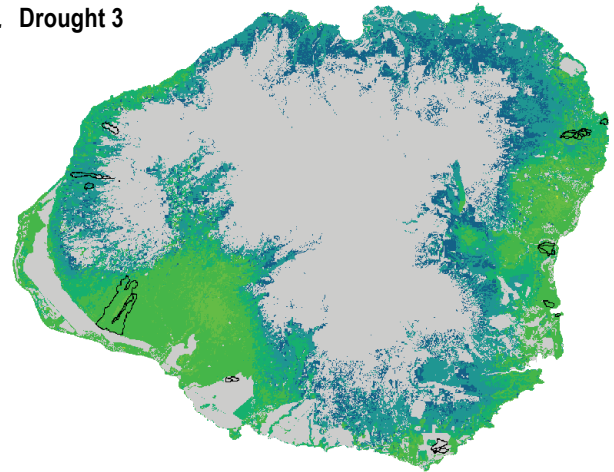
The Drought 3, Future Non-Drought, and Future Drought 3 scenarios all produce increases in the relative frequencies of moisture-stress indicators across extensive areas of Kauaʻi (figs. 21–23). For the Drought 3 scenario, the greatest increase in relative frequency for the three moisture-stress indicators occurs in the southwestern and eastern parts of Kauaʻi, where changes are as high as 0.42 for soil moisture, 0.39 for ET, and 0.33 for CWD (figs. 21A, 22A, 23A). The increases in relative frequency of moisture-stress indicators in these areas imply increased frequency of low fuel-moisture conditions and increased wildfire hazard. Areas of little or no change in relative frequency for moisture-stress indicators imply no increase in the frequency of low fuel-moisture conditions and extend across the central, upland regions of the island. Areas of little or no change in relative frequency for soil moisture and CWD moisture-stress indicators also extend across irrigated agricultural areas along the southwest coast (figs. 4A, 21A, 23A), which is consistent with the concept that irrigation can suppress the frequency of low-moisture conditions.

EXPLANATION
Estimated change in relative frequency of monthly mean soil moisture less than or equal to a value of 0.074—expressed as a fraction of available water capacity

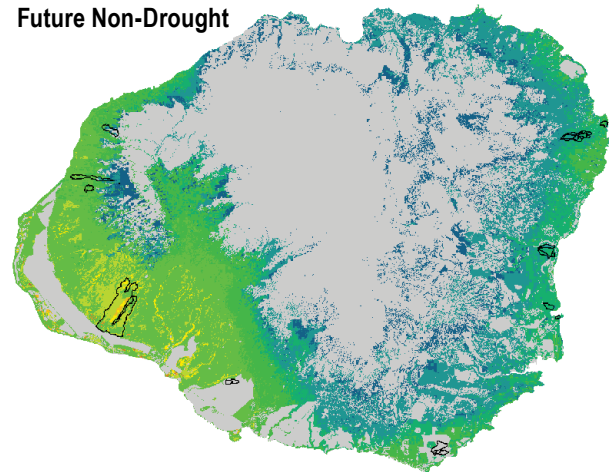


Perimeter of wildfire during 1999–2012
(University of Hawaiʻi at Mānoa, 2021)

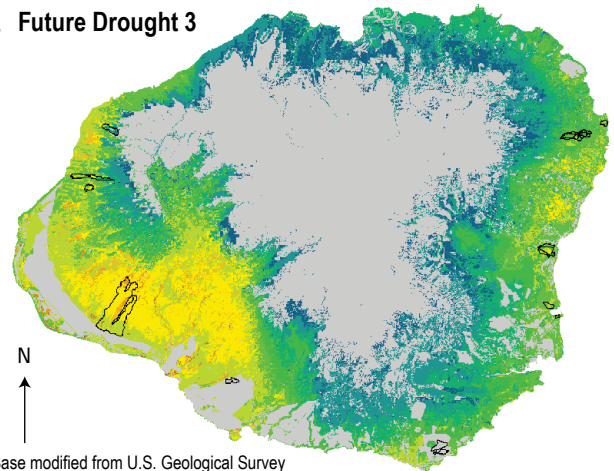
A. Drought 3



B. Future Non-Drought



C. Future Drought 3



Base modified from U.S. Geological Survey
National Hydrography Dataset, Universal
Transverse Mercator projection, zone 4,
North American Datum of 1983.

0 5 10 MILES
0 5 10 KILOMETERS

Figure 21. Maps showing estimated increases in relative frequency of monthly mean soil moisture less than or equal to a value of 0.074 for three water-budget scenarios for Kauaʻi. A, Drought 3 scenario. B, Future Non-Drought scenario. C, Future Drought 3 scenario. All increases in relative frequency are relative to a Non-Drought scenario, which consists of rainfall during 1990–97 and 2003–06 from Frazier and others (2016), and 2020 land cover from Kāne and others (2024a). Drought 3 rainfall is rainfall during 1998–2002 and 2007–12 from Frazier and others (2016), Future Non-Drought rainfall is rainfall during 1990–97 and 2003–06 from Frazier and others (2016) adjusted for a RCP8.5 2071–99 projection from Elison Timm and others (2015), and Future Drought 3 rainfall is rainfall during 1998–2002 and 2007–12 from Frazier and others (2016) adjusted for a RCP8.5 2071–99 projection from Elison Timm and others (2015).

For the Future Non-Drought scenario, the greatest increases in relative frequency for the three moisture-stress indicators occur in the western part of Kauaʻi, where increases are as high as 0.84 for soil moisture, 0.69 for ET, and 0.59 for CWD (figs. 21B, 22B, 23B). These increases in relative frequency of moisture-stress indicators imply that low-moisture conditions expand and increase in duration for much of west Kauaʻi, and indicate increased wildfire hazard for a projected non-drought climate condition. The increases in relative frequency for the eastern part of Kauaʻi are generally smaller and less extensive relative to the Drought 3 condition, which indicates lesser increases in wildfire hazard. Areas of little or no change in relative frequency, implying no change in wildfire hazard, extend across the central, upland regions of the island and across irrigated agricultural areas along the southwest coast (figs. 4A, 21B, 22B, 23B).

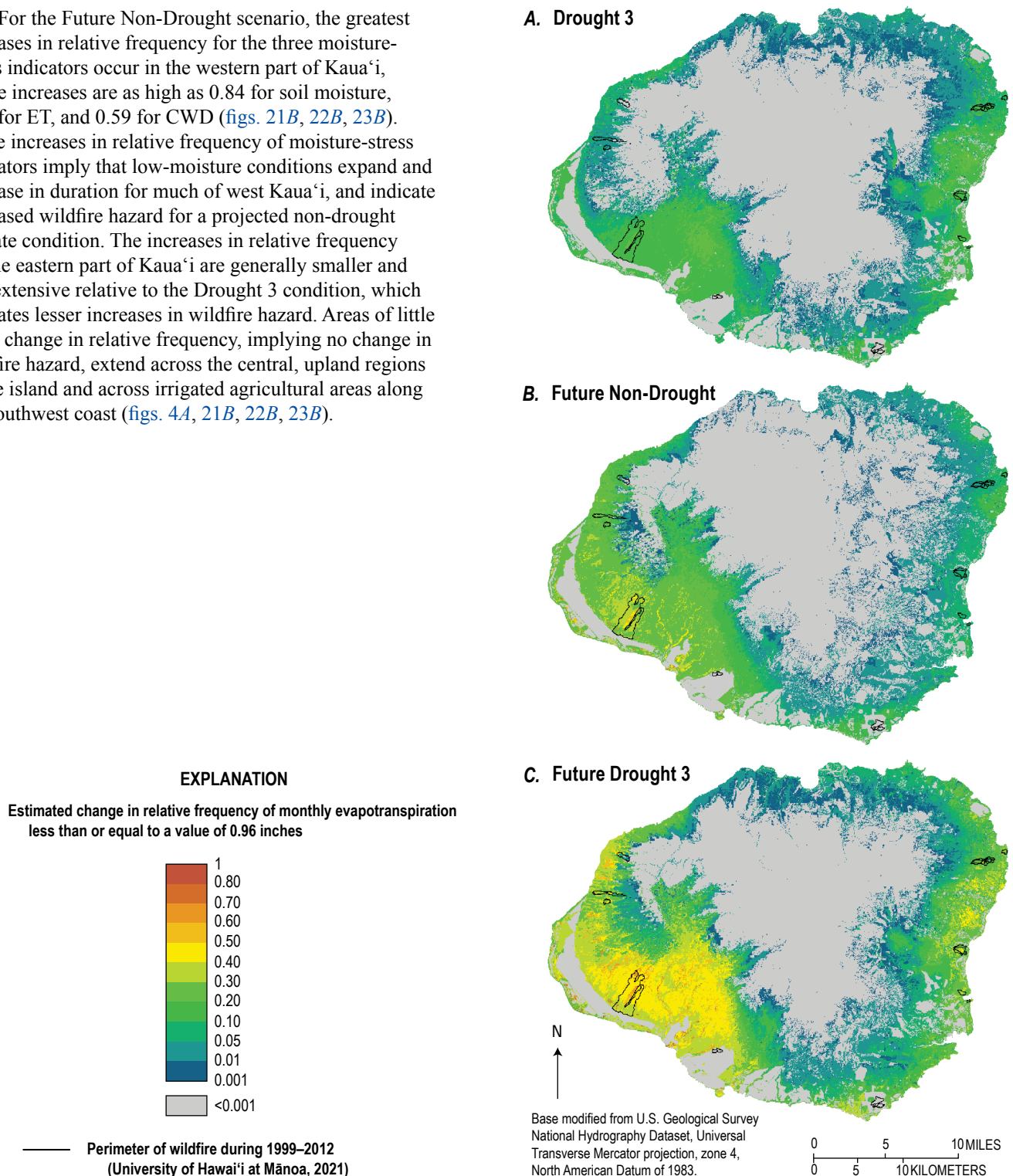
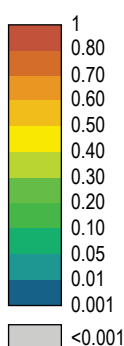


Figure 22. Maps showing estimated increases in relative frequency of monthly evapotranspiration less than or equal to a value of 0.96 inches for three water-budget scenarios for Kauaʻi. A, Drought 3 scenario. B, Future Non-Drought scenario. C, Future Drought 3 scenario. All increases in relative frequency are relative to a Non-Drought scenario, which consists of rainfall during 1990–97 and 2003–06 from Frazier and others (2016), and 2020 land cover from Kāne and others (2024a). Drought 3 rainfall is rainfall during 1998–2002 and 2007–12 from Frazier and others (2016), Future Non-Drought rainfall is rainfall during 1990–97 and 2003–06 from Frazier and others (2016) adjusted for a RCP8.5 2071–99 projection from Elison Timm and others (2015), and Future Drought 3 rainfall is rainfall during 1998–2002 and 2007–12 from Frazier and others (2016) adjusted for a RCP8.5 2071–99 projection from Elison Timm and others (2015).

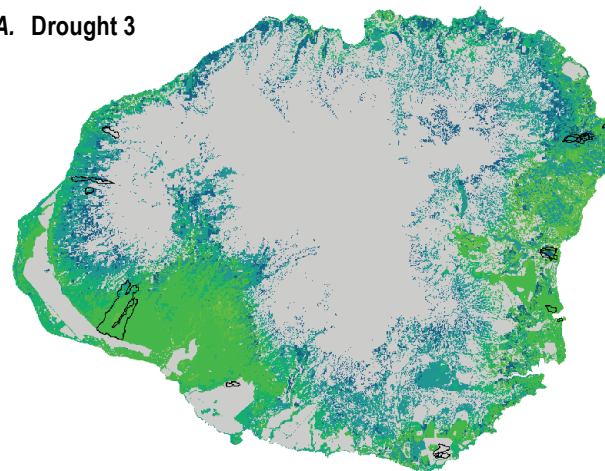
For the Future Drought 3 scenario, the greatest change in relative frequency for the three moisture-stress indicators occurs in the western part of Kauaʻi, where increases are as high as 0.99 for soil moisture, 0.86 for ET, and 0.78 for CWD (figs. 21C, 22C, 23C). These increases in relative frequency are the most extreme among the three scenarios and imply that low-moisture conditions expand and increase in duration for much of west Kauaʻi and areas along the northern, eastern, and southern coast. The extent and magnitude of increases in the frequency of low-moisture conditions implies substantially greater wildfire hazard for the Future Drought 3 scenario. Areas of little or no change in relative frequency, implying no change in wildfire hazard, extend across the central upland regions of the island and across irrigated agricultural areas along the southwest coast (figs. 4A, 21C, 22C, 23C). However, the area of little or no change in relative frequency across the central part of the island contracts relative to the Drought 3 and Future Non-Drought scenarios, which indicates increased wildfire hazard for many upland forest areas of Kauaʻi.

EXPLANATION
Estimated change in relative frequency of monthly climatic water deficit greater than or equal to a value of 0.77—expressed as a fraction of potential evapotranspiration

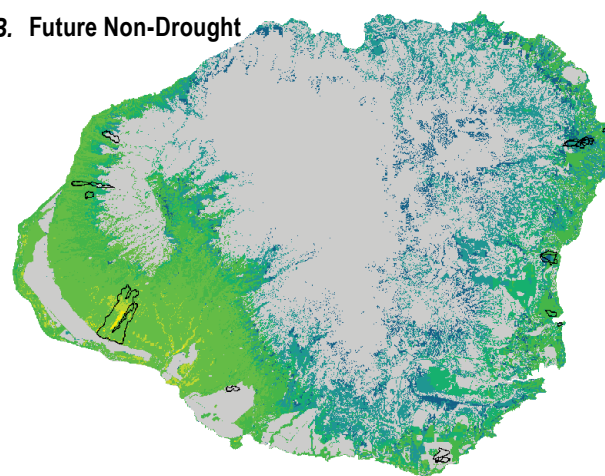


Perimeter of wildfire during 1999–2012
(University of Hawaiʻi at Mānoa, 2021)

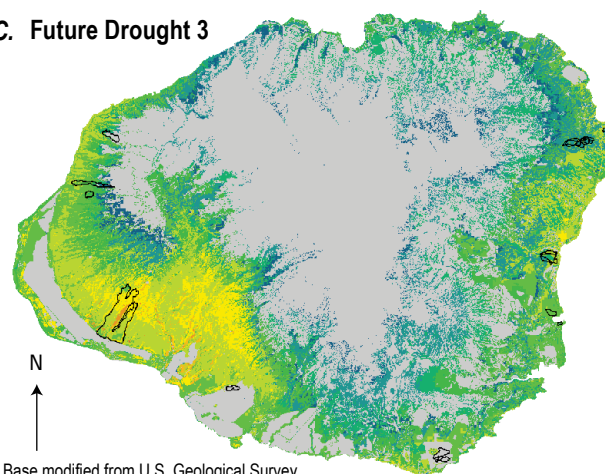
A. Drought 3



B. Future Non-Drought



C. Future Drought 3



Base modified from U.S. Geological Survey
National Hydrography Dataset, Universal
Transverse Mercator projection, zone 4,
North American Datum of 1983.

0 5 10 MILES
0 5 10 KILOMETERS

Figure 23. Maps showing estimated increases in relative frequency of monthly climatic water deficit greater than or equal to a value of 0.77 for three water-budget scenarios for Kauaʻi. A, Drought 3 scenario. B, Future Non-Drought scenario. C, Future Drought 3 scenario. All increases in relative frequency are relative to a Non-Drought scenario, which consists of rainfall during 1990–97 and 2003–06 from Frazier and others (2016), and 2020 land cover from Kāne and others (2024a). Drought 3 rainfall is rainfall during 1998–2002 and 2007–12 from Frazier and others (2016), Future Non-Drought rainfall is rainfall during 1990–97 and 2003–06 from Frazier and others (2016) adjusted for a RCP8.5 2071–99 projection from Elison Timm and others (2015), and Future Drought 3 rainfall is rainfall during 1998–2002 and 2007–12 from Frazier and others (2016) adjusted for a RCP8.5 2071–99 projection from Elison Timm and others (2015).

O‘ahu

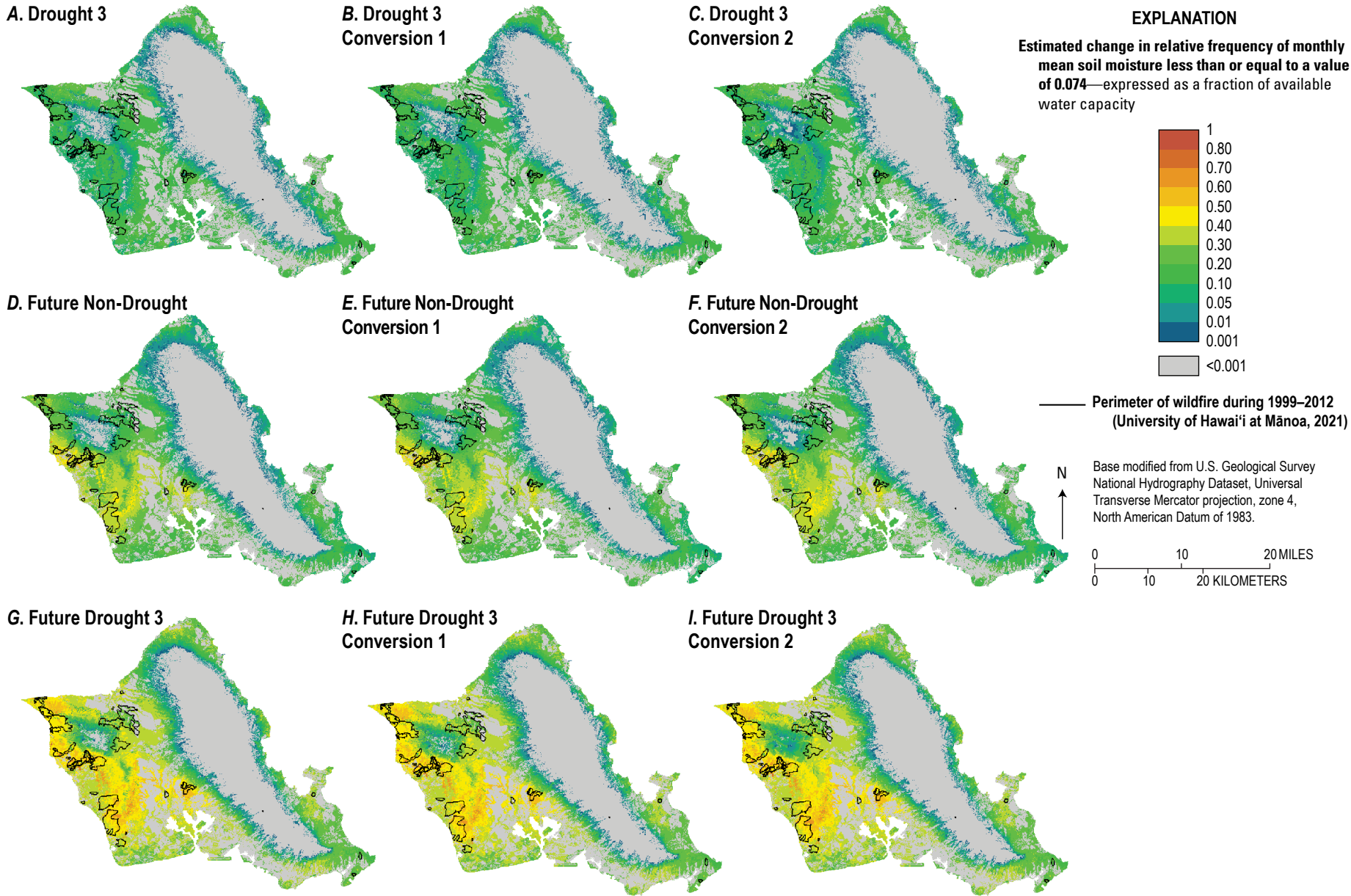
The Drought 3, Future Non-Drought, and Future Drought 3 scenarios all produce increases in the relative frequency of moisture-stress indicators across extensive areas of O‘ahu (figs. 24–26). For the Drought 3 scenario, the greatest change in relative frequency for the three moisture-stress indicators occurs across parts of central and west O‘ahu, and along the east coast, where increases as high as 0.37 for soil moisture, 0.34 for ET, and 0.34 for CWD are indicated (figs. 24A, 25A, 26A). The positive change in relative frequency of moisture-stress indicators in these areas implies an increase in the frequency of low fuel-moisture conditions and increased wildfire hazard. Areas of little or no change in relative frequency, implying no change in wildfire hazard, extend across much of the wet, upland regions of the Ko‘olau Range, parts of the upland regions of the Wai‘anae Range, and across many of the irrigated agricultural, golf course, and developed areas of the island (figs. 1, 4B, 24A, 25A, 26A).

For the Future Non-Drought scenario, the greatest change in relative frequency for the three moisture-stress indicators occurs in the western part of O‘ahu, where increases are as high as 0.92 for soil moisture, 0.72 for ET, and 0.72 for CWD (figs. 24D, 25D, 26D). These increases in relative frequency imply that low-moisture conditions expand and increase in duration across much of western

O‘ahu, and imply increased wildfire hazard for the Future Non-Drought scenario. Areas of little or no change in relative frequency, implying no change in wildfire hazard, extend across the upland regions of the Ko‘olau Range, the northern part of the Wai‘anae Range around Ka‘ala, and the irrigated areas of the island (figs. 1, 4B, 24D, 25D, 26D).

For the Future Drought 3 scenario, the greatest change in relative frequency for the three moisture-stress indicators occurs in central and west O‘ahu, where increases are as high as 0.98 for soil moisture, 0.86 for ET, and 0.8 for CWD (figs. 24G, 25G, 26G). These increases in relative frequency are the most extreme among the three scenarios and imply that low-moisture conditions expand and increase in duration for much of western O‘ahu and areas along the north, east, and south coast. The increase in the extent and magnitude of increases in the frequency of low-moisture conditions implies substantially greater wildfire hazard for the Future Drought 3 scenario. Areas of little or no change in relative frequency, implying no change in wildfire hazard, extend across the upland regions of the Ko‘olau Range, the northern part of the Wai‘anae Range around Ka‘ala, and the irrigated areas of the island (figs. 1, 4B, 24G, 25G, 26G). However, the area of little or no change in relative frequency across the Ko‘olau Range and northern part of the Wai‘anae Range contracts relative to the Drought 3 and Future Non-Drought scenarios, which indicates increased wildfire hazard for many upland forest areas of O‘ahu.

Figure 24. Maps showing estimated increases in relative frequency of monthly mean soil moisture less than or equal to a value of 0.074 for nine water-budget scenarios for O‘ahu. A, Drought 3 scenario. B, Drought 3 Conversion 1 scenario. C, Drought 3 Conversion 2 scenario. D, Future Non-Drought scenario. E, Future Non-Drought Conversion 1 scenario. F, Future Non-Drought Conversion 2 scenario. G, Future Drought 3 scenario. H, Future Drought 3 Conversion 1 scenario. I, Future Drought 3 Conversion 2 scenario. All increases in relative frequency are relative to a Non-Drought scenario, which consists of rainfall during 1990–97 and 2003–06 from Frazier and others (2016), and 2020 land cover from Kāne and others (2024a). Drought 3 rainfall is rainfall during 1998–2002 and 2007–12 from Frazier and others (2016), Future Non-Drought rainfall is rainfall during 1990–97 and 2003–06 from Frazier and others (2016) adjusted for a RCP8.5 2071–99 projection from Elison Timm and others (2015), and Future Drought 3 rainfall is rainfall during 1998–2002 and 2007–12 from Frazier and others (2016) adjusted for a RCP8.5 2071–99 projection from Elison Timm and others (2015). Conversion 1 land cover is land-cover condition in which roughly 50 percent of shrubland and forest areas within the cloud zone are converted to grassland; Conversion 2 land cover is land-cover condition in which 100 percent of shrubland and forest areas within the cloud zone are converted to grassland.



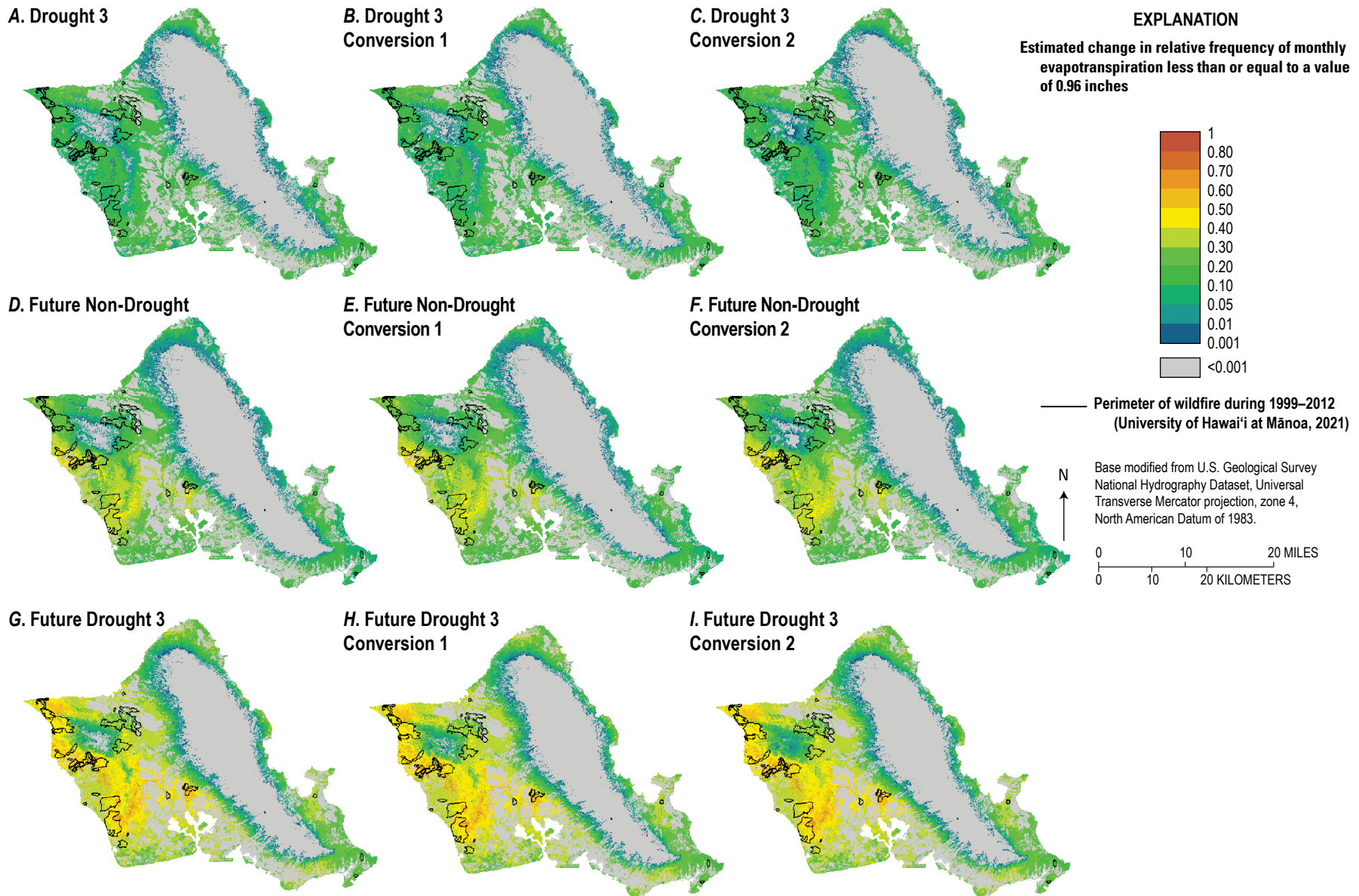


Figure 25. Maps showing estimated increases in relative frequency of monthly evapotranspiration less than or equal to a value of 0.96 inches for nine water-budget scenarios for O'ahu. A, Drought 3 scenario. B, Drought 3 Conversion 1 scenario. C, Drought 3 Conversion 2 scenario. D, Future Non-Drought scenario. E, Future Non-Drought Conversion 1 scenario. F, Future Non-Drought Conversion 2 scenario. G, Future Drought 3 scenario. H, Future Drought 3 Conversion 1 scenario. I, Future Drought 3 Conversion 2 scenario. All increases in relative frequency are relative to a Non-Drought scenario, which consists of rainfall during 1990–97 and 2003–06 from Frazier and others (2016), and 2020 land cover from Kāne and others (2024a). Drought 3 rainfall is rainfall during 1998–2002 and 2007–12 from Frazier and others (2016), RCP8.5 2071–99 Non-Drought rainfall is rainfall during 1990–97 and 2003–06 from Frazier and others (2016) adjusted for a RCP8.5 2071–99 projection from Elison Timm and others (2015), and RCP8.5 2071–99 Drought 3 rainfall is rainfall during 1998–2002 and 2007–12 from Frazier and others (2016) adjusted for a RCP8.5 2071–99 projection from Elison Timm and others (2015). Conversion 1 land cover is land-cover condition in which roughly 50 percent of shrubland and forest areas within the cloud zone are converted to grassland; Conversion 2 land cover is land-cover condition in which 100 percent of shrubland and forest areas within the cloud zone are converted to grassland.

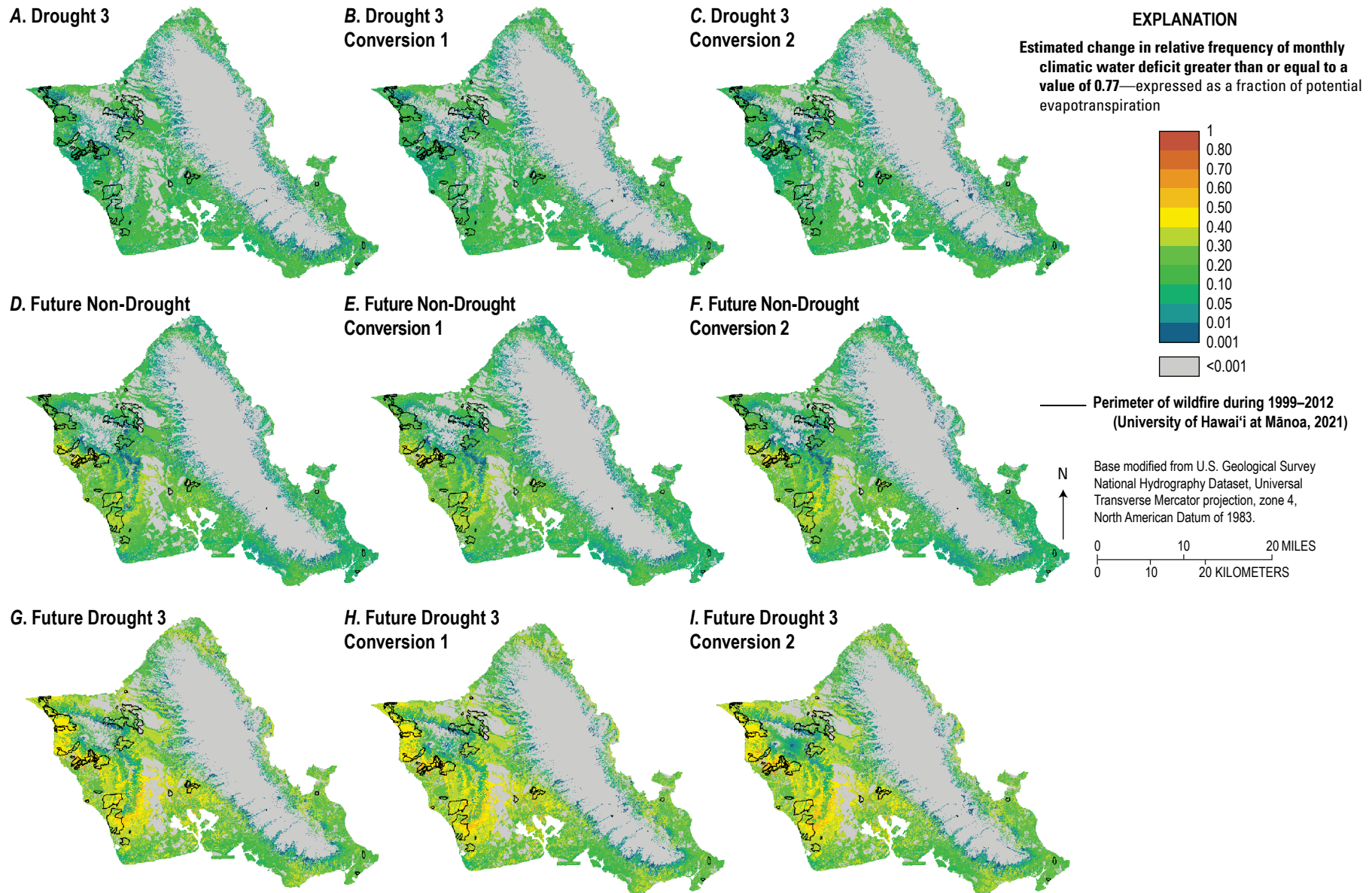


Figure 26. Maps showing estimated increases in relative frequency of monthly climatic water deficit greater than or equal to a value of 0.77 for nine water-budget scenarios for O'ahu. *A*, Drought 3 scenario. *B*, Drought 3 Conversion 1 scenario. *C*, Drought 3 Conversion 2 scenario. *D*, Future Non-Drought scenario. *E*, Future Non-Drought Conversion 1 scenario. *F*, Future Non-Drought Conversion 2 scenario. *G*, Future Drought 3 scenario. *H*, Future Drought 3 Conversion 1 scenario. *I*, Future Drought 3 Conversion 2 scenario. All increases in relative frequency are relative to a Non-Drought scenario, which consists of rainfall during 1990–97 and 2003–06 from Frazier and others (2016), and 2020 land cover from Kāne and others (2024a). Drought 3 rainfall is rainfall during 1998–2002 and 2007–12 from Frazier and others (2016), Future Non-Drought rainfall is rainfall during 1990–97 and 2003–06 from Frazier and others (2016) adjusted for a RCP8.5 2071–99 projection from Elison Timm and others (2015), and Future Drought 3 rainfall is rainfall during 1998–2002 and 2007–12 from Frazier and others (2016) adjusted for a RCP8.5 2071–99 projection from Elison Timm and others (2015). Conversion 1 land cover is land-cover condition in which roughly 50 percent of shrubland and forest areas within the cloud zone are converted to grassland; Conversion 2 land cover is land-cover condition in which 100 percent of shrubland and forest areas within the cloud zone are converted to grassland.

Molokaʻi

The Drought 3, Future Non-Drought, and Future Drought 3 scenarios all produce increases in the relative frequency of moisture-stress indicators across extensive areas of Molokaʻi (figs. 27–29). For the Drought 3 scenario, the greatest change in relative frequency for the three moisture-stress indicators occurs in central Molokaʻi, where increases are as high as 0.41 for soil moisture, 0.40 for ET, and 0.32 for CWD (figs. 27A, 28A, 29A). The positive change in relative frequency in these areas implies an increase in the frequency of low fuel-moisture conditions and increased wildfire hazard. Areas of little or no change in relative frequency, implying no change in wildfire hazard, extend across the eastern, upland regions of the island and across irrigated agricultural areas in central Molokaʻi (figs. 4C, 27A, 28A, 29A).

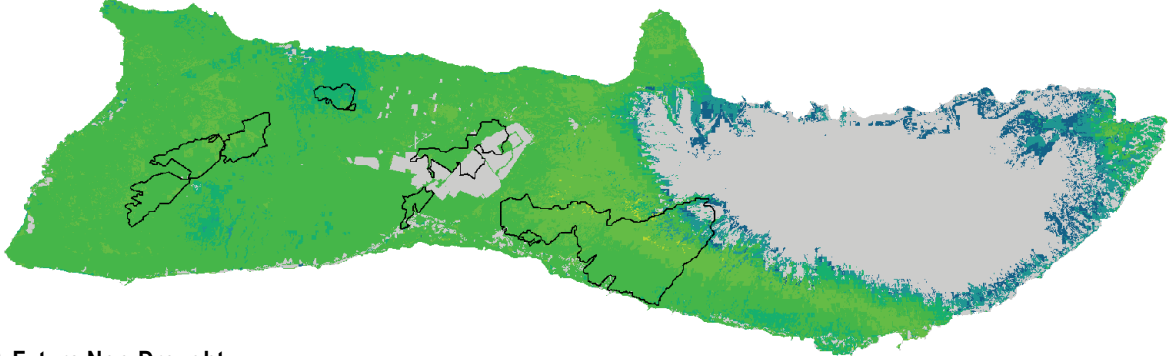
For the Future Non-Drought scenario, the greatest change in relative frequency for the three moisture-stress indicators occurs in west Molokaʻi, where increases are as high as 0.54 for soil moisture, 0.49 for ET, and 0.45 for CWD (figs. 27B, 28B, 29B). These increases in relative frequency imply that low-moisture conditions expand and increase in duration,

which would result in increased wildfire hazard across many parts of Molokaʻi for a Future Non-Drought scenario. Areas of little or no change in relative frequency, implying no change in wildfire hazard, extend across the eastern, upland regions and the irrigated agricultural areas of the island (figs. 4C, 27B, 28B, 29B).

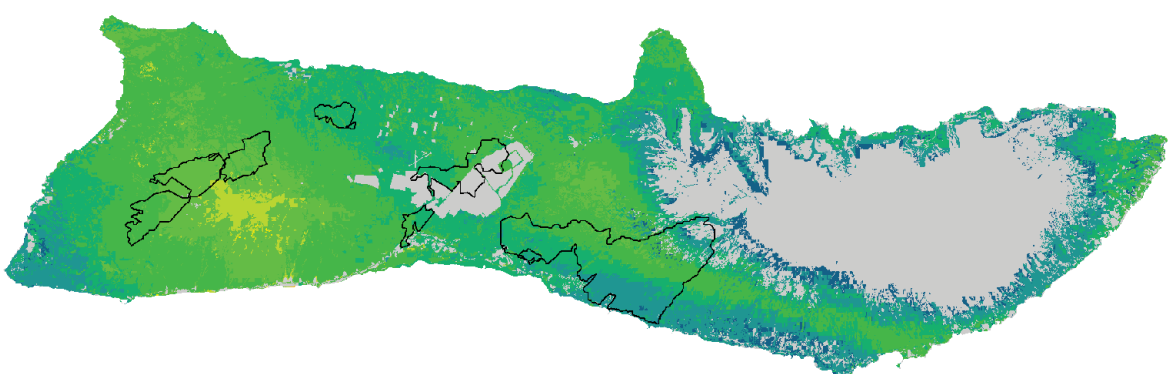
For the Future Drought 3 scenario, the greatest change in relative frequency for the three moisture-stress indicators occurs in central and west Molokaʻi, where increases are as high as 0.68 for soil moisture, 0.68 for ET, and 0.52 for CWD (figs. 27C, 28C, 29C). These increases in relative frequency imply that low-moisture conditions expand and increase in duration in these areas, and increase wildfire hazard during the Future Drought 3 scenario. Areas of little or no change in relative frequency, implying no change in wildfire hazard, extend across the eastern, upland regions of the island and across irrigated agricultural areas in central Molokaʻi (figs. 4C, 27C, 28C, 29C). However, the area of little or no change in relative frequency across eastern, upland regions contracts relative to the Drought 3 and Future Non-Drought scenarios, which indicates increased wildfire hazard for many upland forest areas of Molokaʻi.

Figure 27. Maps showing estimated increases in relative frequency of monthly mean soil moisture less than or equal to a value of 0.074 for three water-budget scenarios for Molokaʻi. A, Drought 3 scenario. B, Future Non-Drought scenario. C, Future Drought 3 scenario. All increases in relative frequency are relative to a Non-Drought scenario, which consists of rainfall during 1990–97 and 2003–06 from Frazier and others (2016), and 2020 land cover from Kāne and others (2024a). Drought 3 rainfall is rainfall during 1998–2002 and 2007–12 from Frazier and others (2016), Future Non-Drought rainfall is rainfall during 1990–97 and 2003–06 from Frazier and others (2016) adjusted for a RCP8.5 2071–99 projection from Alison Timm and others (2015), and Future Drought 3 rainfall is rainfall during 1998–2002 and 2007–12 from Frazier and others (2016) adjusted for a RCP8.5 2071–99 projection from Alison Timm and others (2015).

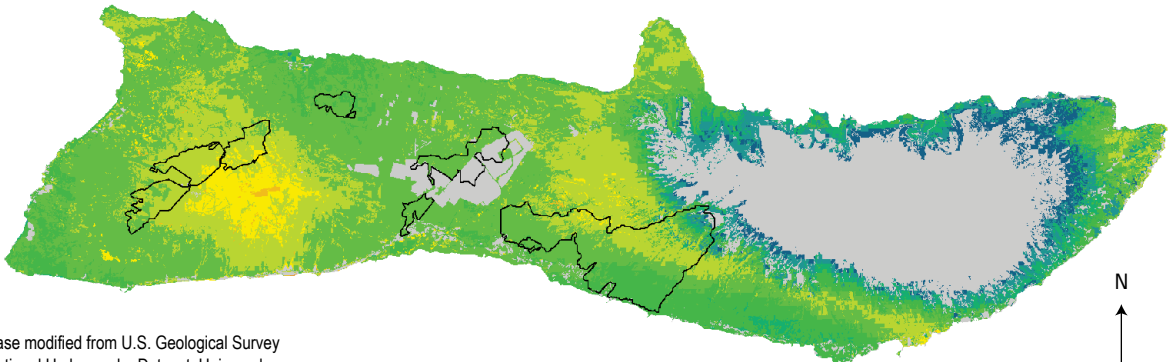
A. Drought 3



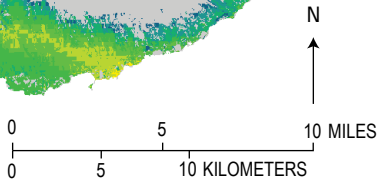
B. Future Non-Drought



C. Future Drought 3



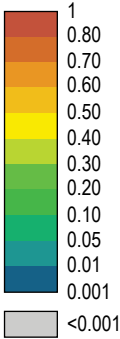
Base modified from U.S. Geological Survey
National Hydrography Dataset, Universal
Transverse Mercator projection, zone 4,
North American Datum of 1983.



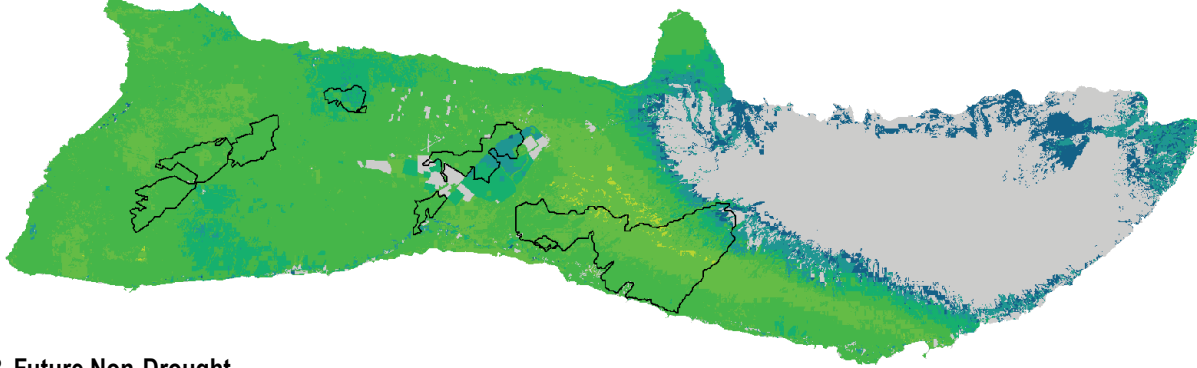
EXPLANATION

Estimated change in relative frequency of monthly mean soil
moisture less than or equal to a value of 0.074—expressed
as a fraction of available water capacity

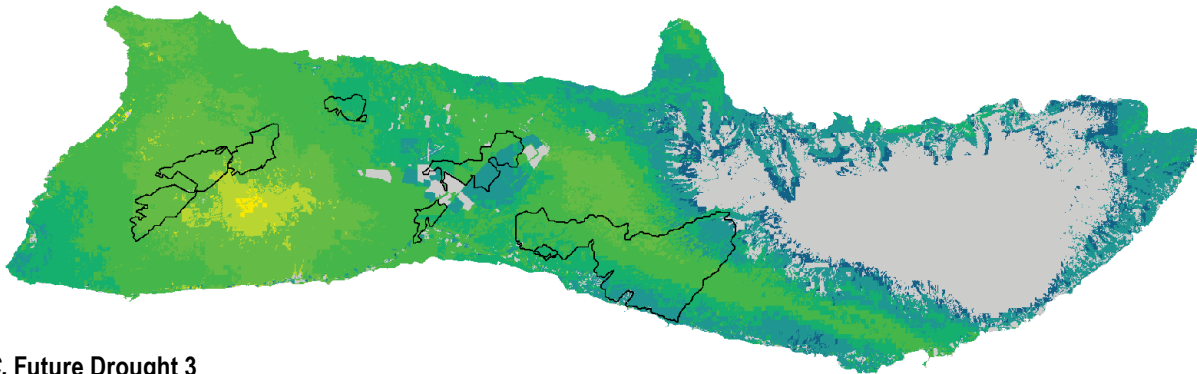
Perimeter of wildfire during 1999–2012
(University of Hawai'i at Mānoa, 2021)



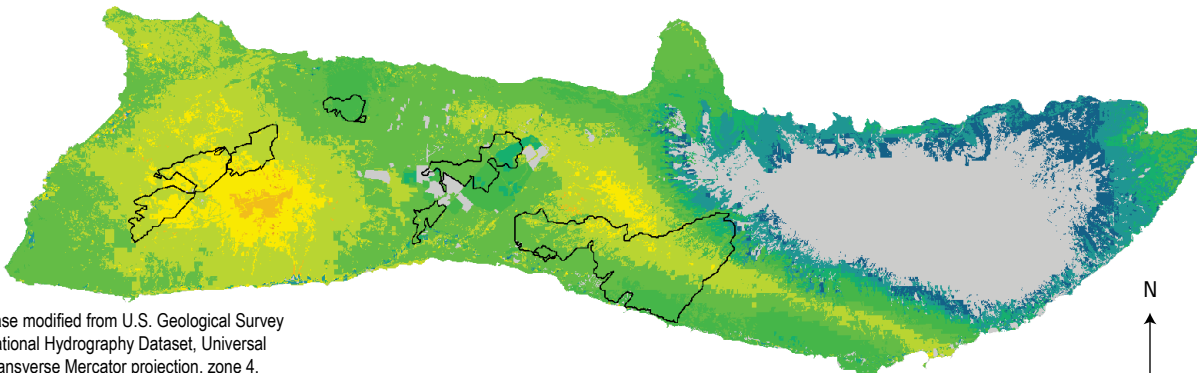
A. Drought 3



B. Future Non-Drought



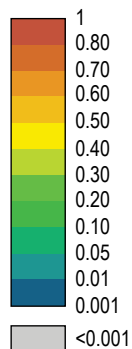
C. Future Drought 3



Base modified from U.S. Geological Survey
National Hydrography Dataset, Universal
Transverse Mercator projection, zone 4,
North American Datum of 1983.

EXPLANATION

Estimated change in relative frequency of monthly
evapotranspiration less than or equal to a value of 0.96 inches



— Perimeter of wildfire during 1999–2012
(University of Hawai'i at Mānoa, 2021)

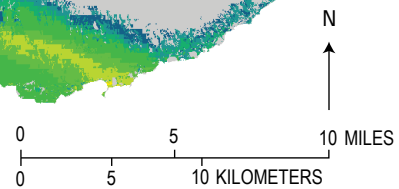
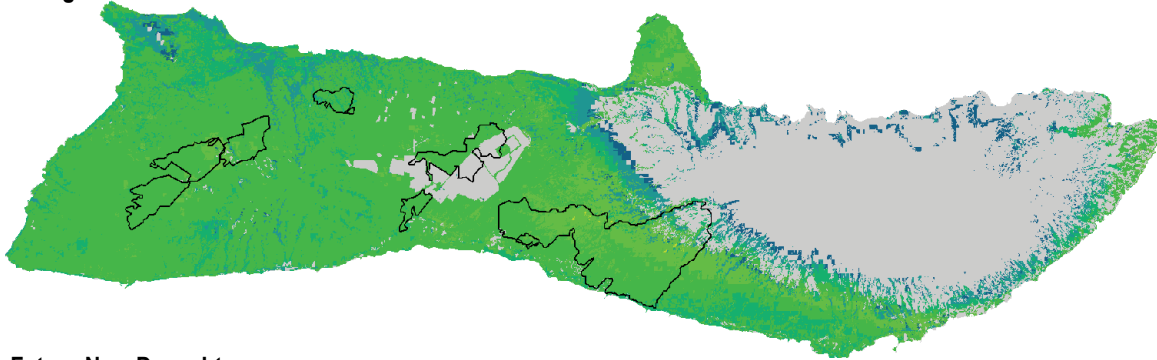
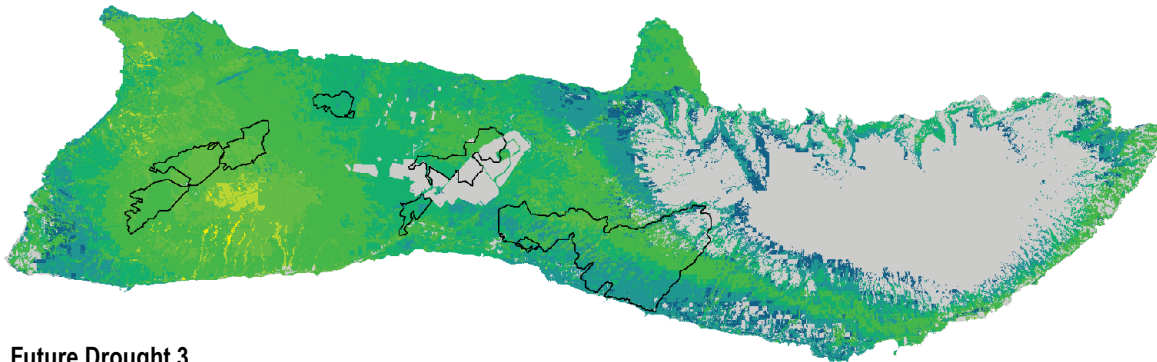
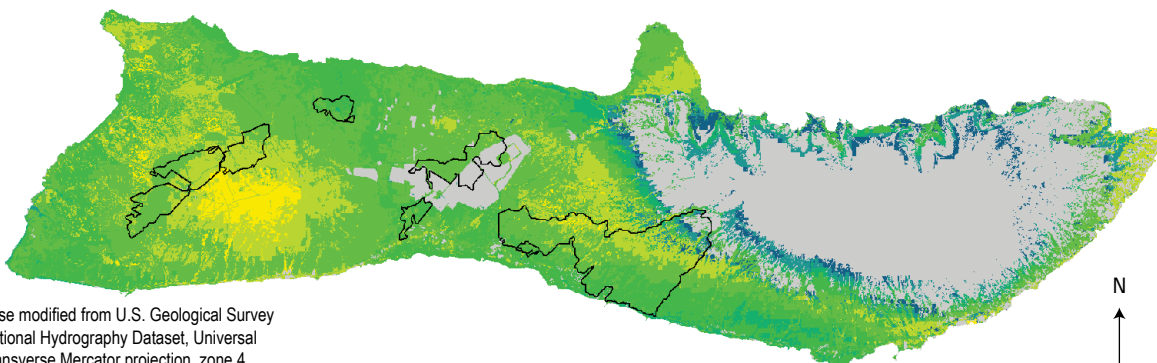


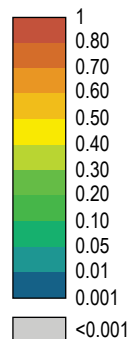
Figure 28. Maps showing estimated increases in relative frequency of monthly evapotranspiration less than or equal to a value of 0.96 inches for three water-budget scenarios for Moloka'i. *A*, Drought 3 scenario. *B*, Future Non-Drought scenario. *C*, Future Drought 3 scenario. All increases in relative frequency are relative to a Non-Drought scenario, which consists of rainfall during 1990–97 and 2003–06 from Frazier and others (2016), and 2020 land cover from Kāne and others (2024a). Drought 3 rainfall is rainfall during 1998–2002 and 2007–12 from Frazier and others (2016), Future Non-Drought rainfall is rainfall during 1990–97 and 2003–06 from Frazier and others (2016) adjusted for a RCP8.5 2071–99 projection from Elison Timm and others (2015), and Future Drought 3 rainfall is rainfall during 1998–2002 and 2007–12 from Frazier and others (2016) adjusted for a RCP8.5 2071–99 projection from Elison Timm and others (2015).

A. Drought 3**B. Future Non-Drought****C. Future Drought 3**

Base modified from U.S. Geological Survey
National Hydrography Dataset, Universal
Transverse Mercator projection, zone 4,
North American Datum of 1983.

EXPLANATION

Estimated change in relative frequency of monthly climatic water deficit greater than or equal to a value of 0.77—expressed as a fraction of potential evapotranspiration



— Perimeter of wildfire during 1999–2012
(University of Hawai'i at Mānoa, 2021)

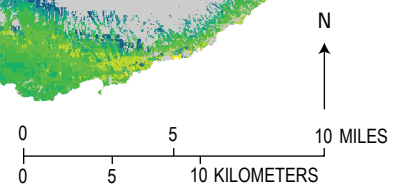


Figure 29. Maps showing estimated increases in relative frequency of monthly climatic water deficit greater than or equal to a value of 0.77 for three water-budget scenarios for Moloka'i. *A*, Drought 3 scenario. *B*, Future Non-Drought scenario. *C*, Future Drought 3 scenario. All increases in relative frequency are relative to a Non-Drought scenario, which consists of rainfall during 1990–97 and 2003–06 from Frazier and others (2016), and 2020 land cover from Kāne and others (2024a). Drought 3 rainfall is rainfall during 1998–2002 and 2007–12 from Frazier and others (2016), Future Non-Drought rainfall is rainfall during 1990–97 and 2003–06 from Frazier and others (2016) adjusted for a RCP8.5 2071–99 projection from Elison Timm and others (2015), and Future Drought 3 rainfall is rainfall during 1998–2002 and 2007–12 from Frazier and others (2016) adjusted for a RCP8.5 2071–99 projection from Elison Timm and others (2015).

Maui

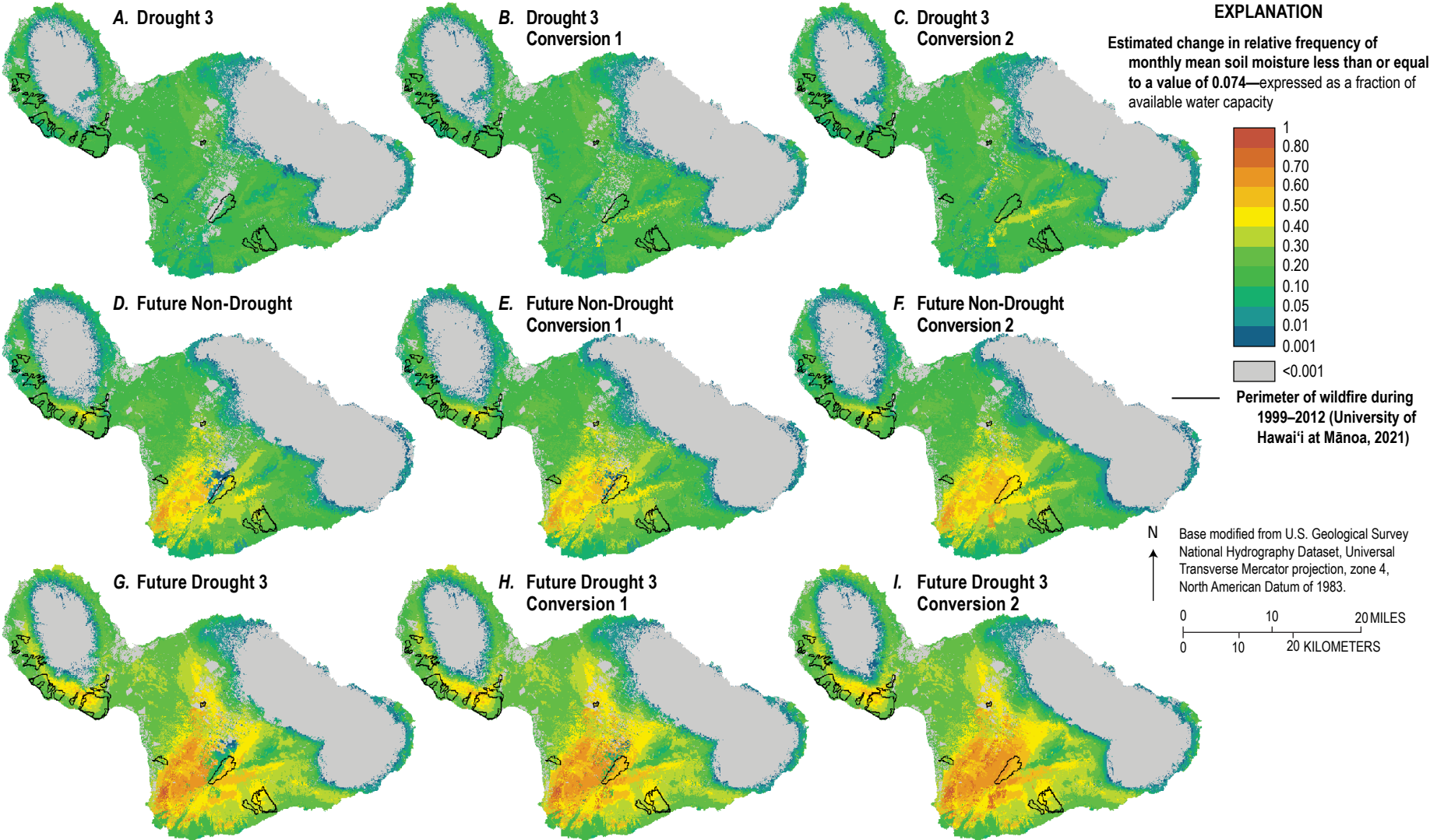
The Drought 3, Future Non-Drought, and Future Drought 3 scenarios produce increases in the relative frequency of moisture-stress indicators across extensive areas of Maui (figs. 30–32). For the Drought 3 scenario, the greatest change in relative frequency for the three moisture-stress indicators occurs across central Maui and low- to mid-altitude parts of West Maui, where increases are as high as 0.35 for soil moisture, 0.34 for ET, and 0.3 for CWD (figs. 30A, 31A, 32A). The positive change in relative frequency in these areas implies an increase in the frequency of low fuel-moisture conditions and wildfire hazard. Areas of little or no change in relative frequency, implying no change in wildfire hazard, include much of the wet, upland regions of West Maui volcano and windward parts of Haleakalā, and the irrigated agricultural, golf course, and developed areas of central and West Maui (figs. 1, 4D, 30A, 31A, 32A).

For the Future Non-Drought scenario, the greatest change in relative frequency for the three moisture-stress indicators occurs across a band of mid-altitude area on the southern slope of West Maui volcano and across the southwestern slope of Haleakalā, where increases are as high as 0.85 for soil moisture, 0.8 for ET, and 0.69 for CWD (figs. 4D, 30D, 31D,

32D). These increases in relative frequency imply that low-moisture conditions increase in duration in these areas, which would result in increased wildfire hazard. Areas of little or no change in relative frequency, implying no change in wildfire hazard, extend across the upland regions of the West Maui volcano and windward parts of Haleakalā, and the irrigated areas of the island (figs. 1, 4D, 30D, 31D, 32D).

For the Future Drought 3 scenario, the greatest change in relative frequency for the three moisture-stress indicators occurs across a band of mid-altitude area on the southern slope of West Maui volcano and across the southwestern slope of Haleakalā, where increases are as high as 0.94 for soil moisture, 0.92 for ET, and 0.8 for CWD (figs. 1, 4D, 30G, 31G, 32G). The extent and magnitude of these increases in relative frequency imply that low-moisture conditions expand and increase in duration in these areas of Maui, which implies substantial increases in wildfire hazard. Areas of little or no change in relative frequency, implying no change in wildfire hazard, extend across the upland regions of West Maui volcano, windward parts of Haleakalā, and the irrigated areas of the island (figs. 1, 4D, 30G, 31G, 32G). However, the areas of little or no change in relative frequency contract relative to the Drought 3 and Future Non-Drought scenarios, which indicates increased wildfire hazard for many upland forest areas of Maui.

Figure 30. Maps showing estimated increases in relative frequency of monthly mean soil moisture less than or equal to a value of 0.074 for nine water-budget scenarios for Maui. A, Drought 3 scenario. B, Drought 3 Conversion 1 scenario. C, Drought 3 Conversion 2 scenario. D, Future Non-Drought scenario. E, Future Non-Drought Conversion 1 scenario. F, Future Non-Drought Conversion 2 scenario. G, Future Drought 3 scenario. H, Future Drought 3 Conversion 1 scenario. I, Future Drought 3 Conversion 2 scenario. All increases in relative frequency are relative to a Non-Drought scenario, which consists of rainfall during 1990–97 and 2003–06 from Frazier and others (2016), and 2020 land cover from Kāne and others (2024a). Drought 3 rainfall is rainfall during 1998–2002 and 2007–12 from Frazier and others (2016), Future Non-Drought rainfall is rainfall during 1990–97 and 2003–06 from Frazier and others (2016) adjusted for a RCP8.5 2071–99 projection from Elison Timm and others (2015), and Future Drought 3 rainfall is rainfall during 1998–2002 and 2007–12 from Frazier and others (2016) adjusted for a RCP8.5 2071–99 projection from Elison Timm and others (2015). Conversion 1 land cover is land-cover condition in which roughly 50 percent of shrubland and forest areas within the cloud zone are converted to grassland; Conversion 2 land cover is land-cover condition in which 100 percent of shrubland and forest areas within the cloud zone are converted to grassland.



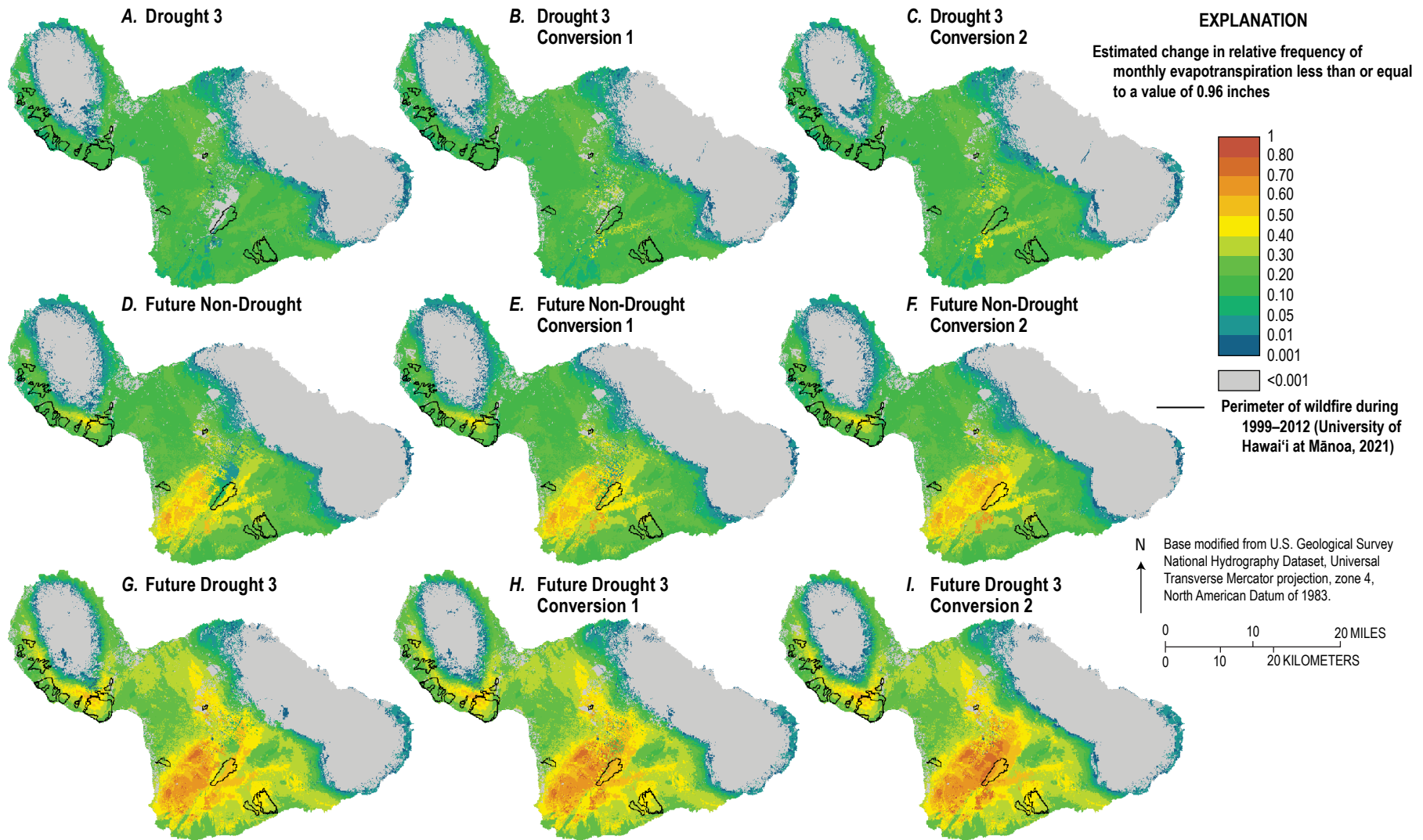


Figure 31. Maps showing estimated increases in relative frequency of monthly evapotranspiration less than or equal to a value of 0.96 inches for nine water-budget scenarios for Maui. A, Drought 3 scenario. B, Drought 3 Conversion 1 scenario. C, Drought 3 Conversion 2 scenario. D, Future Non-Drought scenario. E, Future Non-Drought Conversion 1 scenario. F, Future Non-Drought Conversion 2 scenario. G, Future Drought 3 scenario. H, Future Drought 3 Conversion 1 scenario. I, Future Drought 3 Conversion 2 scenario. All increases in relative frequency are relative to a Non-Drought scenario, which consists of rainfall during 1990–97 and 2003–06 from Frazier and others (2016), and 2020 land cover from Kāne and others (2024a). Drought 3 rainfall is rainfall during 1998–2002 and 2007–12 from Frazier and others (2016), Future Non-Drought rainfall is rainfall during 1990–97 and 2003–06 from Frazier and others (2016) adjusted for a RCP8.5 2071–99 projection from Elison Timm and others (2015), and Future Drought 3 rainfall is rainfall during 1998–2002 and 2007–12 from Frazier and others (2016) adjusted for a RCP8.5 2071–99 projection from Elison Timm and others (2015). Conversion 1 land cover is land-cover condition in which roughly 50 percent of shrubland and forest areas within the cloud zone are converted to grassland; Conversion 2 land cover is land-cover condition in which 100 percent of shrubland and forest areas within the cloud zone are converted to grassland.

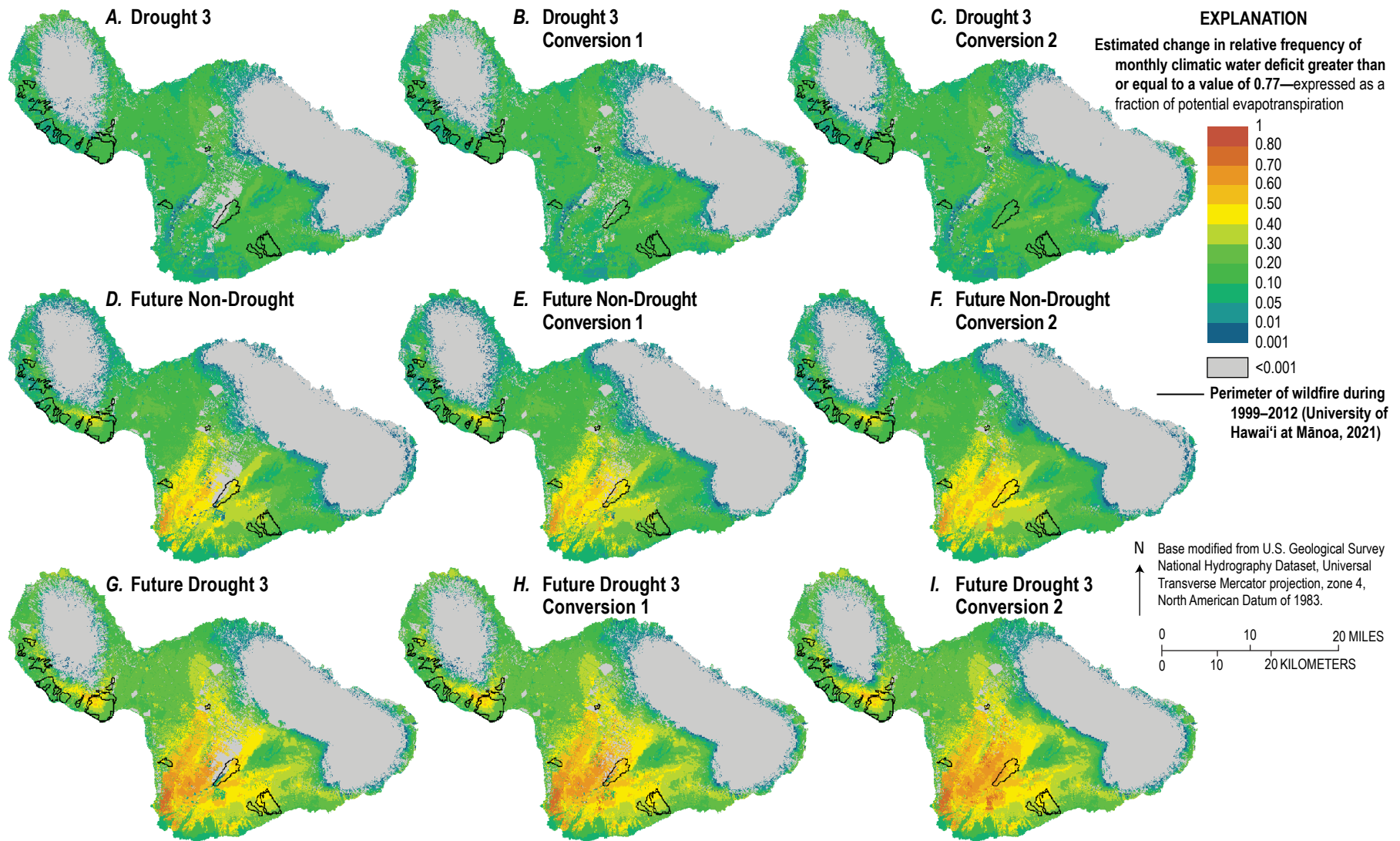


Figure 32. Maps showing estimated increases in relative frequency of monthly climatic water deficit greater than or equal to a value of 0.77 for nine water-budget scenarios for Maui. A, Drought 3 scenario. B, Drought 3 Conversion 1 scenario. C, Drought 3 Conversion 2 scenario. D, Future Non-Drought scenario. E, Future Non-Drought Conversion 1 scenario. F, Future Non-Drought Conversion 2 scenario. G, Future Drought 3 scenario. H, Future Drought 3 Conversion 1 scenario. I, Future Drought 3 Conversion 2 scenario. All increases in relative frequency are relative to a Non-Drought scenario, which consists of rainfall during 1990–97 and 2003–06 from Frazier and others (2016), and 2020 land cover from Kāne and others (2024a). Drought 3 rainfall is rainfall during 1998–2002 and 2007–12 from Frazier and others (2016), Future Non-Drought rainfall is rainfall during 1990–97 and 2003–06 from Frazier and others (2016) adjusted for a RCP8.5 2071–99 projection from Elison Timm and others (2015), and Future Drought 3 rainfall is rainfall during 1998–2002 and 2007–12 from Frazier and others (2016) adjusted for a RCP8.5 2071–99 projection from Elison Timm and others (2015). Conversion 1 land cover is land-cover condition in which roughly 50 percent of shrubland and forest areas within the cloud zone are converted to grassland; Conversion 2 land cover is land-cover condition in which 100 percent of shrubland and forest areas within the cloud zone are converted to grassland.

Island of Hawai‘i

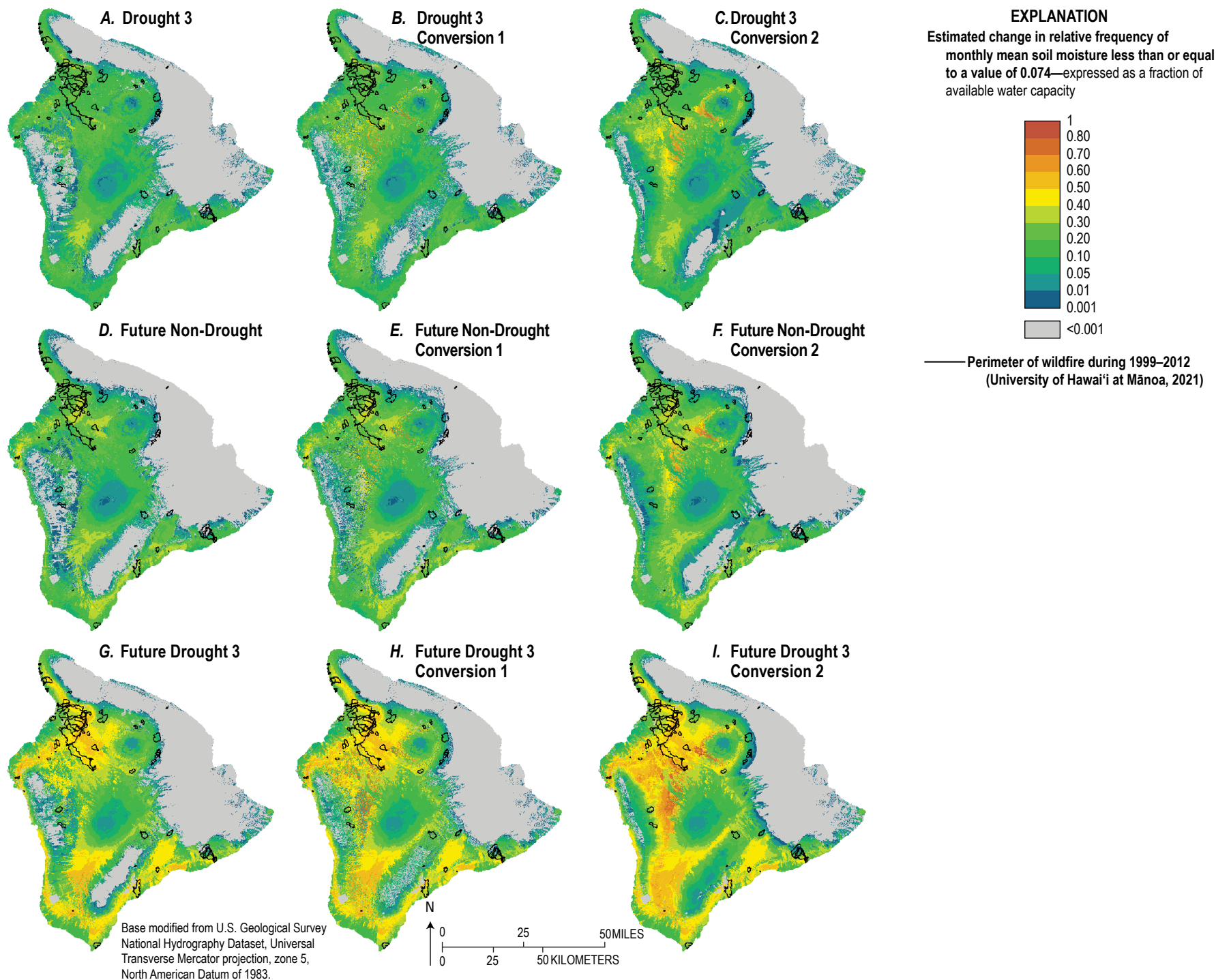
The Drought 3, Future Non-Drought, and Future Drought 3 scenarios produce increases in the relative frequency of moisture-stress indicators across extensive areas of the Island of Hawai‘i (figs. 33–35). For the Drought 3 scenario, the greatest change in relative frequency for the three moisture-stress indicators occurs across the northwestern and southern parts of the Island of Hawai‘i, where increases are as high as 0.52 for soil moisture, 0.50 for ET, and 0.44 for CWD (figs. 33A, 34A, 35A). Areas of little or no change in relative frequency, implying no change in wildfire hazard, extend across the upland region in the southern and western parts of the Island of Hawai‘i, and much of the northeastern region of the Island of Hawai‘i.

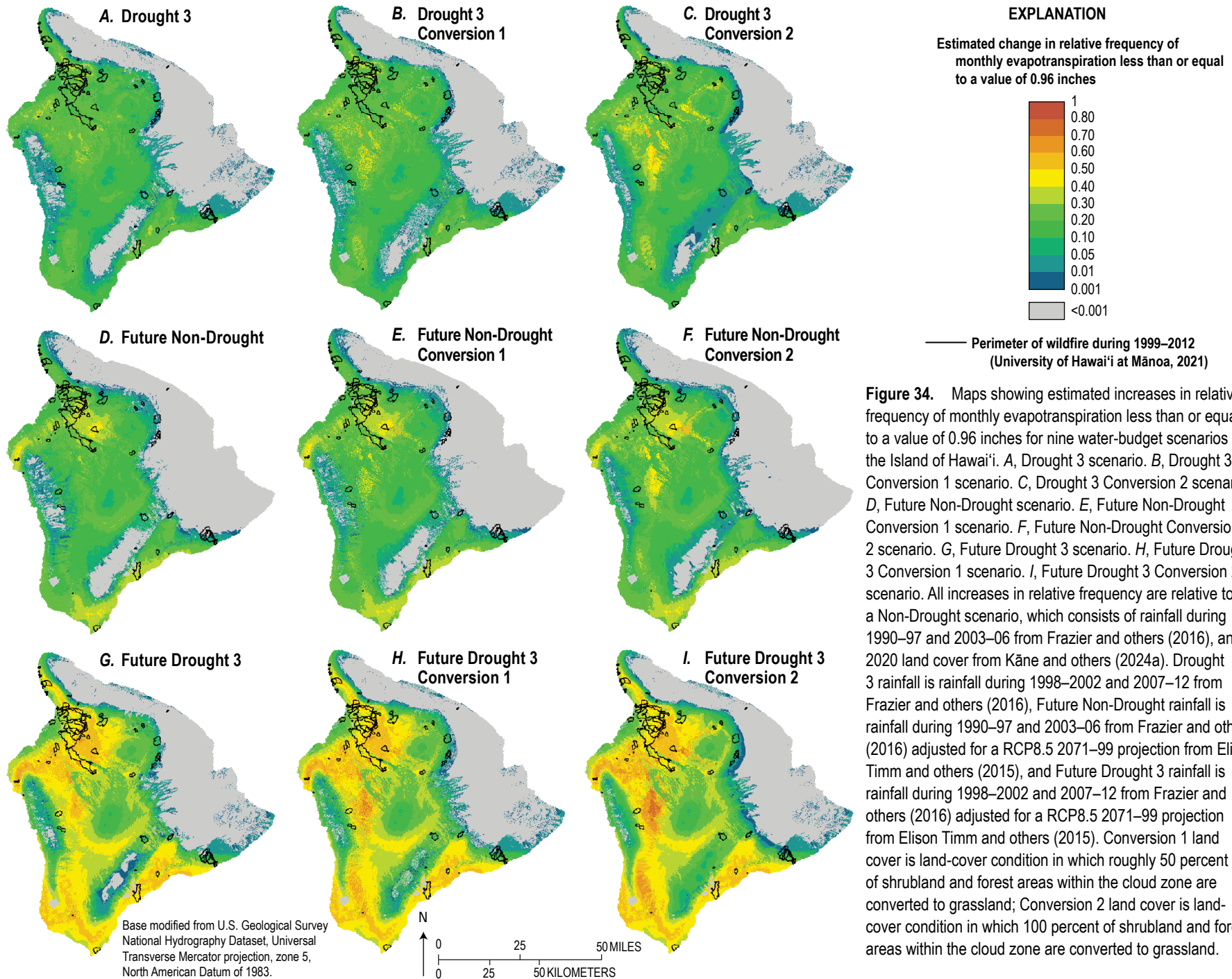
For the Future Non-Drought scenario, the greatest change in relative frequency occurs for the three moisture-stress indicators across northwestern and southern parts of the Island of Hawai‘i, where increases are as high as 0.81 for soil moisture, 0.59 for ET, and 0.58 for CWD (figs. 33D, 34D, 35D). These increases in relative frequency imply that low-moisture conditions increase in duration in these areas, which would result in increased wildfire hazard. Areas of little or no change in relative frequency imply no change in

wildfire hazard, and include the upland region in the southern and western parts of the Island of Hawai‘i, and much of the northeastern region of the Island of Hawai‘i.

For the Future Drought 3 scenario, the greatest change in relative frequency for the three moisture-stress indicators occurs across mid-altitude areas in the northwestern and southern parts of the Island of Hawai‘i, and a low- to mid-altitude band extending from the west coast to Kīlauea, where increases are as high as 0.93 for soil moisture, 0.81 for ET, and 0.72 for CWD (figs. 33G, 34G, 35G). The extent and magnitude of these increases in relative frequency imply that low-moisture conditions expand and increase in duration in these areas of the Island of Hawai‘i, which implies substantial increases in wildfire hazard. Areas of little or no change in relative frequency, implying no change in wildfire hazard, include the upland region in the southern and western parts of the Island of Hawai‘i, and much of the northeastern region of the Island of Hawai‘i. However, the areas of little or no change in relative frequency contract across forest areas in the western and southern parts of the Island of Hawai‘i relative to the Drought 3 and Future Non-Drought scenarios, which indicates increased wildfire hazard for many upland forest areas of the Island of Hawai‘i.

Figure 33. Maps showing estimated increases in relative frequency of monthly mean soil moisture less than or equal to a value of 0.074 for nine water-budget scenarios for the Island of Hawai‘i. A, Drought 3 scenario. B, Drought 3 Conversion 1 scenario. C, Drought 3 Conversion 2 scenario. D, Future Non-Drought scenario. E, Future Non-Drought Conversion 1 scenario. F, Future Non-Drought Conversion 2 scenario. G, Future Drought 3 scenario. H, Future Drought 3 Conversion 1 scenario. I, Future Drought 3 Conversion 2 scenario. All increases in relative frequency are relative to a Non-Drought scenario, which consists of rainfall during 1990–97 and 2003–06 from Frazier and others (2016), and 2020 land cover from Kāne and others (2024a). Drought 3 rainfall is rainfall during 1998–2002 and 2007–12 from Frazier and others (2016), Future Non-Drought rainfall is rainfall during 1990–97 and 2003–06 from Frazier and others (2016) adjusted for a RCP8.5 2071–99 projection from Elison Timm and others (2015), and Future Drought 3 rainfall is rainfall during 1998–2002 and 2007–12 from Frazier and others (2016) adjusted for a RCP8.5 2071–99 projection from Elison Timm and others (2015). Conversion 1 land cover is land-cover condition in which roughly 50 percent of shrubland and forest areas within the cloud zone are converted to grassland; Conversion 2 land cover is land-cover condition in which 100 percent of shrubland and forest areas within the cloud zone are converted to grassland.





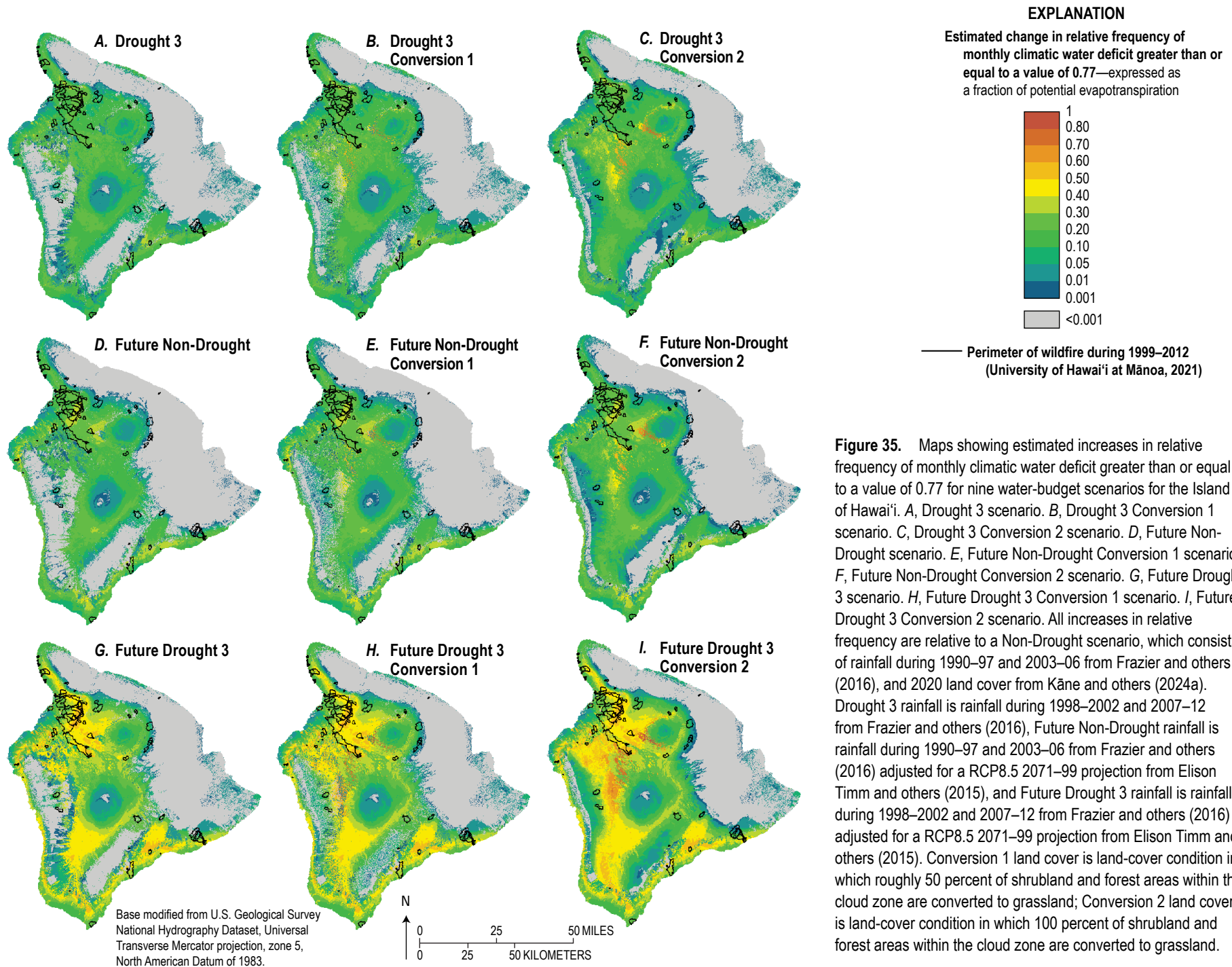


Figure 35. Maps showing estimated increases in relative frequency of monthly climatic water deficit greater than or equal to a value of 0.77 for nine water-budget scenarios for the Island of Hawai'i. *A*, Drought 3 scenario. *B*, Drought 3 Conversion 1 scenario. *C*, Drought 3 Conversion 2 scenario. *D*, Future Non-Drought scenario. *E*, Future Non-Drought Conversion 1 scenario. *F*, Future Non-Drought Conversion 2 scenario. *G*, Future Drought 3 scenario. *H*, Future Drought 3 Conversion 1 scenario. *I*, Future Drought 3 Conversion 2 scenario. All increases in relative frequency are relative to a Non-Drought scenario, which consists of rainfall during 1990–97 and 2003–06 from Frazier and others (2016), and 2020 land cover from Kāne and others (2024a). Drought 3 rainfall is rainfall during 1998–2002 and 2007–12 from Frazier and others (2016), Future Non-Drought rainfall is rainfall during 1990–97 and 2003–06 from Frazier and others (2016) adjusted for a RCP8.5 2071–99 projection from Elison Timm and others (2015), and Future Drought 3 rainfall is rainfall during 1998–2002 and 2007–12 from Frazier and others (2016) adjusted for a RCP8.5 2071–99 projection from Elison Timm and others (2015). Conversion 1 land cover is land-cover condition in which roughly 50 percent of shrubland and forest areas within the cloud zone are converted to grassland; Conversion 2 land cover is land-cover condition in which 100 percent of shrubland and forest areas within the cloud zone are converted to grassland.

Effects of Drought and Reduced Cloud-Water Interception

A total of six water-budget scenarios were added for O'ahu, Maui, and the Island of Hawai'i (table 5) to quantify the effect of reduced CWI during drought conditions as follows:

1. Drought 3 Conversion 1 scenario,
2. Drought 3 Conversion 2 scenario,
3. Future Non-Drought Conversion 1 scenario,
4. Future Non-Drought Conversion 2 scenario,
5. Future Drought 3 Conversion 1 scenario, and
6. Future Drought 3 Conversion 2 scenario.

The effect of drought on moisture stress was evaluated by examining the change in relative frequency of moisture-stress indicators between the Non-Drought scenario and the six water-budget scenarios. The change in relative frequency was computed for each subarea as the difference in relative frequency from the Non-Drought scenario. Increases in the relative frequency indicate an increase in the fraction of months that soil moisture or ET (or CWD) is less than or equal to (or greater than or equal to) the selected threshold value and imply an increase in the relative frequency of low-moisture conditions. Increases in the relative frequency of low-moisture conditions implies higher moisture stress, increased flammability due to low fuel moisture, and greater wildfire hazard, relative to the Non-Drought scenario. The effect of drought and reduced CWI for recent and projected climate conditions on the relative frequency of moisture-stress indicators for O'ahu, Maui, and the Island of Hawai'i is described in the following sections.

O'ahu

The Conversion 1 and 2 land-cover conditions produce increases in the relative frequency of moisture-stress indicators across some upland shrubland and forest areas of O'ahu (figs. 4B, 24–26). The most obvious increases in relative frequency of moisture-stress indicators occur around Ka'ala in the Wai'anae Range and the southeastern part of the Ko'olau Range (figs. 1, 24–26). For example, changes in relative frequency for the soil-moisture indicator in the upland area around Ka'ala indicate increases from less than 0.001 for the Future Drought 3 scenario to as much as 0.2 or more for

the Future Drought 3 Conversion 2 scenario (figs. 24G–I). The positive change in relative frequency in these areas of O'ahu implies increased frequency of low fuel-moisture conditions, which implies increased wildfire hazard attributable to conversions of shrubland and forest areas to grassland land cover within the cloud zone.

Maui

The Conversion 1 and 2 land-cover conditions produce increases in the relative frequency of moisture-stress indicators across upland shrubland and forest areas of Maui (figs. 4D, 30–32). The most obvious increases in relative frequency for the three moisture-stress indicators occur around the southern part of West Maui volcano and across the southwestern slope of Haleakalā (figs. 1, 30–32). For example, changes in relative frequency for the CWD indicator in the upland area of southwest Haleakalā indicate increases from less than 0.001 for the Future Drought 3 scenario to more than 0.6 for the Future Drought 3 Conversion 2 scenario (figs. 32G–I). The increases in relative frequency in these areas of Maui imply potentially substantial increases in the frequency of low fuel-moisture conditions, and increased wildfire hazard attributable to conversions of shrubland and forest areas to grassland land cover within the cloud zone.

Island of Hawai'i

The Conversion 1 and 2 land-cover conditions produce increases in the relative frequency of moisture-stress indicators across upland shrubland and forest areas of the Island of Hawai'i (figs. 4E, 33–35). The most obvious increases in relative frequency for the three moisture-stress indicators occur across the upland regions in the western and southern parts of the Island of Hawai'i. For example, within the cloud zone in the western part of the Island of Hawai'i, changes in relative frequency for the soil-moisture indicator indicate increases from as low as 0.01 for the Future Drought 3 scenario to more than 0.6 for the Future Drought 3 Conversion 2 scenario (figs. 33G–I). Within the cloud zone on the southeastern slope of Mauna Loa, changes in relative frequency for moisture-stress indicators indicate increases from less than 0.001 for the Future Drought 3 scenario to more than 0.2 for the Future Drought 3 Conversion 2 scenario (figs. 33G–I, 34G–I, 35G–I). The positive increases in relative frequency in these areas of the Island of Hawai'i imply potentially substantial increases in the frequency and extent of low fuel-moisture conditions, and increased wildfire hazard attributable to conversions of shrubland and forest areas to grassland land cover within the cloud zone.

Implications of Drought and Reduced Cloud-Water Interception for Groundwater Recharge, Soil Moisture, Evapotranspiration, and Climatic Water Deficit

Groundwater Recharge

The WATRMOD simulations for the historical and future drought conditions, and 2020 land cover show decreases in mean annual groundwater recharge across Kauaʻi, Oʻahu, Molokaʻi, Maui, and the Island of Hawaiʻi, relative to the reference condition consisting of 1978–2007 rainfall and 2020 land cover (figs. 8, 10, 12, 14, and 16). Island-wide recharge for these five islands decreased between 30 and 39 percent for the historical drought condition and between 40 and 51 percent for the future drought condition (table 6). The greatest decrease in island-wide recharge for the historical drought condition occurs on the Island of Hawaiʻi where island-wide recharge is estimated to decrease by 39 percent. The greatest decrease for the future drought condition occurs on Molokaʻi where island-wide recharge is estimated to decrease by 51 percent. In general, absolute changes in recharge from the reference conditions were greatest in wetter, windward parts of each island, whereas relative changes were greatest in drier, leeward parts of each island. In terms of aquifer-system recharge, the greatest decreases in aquifer-system recharge generally occur in the drier, leeward parts of each island. For example, aquifer-system recharge for the historical drought condition is estimated to decrease by 50 percent or more on Kauaʻi (one aquifer system), Oʻahu (11 aquifer systems), Molokaʻi (six aquifer systems), Maui (one aquifer system), and the Island of Hawaiʻi (14 aquifer systems) (figs. 9, 11, 13, 15, and 17). Aquifer-system recharge for the future drought condition is estimated to decrease by 80 percent or more on Kauaʻi (one aquifer system), Oʻahu (eight aquifer systems), Molokaʻi (four aquifer systems), Maui (three aquifer systems), and the Island of Hawaiʻi (seven aquifer systems) (figs. 9, 11, 13, 15, and 17).

Reduced CWI through conversion of forest and shrubland to grassland in the WATRMOD simulations further reduces estimates of island-wide recharge on Oʻahu, Maui, and the Island of Hawaiʻi. In the WATRMOD simulations, conversions of all shrubland and forest areas within the cloud zone to grassland land cover eliminate contributions of CWI and increase losses to ET, which effectively decreases recharge within the cloud zone. For Oʻahu, conversion of all shrubland and forest areas to grassland within the cloud zone for the historical and future drought conditions decreases island-wide recharge by 36 and 49 percent, respectively, relative to the reference condition of 1978–2007 rainfall and 2020 land cover. For Maui and the Island of Hawaiʻi, conversion of all shrubland and forest areas within the cloud zone to grassland

for the historical and future drought conditions decreases island-wide recharge by 44 and 50 percent, respectively, on Maui, and by 52 and 57 percent, respectively, on the Island of Hawaiʻi. For Oʻahu, these decreases in estimated recharge imply that existing shrubland and forest land cover, that is, 2020 land cover, within the cloud zone effectively contributes 11 to 12 Mgal/d more recharge than grassland land cover during similar historical and future drought conditions. For Maui and the Island of Hawaiʻi, existing shrubland and forest land cover within the cloud zone effectively contributes 119 to 135 Mgal/d (Maui) and 689 to 849 Mgal/d (Island of Hawaiʻi) more recharge than grassland land cover during similar drought conditions. In terms of percentage change in island-wide recharge, conversions of all shrubland and forest areas within the cloud zone to grassland land cover during historical and future drought conditions would result in land-cover-related decreases of 3 percent for Oʻahu, 17 percent for Maui, and 19 to 20 percent for the Island of Hawaiʻi.

The results of this study indicate estimated changes in the amount and distribution of groundwater recharge on Kauaʻi, Oʻahu, Molokaʻi, Maui, and the Island of Hawaiʻi for a set of drought and hypothetical land-cover conditions that could affect groundwater availability. Furthermore, these changes in recharge could also affect groundwater levels and salinity in production wells that supply potable drinking water. Changes in recharge could also affect aquatic ecosystems that rely on groundwater discharge to streams and nearshore marine environments. The scope of this study does not include an assessment of groundwater availability related to the estimated changes in groundwater recharge for the drought and hypothetical land-cover conditions included in this study. Assessments of groundwater availability in Hawaiʻi over the past 15 years have involved the use of numerical groundwater-flow models to address information needs related to, but not limited to, the following: (1) quantifying the effects of pumping existing or proposed wells on the salinity of groundwater and discharge of groundwater near the coast, (2) identifying areas for new groundwater development, (3) distributing pumping to increase the overall amount of fresh groundwater withdrawn, and (4) estimating the long-term effects of potential changes in groundwater recharge (Gingerich, 2008; Gingerich and Engott, 2012; Oki and others, 2020; Izuka and Rotzoll, 2021; Rotzoll and others, 2022).

Soil Moisture, Evapotranspiration, and Climatic Water Deficit

Frequency characteristics of soil moisture, ET, and CWD estimates relative to the selected threshold values change substantially during drought conditions and indicate areas of increased moisture stress on vegetation on Kauaʻi, Oʻahu, Molokaʻi, Maui, and the Island of Hawaiʻi. Increases in moisture stress on vegetation decrease fuel moisture, that is, moisture in living and dead vegetation, which increases landscape flammability and wildfire hazard. For historical drought conditions, areas of increased moisture stress occur

in the drier leeward parts of each island where increases in the relative frequency of moisture-stress indicators are as high as 0.35 to 0.52 across parts of the five islands. For future non-drought conditions, relative frequency for the three moisture-stress indicators increase by as much as 0.54 to 0.92, which indicates that future non-drought conditions for the RCP8.5 2071–99 projection produce greater moisture stress on vegetation than estimated for historical drought conditions across parts of each island. For future drought conditions, increases in relative frequency for the three moisture-stress indicators are as high as 0.68 to 0.99 and indicate substantial increases in the extent and frequency of moisture stress on vegetation on each island. Areas of greatest change in moisture stress on vegetation for the future drought condition occur across extensive mid-altitude areas of southwestern Kauaʻi, western Oʻahu, western Molokaʻi, southern West Maui volcano and southwestern Haleakalā on Maui, and the northwestern and southern parts of the Island of Hawaiʻi. Areas of little or no change in moisture stress on vegetation during future drought conditions are generally confined to parts of the wet windward and mountainous regions of each island.

Reduced CWI through hypothetical conversions of shrubland and forest areas to grassland within the cloud zone further increases the frequency of low-moisture conditions that increase moisture stress on vegetation within the cloud zones of Oʻahu, Maui, and the Island of Hawaiʻi. In the WATMod simulations, conversions of shrubland and forest areas within the cloud zone to grassland eliminate contributions of CWI and increase losses to ET, which effectively increases moisture stress on vegetation within the cloud zone. Areas of greatest change in moisture stress on vegetation owing to conversions of shrubland and forest areas to grassland within the cloud zone occur around Kaʻala on Oʻahu, southern West Maui volcano and southwestern Haleakalā on Maui, and western and southeastern Mauna Loa on the Island of Hawaiʻi.

The results of this study indicate estimated increases in the relative frequency of soil moisture, ET, and CWD indicators of moisture stress on Kauaʻi, Oʻahu, Molokaʻi, Maui, and the Island of Hawaiʻi for a set of drought and hypothetical land-cover conditions that could affect the potential range and survivability of native and non-native forest species that rely on adequate fluxes of moisture to the plant-root zone. However, the scope of this study does not include an assessment of projected changes in the range of native and non-native forest species for the future climate condition included in this study.

Study Limitations

This study relies on the availability of various types of physical data for simulating hydrological processes and physical conditions that affect groundwater recharge for a set of drought and land-cover conditions. Lack of data or sparse, uneven distribution of data in space and time, and poor understanding of some hydrologically relevant processes limit the precision and accuracy of study results. This section

describes the limitations imposed by selected model input datasets for simulating the effects of drought and land-cover conditions on groundwater recharge, soil moisture, ET, and CWD. Information that could advance future efforts to reduce the uncertainty associated with recharge, soil moisture, ET, and CWD estimates and to assess the effects of drought and land-cover conditions on groundwater availability and wildfire hazard is also discussed. Descriptions of the WATMod limitations are provided in Oki (2022).

Rainfall—Rainfall is an essential dataset for estimating recharge in the water budget. Although the State of Hawaiʻi has a higher number of rain gages per square mile than most other places, the placement of gages and their periods of operation have commonly been dictated by the water-supply needs of humans—particularly for agriculture (Giambelluca and others, 1986). One of the primary sources of rainfall data used in this study, the Rainfall Atlas of Hawaiʻi by Giambelluca and others (2013), discusses limitations to rainfall regionalization related to the number and distribution of rain gages and the limited periods of record; these limitations translate to limitations in the recharge results of this study. The online version of the rainfall atlas provides maps of rain-gage locations and uncertainty in the extrapolated rainfall estimates. These maps indicate that rain gages are scarce in areas that are less populated or unfavorable for agriculture, such as in the high-altitude interiors of islands or areas that have rugged terrain. Rainfall estimates for these areas thus have a greater degree of uncertainty, yet these tend to be the wettest areas of the islands and the areas where most recharge occurs. For example, the effect of rain-gage scarcity on rainfall estimates is evident in some drainage basins along the windward region of the Island of Hawaiʻi where direct runoff estimates derived from streamgage data exceed concurrent rainfall represented in the monthly mean rainfall maps by Frazier and others (2016). The streamgage data from these wet drainage basins indicate that the monthly mean rainfall maps by Frazier and others (2016) might be underestimating rainfall across the area. Recharge estimates can be improved with rainfall data from these sparsely gaged areas. Cheng and others (2021) evaluated the rainfall monitoring needs for the State of Hawaiʻi and proposed a monitoring network that includes additional rain-gage sites in sparsely gaged areas. To address the need for additional rainfall monitoring stations, rain gages are now being deployed across many sparsely gaged areas of the main Hawaiian Islands (<https://www.hawaii.edu/climate-data-portal/hawaii-mesonet/>).

In this study, daily rainfall frequency refers to the sequence, magnitude, and distribution of daily rainfall for any given subarea and month during a specified simulation period, such as the 1990–2012 time period. The projected effects of potential changes to daily rainfall frequency on recharge and other water-budget components could not be simulated for the RCP8.5 2071–99 projection from Elison Timm and others (2015) because estimates of daily rainfall frequency were not available for this projection. WATMod estimates for future

conditions can be improved with information on projected changes in daily rainfall frequency.

Cloud-water interception—Measurements of CWI in the Hawaiian Islands are particularly scant. Contributions of water from CWI are believed to provide a substantial part of the water available for groundwater recharge over large areas of the Hawaiian Islands but CWI has been measured by only a few studies in a few places. As a result, CWI distribution was applied in a generalized fashion in the recharge calculation. For example, CWI is computed in the WATRMod simulations as a fraction of daily rainfall, which implies that CWI can only occur when daily rainfall occurs and is a limitation of the approach. Water-budget estimates can be improved with better quantification of the spatial and temporal variability of CWI rates, and the ability of different types of vegetation to intercept cloud water.

Projected effects of potential changes to CWI rates and cloud-zone altitudes, and their effect on water-budget estimates, could not be simulated for the selected future climate condition. Contributions of water from CWI may provide an important part of the water available for recharge, soil moisture, and ET on each island. Hence, water-budget estimates for future climate conditions can be improved with information that describes the potential changes in CWI rates and cloud-zone altitudes for future conditions.

Runoff—Runoff in gaged areas is estimated in the model using seasonal runoff-to-rainfall ratios that are derived from monitoring data from a limited number of streamgage stations on each of the islands considered in this study. In ungaged areas, runoff is estimated using runoff-to-rainfall ratios derived from statistical analyses of available streamgage and rain-gage data. For the future climate condition, seasonal runoff-to-rainfall ratios derived from statistical analyses also are used to estimate runoff in all gaged and ungaged areas. Streamgage data indicate that rainfall may be underestimated in some parts of Hawai‘i due to a sparse number of rain gages, and imply that runoff may be underestimated in these ungaged areas. Hence, runoff estimates can be improved with streamgage data from currently ungaged areas and from rainfall data in sparsely gaged areas, which also would improve water-budget estimates for recent and future climate conditions. Cheng and others (2021) evaluated the streamflow monitoring needs for the State of Hawai‘i and proposed a monitoring network that includes additional streamgage sites in ungaged areas.

Reference evapotranspiration—The concept of potential ET, combined with empirical models when soil moisture is limited, is used by WATRMod to estimate ground evaporation and transpiration in daily potential-ET rate for each subarea is computed as the product of its crop coefficient and the daily reference-ET rate. Giambelluca and others (2014) developed spatially dependent (250-m resolution) and temporally dependent (for each month, a mean monthly value and 24-hourly values representing the mean diurnal cycle) maps of reference ET for the main Hawaiian Islands, excluding Ni‘ihau. In this study, the daily reference-ET rate

was computed using the maps of mean monthly reference-ET rates from Giambelluca and others (2014) and assumed to be the same each day of a given month. The use of mean monthly reference-ET rates was necessary because monthly maps of reference-ET rates during 1920–2012, similar to the maps of monthly rainfall during 1920–2012 from Frazier and others (2016), were unavailable. The projected effects of potential changes to reference-ET rates on recharge could not be simulated for the RCP8.5 2071–99 projection used in this study because projections for reference ET were not available. Recharge estimates could be improved with better estimates of how reference ET varies temporally for recent conditions and for each future climate projection.

Canopy evaporation, net precipitation, and transpiration—The current understanding of the regional effects of highly invasive non-native and dominant native forest species on water resources is incomplete. Because of limited data, the WATRMod simulations of canopy evaporation, net precipitation, and transpiration processes in this study are mostly limited to broad categories of forest land cover, such as non-native forest, native forest, tree plantation, and grassland land cover. In this study, for example, transpiration for non-native forest below the cloud zone is estimated using only one set of model input parameter values for root depth, depletion fraction, and crop coefficient (Appendix 1, table 1.1). Canopy evaporation is estimated using only one set of model input parameter values for canopy capacity, trunk-storage capacity, and stemflow rate for all types of forest land cover. For example, values of 0.05 in, 0.01 in, and 0.04 are used for canopy capacity, trunk-storage capacity and stemflow rate, respectively, for subareas with non-native forest land cover. However, Safeeq and Fares (2014) calculated values of 0.05 in, 0.02 in, and 0.37 for canopy capacity, trunk-storage capacity, and stemflow rate, respectively, for simulating canopy evaporation from a monotypic stand of strawberry guava (*Psidium cattleianum*). Strawberry guava has been identified as a high-priority non-native species of concern on several of the main Hawaiian Islands (Johnson and others, 2023) and extensive areas have been identified on Kaua‘i, O‘ahu, Moloka‘i, Lāna‘i, Maui, and the Island of Hawai‘i (Geometrician Associates, LLC, 2011). The higher values for trunk-storage capacity and stemflow rate imply higher canopy evaporation and lower recharge relative to estimates using baseline values in areas dominated by strawberry guava. Water-budget estimates could be improved with the development of these model input parameters for specific types of forest species or forest environments, as well as land-cover maps that reflect specific types of forest species or forest environments (see following discussion of “Land Cover”). Johnson and others (2023) identified a set of information needs to reduce the uncertainty in recharge estimates for three moisture zones (dry, mesic, and wet) on O‘ahu and Maui that includes estimates or measurements of the following: (1) evapotranspiration processes needed to determine crop coefficients for land-cover types in all moisture zones, (2) rooting depths for land-cover types in the dry and

mesic moisture zones, (3) canopy-cover fraction for forests in the wet and mesic moisture zones, (4) ratios of cloud-water interception to rainfall for forests and shrublands in the wet moisture zone, and (5) canopy capacity for forests in the wet and mesic moisture zones.

The projected effects of potential changes to canopy evaporation on recharge and other water-budget components could not be simulated for the RCP8.5 2071–99 projection because projections for canopy evaporation were not available for this projection. Improved spatial estimates of the ratio of the mean evaporation rate to the mean precipitation rate during saturated canopy conditions would be helpful for estimating the spatial distribution of canopy evaporation and the projected effects of future climate conditions on canopy evaporation.

Seepage rates from unlined reservoir, inland water body, and taro land cover—Seepage rates from subareas with unlined reservoir, inland water body, and taro land cover were estimated from limited available data. Seepage rates were assigned to model subareas with unlined reservoir land cover on the basis of available information and generally decrease with age of the soils and substrate associated with each island. For example, published seepage rates for unlined reservoirs range from relatively low values on Kaua‘i, the oldest island, to relatively high values on Maui, one of the youngest islands. However, these studies were conducted at a limited number of locations on Kaua‘i, Moloka‘i, and Maui, and may not capture the full range of reservoir seepage rates for unlined reservoirs on each island and throughout the State of Hawai‘i. The seepage rate assigned to inland water body land cover in this study is based on estimates from published studies. The seepage rates used for unlined reservoir, inland water body, and taro land cover were considered constant values, regardless of possible substantial fluctuations in surface-water availability from episodic dry or wet periods. Water-budget estimates could be improved with better quantification of seepage rates from unlined reservoir, inland water body, and taro land cover on each island and for a range of climate conditions.

Taro cultivation—For this study, only a subset of the wetland taro areas delineated in the land-cover map for each island was considered to be irrigated and cultivated at any one time. The subset of wetland taro areas was determined from the number of acres of irrigated taro in each county that were harvested during a single year as reported in a National Agricultural Statistics Service census of crop production. The information used in the census is provided voluntarily by commercial taro farmers and does not include non-commercial taro farming. Hence, the actual percentage of wetland taro areas being irrigated and cultivated on each island may differ from the census information. Also, the irrigation rate for wetland taro was estimated as the mean value from a limited number of water-use studies of wetland taro in the State of Hawai‘i. Water-budget estimates could be improved with better quantification of wetland taro cultivation areas and of irrigation rates needed to support wetland taro across the range of current and potential cultivation areas.

Areas of groundwater discharge and streambed infiltration—The island-wide water budget models might not accurately estimate recharge in some areas where hydrologic processes are not represented or poorly understood. For example, the water-budget method might overestimate recharge in areas, such as wetlands, where groundwater is discharging because recharge might be rejected. In losing reaches of streams, recharge following a storm can occur for several days following the cessation of rainfall as streamflow recedes. However, due to a limited understanding of groundwater discharge and streambed infiltration rates, these processes are not explicitly represented in the WATRMOD simulations.

Impervious surfaces—The calculations in WATRMOD require that excess water from the impervious fraction be distributed to a pervious part of each subarea, which implies that a subarea cannot be completely impervious and is a limitation of the approach. Therefore, all subareas were reassigned a value of 0.99 for impervious fraction whenever the value computed from the map of impervious surfaces exceeded 0.99.

Land Cover—An understanding of the effects of existing land-cover conditions on water-budget estimates could be improved by linking maps of specific forest species or forest environments with model input parameters for estimating canopy evaporation, net precipitation, and transpiration from those same forest species or forest environments, which could reduce the uncertainty of groundwater recharge, soil moisture, ET, and CWD estimates (see previous discussion of “[Canopy evaporation, net precipitation, and transpiration](#)”). The effects of future land-cover conditions on water-budget estimates were considered for two hypothetical land-cover conditions: (1) conversion of roughly 50 percent of shrubland and forest within the cloud zone to grassland, and (2) conversion of 100 percent of shrubland and forest within the cloud zone to grassland. The hypothetical land-cover conditions were developed to quantify the effect of reduced CWI on groundwater recharge, soil moisture, ET, and CWD. Maps of future land-cover conditions on each island would be helpful for evaluating the effects of (1) planned development, (2) climate-induced changes in the distribution of the dominant types of forest species, and (3) watershed management and restoration efforts including planned revegetation of bare or eroded land, and afforestation of grassland-dominated areas. The approach used for this study, however, did allow for quantifying the effect of reduced CWI on recharge, soil moisture, ET, and CWD.

Fuel biomass—Antecedent wet periods can increase the amount of living and dead vegetation (or fuel biomass) during a drought, which can increase wildfire hazard. In this study, the water-budget modeling approach was used to track water inputs, water outputs, and changes in stored water in the plant-root zone. However, the approach did not track or estimate changes in the amount of fuel biomass. Hence, the estimates of relative frequency for soil moisture, ET, and CWD that were used to identify areas of increased wildfire hazard do not directly account for the duration or magnitude of potential intermonthly changes in fuel biomass.

Summary

The main objectives of this study were to: (1) estimate changes in groundwater recharge, soil moisture, evapotranspiration (ET), and climatic water deficit (CWD) during periods of drought and long-term drying for recent and future climate conditions for Kauaʻi, Oʻahu, Molokaʻi, Maui, and the Island of Hawaiʻi, and (2) quantify the effects of reduced cloud-water interception (CWI) on groundwater recharge, soil moisture, ET, and CWD. The study was divided into two parts, one part to address the effects on groundwater recharge and the second part to address the effects on soil moisture, ET, and CWD. Soil moisture, ET, and CWD can be used as indicators of moisture stress in vegetation and potential wildfire hazard. In this study, wildfire hazard refers to the prevalence of moisture stress in living vegetation that is favorable for wildfire occurrence and propagation.

In the first part of this study, the Water-budget Accounting for Tropical Regions Model (WATRMod) code was used to quantify the effects of drought and reduced CWI on groundwater recharge for historical and future dry-climate conditions. Two drought conditions were defined for each island in the study area: (1) a historical drought condition during 1998–2002 for Kauaʻi, Oʻahu, and Molokaʻi, and during 2007–12 for Maui and the Island of Hawaiʻi, and (2) a future drought condition using projected rainfall conditions during 2071–99 from Elison Timm and others (2015) for a Representative Concentration Pathway (RCP) warming scenario with a total radiative forcing of 8.5 watts per square meter (W/m^2) by the year 2100 (RCP8.5 2071–99 projection) (Intergovernmental Panel on Climate Change, 2014). A map of 2020 land cover was used in the WATRMod simulations for both drought scenarios. The effect of reduced CWI on groundwater recharge was simulated by converting shrubland and forest land cover within the cloud zone to grassland land cover, for which CWI is considered to be negligible. Two hypothetical land-cover conditions were defined for Oʻahu, Maui, and the Island of Hawaiʻi: (1) a land-cover condition in which roughly 50 percent of shrubland and forest areas within the cloud zone were converted to grassland, and (2) a land-cover condition in which 100 percent of shrubland and forest areas within the cloud zone were converted to grassland. Recharge was computed with a water-budget model that used a daily computation interval. Hydrologic processes and physical conditions that affect recharge on Kauaʻi, Oʻahu, Molokaʻi, Maui, and the Island of Hawaiʻi for recent and future climate conditions were simulated in the water-budget model using the most recent datasets available—including maps of 2020 land cover, 1990–2012 monthly rainfall, 1990–2014 daily rainfall, and mean monthly reference ET. A published high-resolution downscaled climate projection was used to modify inputs of monthly rainfall and seasonal runoff for simulating the effects of the RCP8.5 2071–99 projection.

In general, absolute changes in recharge from the reference conditions were greatest in wetter, windward parts of each island, and relative changes were greatest in drier,

leeward parts of each island. For Kauaʻi, island-wide mean annual recharge is 568 million gallons per day (Mgal/d) for the historical drought condition, which is a decrease of 239 Mgal/d (30 percent) from the reference condition consisting of 1978–2007 rainfall and 2020 land cover. For the future drought condition, island-wide mean annual recharge is 433 Mgal/d, which is a decrease of 373 Mgal/d (46 percent) from the reference condition. For Oʻahu, island-wide mean annual recharge is 396 Mgal/d for the historical drought condition, which is a decrease of 201 Mgal/d (34 percent) from the reference condition. For the future drought condition, island-wide mean annual recharge is 316 Mgal/d, which is a decrease of 281 Mgal/d (47 percent) from the reference condition. For Molokaʻi, island-wide mean annual recharge is 145 Mgal/d for the historical drought condition, which is a decrease of 83 Mgal/d (36 percent) from the reference condition. For the future drought condition, island-wide mean annual recharge is 113 Mgal/d, which is a decrease of 116 Mgal/d (51 percent) from the reference condition. For Maui, island-wide mean annual recharge is 798 Mgal/d for the historical drought condition, which is a decrease of 394 Mgal/d (33 percent) from the reference condition. For the future drought condition, island-wide mean annual recharge is 715 Mgal/d, which is a decrease of 477 Mgal/d (40 percent) from the reference condition. For the Island of Hawaiʻi, island-wide mean annual recharge is 4,179 Mgal/d for the historical drought condition, which is a decrease of 2,706 Mgal/d (39 percent) from the reference condition. For the future drought condition, island-wide mean annual recharge is 3,670 Mgal/d, which is a decrease of 3,215 Mgal/d (47 percent) from the reference condition.

Eliminating CWI through complete conversion of shrubland and forest land cover within the cloud zone to grassland land cover reduces groundwater recharge estimates for Oʻahu, Maui, and the Island of Hawaiʻi. For Oʻahu, these hypothetical changes in land cover correspond to land-cover-related decreases in island-wide mean annual recharge of 12 and 11 Mgal/d (3 percent) for the historical and future drought conditions, respectively. For Maui, these hypothetical changes in land cover correspond to land-cover-related decreases in island-wide mean annual recharge of 135 and 119 Mgal/d (17 percent) for the historical and future drought conditions, respectively. For the Island of Hawaiʻi, these hypothetical changes in land cover correspond to land-cover-related decreases in island-wide mean annual recharge of 849 and 689 Mgal/d (20 and 19 percent) for the historical and future drought conditions, respectively.

In the second part of this study, the water-budget models were used to quantify the effects of drought and reduced CWI on soil moisture, ET, and CWD for recent and future dry-climate conditions. Four drought conditions were defined for each island in the study area: (1) a reference condition representative of non-drought climate conditions during 1990–2012, (2) a historical drought condition representative of the driest periods during 1920–2012, (3) a future non-drought condition representative of non-drought climate

conditions for a RCP8.5 2071–99 projection, and (4) a future drought condition representative of drought conditions for a RCP8.5 2071–99 projection. A map of 2020 land cover was used in the WATRMod simulations for each of the drought conditions. The added effect of reduced CWI on soil moisture, ET, and CWD was evaluated using the two hypothetical land-cover conditions for O‘ahu, Maui, and the Island of Hawai‘i. Monthly time series output from the WATRMod simulations were analyzed to determine the relative frequency of soil moisture, ET, and CWD estimates greater or less than selected moisture-stress levels for each island in the study area. For the reference condition, time series of estimated soil moisture, evapotranspiration, and climatic water deficit were each compared to a selected threshold level to determine the spatial distributions of relative frequencies for each indicator of moisture stress and potential wildfire hazard. Relative frequencies for other conditions were then compared to those from the reference condition to determine the spatial distributions of increases in conditions indicative of moisture stress and potential wildfire hazard. Island-wide summaries of the changes in the relative frequency of moisture-stress indicators (soil moisture, ET, and CWD) between the reference condition, and the different drought and hypothetical land-cover conditions were used to identify areas of increased moisture stress and potential wildfire hazard. Increases in the relative frequency of the moisture-stress indicators imply increased frequency of low fuel-moisture conditions and increased wildfire hazard.

For the historical drought condition, the greatest increases in the relative frequency of moisture-stress indicators occur across parts of eastern and southwestern Kaua‘i; central, eastern, and western O‘ahu; central Moloka‘i; central Maui and low- to mid-altitude parts of West Maui volcano; and northwestern and southern parts of the Island of Hawai‘i. For the future non-drought condition, the greatest increases in the relative frequency of moisture-stress indicators occur across parts of western Kaua‘i, O‘ahu, and Moloka‘i; the southern slope of West Maui volcano and southwestern slope of Haleakalā; and northwestern and southern parts of the Island of Hawai‘i. For the future drought condition, the greatest increases in the relative frequency of moisture-stress indicators occur across parts of western Kaua‘i; central and western O‘ahu and Moloka‘i; a band of mid-altitude area on the southern slope of West Maui volcano and across the southwestern slope of Haleakalā; mid-altitude areas of the northwestern and southern parts of the Island of Hawai‘i, and a low- to mid-altitude band extending from the western coastal margins of the Island of Hawai‘i to Kīlauea. Areas of little or no change in relative frequency, implying no change in wildfire hazard, for each drought condition generally extend across parts of the wet mountainous and windward regions of each island. However, the areas of little or no change in relative frequency are reduced during the future drought condition, which indicates increased wildfire hazard for many upland regions on each island.

Eliminating CWI through complete conversion of shrubland and forest within the cloud zone to grassland further increases the change in the relative frequency of moisture-stress indicators within the cloud zones on O‘ahu, Maui, and the Island of Hawai‘i. On O‘ahu, increases in the relative frequency occur around Ka‘ala in the Wai‘anae Range and the southeastern part of the Ko‘olau Range. On Maui, increases occur around the southern part of West Maui volcano and across the southwestern slope of Haleakalā. Increases also occur across the upland regions of the western and southern parts of the Island of Hawai‘i. The magnitude of the changes in relative frequency implies that conversions of shrubland and forest areas to grassland within the cloud zone substantially increase the frequency and extent of low fuel-moisture conditions, and further increase wildfire hazard.

References Cited

- Abatzoglou, J.T., and Williams, A.P., 2016, Impact of anthropogenic climate change on wildfire across western US forests: Proceedings of the National Academy of Sciences, v. 113, no. 42, p. 11770–11775, <https://doi.org/10.1073/pnas.1607171113>.
- Ainsworth, A., and Kauffman, J.B., 2010, Interactions of fire and nonnative species across an elevation/plant community gradient in Hawaii Volcanoes National Park: Biotropica, v. 42, no. 6, p. 647–655, <https://doi.org/10.1111/j.1744-7429.2010.00636.x>.
- Barton, K.E., Jones, C., Edwards, K.F., Shiels, A.B., and Knight, T., 2020, Local adaptation constrains drought tolerance in a tropical foundation tree: Journal of Ecology, v. 108, no. 4, p. 1540–1552, <https://doi.org/10.1111/1365-2745.13354>.
- Bassiouni, M., and Oki, D.S., 2013, Trends and shifts in streamflow in Hawai‘i, 1913–2008: Hydrological Processes, v. 27, no. 10, p. 1484–1500, <https://doi.org/10.1002/hyp.9298>.
- Blumenstock, D.I., and Price, S., 1994, Climates of the states—Hawaii, in Kay, E.A. ed., A Natural History of the Hawaiian Islands, Selected Readings II: Honolulu, Hawai‘i, University of Hawai‘i Press, p. 94–115.
- Bremer, L.L., DeMaagd, N., Wada, C.A., and Burnett, K.M., 2021, Priority watershed management areas for groundwater recharge and drinking water protection—A case study from Hawai‘i Island: Journal of Environmental Management, v. 286, article no. 111622, 12 p., <https://doi.org/10.1016/j.jenvman.2020.111622>.
- Bremer, L.L., Mandle, L., Trauernicht, C., Pascua, P., McMillen, H.L., Burnett, K., Wada, C.A., Kurashima, N., Quazi, S.A., Giambelluca, T., Chock, P., and Ticktin, T., 2018, Bringing multiple values to the table—assessing future land-use and climate change in North Kona, Hawai‘i: Ecology and Society, v. 23, no. 1, article no. 33, 34 p., <https://doi.org/10.5751/ES-09936-230133>.

- Brewington, L., Keener, V., and Mair, A., 2019, Simulating land cover change impacts on groundwater recharge under selected climate projections, Maui, Hawai'i: Remote Sensing, v. 11, no. 24, article no. 3048, 23 p., <https://doi.org/10.3390/rs11243048>.
- Burgan, R.E., 1976, Correlation of plant moisture in Hawaii with the Keetch/Byram Drought Index: U.S. Department of Agriculture, Forest Service, Pacific Southwest Forest and Range Experiment Station Research Note PSW-307, 6 p.
- Cheney, P., and Sullivan, A., 2008, Grassfires—Fuel, weather and fire behaviour (2d ed.): Australia, Csiro Publishing, 160 p.
- Cheng, C.L., Izuka, S.K., Kennedy, J.J., Frazier, A.G., and Giambelluca, T.W., 2021, Water-resource management monitoring needs, State of Hawai'i: U.S. Geological Survey Scientific Investigations Report 2020–5115, 114 p., <https://doi.org/10.3133/sir20205115>.
- Chu, P.-S., and Chen, H., 2005, Interannual and interdecadal rainfall variations in the Hawaiian Islands: Journal of Climate, v. 18, no. 22, p. 4796–4813, <https://doi.org/10.1175/JCLI3578.1>.
- Chu, P.-S., Chen, Y.R., and Schroeder, T.A., 2010, Changes in precipitation extremes in the Hawaiian Islands in a warming climate: Journal of Climate, v. 23, no. 18, p. 4881–4900, <https://doi.org/10.1175/2010JCLI3484.1>.
- Clilverd, H.M., Tsang, Y.-P., Infante, D.M., Lynch, A.J., and Strauch, A.M., 2019, Long-term streamflow trends in Hawai'i and implications for native stream fauna: Hydrological Processes, v. 33, no. 5, p. 699–719, <https://doi.org/10.1002/hyp.13356>.
- D'Antonio, C.M., Hughes, R., and Tunison, J., 2011, Long-term impacts of invasive grasses and subsequent fire in seasonally dry Hawaiian woodlands: Ecological Applications, v. 21, no. 5, p. 1617–1628, <https://doi.org/10.1890/10-0638.1>.
- D'Antonio, C.M., and Vitousek, P.M., 1992, Biological invasions by exotic grasses, the grass/fire cycle, and global change: Annual review of ecology and systematics, v. 23, no. 1, p. 63–87, <https://doi.org/10.1146/annurev.es.23.110192.000431>.
- DeLay, J.K., and Giambelluca, T.W., 2010, History of cloud water interception research in Hawai'i, in Bruijnzeel, L., Scatena, F., and Hamilton, L. eds., Tropical Montane Cloud Forests: Science for Conservation and Management: Cambridge, UK, Cambridge University Press, p. 332–341.
- Diaz, H.F., Giambelluca, T.W., and Eischeid, J.K., 2011, Changes in the vertical profiles of mean temperature and humidity in the Hawaiian Islands: Global and Planetary Change, v. 77, nos. 1–2, p. 21–25, <https://doi.org/10.1016/j.gloplacha.2011.02.007>.
- Dolling, K., Chu, P.-S., and Fujioka, F., 2005, A climatological study of the Keetch/Byram Drought Index and fire activity in the Hawaiian Islands: Agricultural and Forest Meteorology, v. 133, nos. 1–4, p. 17–27, <https://doi.org/10.1016/j.agrformet.2005.07.016>.
- Dolling, K., Chu, P.-S., and Fujioka, F., 2009, Natural variability of the Keetch-Byram Drought Index in the Hawaiian Islands: International Journal of Wildland Fire, v. 18, no. 4, p. 459–475, <https://doi.org/10.1071/WF06146>.
- Ekern, P.C., 1964, Direct interception of cloud water on Lanai, Hawaii: Soil Science Society of America Journal, v. 28, no. 3, p. 419–421, <https://doi.org/10.2136/sssaj1964.03615995002800030035x>.
- Elison Timm, O., 2017, Future warming rates over the Hawaiian Islands based on elevation-dependent scaling factors: International Journal of Climatology, v. 37, no. S1, p. 1093–1104, <https://doi.org/10.1002/joc.5065>.
- Elison Timm, O., Giambelluca, T.W., and Diaz, H.F., 2015, Statistical downscaling of rainfall changes in Hawai'i based on the CMIP5 global model projections: Journal of Geophysical Research: Atmospheres, v. 120, no. 1, p. 92–112, <https://doi.org/10.1002/2014JD022059>.
- Ellsworth, L.M., Litton, C.M., Dale, A.P., and Miura, T., 2014, Invasive grasses change landscape structure and fire behaviour in Hawaii: Applied Vegetation Science, v. 17, no. 4, p. 680–689, <https://doi.org/10.1111/avsc.12110>.
- Ellsworth, L.M., Litton, C.M., Taylor, A.D., and Kauffman, J.B., 2013, Spatial and temporal variability of guinea grass (*Megathyrsus maximus*) fuel loads and moisture on Oahu, Hawaii: International Journal of Wildland Fire, v. 22, no. 8, p. 1083–1092, <https://doi.org/10.1071/WF12051>.
- Emery, N.C., 2016, Foliar uptake of fog in coastal California shrub species: Oecologia, v. 182, no. 3, p. 731–742, <https://doi.org/10.1007/s00442-016-3712-4>.
- Emery, N.C., D'Antonio, C.M., and Still, C.J., 2018, Fog and live fuel moisture in coastal California shrublands: Ecosphere, v. 9, no. 4, article e02167, 19 p., <https://doi.org/10.1002/ecs2.2167>.
- Engott, J.A., 2011, A water-budget model and assessment of groundwater recharge for the Island of Hawai'i: U.S. Geological Survey Scientific Investigations Report 2011–5078, 53 p., <https://doi.org/10.3133/sir20115078>.
- Engott, J.A., Johnson, A.G., Bassiouni, M., Izuka, S.K., and Rotzoll, K., 2017, Spatially distributed groundwater recharge for 2010 land cover estimated using a water-budget model for the Island of O'ahu, Hawai'i (ver 2.0, December 2017): U.S. Geological Survey Scientific Investigations Report 2015–5010, 49 p., <https://doi.org/10.3133/sir20155010>.

- Fandrich, K.M., Timm, O.E., Zhang, C., and Giambelluca, T.W., 2022, Dynamical downscaling of near-term (2026–2035) climate variability and change for the main Hawaiian Islands: *Journal of Geophysical Research, Atmospheres*, v. 127, no. 2, article no. e2021JD035684, 18 p., <https://doi.org/10.1029/2021JD035684>.
- Flint, L.E., Flint, A.L., and Thorne, J.H., 2015, Climate change—Evaluating your local and regional water resources: U.S. Geological Survey Fact Sheet 2014–3098, 6 p., <https://doi.org/10.3133/fs20143098>.
- Frazier, A.G., Elison Timm, O., Giambelluca, T.W., and Diaz, H.F., 2018, The influence of ENSO, PDO and PNA on secular rainfall variations in Hawai‘i: *Climate Dynamics*, v. 51, no. 5, p. 2127–2140, <https://doi.org/10.1007/s00382-017-4003-4>.
- Frazier, A.G., and Giambelluca, T.W., 2017, Spatial trend analysis of Hawaiian rainfall from 1920 to 2012: *International Journal of Climatology*, v. 37, no. 5, p. 2522–2531, <https://doi.org/10.1002/joc.4862>.
- Frazier, A.G., Giambelluca, T.W., Diaz, H.F., and Needham, H.L., 2016, Comparison of geostatistical approaches to spatially interpolate month-year rainfall for the Hawaiian Islands: *International Journal of Climatology*, v. 36, no. 3, p. 1459–1470, <https://doi.org/10.1002/joc.4437>.
- Frazier, A.G., Giardina, C.P., Giambelluca, T.W., Brewington, L., Chen, Y.-L., Chu, P.-S., Berio Fortini, L., Hall, D., Helweg, D.A., Keener, V.W., Longman, R.J., Lucas, M.P., Mair, A., Oki, D.S., Reyes, J.J., Yelenik, S.G., and Trauernicht, C., 2022, A century of drought in Hawai‘i: Geospatial analysis and synthesis across hydrological, ecological, and socioeconomic scales: *Sustainability*, v. 14, no. 19, article no. 12023, 25 p., <https://doi.org/10.3390/su141912023>.
- Garza, J.A., Chu, P.-S., Norton, C.W., and Schroeder, T.A., 2012, Changes of the prevailing trade winds over the islands of Hawaii and the North Pacific: *Journal of Geophysical Research, Atmospheres*, v. 117, no. D11, 18 p., <https://doi.org/10.1029/2011JD016888>.
- Geng, T., Cai, W., Wu, L., Santoso, A., Wang, G., Jing, Z., Gan, B., Yang, Y., Li, S., Wang, S., Chen, Z., and McPhaden, M.J., 2022, Emergence of changing Central-Pacific and Eastern-Pacific El Niño-Southern Oscillation in a warming climate: *Nature Communications*, v. 13, no. 1, article no. 6616, 11 p., <https://doi.org/10.1038/s41467-022-33930-5>.
- Geometrician Associates, LLC, 2011, Final environmental assessment, biocontrol of strawberry guava by its natural control agent for preservation of native forests in the Hawaiian Islands, 577 p., accessed December 20, 2023, at https://files.hawaii.gov/dbedt/erp/EA_EIS_Library/2011-11-08-ST-FEA-Biocontrol-Strawberry-Guava.pdf.
- Giambelluca, T.W., Chen, Q., Frazier, A.G., Price, J.P., Chen, Y.-L., Chu, P.-S., Eischeid, J.K., and Delparte, D.M., 2013, Online rainfall atlas of Hawai‘i: *Bulletin of the American Meteorological Society*, v. 94, no. 3, p. 313–316, <https://doi.org/10.1175/BAMS-D-11-00228.1>.
- Giambelluca, T.W., DeLay, J.K., Nullet, M.A., Scholl, M.A., and Gingerich, S.B., 2011, Canopy water balance of windward and leeward Hawaiian cloud forests on Haleakalā, Maui, Hawai‘i: *Hydrological Processes*, v. 25, no. 3, p. 438–447, <https://doi.org/10.1002/hyp.7738>.
- Giambelluca, T.W., Diaz, H.F., and Luke, M.S.A., 2008, Secular temperature changes in Hawai‘i: *Geophysical Research Letters*, v. 35, no. 12, article no. L12702, 5 p., <https://doi.org/10.1029/2008GL034377>.
- Giambelluca, T.W., Nullet, M.A., and Schroeder, T.A., 1986, Rainfall atlas of Hawai‘i: Hawai‘i Department of Land and Natural Resources, Division of Water and Land Development Report R76, 267 p.
- Giambelluca, T., and Schroeder, T.A., 1998, Climate, in Juvik, S.P., and Juvik, J.O., eds., *Atlas of Hawai‘i*: Honolulu, Hawai‘i, University of Hawai‘i Press, p. 49–59.
- Giambelluca, T.W., Shuai, X., Barnes, M.L., Alliss, R.J., Longman, R.J., Miura, T., Chen, Q., Frazier, A.G., Mudd, R.G., Cuo, L., and Businger, A.D., 2014, Evapotranspiration of Hawai‘i—Final report: Honolulu, University of Hawai‘i at Mānoa Department of Geography, submitted to the U.S. Army Corps of Engineers—Honolulu District, and the Commission on Water Resource Management, State of Hawai‘i, 168 p., accessed March 4, 2014, at <http://evapotranspiration.geography.hawaii.edu/assets/files/PDF/ET%20Project%20Final%20Report.pdf>.
- Gingerich, S.B., 2008, Ground-water availability in the Wailuku area, Maui, Hawai‘i: U.S. Geological Survey Scientific Investigations Report 2008–5236, 95 p., <https://doi.org/10.3133/sir20085236>.
- Gingerich, S.B., and Engott, J.A., 2012, Groundwater availability in the Lahaina District, west Maui, Hawai‘i: U.S. Geological Survey Scientific Investigations Report 2012–5010, 90 p., <https://doi.org/10.3133/sir20125010>.
- Gingerich, S.B., and Oki, D.S., 2000, Ground water in Hawaii: U.S. Geological Survey Fact Sheet 126–00, 6 p., <https://doi.org/10.3133/fs12600>.
- Hardy, W.R., 1996, A numerical ground-water model for the Island of Lana‘i, Hawaii: Commission on Water Resource Management, Department of Land and Natural Resources, State of Hawaii, 136 p. plus appendixes, accessed August 3, 2020, at <https://files.hawaii.gov/dlnr/cwrm/publishedreports/CWRM-1.pdf>.

- Hawbaker, T.J., Trauernicht, C., Howard, S.M., Litton, C.M., Giardina, C.P., Jacobi, J.D., Fortini, L.B., Hughes, R.F., Selmants, P.C., and Zhu, Z., 2017, Wildland fires and greenhouse gas emissions in Hawai‘i, *in* Selmants, P.C., Giardina, C.P., Jacobi, J.D., and Zhu, Zhiliang, eds., *Baseline and projected future carbon storage and carbon fluxes in ecosystems of Hawai‘i*: U.S. Geological Survey Professional Paper 1834, p. 57–73, <https://doi.org/10.3133/pp1834>.
- Heath, J.A., and Huebert, B.J., 1999, Cloudwater deposition as a source of fixed nitrogen in a Hawaiian montane forest: *Biogeochemistry*, v. 44, no. 2, p. 119–134, <https://doi.org/10.1023/A:1006091429143>.
- Heim, R.R., 2002, A review of twentieth-century drought indices used in the United States: *Bulletin of the American Meteorological Society*, v. 83, no. 8, p. 1149–1166, <https://doi.org/10.1175/1520-0477-83.8.1149>.
- Hillel, D., 1998, *Environmental Soil Physics*: London, Academic Press, 801 p.
- Intergovernmental Panel on Climate Change, 2014, *Climate change 2014—Synthesis report—Contribution of working groups I, II and III to the fifth assessment report of the Intergovernmental Panel on Climate Change*: Geneva, Switzerland, Intergovernmental Panel on Climate Change, 151 p., accessed April 3, 2019, at <https://www.ipcc.ch/report/ar5/syr/>.
- Izuka, S.K., Engott, J.A., Rotzoll, K., Bassiouni, M., Johnson, A.G., Miller, L.D., and Mair, A., 2018, Volcanic aquifers of Hawai‘i—Hydrogeology, water budgets, and conceptual models (ver. 2.0, March 2018): U.S. Geological Survey Scientific Investigations Report 2015–5164, 158 p., <https://doi.org/10.3133/sir20155164>.
- Izuka, S.K., Oki, D.S., and Chen, C., 2005, Effects of irrigation and rainfall reduction on ground-water recharge in the Lihue Basin, Kauai, Hawaii: U.S. Geological Survey Science Investigations Report 2005–5146, 48 p., <https://doi.org/10.3133/sir20055146>.
- Izuka, S.K., Rotzoll, K., and Nishikawa, T., 2021, Volcanic aquifers of Hawai‘i—Construction and calibration of numerical models for assessing groundwater availability on Kaua‘i, O‘ahu, and Maui: U.S. Geological Survey Scientific Investigations Report 2020–5126, 63 p., <https://doi.org/10.3133/sir20205126>.
- Izuka, S.K., and Rotzoll, K., 2021, Groundwater availability in the volcanic aquifers of Hawai‘i: U.S. Geological Survey Professional Paper 2020–5126, 63 p., <https://doi.org/10.3133/sir20205126>.
- Jensen, D., Reager, J.T., Zajic, B., Rousseau, N., Rodell, M., and Hinkley, E., 2018, The sensitivity of US wildfire occurrence to pre-season soil moisture conditions across ecosystems: *Environmental Research Letters*, v. 13, no. 1, article no. 014021, 11 p., <http://dx.doi.org/10.1088/1748-9326/aa9853>.
- Johnson, A.G., Engott, J.A., Bassiouni, M., and Rotzoll, K., 2018, Spatially distributed groundwater recharge estimated using a water-budget model for the Island of Maui, Hawai‘i, 1978–2007 (ver. 2.0, February 2018): U.S. Geological Survey Scientific Investigations Report 2014–5168, 64 p., <https://doi.org/10.3133/sir20145168>.
- Johnson, A.G., Mair, A., and Oki, D.S., 2023, Identification of water-budget information needed to accurately quantify how recharge for the Hawaiian Islands is affected by land-cover change: U.S. Geological Survey Scientific Investigations Report 2023–5022, 28 p., <https://doi.org/10.3133/sir20235022>.
- Juvik, J.O., DeLay, J.K., Kinney, K.M., and Hansen, E.W., 2011, A 50th anniversary reassessment of the seminal ‘Lāna‘i fog drip study’ in Hawai‘i: *Hydrological Processes*, v. 25, no. 3, p. 402–410, <https://doi.org/10.1002/hyp.7803>.
- Juvik, J.O., and Ekern, P.C., 1978, A climatology of mountain fog on Mauna Loa, Hawai‘i Island, Technical Report 118: Honolulu, Hawai‘i, Water Resources Research Center, University of Hawai‘i at Mānoa, 63 p., accessed July 9, 2020, at <http://hdl.handle.net/10125/2006>.
- Juvik, J.O., and Nullet, D., 1995, Relationships between rainfall, cloud-water interception, and canopy throughfall in a Hawaiian montane forest, *in* Hamilton, L.S., Juvik, J.O., and Scatena, F.N., eds., *Tropical montane cloud forests*: New York, Springer, p. 165–182.
- Kagawa-Viviani, A., and Giambelluca, T., 2020, Spatial patterns and trends in surface air temperatures and implied changes in atmospheric moisture across the Hawaiian Islands, 1905–2017: *Journal of Geophysical Research: Atmospheres*, v. 125, no. 2, article no. e2019JD031571, 17 p., <https://doi.org/10.1029/2019JD031571>.
- Kane, V.R., Lutz, J.A., Cansler, C.A., Povak, N.A., Churchill, D.J., Smith, D.F., Kane, J.T., and North, M.P., 2015, Water balance and topography predict fire and forest structure patterns: *Forest Ecology and Management*, v. 338, p. 1–13, <https://doi.org/10.1016/j.foreco.2014.10.038>.
- Kāne, H.L., Mair, A., Johnson, A.G., Rotzoll, K., Mifflin, J., and Oki, D.S., 2024a, Estimated groundwater recharge for mid-century and end-of-century climate projections, Kaua‘i, O‘ahu, Moloka‘i, Lāna‘i, Maui, and the Island of Hawai‘i: U.S. Geological Survey Scientific Investigations Report 2023–5130, 133 p., <https://doi.org/10.3133/sir20235130>.
- Kāne, H.L., Mifflin, J., and Mair, A., 2024b, Mean annual water-budget components for Kaua‘i, O‘ahu, Moloka‘i, Lāna‘i, Maui, and the Island of Hawai‘i, for a set of recent and future climate conditions, and 2020 land cover: U.S. Geological Survey data release, <https://doi.org/10.5066/P972KMSL>.

- Krueger, E.S., Ochsner, T.E., Engle, D.M., Carlson, J.D., Twidwell, D., and Fuhlendorf, S.D., 2015, Soil moisture affects growing-season wildfire size in the southern Great Plains: *Soil Science Society of America Journal*, v. 79, no. 6, p. 1567–1576, <https://doi.org/10.2136/sssaj2015.01.0041>.
- Krueger, E.S., Ochsner, T.E., Quiring, S.M., Engle, D.M., Carlson, J.D., Twidwell, D., and Fuhlendorf, S.D., 2017, Measured soil moisture is a better predictor of large growing-season wildfires than the Keetch–Byram drought index: *Soil Science Society of America Journal*, v. 81, no. 3, p. 490–502, <https://doi.org/10.2136/sssaj2017.01.0003>.
- Krushelnysky, P.D., Loope, L.L., Giambelluca, T.W., Starr, F., Starr, K., Drake, D.R., Taylor, A.D., and Robichaux, R.H., 2013, Climate-associated population declines reverse recovery and threaten future of an iconic high-elevation plant: *Global Change Biology*, v. 19, no. 3, p. 911–922, <https://doi.org/10.1111/gcb.12111>.
- Krushelnysky, P.D., Starr, F., Starr, K., Longman, R.J., Frazier, A.G., Loope, L.L., and Giambelluca, T.W., 2016, Change in trade wind inversion frequency implicated in the decline of an alpine plant: *Climate Change Responses*, v. 3, no. 1, article no. 1, 13 p., <https://doi.org/10.1186/s40665-016-0015-2>.
- Kug, J.-S., Jin, F.-F., and An, S.-I., 2009, Two types of El Niño events—Cold tongue El Niño and warm pool El Niño: *Journal of Climate*, v. 22, no. 6, p. 1499–1515, <https://doi.org/10.1175/2008JCLI2624.1>.
- Kunz, M., 2021, Understanding ecological drought effects and natural resource management needs in Hawai‘i: Honolulu, University of Hawai‘i at Mānoa, Master’s of Environmental Management capstone report, 37 p., accessed February 9, 2023, at <http://hdl.handle.net/10125/75712>.
- LaRosa, A.M., Tunison, J., Ainsworth, A., Kauffman, J.B., and Hughes, R.F., 2008, Chapter 11—Fire and nonnative invasive plants in the Hawaiian Islands bioregion, *in* Zouhar, K., Smith, J.K., Sutherland, S., and Brooks, M.L. eds., *Wildland fire in ecosystems: fire and nonnative invasive plants*. General Technical Report RMRS-GTR-42-vol. 6: U.S. Department of Agriculture, Forest Service, Rocky Mountain Research Station, Ogden, UT, p. 225–242, accessed October 1, 2022, at https://www.fs.usda.gov/rm/pubs/rmrs_gtr042_6/rmrs_gtr042_6_225_242.pdf.
- Lohse, K.A., Nullet, D., and Vitousek, P.M., 1995, Effects of extreme drought on vegetation of a lava flow on Mauna Loa, Hawai‘i: *Pacific Science*, v. 49, no. 3, p. 212–220, accessed November 1, 2022, at <http://hdl.handle.net/10125/2891>.
- Longman, R.J., Diaz, H.F., and Giambelluca, T.W., 2015, Sustained increases in lower-tropospheric subsidence over the central tropical north Pacific drive a decline in high-elevation rainfall in Hawaii: *Journal of Climate*, v. 28, no. 22, p. 8743–8759, <https://doi.org/10.1175/JCLI-D-15-0006.1>.
- Longman, R.J., Frazier, A.G., Giardina, C.P., Parsons, E.W., and McDaniel, S., 2022, The Pacific Drought Knowledge Exchange—A co-production approach to deliver climate resources to user groups: *Sustainability*, v. 14, no. 17, article no. 10554, 14 p., <https://doi.org/10.3390/su141710554>.
- Longman, R.J., Frazier, A.G., Newman, A.J., Giambelluca, T.W., Schanzenbach, D., Kagawa-Viviani, A., Needham, H., Arnold, J.R., and Clark, M.P., 2019, High-resolution gridded daily rainfall and temperature for the Hawaiian Islands (1990–2014): *Journal of Hydrometeorology*, v. 20, no. 3, p. 489–508, <https://doi.org/10.1175/JHM-D-18-0112.1>.
- Longman, R.J., Giambelluca, T.W., Alliss, R.J., and Barnes, M.L., 2014, Temporal solar radiation change at high elevations in Hawai‘i: *Journal of Geophysical Research: Atmospheres*, v. 119, no. 10, p. 6022–6033, <https://doi.org/10.1002/2013JD021322>.
- Lopez, H., Lee, S.-K., Kim, D., Wittenberg, A.T., and Yeh, S.-W., 2022, Projections of faster onset and slower decay of El Niño in the 21st century: *Nature Communications*, v. 13, no. 1, article no. 1915, 13 p., <https://doi.org/10.1038/s41467-022-29519-7>.
- Lu, B.-Y., Chu, P.-S., Kim, S.-H., and Karamperidou, C., 2020, Hawaiian regional climate variability during two types of El Niño: *Journal of Climate*, v. 33, no. 22, p. 9929–9943, <https://doi.org/10.1175/JCLI-D-19-0985.1>.
- Lucas, M.P., Longman, R.J., Giambelluca, T.W., Frazier, A.G., Mclean, J., Cleveland, S.B., Huang, Y.-F., and Lee, J., 2022, Optimizing automated kriging to improve spatial interpolation of monthly rainfall over complex terrain: *Journal of Hydrometeorology*, v. 23, no. 4, p. 561–572, <https://doi.org/10.1175/JHM-D-21-0171.1>.
- Macdonald, G.A., Abbott, A.T., and Peterson, F.L., 1983, *Volcanoes in the sea—The geology of Hawai‘i*, 2d edition: Honolulu, University of Hawai‘i Press, 554 p.
- Mair, A., 2024a, Frequency characteristics of soil moisture, evapotranspiration, and climatic water deficit for Kaua‘i, O‘ahu, Moloka‘i, Maui, and the Island of Hawai‘i, for a set of rainfall and land-cover conditions: U.S. Geological Survey data release, <https://doi.org/10.5066/P9HGHWS4>.
- Mair, A., 2024b, Mean annual groundwater recharge rates for Kaua‘i, O‘ahu, Moloka‘i, Maui, and the Island of Hawai‘i, for a set of drought and land-cover conditions: U.S. Geological Survey data release, <https://doi.org/10.5066/P9DDP1C6>.
- Mair, A., Johnson, A.G., Rotzoll, K., and Oki, D.S., 2019, Estimated groundwater recharge from a water-budget model incorporating selected climate projections, Island of Maui, Hawai‘i: U.S. Geological Survey Scientific Investigations Report 2019–5064, 46 p., <https://doi.org/10.3133/sir20195064>.

- McKee, T.B., Doesken, N.J., and Kleist, J., 1993, The relationship of drought frequency and duration to time scales, *in* Conference on Applied Climatology, 8th, Anaheim, Calif., January 17–22, 1993, [Program]: Anaheim, Calif., American Meteorological Society, 6 p.
- McKenzie, M.M., Giambelluca, T.W., and Diaz, H.F., 2019, Temperature trends in Hawai‘i—A century of change, 1917–2016: *International Journal of Climatology*, v. 39, no. 10, p. 3987–4001, <https://doi.org/10.1002/joc.6053>.
- Murphy, S.F., Alpers, C.N., Anderson, C.W., Banta, J.R., Blake, J.M., Carpenter, K.D., Clark, G.D., Clow, D.W., Hempel, L.A., Martin, D.A., Meador, M.R., Mendez, G.O., Mueller-Solger, A.B., Stewart, M.A., Payne, S.E., Peterman, C.L., and Ebel, B.A., 2023, A call for strategic water-quality monitoring to advance assessment and prediction of wildfire impacts on water supplies: *Frontiers in Water*, v. 5, 9 p., <https://doi.org/10.3389/frwa.2023.1144225>.
- Nakićenović, N., Alcamo, J., Davis, G., de Vries, B., Fenhann, J., Gaffin, S., Gregory, K., Grübler, A., Jung, T.Y., Kram, T., Lebre La Rovere, E., Michaelis, L., Mori, S., Morita, T., Pepper, W., Pitcher, H., Price, L., Riahi, K., Roehrl, A., Rogner, H.-H., Sankovski, A., Schlesinger, M., Shukla, P., Smith, S., Swart, R., van Rooijen, S., Victor, N., and Dadi, Z., 2000, Special report on emissions scenarios, A special report of Working Group III of the Intergovernmental Panel on Climate Change: Cambridge, United Kingdom, Cambridge University Press, 599 p.
- Nugent, A.D., Longman, R.J., Trauernicht, C., Lucas, M.P., Diaz, H.F., and Giambelluca, T.W., 2020, Fire and rain—The legacy of Hurricane Lane in Hawai‘i: *Bulletin of the American Meteorological Society*, v. 101, no. 6, p. E954–E967, <https://doi.org/10.1175/BAMS-D-19-0104.1>.
- O’Connor, C.F., Chu, P.-S., Hsu, P.-C., and Kodama, K., 2015, Variability of Hawaiian winter rainfall during La Niña events since 1956: *Journal of Climate*, v. 28, no. 19, p. 7809–7823, <https://doi.org/10.1175/JCLI-D-14-00638.1>.
- Oki, D.S., 2004, Trends in streamflow characteristics at long-term gaging stations, Hawaii: U.S. Geological Survey Scientific Investigations Report 2004–5080, 116 p., <https://doi.org/10.3133/sir20045080>.
- Oki, D.S., 2005, Numerical simulation of the effects of low-permeability valley-fill barriers and the redistribution of ground-water withdrawals in the Pearl Harbor area, Oahu, Hawaii: U.S. Geological Survey Scientific Investigations Report 2005–5253, 111 p., <https://doi.org/10.3133/sir20055253>.
- Oki, D.S., 2022, Water-budget accounting for tropical regions model (WATRMod) documentation: U.S. Geological Survey Open-File Report 2022–1013, 77 p., <https://doi.org/10.3133/ofr20221013>.
- Oki, D.S., Engott, J.A., and Rotzoll, K., 2020, Numerical simulation of groundwater availability in central Moloka‘i, Hawai‘i: U.S. Geological Survey Scientific Investigations Report 2019–5150, 95 p., <https://doi.org/10.3133/sir20195150>.
- Partyka, G., and Erdman, B., 2023, Meteorologic analysis of the August 2023 Maui wildfires: National Aeronautics and Space Administration Global Modeling and Assimilation Office webpage, accessed January 18, 2024, at https://gmao.gsfc.nasa.gov/research/science_snapshots/2023/meteorologic-analysis-maui-wildfires.php.
- Pickett, E., 2016, Hawaii has a devastating wildfire problem: Hawaii Wildfire Management Organization, 2 p., accessed October 12, 2023, at https://static1.squarespace.com/static/5254fbc2e4b04bb53b57821/t/64e534e8701623136866b88f/1692742896702/Fire+Impacts+in+Hawaii_++June+2016_MkNotes.pdf.
- Rotzoll, K., and Johnson, A.G., 2023, Mean annual water-budget components for Oahu, Hawaii, for future-climate conditions, CMIP5 RCP8.5 2041–70 scenario rainfall and 2010 land cover: U.S. Geological Survey data release, <https://doi.org/10.5066/P9L4N2ZI>.
- Rotzoll, K., Oki, D.S., Johnson, A.G., and Souza, W.R., 2022, Long-term groundwater availability in the Waihe‘e, ‘Iao, and Waikapū aquifer systems, Maui, Hawai‘i: U.S. Geological Survey Scientific Investigations Report 2021–5113, 80 p., <https://doi.org/10.3133/sir20215113>.
- Safeeq, M., and Fares, A., 2014, Interception losses in three non-native Hawaiian forest stands: *Hydrological Processes*, v. 28, no. 2, p. 237–254, <https://doi.org/10.1002/hyp.9557>.
- Sanderson, M., ed., 1993, Prevailing trade winds—Climate and weather in Hawai‘i: Honolulu, University of Hawai‘i Press, 156 p.
- Scholl, M.A., and Giambelluca, T.W., 2010, Stable isotope techniques to investigate cloud water in forested mountain watersheds in the trade wind latitudes—Hawaii and Puerto Rico [abs.], *in* International Conference on Fog, Fog Collection, and Dew, 5th, Münster, Germany, July 25–30, 2010, Programme: International Conference on Fog, Fog Collection, and Dew, FOGDEW2010-118.
- Schroeder, M.J., and Buck, C.C., 1970, Fire weather—A guide for application of meteorological information to forest fire control operations: U.S. Department of Agriculture, Forest Service Agriculture Handbook 360, 229 p., accessed June 2, 2022, at <https://handle.nal.usda.gov/10113/CAT87208488>.
- Scott, J.H., Thompson, M.P., and Calkin, D.E., 2013, A wildfire risk assessment framework for land and resource management: U.S. Department of Agriculture, Forest Service, Rocky Mountain Research Station, General Technical Report RMRS-GTR-315, 83 p., <https://doi.org/10.2737/rmrs-gtr-315>.

- Sharma, S., Carlson, J.D., Krueger, E.S., Engle, D.M., Twidwell, D., Fuhlendorf, S.D., Patrignani, A., Feng, L., and Ochsner, T.E., 2021, Soil moisture as an indicator of growing-season herbaceous fuel moisture and curing rate in grasslands: *International Journal of Wildland Fire*, v. 30, no. 1, p. 57–69, <https://doi.org/10.1071/WF19193>.
- Sharma, S., and Dhakal, K., 2021, Boots on the ground and eyes in the sky—A perspective on estimating fire danger from soil moisture content: *Fire*, v. 4, no. 3, article no. 45, 12 p., <https://doi.org/10.3390/fire4030045>.
- Sherrod, D.R., Sinton, J.M., Watkins, S.E., and Brunt, K.M., 2007, Geologic map of the State of Hawai‘i: U.S. Geological Survey Open-File Report 2007–1089, <https://doi.org/10.3133/ofr20071089>.
- State of Hawai‘i Department of Land and Natural Resources, Commission on Water Resource Management, 2014, Aquifer sector area and aquifer system area boundaries: Hawaii Statewide GIS Program database, accessed August 6, 2020, at <https://geoportal.hawaii.gov/datasets/HiStateGIS::dlr-aquifers/about>.
- State of Hawai‘i Office of Planning, 2014a, 100 ft contours for Hawaii Island: Hawaii Statewide GIS Program database, accessed February 5, 2021, at <https://geoportal.hawaii.gov/datasets/HiStateGIS::hawaii-elevation-contours-100ft/about>.
- State of Hawai‘i Office of Planning, 2014b, 100 ft contours for Kauai Island: Hawaii Statewide GIS Program database, accessed February 5, 2021, at <https://geoportal.hawaii.gov/datasets/HiStateGIS::kauai-elevation-contours-100ft/about>.
- State of Hawai‘i Office of Planning, 2014c, 100 ft contours for Maui Island: Hawaii Statewide GIS Program database, accessed February 5, 2021, at <https://geoportal.hawaii.gov/datasets/HiStateGIS::maui-elevation-contours-100ft/about>.
- State of Hawai‘i Office of Planning, 2014d, 100 ft contours for Molokai Island: Hawaii Statewide GIS Program database, accessed February 5, 2021, at <https://geoportal.hawaii.gov/datasets/HiStateGIS::molokai-elevation-contours-100ft/about>.
- State of Hawai‘i Office of Planning, 2014e, 100 ft contours for Oahu Island: Hawaii Statewide GIS Program database, accessed February 5, 2021, at <https://geoportal.hawaii.gov/datasets/HiStateGIS::oahu-elevation-contours-100ft/about>.
- Stearns, H.T., and Macdonald, G.A., 1947, Geology and ground-water resources of the island of Molokai, Hawaii, Bulletin 11: Hawaii Division of Hydrography 11, 113 p., accessed October 3, 2023, at <https://pubs.usgs.gov/publication/70161790>.
- Stebblein, P.F., Loehman, R.A., Miller, M.P., Holomuzki, J.R., Soileau, S.C., Brooks, M.L., Drane-Maury, M., Hamilton, H.M., Kean, J.W., Keeley, J.E., Mason Jr., R.R., McKerrow, A.J., Meldrum, J.R., Molder, E.B., Murphy, S.F., Peterson, B., Plumlee, G.S., Shinneman, D.J., van Mantgem, P.J., and York, A., 2021, U.S. Geological Survey wildland fire science strategic plan, 2021–26: U.S. Geological Survey Circular 1471, 30 p., <https://doi.org/10.3133/cir1471>.
- Takahashi, M., Giambelluca, T.W., Mudd, R.G., DeLay, J.K., Nullet, M.A., and Asner, G.P., 2011, Rainfall partitioning and cloud water interception in native forest and invaded forest in Hawai‘i Volcanoes National Park: *Hydrological Processes*, v. 25, no. 3, p. 448–464, <https://doi.org/10.1002/hyp.7797>.
- Townscape, Inc., 2019, Hawai‘i Water Plan, Water Resource Protection Plan, 2019 Update: Honolulu, State of Hawai‘i, Department of Land and Natural Resources, Commission on Water Resource Management, prepared by Townscape, Inc., 746 p., accessed November 1, 2022, at <https://dlr.hawaii.gov/cwrp/planning/hiwaterplan/wrpp/>.
- Trauernicht, C., 2019, Vegetation—Rainfall interactions reveal how climate variability and climate change alter spatial patterns of wildland fire probability on Big Island, Hawaii: *Science of The Total Environment*, v. 650, p. 459–469, <https://doi.org/10.1016/j.scitotenv.2018.08.347>.
- Trauernicht, C., and Kunz, M., 2019, Fuel breaks and fuels-management strategies for Pacific Island grasslands and savannas: Honolulu, University of Hawai‘i at Mānoa, College of Tropical Agriculture and Human Resources, RM-22, 17 p., accessed February 6, 2023, at <https://www.ctahr.hawaii.edu/oc/freepubs/pdf/RM-22.pdf>.
- Trauernicht, C., Pickett, E., Giardina, C.P., Litton, C.M., Cordell, S., and Beavers, A., 2015, The contemporary scale and context of wildfire in Hawai‘i: *Pacific Science*, v. 69, no. 4, p. 427–444, <https://doi.org/10.2984/69.4.1>.
- Tseng, H., 2021, Cloud water interception in Hawai‘i: Honolulu, University of Hawai‘i at Mānoa, Ph.D. Dissertation, 204 p., accessed January 13, 2023, at <http://hdl.handle.net/10125/81641>.
- Tseng, H., Fortini, L., Mair, A., Kagawa-Viviani, A., Yelenik, S.G., Miyazawa, Y., Nullet, M.A., Kennedy, J., DeLay, J., Leopold, C., and Giambelluca, T., 2021, Cloud water interception in Hawai‘i—Developing capacity to characterize the spatial patterns and effects on water and ecological processes responses in Hawai‘i: Climate Adaption Science Centers, Final Technical Report, 57 p., <https://pubs.er.usgs.gov/publication/70226917>.

- University of Hawai‘i at Mānoa, 2021, Hawaii fire perimeters 1999–2019: College of Tropical Agriculture and Human Resources, Department of Natural Resources and Environmental Management database, accessed April 27, 2021, at <https://www.nrem-fire.org/hawaii-fire-history>.
- U.S. Census Bureau, 2021, Historical population change data (1910–2020): U.S. Census Bureau web page, accessed April 26, 2021, at <https://www.census.gov/data/tables/time-series/dec/popchange-data-text.html>.
- Vitousek, P.M., 1992, Effects of alien plants on native ecosystems, *in* Stone, C.P., Smith, C.W., and Tunison, J.T. eds., *Alien plant species in native ecosystems of Hawai‘i—Management and research*: Honolulu, University of Hawai‘i Cooperative National Park Resources Studies Unit, p. 29–41.
- Wada, C.A., Bremer, L.L., Burnett, K., Trauernicht, C., Giambelluca, T., Mandle, L., Parsons, E., Weil, C., Kurashima, N., and Ticktin, T., 2017, Estimating cost-effectiveness of Hawaiian dry forest restoration using spatial changes in water yield and landscape flammability under climate change: *Pacific Science*, v. 71, no. 4, p. 401–424, <https://doi.org/10.2984/71.4.2>.
- Westerling, A.L., and Bryant, B.P., 2008, Climate change and wildfire in California: *Climatic Change*, v. 87, Supplement 1, p. 231–249, <https://doi.org/10.1007/s10584-007-9363-z>.
- Yamanaga, G., 1972, Evaluation of the streamflow-data program in Hawaii: U.S Geological Survey Open-File Report 72–453, 28 p., <https://doi.org/10.3133/ofr72453>.
- Zhang, C., and Wang, Y., 2017, Projected future changes of tropical cyclone activity over the western North and South Pacific in a 20-km-mesh regional climate model: *Journal of Climate*, v. 30, no. 15, p. 5923–5941, <https://doi.org/10.1175/JCLI-D-16-0597.1>.
- Zhang, C., Wang, Y., Hamilton, K., and Lauer, A., 2016, Dynamical downscaling of the climate for the Hawaiian Islands, Part II—Projection for the late twenty-first century: *Journal of Climate*, v. 29, no. 23, p. 8333–8354, <https://doi.org/10.1175/JCLI-D-16-0038.1>.
- Zhang, C., Wang, Y., Lauer, A., Hamilton, K., and Xie, F., 2012, Cloud base and top heights in the Hawaiian region determined with satellite and ground-based measurements: *Geophysical Research Letters*, v. 39, no. 15, 6 p., <https://doi.org/10.1029/2012GL052355>.

Appendixes 1–2

Appendix 1. Model Input

This study incorporates a separate set of model input datasets to characterize rainfall, direct runoff, and land cover for each water-budget scenario. For the remaining model inputs, a common set of model input datasets was used in all water-budget scenarios that included but were not limited to, datasets used to characterize reference-evapotranspiration (reference-ET) rates, soil moisture-storage capacities, cloud-water interception (CWI) rates, irrigation methods, septic effluent discharge rates, and storm-drain capture conditions. This appendix describes the development of model input datasets. The model input datasets were input to a water-budget code known as WATRMod, a Water-budget Accounting for Tropical Regions Model (Oki, 2022), that simulated spatially variable daily water-budget components, including groundwater recharge, soil moisture, and ET, for each water-budget scenario developed for Kauaʻi, Oʻahu, Molokaʻi, Maui, and the Island of Hawaiʻi.

Land Cover

Land-cover maps representative of land-cover conditions in 2020 and developed by Kāne and others (2024a) were used for the water-budget scenarios for each island, hereinafter the 2020 land-cover maps (fig. 4). Detailed descriptions of the development of the 2020 land-cover map for each island are described in Kāne and others (2024a) and in the metadata of Kāne and others (2024b). In this study, the effects of reduced CWI on groundwater recharge during drought were evaluated for Oʻahu, Maui, and the Island of Hawaiʻi. In the WATRMod simulations, CWI is assumed to occur only in non-native forest, native forest, tree plantation, kiawe, shrubland, coffee, and macadamia land cover within the cloud zone. The effect of reduced CWI was evaluated in the WATRMod simulations by converting forest and shrubland land cover within the cloud zone to grassland, for which CWI is considered to be negligible. To simulate the effects of reduced CWI, two hypothetical land-cover conditions were applied to Oʻahu, Maui, and the Island of Hawaiʻi: (1) Conversion 1, a land-cover condition in which roughly 50 percent of subareas with shrubland and forest land cover within the cloud zone were randomly selected and converted to grassland, and (2) Conversion 2, a land-cover condition in which 100 percent of shrubland and forest areas within the cloud zone were converted to grassland.

Impervious Surfaces

Impervious surfaces include paved surfaces and buildings. In the water-budget calculations, excess water from the impervious surfaces of a subarea is distributed to the pervious surfaces of the subarea and depends on the impervious fraction of the subarea. The impervious fraction of each subarea was computed by Kāne and others (2024a). Subareas with a water body, reservoir, or taro land-cover classification were assigned a value of zero for impervious

fraction. WATRMod requires that excess water from the impervious fraction be distributed to a pervious part of each subarea, which implies that a subarea cannot be completely impervious. Therefore, all remaining subareas were reassigned a value of 0.99 for impervious fraction whenever the value computed from the map of impervious surfaces exceeded 0.99.

Rainfall

1990–2012 Monthly Rainfall

In the WATRMod simulations, the spatial and temporal distributions of rainfall during 1990–2012 were defined using gridded 250-meter (m) resolution maps of rainfall for the 276 months during 1990–2012. These maps are a subset of the 1,116 maps of rainfall for each month during 1920–2012 for the Hawaiian Islands that Frazier and others (2016) generated for the Rainfall Atlas of Hawaiʻi (Giambelluca and others, 2013). Monthly rainfall for each subarea was computed in WATRMod as the product of the monthly rainfall value from Frazier and others (2016) and a mean monthly adjustment factor. Adjustment factors were developed by Kāne and others (2024a) because cell-by-cell comparisons between mean monthly rainfall calculated for 1978–2007 from the Frazier and others (2016) dataset and the mean monthly values in Giambelluca and others (2013) showed small differences. Kāne and others (2024a) assigned a set of 12 mean monthly adjustment factors to each rainfall grid cell. In this study, the set of mean monthly adjustment factors developed by Kāne and others (2024a) were assigned to each rainfall grid cell. The mean monthly rainfall adjustment factors were applied to the 1990–2012 monthly rainfall maps. The maps of adjusted monthly rainfall were used as the rainfall dataset for the WATRMod simulations of historical climate conditions.

Future Monthly Rainfall

The availability of high-resolution downscaled climate data, such as the output data from regional climate models (RCMs), enables the direct application of these climate data for hydrologic studies at the regional and watershed scales. However, systematic biases are often evident in RCM data from comparisons of simulated and observed reference climate conditions, and these biases can affect the output of hydrologic models (Graham and others, 2007; van Roosmalen and others, 2010, 2011). Hence, bias correction is recommended before using RCM data in hydrologic models (Wilby and others, 2000). A common bias-correction approach is the change-factor method (Hay and others, 2000), which is done by perturbing a reference climate series with relative change factors derived from the comparison of RCM data from a simulated reference climate and a projected future climate (van Roosmalen and others, 2007, 2009, 2010, 2011; Navarro-Racines and others, 2020). The main underlying assumptions of the change-factor method are: (1) the biases for the reference and future climate

simulations are equal, and (2) the RCMs simulate relative changes better than absolute values.

In this study, the change-factor method was used to develop datasets of future monthly rainfall by adjusting datasets of monthly rainfall during a selected reference period (Frazier and others, 2016) with relative change factors. Kāne and others (2024a) developed a set of change factors for monthly rainfall from wet- and dry-season rainfall anomalies of the RCP8.5 2071–99 projection for Kaua‘i, O‘ahu, Moloka‘i, Maui, and the Island of Hawai‘i (Elison Timm and others, 2015). The same set of change factors was then used to adjust 1990–2012 monthly rainfall to produce a future monthly rainfall dataset for each island for the WATRMod simulations of projected future climate conditions.

1990–2012 Daily Rainfall

WATRMod generated daily rainfall for the simulations by disaggregating the monthly values of the 1990–2012 rainfall distribution maps using the method of fragments (for example, Oki, 2002). High-resolution maps of daily rainfall during 1990–2014 for the Hawaiian Islands were developed by Longman and others (2019) at a grid size of roughly 250 m. The rainfall maps from Frazier and others (2016) and Longman and others (2019) both use the same grid to quantify the spatial distribution of rainfall across the five islands. However, the sum of daily rainfall values at each overlapping grid cell during 1990–2012 from Longman and others (2019) do not necessarily match the monthly rainfall values during 1990–2012 from Frazier and others (2016). Hence, the daily rainfall maps from Longman and others (2019) were used to disaggregate monthly rainfall into daily rainfall fragments for WATRMod. For each grid cell, daily rainfall fragments were computed by dividing each daily rainfall value during a particular month by the total rainfall at the cell for that month computed from the sum of the daily values. This resulted in a set of fragments for that month in which the total number of fragments was equal to the number of days in the month. Fragment sets were compiled for every cell for every month during the 1990–2012 simulation period, except for grid cells where the monthly rainfall computed from the daily maps was zero. In these cases, a set of non-zero values was substituted for the fragment set at a particular grid cell during months with no rainfall (one non-zero fragment value for each day of the month). The set of non-zero daily values was then used to disaggregate non-zero monthly rainfall values from Frazier and others (2016) for those grid cells with zero monthly rainfall from the daily maps. This approach to disaggregating rainfall for grid cells with zero monthly rainfall from the daily maps is conservative because the synthesized rainfall allows for rainfall to occur on each day of the month, which can increase ET and lessen the amount of water available for episodic recharge when compared to fragment sets that concentrate monthly rainfall over only a few days.

Fragment sets were grouped by grid cell and month of the year during 1990–2012 for each island and then used in the WATRMod simulations. For each grid cell, and for a given month and year during the simulation (for example, March 1995), WATRMod selected the fragment set for that grid cell, month, and year. Daily rainfall for a given month was synthesized by multiplying the total rainfall for that month (from the monthly rainfall maps) by each fragment in the set.

Future Daily Rainfall

The daily rainfall fragment sets developed for the WATRMod simulations of historical climate conditions (1990–2012) were also used for the simulations of projected future climate conditions (RCP8.5 2071–99) because of a lack of information on projected changes in the frequency, magnitude, or duration of daily rainfall. For the RCP8.5 2071–99 projection, the fragment set used for a given grid cell for a given month and year (for example, January, year 1 of the 23-year simulation) was selected to correspond with the fragment set from the same sequence used for the simulations of historical climate conditions (1990–2012) (for example, January 1990).

Cloud-Water Interception

For Kaua‘i, O‘ahu, and Moloka‘i, all areas at or above 2,000 feet (ft) were assumed to be within the cloud zone and all areas below 2,000 ft were assumed to be below the cloud zone (figs. 4A–C), consistent with earlier studies (Izuka and others, 2018; Oki and others, 2020; Kāne and others, 2024a). For Maui and the Island of Hawai‘i, all areas at or above 2,000 ft in windward areas and all areas at or above 2,600 ft in leeward areas were assumed to be within the cloud zone, and all areas below 2,000 ft in windward areas and below 2,600 ft in leeward areas were assumed to be below the cloud zone (figs. 4D, E), the same as that assumed by recent studies (Johnson and others, 2023; Kāne and others, 2024a).

For each island, CWI was assumed to be limited to non-native forest, native forest, tree plantation, kiawe, shrubland, coffee, and macadamia land cover within the cloud zone. CWI was assumed to be negligible for all areas below the cloud zone. In the water budget, CWI was assumed to occur only on days with rainfall and daily CWI was computed as a fraction of daily rainfall using fog-to-rainfall ratios. For O‘ahu, Moloka‘i, and the Island of Hawai‘i, daily CWI was computed using ratios of mean monthly fog-to-rainfall ratios from Kāne and others (2024a) (see table 5 in Kāne and others [2024a]). For Kaua‘i and Maui, mean annual CWI from Kāne and others (2024a) was assumed to be uniformly distributed to each month. Daily CWI in each subarea was computed as a fraction of daily rainfall equivalent to the ratio of mean monthly CWI and mean monthly rainfall during 1978–2007. These resulting fog-to-rainfall ratios were used to compute recharge for each water-budget scenario.

Irrigation

Irrigation rates were estimated in WATRMd for subareas on each island that were classified as agriculture (coffee, diversified agriculture, pineapple, seed corn, and taro) or other land-cover classes (golf course, high-intensity developed, and medium-intensity developed) that were assumed to contain irrigated lawns and landscapes. Irrigation rates were also estimated for subareas with macadamia land cover on the Island of Hawai'i consistent with the approach of Engott (2011). However, no irrigation was applied in WATRMd to subareas with macadamia on Maui consistent with the approach of earlier studies (Johnson and others, 2018; Brewington and others, 2019; Mair and others, 2019; Kāne and others, 2024a). Irrigation rates were estimated in WATRMd using two methods: (1) a supply-based approach with specified monthly irrigation depths, and (2) a demand-based approach that considers rainfall and potential ET. A supply-based approach was used for taro, whereas a demand-based approach was used for all other irrigated land-cover classes. For each irrigated land-cover class, model input was formatted to specify the days on which irrigation was applied and whether irrigation was determined using the supply- or demand-based approach. The approach described herein was used to estimate irrigation rates for each of the water-budget scenarios.

All subareas of the taro land-cover class were assigned an irrigation rate of 455 inches per year in WATRMd on the basis of water-use studies for various taro pond fields in Hawai'i (Miles, 1931, as cited in Penn, 1997; Watson, 1964; De la Pena and Melchor, 1984; Berg and others, 1997), although local differences in irrigation rates likely exist. For this study, the percentage of subareas with taro that is cultivated at any one time, hereinafter taro-cultivation rate, was estimated using the values from Kāne and others (2024a) as follows: (1) 30 percent for Kaua'i, (2) 100 percent for O'ahu, (3) 93 percent for Moloka'i and Maui, and (4) 87 percent for the Island of Hawai'i. The remaining percentage of land area for each subarea with taro land cover was treated in WATRMd as developed open space land cover. In the WATRMd simulations, the monthly irrigation depths for taro were evenly distributed on each day of the month, about 1.25 inches per day (in/d), regardless of the rainfall on the day.

For irrigated land-cover classes other than taro, irrigation rates were estimated using equation 7 in Kāne and others (2024a). Irrigation-method efficiency is the fraction of applied irrigation water that becomes available for plant consumption. The irrigation efficiencies used in the water budget for all irrigated land-cover classes were taken from Kāne and others (2024a) (table 1.1). For all irrigated land-cover classes other than pineapple and taro, monthly irrigation estimated from equation 7 in Kāne and others (2024a) was allocated in equal amounts for each day of a given month. Similar to the approach taken in Engott and Vana (2007) for pineapple irrigation, the monthly irrigation volume calculated for pineapple using equation 16 in Johnson and others (2018) was uniformly distributed on days 1, 2, 3, 8, 9, 10, 15, 16, 17, 22, 23, 24, and

28 of each month. Simulation of the pineapple-cultivation cycle was not represented in this study and irrigation was assumed for all months of the simulation period. Seed corn irrigation for this study is based on a cultivation cycle of two crops per year. Only 25 percent of each subarea classified as seed corn is cultivated at any one time, leaving the remaining 75 percent of the subarea to be classified as bare soil. This approach was developed on the basis of cultivation practices on Moloka'i and used in earlier studies (Engott and others, 2017; Kāne and others, 2024a) for estimating corn irrigation.

WATRMd's irrigation estimates for diversified agriculture and medium- and high-intensity developed land-cover types were adjusted with irrigation-adjustment factors used by Kāne and others (2024a) (table 1.1). These factors ensured that WATRMd's irrigation estimates were, on average, consistent with reported rates of irrigation and rates of water available for irrigation. The estimated irrigation rates for coffee, golf course, pineapple, taro, and seed corn were not adjusted. Irrigated subareas classified as agriculture (coffee, diversified agriculture, pineapple, seed corn, and taro) and other land-cover classes (golf course, high-intensity developed, and medium-intensity developed) occupy about 4 percent of the total land area on Kaua'i, O'ahu, Moloka'i, Maui, and the Island of Hawai'i (Mair, 2024).

Septic Effluent

Septic effluent for this study consisted of cesspool seepage and septic-system leachate. In the WATRMd simulations, cesspool seepage was counted as direct recharge, whereas septic-system leachate was added to the plant-root zone where it was subject to evapotranspiration. Some buildings and premises on each island use onsite sewage disposal systems (OSDS) to dispose of wastewater. Whittier and El-Kadi (2009, 2014) compiled an inventory of OSDS on Kaua'i, O'ahu, Moloka'i, Maui, and the Island of Hawai'i.

For each tax map key (TMK) parcel, Whittier and El-Kadi (2009, 2014) specified the number and type (class) of OSDS and the total estimated septic effluent flux for each type of OSDS. Each TMK parcel may contain one or more model subareas. Hence, all subareas, including those not in the developed land-cover class, within a TMK parcel that contain an OSDS can have septic effluent. For TMK parcels with cesspools, the total estimated septic effluent flux was transformed into an equivalent depth per unit time by dividing the flux by the parcel area, hereinafter the cesspool seepage rate. For subareas within TMK parcels with cesspools, the cesspool seepage rate was applied as direct recharge (see "Direct Recharge" section). For TMK parcels with other types of OSDS, the effluent flux was transformed into equivalent depth per unit time, hereinafter the septic-system leachate rate. For subareas within TMK parcels with other types of OSDS, the septic-system leachate rate applied only to the pervious fraction. However, the septic-system leachate rate in each subarea was adjusted by dividing the rate by the pervious fraction. The adjustment to the septic-system leachate

Table 1.1. Land-cover parameters used in the WATRMod simulations.

[--, not applicable; for forest land covers, crop coefficients were used to compute the sum of transpiration and ground evaporation, canopy evaporation was computed separately; for non-forest land covers, crop coefficients were used to compute the sum of all evaporative components]

Land-cover description	Root depth, in inches	Depletion fraction	Crop coefficient	Canopy capacity, in inches	Trunk-storage capacity, in inches	Fraction of precipitation diverted to stemflow	Fog-catch efficiency	Irrigation method	Irrigation-method efficiency	Irrigation-adjustment factor
Forest land covers										
Native forest, fog	30	0.50	0.30	0.05	0.01	0.04	1	--	--	--
Native forest, no fog	30	0.50	0.30	0.05	0.01	0.04	--	--	--	--
Non-native forest, fog	60	0.50	0.33	0.05	0.01	0.04	1	--	--	--
Non-native forest, no fog	60	0.50	0.44	0.05	0.01	0.04	--	--	--	--
Tree plantation, fog	60	0.50	0.33	0.05	0.01	0.04	1	--	--	--
Tree plantation, no fog	60	0.50	0.44	0.05	0.01	0.04	--	--	--	--
Kiawe, fog	71	0.50	0.23	0.05	0.01	0.04	1	--	--	--
Kiawe, no fog	71	0.50 ^b , 1.00 ^c	0.23	0.05	0.01	0.04	--	--	--	--
Non-forest land covers										
Bare soil ^a	6	0.60	0.25	0	0	0	0	--	--	--
Coffee	48	0.40	0.91	0	0	0	0.5	Micro-spray	0.80	1
Diversified agriculture	10	0.35	1.00	0	0	0	0	Drip	0.85	0.40 ^f , 0.41 ^g , 0.55 ^h
Macadamia	60	0.50	0.91	0	0	0	1	Micro-spray ^e	0.80 ^e	1 ^e
Pineapple	18	0.50	0.30	0	0	0	0	Drip	0.85	1
Seed corn	18	0.60	0.29–1.20 ^d	0	0	0	0	Drip	0.85	1
Taro	15	1.00	1.25	0	0	0	0	Flood	1	1
Developed, open space	12	0.50	1.18	0	0	0	0	--	--	--
Developed, low intensity	12	0.50	1.18	0	0	0	0	--	--	--
Developed, medium intensity	12	0.50	1.18	0	0	0	0	Sprinkler	0.70	0.37
Developed, high intensity	12	0.50	1.18	0	0	0	0	Sprinkler	0.70	0.37
Golf course	30	0.50	0.85	0	0	0	0	Sprinkler	0.70	1
Grassland	39	0.60	0.95	0	0	0	0	--	--	--
Shrubland, fog	12	0.50	1.00	0	0	0	0.5	--	--	--
Shrubland, no fog	12	0.50	1.00	0	0	0	0	--	--	--
Sparsely vegetated	5	0.50	1.18	0	0	0	0	--	--	--
Reservoir, lined	0	1.00	1.05	0	0	0	0	--	--	--
Reservoir, unlined	0	1.00	1.05	0	0	0	0	--	--	--

Table 1.1. Land-cover parameters used in the WATRMod simulations.—Continued

Land-cover description	Root depth, in inches	Depletion fraction	Crop coefficient	Canopy capacity, in inches	Trunk-storage capacity, in inches	Fraction of precipitation diverted to stemflow	Fog-catch efficiency	Irrigation method	Irrigation-method efficiency	Irrigation-adjustment factor
Coastal water body	0	1.00	1.05	0	0	0	0	--	--	--
Inland water body	0	1.00	1.05	0	0	0	0	--	--	--
Wetland	39	0.50	1.18	0	0	0	0	--	--	--

^aUsed in mixed land-cover designation for seed corn (see “[Irrigation](#)” section for explanation).

^bValue used at altitude above 49 feet.

^cValue used at altitude equal to or less than 49 feet.

^dVaries by month (see “[Potential Evapotranspiration](#)” section for explanation).

^eIsland of Hawai‘i only; irrigation of macadamia on Maui considered negligible.

^fValue used on Moloka‘i.

^gValue used on Maui and Island of Hawai‘i.

^hValue used on Kaua‘i and O‘ahu.

rate was needed to maintain the same volumetric rate of discharge within each subarea. In the WATRMd simulations, the adjusted septic-system leachate rate was added to the plant-root zone of the subarea. For this study, no changes in cesspool seepage and septic-system leachate rates, and no changes in the pervious fraction of each subarea were assumed for the water-budget scenarios.

The area and spatial extent of each TMK parcel were determined in a geographic information system using polygon shapefiles of TMK parcels (City and County of Honolulu, 2020; Counties of Kauai, Maui, and Hawaii, 2019). Dozens of TMK numbers in the shapefiles of OSDS points did not match any TMK numbers in the shapefiles of TMK parcels; in each of these instances, the cesspool and septic-system leachate for an OSDS point was included in the leachate values assigned to the nearest TMK parcel.

Storm-Drain Systems

Some developed areas in Hawai'i have storm-drain systems that collect and divert stormwater runoff. In the WATRMd simulations, only subareas with developed, medium-intensity and developed, high-intensity land cover on each island were considered to have storm-drain systems (fig. 4). In these subareas, excess water that flows off impervious surfaces was assumed to be collected by storm-drain systems instead of flowing to adjacent pervious surfaces.

Soil-Infiltration Capacity

Infiltration is the downward entry of water from the ground surface into the plant-root zone. Liquid water in the plant-root zone that is not lost to ET can percolate deeper below the plant-root zone to recharge groundwater. The soil-infiltration capacity is the maximum rate of infiltration and typically decreases during the early part of a precipitation event due to increases in soil moisture. Measurements of field-saturated hydraulic conductivity, K_{fs} (Nimmo and others, 2009), an indicator of soil-infiltration capacity, have been conducted at multiple sites across the Hawaiian Islands (Perkins and others, 2018; Kennedy and others, 2019a, b; Fortini and others, 2020). Results of these studies indicate that median values of K_{fs} vary from about 8 in/d at a site dominated by bare soil (Perkins and others, 2018) to about 14,000 in/d at a site dominated by forest species (Kennedy and others, 2019a). These data indicate a wide range of variability in soil-infiltration capacities across the Hawaiian Islands. For each subarea, WATRMd requires a specified value for soil-infiltration capacity, which limits infiltration during a day. However, direct runoff in this study is computed separately using runoff-to-rainfall ratios, an approach that is intended to include runoff generated from precipitation rates in excess of the soil-infiltration capacity (see the “[Direct Runoff](#)” section of this appendix for a full description). Therefore, the

soil-infiltration capacity in the water budget was set to 9,999 in/d, a value greater than the daily maximum precipitation rate, to ensure that direct runoff computed by WATRMd was derived solely from the application of runoff-to-rainfall ratios.

Direct Runoff

Direct runoff of rainfall, hereinafter runoff, is the fraction of rainfall that does not contribute to net moisture gain within the plant-root zone. Runoff consists of overland flow and subsurface storm flow that rapidly transports infiltrated water to the stream (Oki, 2003). In the WATRMd simulations, direct runoff was estimated as a fraction of rainfall using runoff-to-rainfall ratios, hereinafter runoff ratios. This approach was also used in previous water-budget studies of Hawai'i and other Pacific islands (Johnson, 2012; Engott and others, 2017; Izuka and others, 2018; Johnson and others, 2018; Oki and others, 2020; Johnson and others, 2023; Kāne and others, 2024a) and provides reasonable estimates of regional average runoff using a minimal level of complexity. Details of the approach used to develop the runoff ratios for the WATRMd simulations in this study are described in Kāne and others (2024a).

The spatial variability of runoff ratios depends on numerous factors including geology, climate, soil type, topography, and land cover. Runoff ratios are expected to be highest where the rainfall amount and intensity are high, permeability of the soils and substrate is low, slopes are steep, and soil moisture is high (Oki, 2003). The temporal variability in runoff ratios used in this study reflects factors including antecedent soil moisture and rainfall intensity. In Hawai'i, runoff ratios generally follow a seasonal pattern. Runoff ratios are highest during the wet-season months and lowest during the dry-season months. The months of November through April and May through October were considered the wet and dry seasons, respectively, for this study. Daily runoff was calculated in WATRMd by multiplying daily rainfall by seasonal (wet and dry season) runoff ratios assigned to catchment zones.

Separate sets of runoff ratios were computed for the WATRMd simulations of historical climate (1990–2012) and projected future climate conditions (RCP8.5 2071–99) for each island. Runoff ratios within a catchment zone for the WATRMd simulations of historical climate conditions (1990–2012) consist of four types of ratios as follows: (1) observed seasonal ratios, (2) mean seasonal ratios, (3) estimated ratios using a regional-regression analysis that considered 30 different basin characteristics including soil, climate, land-cover, and morphometric characteristics (Izuka and others, 2018), or (4) a combination of these ratios (Oki and others, 2020). For the WATRMd simulations using projected future climate conditions (RCP8.5 2071–99), runoff ratios were adjusted for interannual variability to account for differences in rainfall compared to 1978–2007 mean rainfall using the approach described by Kāne and others (2024a).

Evapotranspiration

Evapotranspiration (ET) is the sum of all water that is evaporated or transpired from a land surface, including bare soil, the soil surface and overlying litter and mulch layers of vegetated surfaces, and the plant-root zone. The process of ET can be divided into three main evaporative subprocesses as follows: (1) canopy evaporation, which is evaporation of intercepted rain and cloud water from the surface of vegetation; (2) ground evaporation, which is evaporation of water from the soil surface and overlying litter and mulch layers; and (3) transpiration, the process by which soil moisture or groundwater taken up by vegetation is transported to leaves where it is released to the atmosphere through leaf stomata (Viessman and Lewis, 2003; Brooks and others, 2003). All three ET subprocesses (canopy evaporation, ground evaporation, and transpiration) are represented in the total-ET estimates of WATRMod.

Canopy evaporation in forest areas can substantially reduce the rainfall that reaches the ground beneath a forest canopy (Gaskill, 2004; DeLay, 2005; McJannet and others, 2007; Giambelluca and others, 2011; Safeeq and Fares, 2014). Because of the height of trees and their canopy structure, turbulent diffusion is much more efficient at removing intercepted water from forest canopies than from shorter vegetation. Moreover, canopy evaporation in forests tends to operate on much shorter time scales (hours) than transpiration (weeks or longer) (Savenije, 2004). Thus, accurate estimates of ET from forests generally require transpiration and canopy evaporation to be evaluated separately (Shuttleworth, 1993).

For this study, total ET from subareas of the forest land-cover class is computed by separately estimating forest-canopy evaporation and combined ground evaporation and transpiration from the plant-root zone. Evaporation from the forest canopy and ET from the plant-root zone are added together to yield total ET. For subareas of non-forest land-cover classes, ET is computed using a more traditional approach in which canopy evaporation, ground evaporation, and transpiration are not separately estimated. The concept of potential ET, combined with empirical models that account for periods when soil moisture is limited, is used to estimate ground evaporation and transpiration in forests and total ET for all other land-cover classes. The same approach to estimating total ET was used by Kāne and others (2024a) for Kauaʻi, Oʻahu, Molokaʻi, Maui, and the Island of Hawaiʻi.

Forest-Canopy Evaporation and Net Precipitation

As rain falls on a vegetated surface, a fraction of the droplets will accumulate on the leaves, trunks, or stems of the vegetation. Additional moisture from CWI may increase the amount of water that accumulates on vegetation. Net precipitation is the part of precipitation that reaches the forest floor.

In this study, the method derived from the Gash model (Gash and others, 1995) was used to calculate forest-canopy evaporation for the following reasons. First, the Gash model accounts for gaps in the forest canopy, and this allows for

a sparse canopy to be differentiated from a dense canopy. Second, canopy evaporation during a period of precipitation is dependent on the amount of precipitation during that period. Third, the Gash model has the capacity to account for spatial differences in climate, including climate differences between windward and leeward forests. One disadvantage of the Gash model, however, is that it is theoretical, which implies that a Gash model parameter must be adjusted for model estimates to match either empirical data or a reference dataset. Therefore, one of the parameters of the Gash model used by WATRMod to calculate forest-canopy evaporation required calibration to the wet-canopy evaporation maps of Giambelluca and others (2014) as described below. Use of the Gash model, instead of the mean wet-canopy evaporation maps, in the water budget allows forest-canopy evaporation to be calculated daily in response to daily variations in precipitation.

The estimation of forest-canopy evaporation by WATRMod requires values for rainfall and the following five Gash model parameters: (1) canopy cover, (2) canopy capacity, (3) trunk-storage capacity, (4) fraction of precipitation diverted to stemflow (precipitation that flows to the ground along tree trunks or plant stems), and (5) the ratio of the mean evaporation rate to mean precipitation rate during saturated conditions (V). The values assigned to the first four parameters in the WATRMod simulations were derived from published data for areas on several of the main Hawaiian Islands (Gaskill, 2004; DeLay, 2005; Takahashi and others, 2011; Giambelluca and others, 2014; Safeeq and Fares, 2014). The values assigned to V were derived using a method developed in a previous study (Johnson and others, 2018) that uses maps of mean wet-canopy evaporation for Kauaʻi, Oʻahu, and Maui (Giambelluca and others, 2014).

Canopy cover of forest land-cover classes varies spatially across each island. The canopy cover of each forest land-cover class subarea in the water budget was estimated from a map of mean annual vegetation cover fraction (Giambelluca and others, 2014) and was assumed to be the same for each time period simulated. This map quantifies the vegetation cover fraction at a spatial resolution of about 14 acres. A canopy cover of 0 implies an absence of canopy cover, whereas a value of 1 implies a dense canopy with no gaps.

Canopy capacity, trunk-storage capacity, and the fraction of precipitation diverted to stemflow were set to 0.05 inches (in.), 0.01 in., and 0.04, respectively, for each subarea with a forest land-cover classification (table 1.1). These values were estimated by Johnson and others (2018) on the basis of published data from studies conducted on Oʻahu and the Island of Hawaiʻi at forest sites that were each dominated by either native or non-native species (Gaskill, 2004; DeLay, 2005; Takahashi and others, 2011; Safeeq and Fares, 2014). Takahashi and others (2011) and Safeeq and Fares (2014) each monitored stemflow at an additional forest site dominated by *Psidium cattleianum* (strawberry guava) and measured stemflow rates (fraction of precipitation diverted to stemflow) ranging from 0.29 to 0.34. The high stemflow values from these two additional forest sites were excluded

from the calculated stemflow mean of 0.04 used for all forest land-cover types in the WATRMod simulations, which is consistent with earlier studies (Johnson and others, 2018; Izuka and others, 2018; Mair and others, 2019; Kāne and others, 2024a). Johnson and others (2018) tested the effect of using a stemflow rate of 0.37 for non-native forest in their water-budget model for Maui and reported a decrease of 0.4 percent in recharge summed across all subareas with non-native forest.

The spatial distribution of V was estimated using equation 11 from Kāne and others (2024a). Values of V ranged from 0.01 to 0.50, with wetter areas typically having lower values than drier areas. The spatial distribution of V from Kāne and others (2024a) was used for the WATRMod simulations of historical climate conditions (1990–2012) and the WATRMod simulations of projected future climate conditions (RCP8.5 2071–99) because of a lack of information to estimate potential changes in V . For example, projected changes in wind speed are needed to estimate potential changes in V ; however, this information is lacking for the RCP8.5 2071–99 projection.

Potential Evapotranspiration

The potential-ET rate is the maximum rate that water can be removed from the plant-root zone by ET if soil moisture is nonlimiting (Giambelluca, 1983). The actual plant-root zone rate of ET, referred to as the actual-ET rate, is computed in the water budget as a function of potential ET, soil-moisture content, and threshold-moisture content (see equation 14 in Oki [2022]). The actual-ET rate becomes less than the potential-ET rate with the onset of soil-moisture stress. As the soil dries, capillary and adsorptive forces bind the remaining water to the soil matrix, reducing the water available to roots. Soil-moisture stress occurs when the reduced availability of water to the root system induces a response in the plant to slow down transpiration and prevent desiccation. The threshold-moisture content at which a plant begins to react to soil drying varies with the type of plant.

The potential-ET rate is needed to compute the actual-ET rate in WATRMod. WATRMod computes the potential-ET rate for each subarea as the product of its crop coefficient and reference-ET rate. Crop coefficients are used to represent the integrated effects of land-cover and vegetation characteristics on the potential-ET rate. The reference-ET rate is the ET rate of a hypothetical grass surface of uniform height that is completely shading the ground and has optimum soil-water conditions for given climatic conditions (Allen and others, 1998). The mean annual reference-ET rate ranges from about 26 to 114 inches across the Hawaiian Islands (Giambelluca and others, 2014, map of grass reference surface potential ET available at <http://evapotranspiration.geography.hawaii.edu/interactivemap.html>). In the WATRMod simulations, the monthly reference-ET rate was not varied from year to year, and it was assumed to equal the mean monthly reference-ET rate. Reference ET was assumed to be the same each day of a given month.

Crop coefficients were assigned to each subarea based on the subarea's land-cover type (table 1.1). The crop coefficients used for this study's scenarios were the same as those used by Kāne and others (2024a). For non-forest land-cover classes, crop coefficients integrated the effects of transpiration, ground evaporation, and canopy evaporation. For forest land-cover classes, crop coefficients integrated the effects of transpiration and ground evaporation only because canopy evaporation was accounted for separately. The crop coefficients for corn vary monthly and are based on information in the Hawai'i Agricultural Water Use and Development Plan (University of Hawai'i at Mānoa, 2008). The crop coefficients used for corn were 0.85, 0.50, 0.29, 0.40, 0.80, 1.20, 0.85, 0.50, 0.29, 0.40, 0.80, and 1.20 for the months of January through December, respectively. The values for seed corn were the same as those used by Kāne and others (2024a) for Kaua'i, O'ahu, Moloka'i, Maui, and the Island of Hawai'i.

Monthly reference ET for each model subarea was estimated for the WATRMod simulations of historical climate conditions (1990–2012) using maps of mean monthly grass reference surface ET (Giambelluca and others, 2014). The monthly reference ET for each model subarea for the WATRMod simulations of historical climate conditions (1990–2012) was also used for the WATRMod simulations of projected future climate conditions (RCP8.5 2071–99) because of a lack of information needed to estimate potential changes in reference ET. The same approach was used by Kāne and others (2024a) for the RCP8.5 2071–99 projection.

Total Evapotranspiration

In this study, total ET in each subarea represents the sum of transpiration, ground evaporation, and canopy evaporation. However, the approach used to compute the amount attributable to each ET process varies with land-cover class. For subareas of the non-forest land-cover class, WATRMod estimates of plant-root zone ET were used to represent all three ET processes and quantify total ET. For subareas of the forest land-cover class, WATRMod estimates of plant-root zone ET were used to represent transpiration and ground evaporation, whereas estimates of ET losses from the rainfall-interception model were used to represent canopy evaporation. Total ET for subareas of the forest land-cover class, including tree plantation, was computed as the sum of plant-root zone ET and canopy evaporation.

Plant-root zone ET for each subarea was computed by WATRMod on the basis of potential ET, moisture storage in the plant-root zone, and threshold-moisture storage (Oki, 2022). When moisture storage was greater than or equal to the threshold-moisture storage, the plant-root-zone-ET rate was assumed to be equal to the potential-ET rate. When moisture storage was less than the threshold-moisture storage, the plant-root-zone-ET rate was less than the potential-ET rate and declined linearly with soil-moisture content. Threshold-moisture storage was computed on the basis of the depletion fraction and moisture-storage capacity of the plant-root zone (see equation 25 in Oki [2022]). Values for depletion fraction

assigned to each land-cover class (table 1.1) were the same as those used by Kāne and others (2024a).

Moisture-Storage Capacity of the Plant-Root Zone

The moisture-storage capacity of the plant-root zone for each subarea was computed by WATRMod as the product of its assigned root depth and the available water capacity of its soil unit (see equation 12 in Johnson and others [2018]). The root depth of each subarea was set to the root depth assigned to its land-cover class (table 1.1). The available water capacities of soils were assumed to be time-invariant and were estimated from the Natural Resources Conservation Service (2019) soil map and corresponding tables of available water capacities. For each soil unit, the tables listed the minimum and maximum available water capacities for various ranges of depth. A depth-weighted mean of available water capacity was computed for each soil type in WATRMod. All depths of the “rock outcrop” soil unit, however, had zero available water capacity according to Natural Resources Conservation Service (2019). For this study, zero available water capacity was considered too low for this soil unit because many areas with this soil unit were mapped as grassland or shrubland. Therefore, in the WATRMod simulations, a value of 0.01 was substituted for all subareas with the “rock outcrop” soil unit, which is consistent with the approach used by Kāne and others (2024a).

Direct Recharge

In the WATRMod simulations, direct recharge represents water seepage that was not subject to the direct runoff or ET process because it bypassed the plant-root zone. Direct recharge in this study was estimated for subareas with cesspool seepage and for subareas with reservoir and water body land cover (fig. 4). Methods used to estimate cesspool seepage for each scenario were explained in the “Septic Effluent” section. Specified rates of constant recharge were assigned as daily values to subareas of reservoir and water body land cover in the WATRMod simulations. The rates of constant recharge used in this study were the same as those used by Kāne and others (2024a) (see table 11 in Kāne and others [2024a]).

Initial Conditions

In addition to the water-budget inputs already listed, several other parameter inputs were required. The initial moisture storage for the pervious fraction of subareas was set at 50 percent of the soil moisture-storage capacity. The initial moisture storage for the impervious fraction of subareas was set at 0.125 in., which was calculated as 50 percent of the rainfall-retention capacity of 0.25 in. These values were also used for other recent water budgets for Kauaʻi, Oʻahu, Molokaʻi, Maui, and the Island of Hawaiʻi (Izuka and others, 2018; Oki and others, 2020; Kāne and others, 2024a). These values were also used in each of the WATRMod simulations. The effects of these inputs on regional-scale mean annual

recharge generally were minor because they either pertained to only a small area or were only applicable during a small fraction of time.

References Cited

- Allen, R.G., Pereira, L.S., Raes, D., and Smith, M., 1998, Crop evapotranspiration—Guidelines for computing crop water requirements: Food and Agriculture Organization of the United Nations, Irrigation and Drainage paper 56, accessed April 1, 2020, at <https://www.fao.org/3/x0490e/x0490e00.htm>.
- Berg, N., McGurk, B., and Calhoun, R., 1997, Hydrology and land use effects on the Hanalei National Wildlife Refuge, Kauai, Hawaii, Final Report: U.S. Department of Agriculture, Forest Service, Pacific Southwest Research Station, Interagency Agreement 14-48-0001-94588, 62 p.
- Brewington, L., Keener, V., and Mair, A., 2019, Simulating Land Cover Change Impacts on Groundwater Recharge under Selected Climate Projections, Maui, Hawaiʻi: Remote Sensing, v. 11, no. 24, <https://doi.org/10.3390/rs11243048>.
- Brooks, K.N., Ffolliott, P.F., Gregersen, H.M., and DeBano, L.F., 2003, Hydrology and the management of watersheds, 3rd Edition: Ames, Iowa, Iowa State Press, 574 p.
- City and County of Honolulu, 2020, Parcel—Tax [originally published March 18, 2016]: City and County of Honolulu database, accessed February 13, 2020, at <https://honolulu.cchnl.opendata.arcgis.com/datasets/cchnl::parcels-tax/about>.
- Counties of Kauai, Maui, and Hawaii, 2019, 015—Cadastral and Land Descriptions—TMK Parcels (All Islands), Neighbor Islands: State of Hawaiʻi Office of Planning and Sustainable Development database, accessed February 25, 2020, at <http://planning.hawaii.gov/gis/download-gis-data-expanded/>.
- De la Pena, R., and Melchor, F., 1984, Water use and efficiency in lowland taro production, in 6. Symposium of the International Society for Tropical Root Crops, Lima (Peru), 21-26 Feb 1983.
- DeLay, J.K., 2005, Canopy water balance on an elfin cloud forest at Alakahi, Hawaiʻi: Honolulu, University of Hawaiʻi, M.S. thesis, 78 p., accessed April 4, 2020, at <http://hdl.handle.net/10125/11633>.
- Elison Timm, O., Giambelluca, T.W., and Diaz, H.F., 2015, Statistical downscaling of rainfall changes in Hawaiʻi based on the CMIP5 global model projections: Journal of Geophysical Research, Atmospheres, v. 120, no. 1, p. 92–112, <https://doi.org/10.1002/2014JD022059>.
- Engott, J.A., 2011, A water-budget model and assessment of groundwater recharge for the Island of Hawaiʻi: U.S. Geological Survey Scientific Investigations Report 2011–5078, 53 p., <https://doi.org/10.3133/sir20115078>.

- Engott, J.A., Johnson, A.G., Bassiouni, M., Izuka, S.K., and Rotzoll, K., 2017, Spatially distributed groundwater recharge for 2010 land cover estimated using a water-budget model for the Island of O‘ahu, Hawai‘i (ver 2.0, December 2017): U.S. Geological Survey Scientific Investigations Report 2015–5010, 49 p., <https://doi.org/10.3133/sir20155010>.
- Engott, J.A., and Vana, T.T., 2007, Effects of agricultural land-use changes and rainfall on ground-water recharge in Central and West Maui, Hawai‘i, 1926–2004: U.S. Geological Survey Scientific Investigations Report 2007–5103, 56 p., <https://doi.org/10.3133/sir20075103>.
- Fortini, L.B., Leopold, C.R., Perkins, K., Chadwick, O.A., Yelenik, S.G., Jacobi, J.D., Bishaw II, K., Gregg, M., and Rosa, S., 2020, Hawaiian Islands datasets quantifying the effects of invasive animals and plants on native forests across the archipelago 2019 (ver. 2.0 April 2020): U.S. Geological Survey data release, <https://doi.org/10.5066/P9J35LMQ>.
- Frazier, A.G., Giambelluca, T.W., Diaz, H.F., and Needham, H.L., 2016, Comparison of geostatistical approaches to spatially interpolate month-year rainfall for the Hawaiian Islands: *International Journal of Climatology*, v. 36, no. 3, p. 1459–1470, <https://doi.org/10.1002/joc.4437>.
- Gash, J.H.C., Lloyd, C.R., and Lachaud, G., 1995, Estimating sparse forest rainfall interception with an analytical model: *Journal of Hydrology*, v. 170, no. 1–4, p. 79–86, [https://doi.org/10.1016/0022-1694\(95\)02697-N](https://doi.org/10.1016/0022-1694(95)02697-N).
- Gaskill, T.G.R., 2004, Hydrology of forest ecosystems in the Honouliuli Preserve—Implications for groundwater recharge and watershed restoration: Botanical Sciences, University of Hawai‘i at Mānoa PhD Dissertation, 177 p., accessed January 27, 2015, at <http://scholarspace.manoa.hawaii.edu/handle/10125/12116>.
- Giambelluca, T.W., 1983, Water balance of the Pearl Harbor-Honolulu basin, Hawaii, 1946–1975: Honolulu, University of Hawai‘i at Mānoa, Water Resources Research Center Technical Report 151, 151 p., accessed February 8, 2010, at <https://scholarspace.manoa.hawaii.edu/handle/10125/1992>.
- Giambelluca, T.W., Chen, Q., Frazier, A.G., Price, J.P., Chen, Y.-L., Chu, P.-S., Eischeid, J.K., and Delparte, D.M., 2013, Online rainfall atlas of Hawai‘i: *Bulletin of the American Meteorological Society*, v. 94, no. 3, p. 313–316, <https://doi.org/10.1175/BAMS-D-11-00228.1>.
- Giambelluca, T.W., DeLay, J.K., Nullet, M.A., Scholl, M.A., and Gingerich, S.B., 2011, Canopy water balance of windward and leeward Hawaiian cloud forests on Haleakalā, Maui, Hawai‘i: *Hydrological Processes*, v. 25, no. 3, p. 438–447. <https://doi.org/10.1002/hyp.7738>.
- Giambelluca, T.W., Shuai, X., Barnes, M.L., Alliss, R.J., Longman, R.J., Miura, T., Chen, Q., Frazier, A.G., Mudd, R.G., Cuo, L., and Businger, A.D., 2014, Evapotranspiration of Hawai‘i—Final report: Honolulu, University of Hawai‘i at Mānoa Department of Geography, submitted to the U.S. Army Corps of Engineers—Honolulu District, and the Commission on Water Resource Management, State of Hawai‘i, 168 p., accessed March 4, 2014, at <http://evapotranspiration.geography.hawaii.edu/assets/files/PDF/ET%20Project%20Final%20Report.pdf>.
- Graham, L.P., Hagemann, S., Jaun, S., and Beniston, M., 2007, On interpreting hydrological change from regional climate models: *Climatic Change*, v. 81, no. 1, p. 97–122. <http://dx.doi.org/10.1007/s10584-006-9217-0>.
- Hay, L.E., Wilby, R.L., and Leavesley, G.H., 2000, A comparison of delta change and downscaled GCM scenarios for three mountainous basins in the United States: *Journal of the American Water Resources Association*, v. 36, no. 2, p. 387–397. <http://dx.doi.org/10.1111/j.1752-1688.2000.tb04276.x>.
- Izuka, S.K., Engott, J.A., Rotzoll, K., Bassiouni, M., Johnson, A.G., Miller, L.D., and Mair, A., 2018, Volcanic aquifers of Hawai‘i—Hydrogeology, water budgets, and conceptual models (ver. 2.0, March 2018): U.S. Geological Survey Scientific Investigations Report 2015–5164, 158 p., <https://doi.org/10.3133/sir20155164>.
- Johnson, A.G., 2012, A water-budget model and estimates of groundwater recharge for Guam: U.S. Geological Survey Scientific Investigations Report 2012–5028, 53 p., <https://doi.org/10.3133/sir20125028>.
- Johnson, A.G., Engott, J.A., Bassiouni, M., and Rotzoll, K., 2018, Spatially distributed groundwater recharge estimated using a water-budget model for the Island of Maui, Hawai‘i, 1978–2007 (ver. 2.0, February 2018): U.S. Geological Survey Scientific Investigations Report 2014–5168, 53 p., <https://doi.org/10.3133/sir20145168>.
- Johnson, A.G., Mair, A., and Oki, D.S., 2023, Identification of water-budget information needed to accurately quantify how recharge for the Hawaiian Islands is affected by land-cover change: U.S. Geological Survey Scientific Investigations Report 2023–5022, 28 p., <https://doi.org/10.3133/sir20235022>.
- Kāne, H.L., Mair, A., Johnson, A.G., Rotzoll, K., Mifflin, J., and Oki, D.S., 2024a, Estimated groundwater recharge for mid-century and end-of-century climate projections, Kaua‘i, O‘ahu, Moloka‘i, Lāna‘i, Maui, and the Island of Hawai‘i: U.S. Geological Survey Scientific Investigations Report 2023–5130, 133 p., <https://doi.org/10.3133/sir20235130>.

- Kāne, H.L., Mifflin, J., and Mair, A., 2024b, Mean annual water-budget components for Kauaʻi, Oʻahu, Molokaʻi, Lānaʻi, Maui, and the Island of Hawaiʻi, for a set of recent and future climate conditions, and 2020 land cover: U.S. Geological Survey data release, <https://doi.org/10.5066/P972KMSL>.
- Kennedy, J.J., Mair, A., and Perkins, K.S., 2019a, Summary of soil field-saturated hydraulic conductivity, hydrophobicity, preferential-flow, and particle-size measurements collected at four study sites on the island of Maui, Hawaii, September 2017–August 2018: U.S. Geological Survey data release, <https://doi.org/10.5066/P9OP3BHM>.
- Kennedy, J.J., Mair, A., Perkins, K.S., Nullet, M.A., Tseng, H., and Miyazawa, Y., 2019b, Summary of soil field-saturated hydraulic conductivity, hydrophobicity, and preferential-flow measurements and soil laboratory-testing results collected at three sites on the islands of Maui and Hawaii, Hawaii, July 2016–January 2018: U.S. Geological Survey data release, <https://doi.org/10.5066/P9J5SESD>.
- Longman, R.J., Frazier, A.G., Newman, A.J., Giambelluca, T.W., Schanzenbach, D., Kagawa-Viviani, A., Needham, H., Arnold, J.R., and Clark, M.P., 2019, High-resolution gridded daily rainfall and temperature for the Hawaiian Islands (1990–2014): *Journal of Hydrometeorology*, v. 20, no. 3, p. 489–508, <https://doi.org/10.1175/JHM-D-18-0112.1>.
- Mair, A., 2024, Mean annual groundwater recharge rates for Kauaʻi, Oʻahu, Molokaʻi, Maui, and the Island of Hawaiʻi, for a set of drought and land-cover conditions: U.S. Geological Survey data release, <https://doi.org/10.5066/P9DDP1C6>.
- Mair, A., Johnson, A.G., Rotzoll, K., and Oki, D.S., 2019, Estimated groundwater recharge from a water-budget model incorporating selected climate projections, Island of Maui, Hawaiʻi: U.S. Geological Survey Scientific Investigations Report 2019–5064, 46 p., <https://doi.org/10.3133/sir20195064>.
- McJannet, D., Wallace, J., and Reddell, P., 2007, Precipitation in Australian tropical rainforests: I. Measurement of stemflow, throughfall and cloud interception: *Hydrological Processes*, v. 21, no. 13, p. 1692–1702, <https://doi.org/10.1002/hyp.6347>.
- Miles, K., 1931, Report on study of water requirements of taro in Hanapēpē Valley, cooperative study by the Territory of Hawaiʻi and McBryde Sugar Co.: ‘Eleʻele, Hawaiʻi, 52 p. [As cited in Penn, 1997.]
- Natural Resources Conservation Service, 2019, Web Soil Survey—Soil survey geographic (SSURGO) database for the Islands of Kauaʻi, Oʻahu, Molokaʻi, Lānaʻi, Maui, and Hawaiʻi: U.S. Department of Agriculture, Natural Resources Conservation Service web page, accessed December 5, 2019, at <https://websoilsurvey.nrcs.usda.gov/app/>.
- Navarro-Racines, C., Tarapues, J., Thornton, P., Jarvis, A., and Ramirez-Villegas, J., 2020, High-resolution and bias-corrected CMIP5 projections for climate change impact assessments: *Scientific Data*, v. 7, no. 1, article no. 7, 14 p., <https://doi.org/10.1038/s41597-019-0343-8>.
- Nimmo, J.R., Schmidt, K.M., Perkins, K.S., and Stock, J.D., 2009, Rapid measurement of field-saturated hydraulic conductivity for areal characterization: *Vadose Zone Journal*, v. 8, no. 1, p. 142–149, <https://doi.org/10.2136/vzj2007.0159>.
- Oki, D.S., 2002, Reassessment of ground-water recharge and simulated ground-water availability for the Hawi area of north Kohala, Hawaii: U.S. Geological Survey Water-Resources Investigations Report 02–4006, 62 p., <https://doi.org/10.3133/wri20024006>.
- Oki, D.S., 2003, Surface water in Hawaii: U.S. Geological Survey Fact Sheet 045–03, 6 p., <https://doi.org/10.3133/fs04503>.
- Oki, D.S., 2022, Water-budget accounting for tropical regions model (WATRMd) documentation: U.S. Geological Survey Open-File Report 2022–1013, 77 p., <https://doi.org/10.3133/ofr20221013>.
- Oki, D.S., Engott, J.A., and Rotzoll, K., 2020, Numerical simulation of groundwater availability in central Molokaʻi, Hawaiʻi: U.S. Geological Survey Scientific Investigations Report 2019–5150, 95 p., <https://doi.org/10.3133/sir20195150>.
- Penn, D.C., 1997, Water and energy flows in Hawaiʻi taro pondfields: Honolulu, University of Hawaiʻi at Mānoa, Ph.D. Dissertation, 395 p.
- Perkins, K.S., Stock, J.D., and Nimmo, J.R., 2018, Vegetation influences on infiltration in Hawaiian soils: *Ecohydrology*, v. 11, no. 5, article no. e1973, 6 p., <https://doi.org/10.1002/eco.1973>.
- van Roosmalen, L., Christensen, J.H., Butts, M.B., Jensen, K.H., and Refsgaard, J.C., 2010, An intercomparison of regional climate model data for hydrological impact studies in Denmark: *Journal of Hydrology*, v. 380, no. 3–4, p. 406–419, <https://doi.org/10.1016/j.jhydrol.2009.11.014>.

- van Roosmalen, L., Christensen, B.S.B., and Sonnenborg, T.O., 2007, Regional differences in climate change impacts on groundwater and stream discharge in Denmark: *Vadose Zone Journal*, v. 6, no. 3, p. 554–571, <https://doi.org/10.2136/vzj2006.0093>.
- van Roosmalen, L., Sonnenborg, T.O., and Jensen, K.H., 2009, Impact of climate and land use change on the hydrology of a large-scale agricultural catchment: *Water Resources Research*, v. 45, no. 7, 18 p., <https://doi.org/10.1029/2007WR006760>.
- van Roosmalen, L., Sonnenborg, T.O., Jensen, K.H., and Christensen, J.H., 2011, Comparison of hydrological simulations of climate change using perturbation of observations and distribution-based scaling: *Vadose Zone Journal*, v. 10, no. 1, p. 136–150, <https://doi.org/10.2136/vzj2010.0112>.
- Safeeq, M., and Fares, A., 2014, Interception losses in three non-native Hawaiian forest stands: *Hydrological Processes*, v. 28, no. 2, p. 237–254, <https://doi.org/10.1002/hyp.9557>.
- Savenije, H.H.G., 2004, The importance of interception and why we should delete the term evapotranspiration from our vocabulary: *Hydrological Processes*, v. 18, no. 8, p. 1507–1511, <https://doi.org/10.1002/hyp.5563>.
- Shuttleworth, W.J., 1993, Evaporation, *in* Maidment, D.R. ed., *Handbook of hydrology*: New York, McGraw-Hill, p. 4.1–4.53.
- Takahashi, M., Giambelluca, T.W., Mudd, R.G., DeLay, J.K., Nullet, M.A., and Asner, G.P., 2011, Rainfall partitioning and cloud water interception in native forest and invaded forest in Hawai‘i Volcanoes National Park: *Hydrological Processes*, v. 25, no. 3, p. 448–464, <https://doi.org/10.1002/hyp.7797>.
- University of Hawai‘i at Mānoa, 2008, Hawaii agricultural water use and development plan: Honolulu, State of Hawaii Department of Agriculture, prepared by University of Hawai‘i at Mānoa, 135 p.
- Viessman, W., and Lewis, G.L., 2003, *Introduction to Hydrology*, 5th Edition: Upper Saddle River, New Jersey, Prentice Hall, Pearson Education, Inc., 624 p.
- Watson, L.J. (ed.), 1964, Observations made with respect to irrigation and growth of taro at certain patches at Waiāhole and Kahaluu: Honolulu, Hawai‘i, City & County of Honolulu Board of Water Supply Water Resources Division, *in* Reppun v. Board of Water Supply: variously paged.
- Whittier, R.B., and El-Kadi, A.I., 2009, Human and environmental risk ranking of onsite sewage disposal systems for Oahu: Honolulu, Hawai‘i Department of Health Safe Drinking Water Branch, prepared by University of Hawai‘i at Mānoa, 142 p., accessed February 13, 2020, at <https://hdl.handle.net/10125/50770>.
- Whittier, R.B., and El-Kadi, A.I., 2014, Human and environmental risk ranking of onsite sewage disposal systems for the Hawaiian islands of Kauai, Molokai, Maui, and Hawaii: Honolulu, Hawai‘i Department of Health Safe Drinking Water Branch, prepared by University of Hawai‘i at Mānoa, 257 p., accessed February 13, 2020, at <https://hdl.handle.net/10125/50771>.
- Wilby, R.L., Hay, L.E., Gutowski, W.J., Arritt, R.W., Takle, E.S., Pan, Z., Leavesley, G.H., and Clark, M.P., 2000, Hydrological responses to dynamically and statistically downscaled climate model output: *Geophysical Research Letters*, v. 27, no. 8, p. 1199–1202, <https://doi.org/10.1029/1999GL006078>.

Appendix 2. Evaluation of Moisture-Stress Thresholds for Soil Moisture, Evapotranspiration, and Climatic Water Deficit

A set of thresholds was developed for assessing the frequency characteristics of moisture-stress indicators, including soil moisture, evapotranspiration (ET), and climatic water deficit (CWD) for each water-budget scenario. This appendix describes the approach used to select a single moisture-stress threshold for assessing the frequency characteristics of each moisture-stress indicator. Selected threshold levels of moisture stress were median values during the month of occurrence of each wildfire. Threshold values of 0.074, 0.96 inches, and 0.77 were selected for soil moisture (expressed as a fraction of available water capacity), ET, and CWD (expressed as a fraction of potential ET), respectively. The frequency characteristics of soil moisture, ET, and CWD are examined in the “[Soil Moisture, Evapotranspiration, and Climatic Water Deficit Frequency Characterization](#)” section of the report.

Definitions of Soil Moisture, Evapotranspiration, and Climatic Water Deficit

In the water-budget model, soil moisture is expressed as an equivalent water depth (Oki, 2022), which is defined as the volumetric soil water content multiplied by the soil depth (Brouwer and others, 1985). For this analysis, soil moisture is expressed as a fraction of available water capacity, defined as the maximum amount of plant-available water a soil can provide (Natural Resources Conservation Service, 2008). Expressing soil moisture as a fraction of available water capacity is preferable to using equivalent water depth because this relative soil-moisture representation accounts for the effect of soil properties on moisture available for vegetation (Allen and others, 1998). A depth-weighted mean available water capacity was computed for each soil type in the water-budget model on the basis of soil maps and corresponding tables of available water capacities for Kaua‘i, O‘ahu, Moloka‘i, Maui, and the Island of Hawai‘i (Natural Resources Conservation Service, 2019). The depth-weighted mean available water capacities were used to express soil moisture as a fraction of available water capacity for each subarea. A time series of monthly mean soil moisture, expressed as a fraction of available water capacity, from each water-budget simulation was used to determine the frequency characteristics of soil moisture for each model subarea.

In this study, ET in each subarea represents the sum of transpiration, ground evaporation, and canopy evaporation. A time series of monthly ET from each water-budget scenario was used to determine the frequency characteristics of ET

for each model subarea. Potential ET is the maximum rate that water can be removed from the plant-root zone by ET if soil moisture is non-limiting (Giambelluca, 1983). Climatic water deficit is defined as the evaporative demand that exceeds available water and is calculated as the difference between potential ET and actual ET (Flint and others, 2015). For this analysis, CWD is expressed as a fraction of potential ET, which is preferable to using the difference between potential ET and actual ET because this CWD representation accounts for the variability in evaporative demand and vegetation across each island. This CWD representation implies that CWD for each model subarea can vary from 0 (low moisture stress) to 1 (high moisture stress). A time series of monthly CWD, expressed as a fraction of potential ET, from each water-budget scenario was used to determine the frequency characteristics of CWD for each model subarea.

Effects of Drought on Soil Moisture, Evapotranspiration, and Climatic Water Deficit Estimates

Moisture stress on vegetation decreases during relatively wet periods and increases during relatively dry periods. Water-budget model results were evaluated to assess how changes in rainfall affect indicators of moisture stress on vegetation, including estimates of soil moisture, ET, and CWD, during recent and future drought conditions. Frequency characteristics of soil moisture, ET, and CWD were computed using a set of threshold values ([table 2.1](#)) developed for four water-budget scenarios: (1) a reference condition representative of non-drought rainfall conditions during 1990–2012 and 2020 land cover, (2) rainfall conditions representative of the driest periods during 1920–2012 and 2020 land cover, (3) rainfall conditions representative of non-drought conditions during a future dry-climate condition and 2020 land cover, and (4) rainfall conditions representative of the driest periods during a future dry-climate condition and 2020 land cover. The threshold values for the indicator variables were selected using a trial-and-error approach to capture a range of values for developing cumulative frequency curves. Rainfall conditions during 1990–97 and 2003–06 from Frazier and others (2016), hereinafter Non-Drought rainfall, were selected to represent the reference conditions and used with 2020 land cover, hereinafter Non-Drought scenario ([table 5](#)). Rainfall conditions during 1998–2002 and 2007–12 from Frazier and others (2016), hereinafter Drought 3 rainfall, were selected to represent the driest periods during 1920–2012 and used with

Table 2.1. Summary of threshold values for computing relative frequency of soil moisture, evapotranspiration, and climatic water deficit.

[--, not applicable; selected threshold value for mapping relative frequency is bolded.]

Monthly mean soil moisture, in fraction of available water capacity	Monthly evapotranspiration, in inches	Monthly climatic water deficit, in fraction of potential evapotranspiration
0.01	0.1	0.01
0.074	0.96	0.1
0.1	2	0.3
0.3	3	0.5
0.5	4	0.7
0.7	5	0.77
0.9	6	0.8
0.99	--	0.9
--	--	0.99

2020 land cover, hereinafter Drought 3 scenario. The future dry-climate condition was developed using projected rainfall conditions during 2071–99 from Elison Timm and others (2015) for a Representative Concentration Pathway (RCP) warming scenario with a total radiative forcing of 8.5 watts per square meter (W/m^2) by the year 2100 (Intergovernmental Panel on Climate Change, 2014), hereinafter RCP8.5 2071–99 projection. Rainfall conditions during 1990–97 and 2003–06 adjusted for a RCP8.5 2071–99 projection, hereinafter RCP8.5 2071–99 Non-Drought rainfall, were selected to represent non-drought conditions during the future dry-climate condition and used with 2020 land cover, hereinafter Future Non-Drought scenario. Finally, rainfall conditions during 1998–2002 and 2007–12 adjusted for a RCP8.5 2071–99 projection, hereinafter RCP8.5 2071–99 Drought 3 rainfall, were selected to represent the driest periods during the future dry-climate condition and used with 2020 land cover, hereinafter Future Drought 3 scenario. For each water-budget scenario, a time series of monthly soil moisture, ET, and CWD for each subarea was used to compute the relative frequency for each threshold value. In this study, relative frequency describes the fraction of months that soil moisture and ET are less than or equal to a threshold value without regard for the sequence or intensity of occurrence. For CWD, relative frequency describes the fraction of months that estimates are greater than or equal to a threshold value.

The following steps were completed using time series results from each of the selected water-budget simulations for Kaua‘i, O‘ahu, Moloka‘i, Maui, and the Island of Hawai‘i. First, the relative frequency of each moisture-stress indicator (soil moisture, ET, CWD) was computed for each model subarea using a set of threshold values (table 2.1). Next, an island-wide area-weighted mean of relative frequency for each

moisture-stress indicator was computed for each threshold value. Finally, cumulative frequency curves were developed by plotting the island-wide area-weighted mean of relative frequency for soil moisture, ET, and CWD against the set of threshold values. The cumulative frequency curves were used to illustrate how changes in rainfall for each water-budget scenario can affect island-wide estimates of soil moisture, ET, and CWD.

Soil Moisture

The cumulative frequency curves show that the relative frequency of soil moisture changes with each water-budget scenario (fig. 2.1). As expected, the lowest relative frequencies of soil moisture are evident for the Non-Drought scenario, which indicates that moisture stress on vegetation occurs less often and over a smaller area of each island relative to the other three scenarios. The highest relative frequencies of soil moisture are evident for the Future Drought 3 scenario, which indicates more frequent and widespread moisture stress on vegetation on each island relative to the other three scenarios. Among the five islands, Kaua‘i has the lowest relative frequencies for each soil-moisture threshold and water-budget scenario (fig. 2.1A), whereas Moloka‘i has the highest relative frequencies (fig. 2.1C). These results indicate that moisture stress on vegetation is most frequent and widespread on Moloka‘i, and least frequent and widespread on Kaua‘i. More frequent and widespread moisture stress implies a greater potential wildfire hazard, which implies that Moloka‘i has the greatest wildfire hazard and Kaua‘i has the lowest wildfire hazard among the five islands. These results are consistent with estimates of island-wide mean annual rainfall. For example, Moloka‘i had the lowest island-wide mean annual rainfall during 1978–2007 among the five

islands, whereas Kauaʻi had the highest (table 4). These results are also consistent with the total burned area documented during 1999–2012 on each island. Kauaʻi had the lowest total burned area, expressed as a fraction of land area, during 1999–2012 among the five islands, whereas Molokaʻi had the highest (table 2). Relative frequencies of soil moisture on each island for the Drought 3 and Future Non-Drought scenarios are similar, which indicates that these two scenarios may have similar effects on the spatial extent and frequency of moisture stress on vegetation.

Evapotranspiration

The cumulative frequency curves show that the relative frequency of ET changes with each water-budget scenario (fig. 2.2). The lowest relative frequencies of ET are evident for the Non-Drought scenario, which indicates that moisture stress on vegetation occurs less often and over a smaller area on each island relative to the other three scenarios. The highest relative frequencies of ET are evident for the Future Drought 3 scenario, which indicates more frequent and widespread moisture stress on vegetation on each island

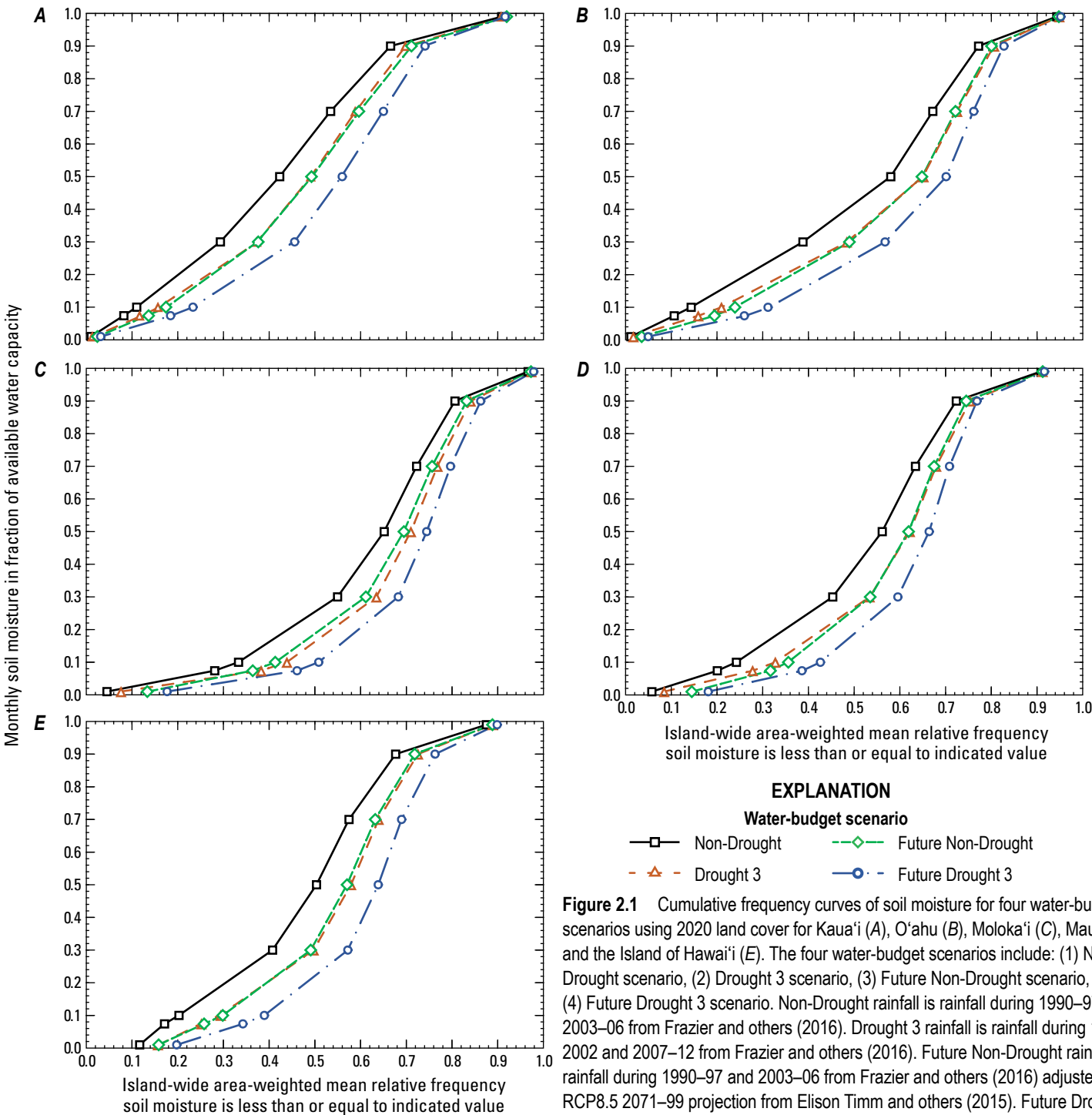


Figure 2.1 Cumulative frequency curves of soil moisture for four water-budget scenarios using 2020 land cover for Kauaʻi (A), Oʻahu (B), Molokaʻi (C), Maui (D), and the Island of Hawaiʻi (E). The four water-budget scenarios include: (1) Non-Drought scenario, (2) Drought 3 scenario, (3) Future Non-Drought scenario, and (4) Future Drought 3 scenario. Non-Drought rainfall is rainfall during 1990–97 and 2003–06 from Frazier and others (2016). Drought 3 rainfall is rainfall during 1998–2002 and 2007–12 from Frazier and others (2016). Future Non-Drought rainfall is rainfall during 1990–97 and 2003–06 from Frazier and others (2016) adjusted for a RCP8.5 2071–99 projection from Elison Timm and others (2015). Future Drought 3 rainfall is rainfall during 1998–2002 and 2007–12 from Frazier and others (2016) adjusted for a RCP8.5 2071–99 projection from Elison Timm and others (2015).

relative to the other three scenarios. Among the five islands, Kaua'i and O'ahu have the lowest relative frequencies of ET for each ET threshold and water-budget scenario (fig. 2.2A, B). These results indicate that moisture stress on vegetation is less frequent and widespread on Kaua'i and O'ahu, relative to the other islands. However, the relative frequencies for O'ahu include large areas of irrigated agriculture (fig. 4B) which increases ET in these areas and may bias estimates of island-wide relative frequency of ET. Relative frequencies of ET on each island for the Drought 3 and Future Non-Drought

scenarios are similar, which indicates that these two scenarios may have similar effects on the extent and frequency of moisture stress on vegetation.

Climatic Water Deficit

The cumulative frequency curves show that the relative frequency of CWD changes with each water-budget scenario (fig. 2.3). The lowest relative frequencies of CWD are evident for the Non-Drought scenario, which indicates that moisture stress on vegetation occurs less often and over a smaller

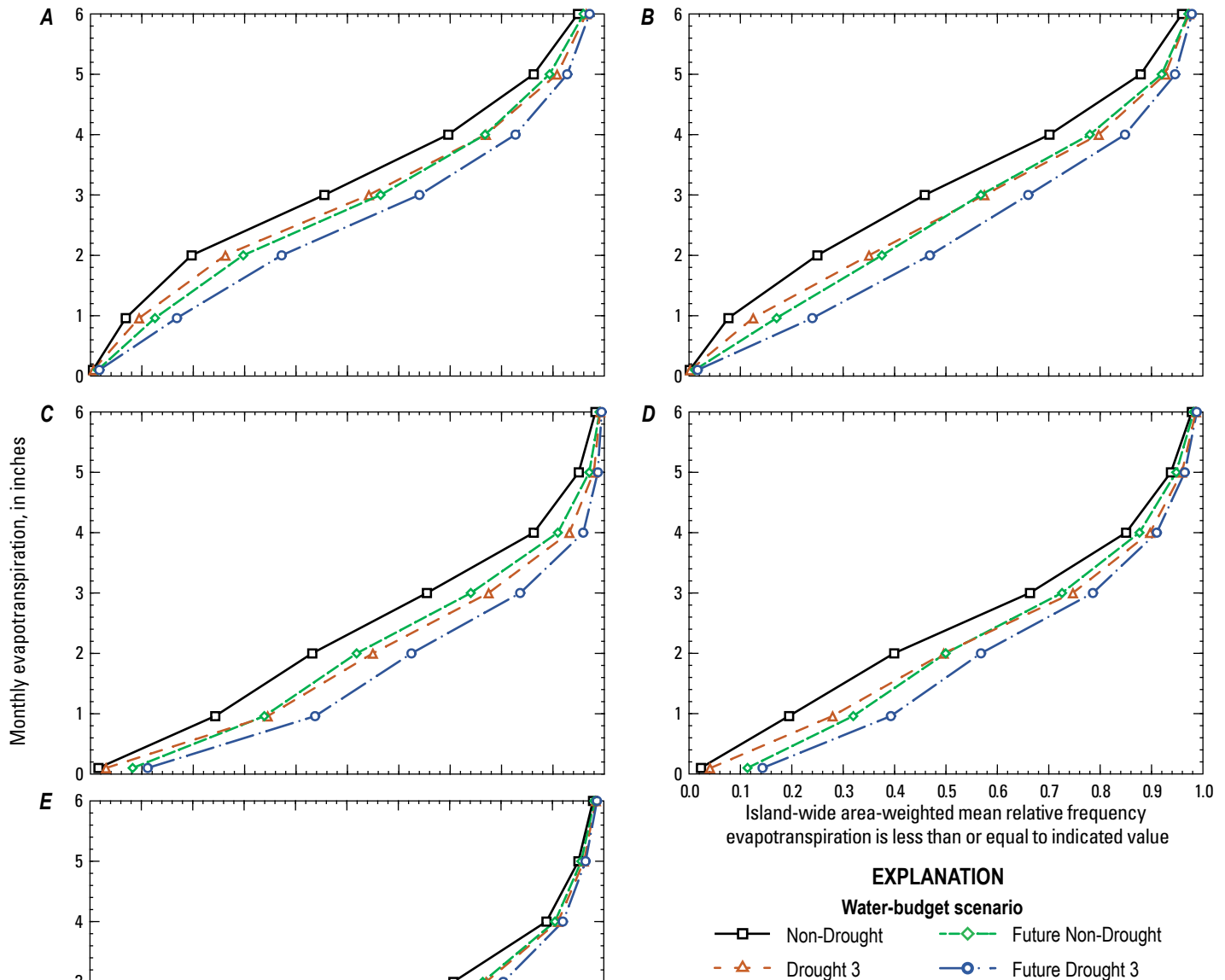
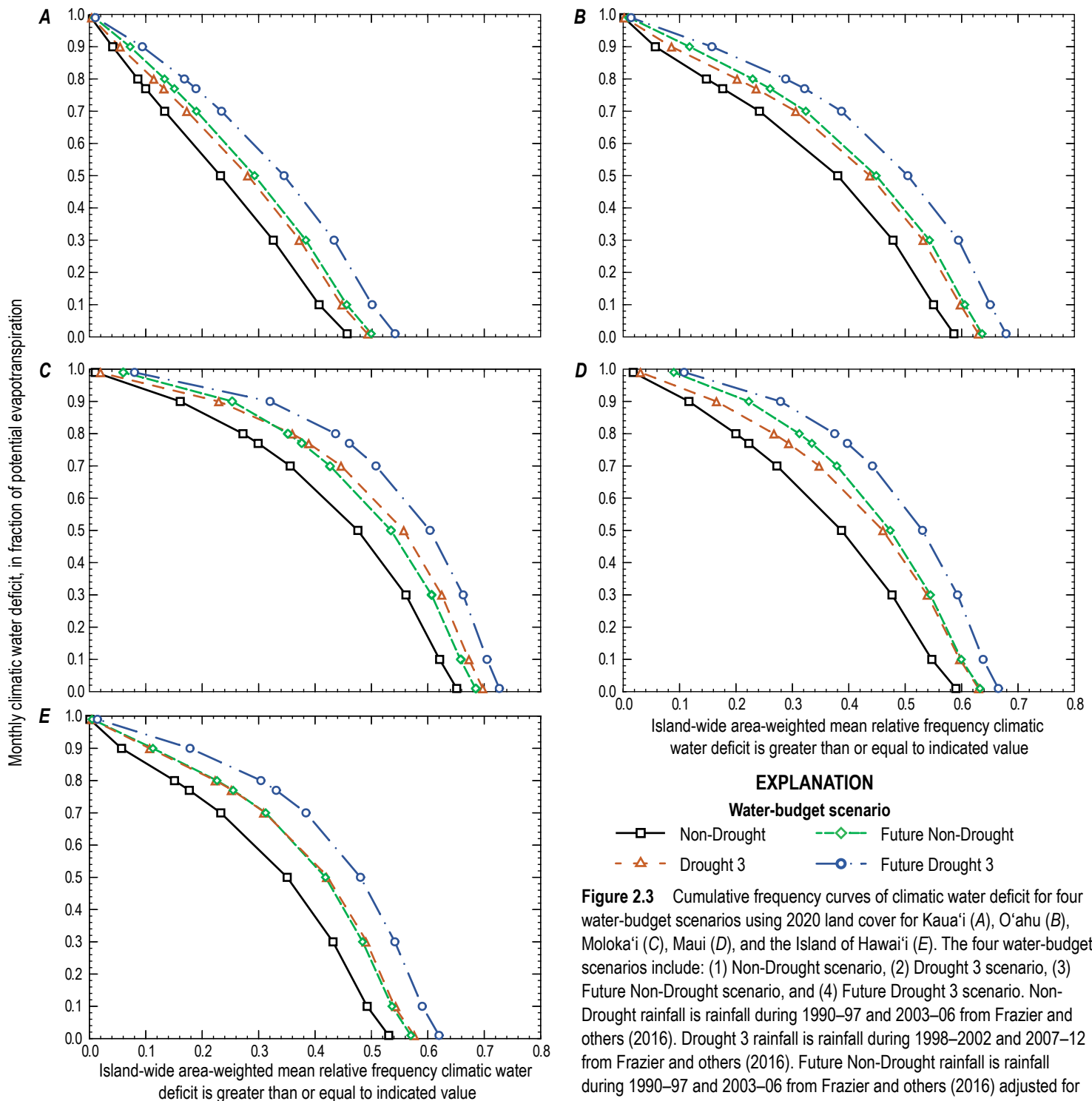


Figure 2.2 Cumulative frequency curves of evapotranspiration for four water-budget scenarios using 2020 land cover for Kaua'i (A), O'ahu (B), Moloka'i (C), Maui (D), and the Island of Hawai'i (E). The four water-budget scenarios include: (1) Non-Drought scenario, (2) Drought 3 scenario, (3) Future Non-Drought scenario, and (4) Future Drought 3 scenario. Non-Drought rainfall is rainfall during 1990–97 and 2003–06 from Frazier and others (2016). Drought 3 rainfall is rainfall during 1998–2002 and 2007–12 from Frazier and others (2016). Future Non-Drought rainfall is rainfall during 1990–97 and 2003–06 from Frazier and others (2016) adjusted for a RCP8.5 2071–99 projection from Elison Timm and others (2015). Future Drought 3 rainfall is rainfall during 1998–2002 and 2007–12 from Frazier and others (2016) adjusted for a RCP8.5 2071–99 projection from Elison Timm and others (2015).

area on each island relative to the other three scenarios. The highest relative frequencies of CWD are evident for the Future Drought 3 scenario, which indicates more frequent and widespread moisture stress on vegetation on each island relative to the other three scenarios. Among the five islands,

Kaua'i has the lowest relative frequencies of CWD for each CWD threshold and water-budget scenario (fig. 2.3A), whereas Moloka'i has the highest relative frequencies (fig. 2.3C). These results indicate that moisture stress on vegetation is most frequent and widespread on Moloka'i, and least frequent



and widespread on Kaua‘i. Relative frequencies of CWD on Kaua‘i, O‘ahu, and Maui for the Drought 3 scenario are slightly less than those for the Future Non-Drought scenarios (figs. 2.3A, B, D), which indicates the Future Non-Drought scenario causes more frequent and extensive moisture stress on vegetation. Relative frequencies of CWD on the Island of Hawai‘i for the Drought 3 and Future Non-Drought scenarios are similar, which indicates that these two scenarios have similar effects on the spatial extent and frequency of moisture stress on vegetation.

Comparison of Soil Moisture, Evapotranspiration, and Climatic Water Deficit Estimates within Wildfire Perimeters

Two-group statistical significance testing was conducted to assess potential differences in the estimates of soil moisture, ET, and CWD within the perimeters of documented wildfires between each of the water-budget scenarios. The purpose of these analyses was to determine whether estimates of these moisture-stress indicators change significantly within areas of documented wildfires. University of Hawai‘i at Mānoa (2021) documented the perimeters of wildfires in the Hawaiian Islands during 1999–2019. A subset of 187 wildfires that occurred during 1999–2012 on Kaua‘i, O‘ahu, Moloka‘i, Maui, and the Island of Hawai‘i (table 2, fig. 6) was used to overlap with the water-budget simulation period during 1990–2012 (see the “Water-Budget Scenarios” section of the report). The non-parametric Mann-Whitney *U* test (Mann and Whitney, 1947) and a significance level of 0.05 (two-sided test) were used to test for statistically significant differences between all two-group comparisons.

A set of statistical comparisons was conducted for the estimates of each moisture-stress indicator including soil moisture, ET, and CWD. First, maps of subareas used in the water-budget model simulations were clipped to the perimeter of each wildfire to create a total of 187 clipped maps of subareas from Kaua‘i, O‘ahu, Moloka‘i, Maui, and the Island of Hawai‘i. Next, the time series of monthly water-budget scenario results for each subarea were used to compute a wildfire perimeter, area-weighted mean value of soil moisture, ET, and CWD for each wildfire during the month of each wildfire’s occurrence. Next, the same time series of monthly results were used to compute a mean monthly value of soil moisture, ET, and CWD for each subarea during each of the four water-budget scenarios. The mean monthly values were then used to compute an area-weighted mean value of soil moisture, ET, and CWD for each wildfire perimeter and for each of the four water-budget scenarios. Finally, two-group statistical comparisons were conducted to assess differences in the area-weighted mean values of soil moisture, ET, and CWD between the different water-budget scenarios.

Soil Moisture

The distributions of area-weighted mean values of soil moisture within each of the 187 wildfires show substantial variability between the month of each wildfire and the four water-budget scenarios (fig. 2.4A). For example, estimates of soil moisture during the Drought 3, Future Non-Drought, and Future Drought 3 scenarios are significantly lower ($p < 0.01$) than those reported during the Non-Drought scenario (table 2.2). These results indicate increased moisture stress on vegetation, which implies increased flammability due to lower fuel moisture, that is, moisture in living and dead vegetation, and increased wildfire hazard during the Drought 3, Future Non-Drought, and Future Drought 3 scenarios, relative to the Non-Drought scenario. Furthermore, estimates of soil moisture during the Future Drought 3 scenario are not significantly different from those estimated during the month of the wildfire ($p = 0.95$), which implies no significant difference in moisture stress on vegetation between the episodic wildfires during 1999–2012 and the Future Drought 3 scenario.

Evapotranspiration

The distributions of area-weighted mean values of ET within each of the 187 wildfires show substantial variability between the month of each wildfire and the four water-budget scenarios (fig. 2.4B). For example, estimates of ET during the Drought 3, Future Non-Drought, and Future Drought 3 scenarios are significantly lower ($p < 0.01$) than those reported during the Non-Drought scenario (table 2.2). These results indicate increased moisture stress on vegetation, which implies increased flammability and increased wildfire hazard during the Drought 3, Future Non-Drought, and Future Drought 3 scenarios, relative to the Non-Drought scenario. Furthermore, estimates of ET for the Future Drought 3 scenario are not statistically dissimilar from those estimated during the month of the wildfire ($p = 0.32$), which implies no significant difference in moisture stress on vegetation between the episodic wildfires during 1999–2012 and the Future Drought 3 scenario.

Climatic Water Deficit

The distributions of area-weighted mean values of CWD within each of the 187 wildfires show substantial variability between the month of each wildfire and the four water-budget scenarios (fig. 2.4C). For example, estimates of CWD during the Drought 3, Future Non-Drought, and Future Drought 3 scenarios are significantly higher ($p < 0.01$) than those reported during the Non-Drought scenario (table 2.2). These results indicate increased moisture stress on vegetation, which implies increased flammability and increased wildfire hazard during the Drought 3, Future Non-Drought, and Future Drought 3 scenarios, relative to the Non-Drought scenario. Furthermore, estimates of CWD during the Future Drought 3 scenario are not

statistically dissimilar from those estimated during the month of the wildfire ($p=0.66$), which implies no significant difference in moisture stress on vegetation between the episodic wildfires during 1999–2012 and the Future Drought 3 scenario.

Selection of Moisture-Stress Levels for Soil Moisture, Evapotranspiration, and Climatic Water Deficit

Moisture-stress levels for computing frequency characteristics were selected for soil moisture, ET, and CWD using a trial-and-error approach aimed at distinguishing the frequency of low-moisture conditions during the occurrence of documented wildfires. A range of moisture-stress levels

similar to those estimated during the occurrence of wildfires during 1999–2012 were tested to identify areas of increased moisture stress and wildfire hazard. The median value of the area-weighted mean values within each wildfire perimeter during the month in which each wildfire occurred was selected as the threshold for computing frequency maps. For example, the median values of 0.074, 0.96 inches, and 0.77 were selected as the threshold values for soil moisture, ET, and CWD, respectively (table 2.1, fig. 2.4). The threshold values were then used in a frequency analysis of monthly time series data produced by each water-budget scenario. The frequency characterization is described in the “[Soil Moisture, Evapotranspiration, and Climatic Water Deficit Frequency Characterization](#)” section of the report.

Table 2.2. Summary of level of significance (p values) for two-group statistical comparisons of area-weighted mean values of estimated soil moisture, evapotranspiration, and climatic water deficit within the perimeters of wildfires during 1999–2012.

[<, less than; --, not applicable; RCP8.5, Representative Concentration Pathway warming scenario with total radiative forcing of 8.5 Watts per square meter by the year 2100 from Intergovernmental Panel on Climate Change (2014); Non-Drought scenario is 1990–97 and 2003–06 rainfall from Frazier and others (2016), and 2020 land cover; Drought 3 scenario is 1998–2002 and 2007–12 rainfall from Frazier and others (2016), and 2020 land cover; Future Non-Drought scenario is 1990–97 and 2003–06 rainfall from Frazier and others (2016) adjusted for a RCP8.5 2071–99 projection from Elison Timm and others (2015), and 2020 land cover; Future Drought 3 scenario is 1998–2002 and 2007–12 rainfall from Frazier and others (2016) adjusted for a RCP8.5 2071–99 projection from Elison Timm and others (2015), and 2020 land cover.]

Water-budget scenario	p values for indicated period or scenario			
	Month of wildfire	Non-Drought	Drought 3	Future Non-Drought
Soil moisture				
Non-Drought	<0.01	--	--	--
Drought 3	<0.01	<0.01	--	--
Future Non-Drought	<0.01	<0.01	0.09	--
Future Drought 3	0.95	<0.01	<0.01	<0.01
Evapotranspiration				
Non-Drought	<0.01	--	--	--
Drought 3	<0.01	<0.01	--	--
Future Non-Drought	<0.01	<0.01	0.04	-
Future Drought 3	0.32	<0.01	<0.01	<0.01
Climatic water deficit				
Non-Drought	<0.01	--	--	--
Drought 3	<0.01	<0.01	--	--
Future Non-Drought	<0.01	<0.01	0.16	--
Future Drought 3	0.66	<0.01	<0.01	<0.01

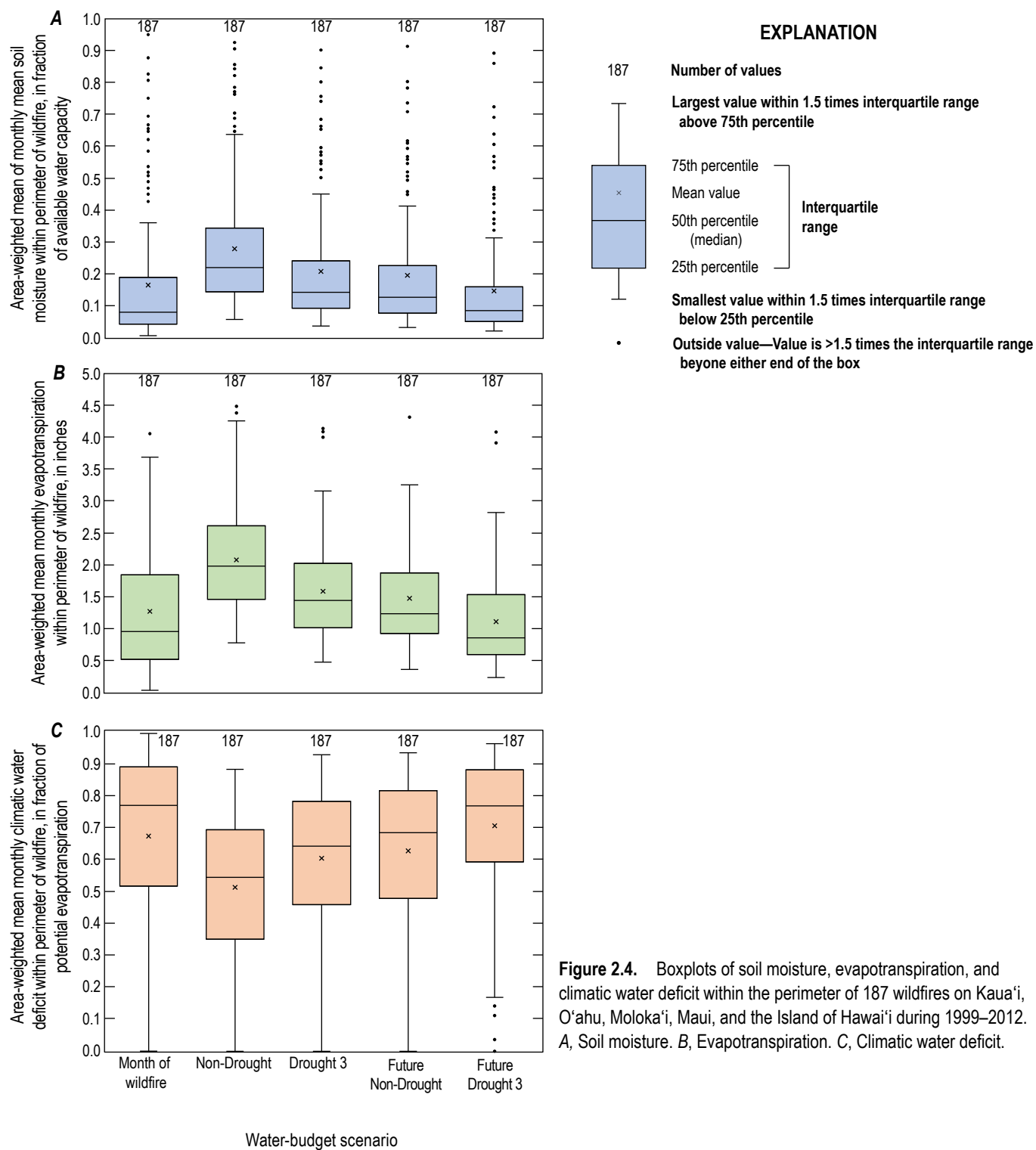


Figure 2.4. Boxplots of soil moisture, evapotranspiration, and climatic water deficit within the perimeter of 187 wildfires on Kaua'i, O'ahu, Moloka'i, Maui, and the Island of Hawai'i during 1999–2012. A, Soil moisture. B, Evapotranspiration. C, Climatic water deficit.

References Cited

- Allen, R.G., Pereira, L.S., Raes, D., and Smith, M., 1998, Crop evapotranspiration—Guidelines for computing crop water requirements: Food and Agriculture Organization of the United Nations, FAO Irrigation and Drainage Paper 56, 300 p., accessed June 9, 2011, at <http://www.fao.org/docrep/X0490E/X0490E00.htm>.
- Brouwer, C., Goffeau, A., and Heibloem, M., 1985, Irrigation Water Management—Training Manual No. 1—Introduction to Irrigation: Food and Agriculture Organization of the United Nations, accessed May 6, 2022, at <https://www.fao.org/3/R4082E/r4082e00.htm#Contents>.
- Elison Timm, O., Giambelluca, T.W., and Diaz, H.F., 2015, Statistical downscaling of rainfall changes in Hawai‘i based on the CMIP5 global model projections: *Journal of Geophysical Research: Atmospheres*, v. 120, no. 1, p. 92–112, <https://doi.org/10.1002/2014JD022059>.
- Flint, L.E., Flint, A.L., and Thorne, J.H., 2015, Climate change—Evaluating your local and regional water resources: U.S. Geological Survey Fact Sheet 2014–3098, 6 p., <https://doi.org/10.3133/fs20143098>.
- Frazier, A.G., Giambelluca, T.W., Diaz, H.F., and Needham, H.L., 2016, Comparison of geostatistical approaches to spatially interpolate month-year rainfall for the Hawaiian Islands: *International Journal of Climatology*, v. 36, no. 3, p. 1459–1470, <https://doi.org/10.1002/joc.4437>.
- Giambelluca, T.W., 1983, Water balance of the Pearl Harbor-Honolulu basin, Hawaii, 1946–1975. Water Resources Research Center Technical Report 151: University of Hawaii at Manoa, Honolulu, 151 p., accessed February 8, 2010, at <https://scholarspace.manoa.hawaii.edu/handle/10125/1992>.
- Mann, H.B., and Whitney, D.R., 1947, On a test of whether one of 2 random variables is stochastically larger than the other: *Annals of Mathematical Statistics*, v. 18, no. 1, p. 50–60, <https://www.jstor.org/stable/2236101>.
- Natural Resources Conservation Service, 2008, Soil quality indicators: U.S. Department of Agriculture, 2 p., accessed September 1, 2022, at https://www.nrcs.usda.gov/sites/default/files/2022-10/nrcs142p2_051590.pdf.
- Natural Resources Conservation Service, 2019, Soil survey geographic (SSURGO) database for the Islands of Kaua‘i, O‘ahu, Moloka‘i, Lāna‘i, Maui, and Hawai‘i: U.S. Department of Agriculture, accessed December 5, 2019, at <https://websoilsurvey.nrcs.usda.gov/app/>.
- Oki, D.S., 2022, Water-budget accounting for tropical regions model (WATRMod) documentation: U.S. Geological Survey Open-File Report 2022–1013, 77 p., <https://doi.org/10.3133/ofr20221013>.
- Trauernicht, C., 2019, Vegetation—Rainfall interactions reveal how climate variability and climate change alter spatial patterns of wildland fire probability on Big Island, Hawaii: *Science of The Total Environment*, v. 650, p. 459–469, <https://doi.org/10.1016/j.scitotenv.2018.08.347>.
- University of Hawai‘i at Mānoa, 2021, Hawaii Fire Perimeters 1999 -2019: College of Tropical Agriculture and Human Resources, Department of Natural Resources and Environmental Management database, accessed April 27, 2021, at <https://www.nrem-fire.org/hawaii-fire-history>.

